

Miguel Ângelo Rodrigues Larginho

Licenciado em Biologia Celular e Molecular

**Gold Nanoparticles for the Detection of
DNA Adducts as Biomarkers of
Exposure to Acrylamide**

Dissertação para obtenção do Grau de
Doutor em Biologia, Especialidade
Biotecnologia, pela Universidade Nova de
Lisboa, Faculdade de Ciências e Tecnologia

Dezembro de 2014

COPYRIGHT

Autorizo os direitos de copyright da minha tese de doutoramento, com o título:
“Gold nanoparticles for the detection of DNA adducts as biomarkers of exposure to acrylamide”.

A Faculdade de Ciências e Tecnologia e a Universidade Nova de Lisboa têm o direito, perpétuo e sem limites geográficos, de arquivar e publicar esta dissertação através de exemplares impressos reproduzidos em papel ou de forma digital, ou por qualquer outro meio conhecido ou que venha a ser inventado, e de a divulgar através de repositórios científicos e de admitir a sua cópia e distribuição com objectivos educacionais ou de investigação, não comerciais, desde que seja dado crédito ao autor e editor.

ACKNOWLEDGEMENTS

I would like to thank all people who contributed to the results presented in this thesis. Without your help and guidance, the work here presented could not have been accomplished. I would also like to thank all people who contributed to make me the person I am today, having contributed indirectly to this thesis. Without them I would be so much less. Words alone cannot express my immense gratitude to you all, but I will give it a shot anyway (I am sorry in advance if I forget anyone!).

- **To my supervisor, prof. Pedro Baptista** I would like to thank you for the unconditional support you have given me for these last years. I was extremely lucky to have been handpicked from the haystack of students wishing to work with you. You have the capacity to turn around one's train of thought, and turn nihilism into joy and hope! Your force of will, knowledge, rigor and amiability make you one of the best examples that has ever been set before me. I am both proud and honoured to have been given the opportunity to know you, as a supervisor, as a professor, as a leader, as a scientist, as a friend. Thank you for everything...and stay tuned because there's still more to come...

- **To my co-supervisor, prof. José Luís Capelo** I would like to thank you for the immense support you have given me all these years. For welcoming me into your family in Galicia like only you know how, for all the "claras con limón", "patatas bravas" and the "pulpo"...but most of all, for advising me when I needed and for not sugarcoating the truth, when it needed to be said. For all you have invested in me, and for always being there when I needed. I feel very fortunate to have known you both inside and outside of the laboratory, and to have worked with you in an area that was almost foreign to me...maybe still is. Thank you for everything...and I am still waiting to try that "assessina".

- **To Dr. Mário Diniz**, I would like to thank you for the neverending support I have given me since we have met, and the influence you had on my future career. I have learnt a great deal from you, both professionally and personally and it is a pleasureable and a privileged experience to work with you. **To Dr. Pedro Costa**, I would like to thank the neverending availability and amiability you have shown, whether for teaching me about toxicology, statistics or tell some jokes while smoking a cigarette. To both of you I thank the opportunity to work and learn in toxicology, your professionalism and knowledge. You have been trusted advisors, teachers and friends, and I am in your debt.

- **To all my colleagues from Lab 315:** Fábio, Sara, Rita, Raquel, Bruno, Milton, Pedrosa, Daniela, Catarina, Cláudia, Joana, Alexandra, Conde, Guida, for the unconditional support and

companionship these last few years both in and out of work. You are both spectacular persons and outstanding professionals. **To the 315 kids:** Catraia, Bárbara, Ana F, Carlota, Daniela C, Gonçalo Sousa, Marisa, Sofia, Tiago, Zé Nobre, Zé Cristóvão, thank you for becoming a part of my journey so far. I have probably learnt more from you, than you have from me. I hope to continue to see you grow! **To the old school team:** Gonças, VP, Rosa, Goku, Red, Letícia, Ana, Carina, Maria, for everything you have taught me, shared with me, discussed with me and laughed with me, for turning the workplace into a second home and fellow colleagues into family. Few people have had the good fortune to experience this feeling, and I am lucky I have been one of them. Also, I find it difficult to excel both at a personal and professional level, but you really know how to do it right. Cheers!

- **To all people from Bioscope:** Hugo, Bete, Cris, Bruno, Javi, Julio, Eduardo, Susana, Hajer, Carla, Daniela, David, Noemí, for all the special moments that made abroad feel like home; I will always remember those great nights with fruitful discussions in castellaño, and the hamburger with 50 cm diameter. A particular word of appreciation to Carlos Lodeiro, for his support during my PhD work, and also for giving me an opportunity many years ago, that marked my first contact with a research laboratory.

- **To all my colleagues from the Department of Life Sciences,** for all the help provided inside and outside of the laboratories.

- **To prof. António Laires and prof. Ana Mota** for all the support and for accepting the invitation to be a part of my thesis.

- **To friends from REQUIMTE:** Lima, Artur, Avó, Filipe, Cristina, for all the support, motivation and discussions about an endless number of subjects and for what I have learnt from you.

- **To Fundação para a Ciência e Tecnologia/MEC** for the financial support; without it this work would not have been possible (SFRH/BD/ 64026/2009). Also, **to Xunta de Galicia,** for additional funding.

- **To the people from Plant Genetics@ISA:** Nuno, Wanda, Leonor, Manuela, Guida, Miguel and Márcia, for all the special and primordial moments that forged my scientific journey.

- **To Ana,** my love and my inspiration, I really would have not made it this far without your help; both in personal and professional life I would be so much less. Your spirit, guidance and perseverance are an example to everyone. You possess true Valor, more than you know, and I am extremely fortunate and privileged to have you with me. And it's only the beginning...

- **To João**, thank you for all the moments we spent together, talking about science, girls, martial arts, Pokémon, King of Fighters or *Arabidopsis*. Ten years!!! You possess remarkable brain damage, matched only by my own, and I treasure you for that.

Bixo, tu é que sabes! おら,いぎませ!

- **To all my brothers from kung-fu and taijiquan**, all those who taught me, practiced with me and those who still do, from Portugal and abroad, you have my thanks. To my brothers in Almada, Amadora, Lisboa, Boston, New Jersey and France for making possible those rare occasions of both pain and pleasure. To Raul, Nuno, Sandro, Tony, Dave, Dario, Tiago, Tonet, Marcio and Quim an enormous thanks for everything. Most often, an intensive martial arts training would turn into extensive discussions about how the human mind works, or the floating cat theory. All of you have played your part in shaping me into the person I am today and for that I am extremely grateful. Last but definitely not least, a special acknowledgment filled with awesomeness to Ricardo. I've know you for half my life, and I can definitely say the road so far would have not been half as fun, half as educational and half as painful without you. I am lucky and honoured to have you as my brother. Thank you.

- **To all my friends**, for all the support throughout these years, for the endless discussions about the most serious and the most ridiculous subjects, and for bringing me into a different reality and forcing me to think in alternate ways! Thank you.

- **Last but definitely not least, to my family**, especially my sister, my parents and their parents as well. You are honestly the best persons I have ever known. Everything you have given me, taught me and provided me with I will never be able to repay, so I might as well just keep trying. I am what I am and where I am today because of you. I love you all from the bottom of my heart. **Marta**, you're an idiot! I really love you. Cheers!

If life seems jolly rotten, there's something you've forgotten

And that's how to laugh and dance and sing!

When you're feeling in the dumps, don't be silly chumps

Just purse your lips and whistle – that's the thing!

And...always look on the bright side of life!

RESUMO

O principal objectivo desta dissertação foi o desenvolvimento de um método baseado em nanopartículas de ouro para detecção de aductos de DNA como biomarcadores, para complementar as desvantagens existentes nos métodos actualmente utilizados. O trabalho experimental foi dividido em 3 componentes: preparação da amostra, detecção e avaliação de um modelo biológico de exposição.

Foram implementadas e combinadas diferentes técnicas de purificação de amostras de DNA (incluindo ultra-sons, endonucleases e cromatografia) num protocolo completo para preparação da amostra de DNA, antes da detecção.

A detecção de nucleótidos alquilados utilizando nanopartículas de ouro foi realizada por dois métodos distintos: espectrometria de massa e colorimétrico. No primeiro, as nanopartículas de ouro foram utilizadas para ionização por laser em vez da matriz orgânica normalmente utilizada. Foi possível a identificação de nucleótidos através de sinais de massa específicos no espectro. No entanto, não foram observados sinais correspondentes aquando da análise de amostras biológicas. Um método alternativo baseado nas propriedades colorimétricas das nanopartículas de ouro foi também utilizado para detecção. Este método inspirado pelo método de *non-cross-linking* permitiu a identificação de guaninas alquiladas e aductos do DNA produzidos numa reacção *in vitro*.

Para avaliação de um modelo de exposição à acrilamida foram testados dois organismos: o peixe-dourado e o mexilhão. Os organismos foram expostos à acrilamida na água, a mortalidade foi avaliada e foram estimadas as concentrações letais. No caso do peixe-dourado, a genotoxicidade e alterações metabólicas mostraram relações entre concentração de exposição e resposta dos biomarcadores. Alterações histopatológicas foram verificadas principalmente nas células pancreáticas, mas também ao nível dos hepatócitos. Nos mexilhões foram observadas concentrações letais maiores que as estimadas para os peixes-dourados. A análise de biomarcadores de stress oxidativo após exposição prolongada mostrou que a acrilamida causa alterações no estado oxidativo da célula e induz actividade de enzimas envolvidas na destoxificação de radicais. Uma análise histopatológica qualitativa revelou gonadotoxicidade acentuada em mexilhões fêmea, o que pode constituir um risco para a dinâmica populacional.

ABSTRACT

The main objective of this thesis was the development of a gold nanoparticle-based methodology for detection of DNA adducts as biomarkers, to try and overcome existing drawbacks in currently employed techniques. For this objective to be achieved, the experimental work was divided in three components: sample preparation, method of detection and development of a model for exposure to acrylamide.

Different techniques were employed and combined for de-complexation and purification of DNA samples (including ultrasonic energy, nuclease digestion and chromatography), resulting in a complete protocol for sample treatment, prior to detection.

The detection of alkylated nucleotides using gold nanoparticles was performed by two distinct methodologies: mass spectrometry and colorimetric detection. In mass spectrometry, gold nanoparticles were employed for laser desorption/ionisation instead of the organic matrix. Identification of nucleotides was possible by fingerprint, however no specific mass signals were denoted when using gold nanoparticles to analyse biological samples. An alternate method using the colorimetric properties of gold nanoparticles was employed for detection. This method inspired in the non-cross-linking assay allowed the identification of glycidamide-guanine adducts and DNA adducts generated *in vitro*.

For the development of a model of exposure, two different aquatic organisms were studied: a goldfish and a mussel. Organisms were exposed to waterborne acrylamide, after which mortality was recorded and effect concentrations were estimated. In goldfish, both genotoxicity and metabolic alterations were assessed and revealed dose-effect relationships of acrylamide. Histopathological alterations were verified primarily in pancreatic cells, but also in hepatocytes. Mussels showed higher effect concentrations than goldfish. Biomarkers of oxidative stress, biotransformation and neurotoxicity were analysed after prolonged exposure, showing mild oxidative stress in mussel cells, and induction of enzymes involved in detoxification of oxygen radicals. A qualitative histopathological screening revealed gonadotoxicity in female mussels, which may present some risk to population equilibrium.

LIST OF ABBREVIATIONS

- μM:** micromoles per liter
- μmol:** micromoles
- 3-HPA:** 3-hydroxypicolinic acid
- AChE:** acetylcholinesterase
- AgNP:** silver nanoparticle
- Ahr:** aryl-hydrocarbon receptor
- ampl:** amplitude
- ARE:** antioxidante response element
- AuNP:** gold nanoparticle
- bp:** base pairs
- CAT:** catalase
- CHCA:** α-cyano-4-hydroxycinnamic acid
- CI:** chemical ionisation
- Cl-Ph-AA:** 3-(4-chloro-phenyl)-2-cyano acrylic acid
- CoNPs:** cobalt nanoparticles
- CSNPs:** core-shell nanoparticles
- CYP1A:** cytochrome P450 1A
- dATP:** deoxyadenosine triphosphate
- dCTP:** deoxycytidine triphosphate
- dGTP:** deoxyguanosine triphosphate
- DHB:** 2,5-dihydroxybenzoic acid
- DIOS:** desorption/ionisation on silicon
- DLS:** dynamic light scattering
- DNA:** deoxyribonucleic acid
- dNTP:** deoxynucleotide triphosphate
- dTTP:** deoxythymidine triphosphate
- EI:** electron ionisation
- ELISA:** enzyme-linked immunosorbent assay
- ENA:** erythrocyte nuclear abnormality
- EROD:** ethoxyresorufin-O-deethylase
- fM:** femtomoles per liter
- fmol:** femtomoles
- GA:** glycidamide
- GST:** glutathione S-transferase

HABA: 2-(4'-hydroxybenzeneazo)benzoic acid
ICP: inductively coupled plasma
LDI: laser desorption/ionisation
m/z: mass-to-charge ratio
M: moles per liter
MALDI: matrix-assisted laser desorption/ionisation
MFO: mixed function oxidases
min: minutes
mM: millimoles per liter
mmol: millimoles
MS: mass spectrometry
nano-PALDI: nanoparticle-assisted laser desorption/ionisation
nM: nanomoles per liter
nmol: nanomoles
NP: nanoparticle
pM: picomoles per liter
pmol: picomoles
PMS: post microsomal supernatant
PtNPs: platinum nanoparticles
ROS: reactive oxygen species
S/N: signal-to-noise ratio
SA: sinapinic acid
SALDI: surface-assisted laser desorption/ionisation
SERS: surface-enhanced Raman scattering
SiO₂: silica
TAC: total antioxidant capacity
TEM: transmission electron microscopy
THAP: 2',4',6'-trihydroxyacetophenone
TOF: time-of-flight
UP: ultrasonic probe
vol: volume
ζ-potential: zeta-potential

TABLE OF CONTENTS

ACKNOWLEDGEMENTS	V
RESUMO	IX
ABSTRACT	XI
LIST OF ABBREVIATIONS	XIII
TABLE OF CONTENTS	XVII
FIGURE INDEX	XXIII
TABLE INDEX	XXVII
CHAPTER 1. GENERAL INTRODUCTION	1
1.1 Nanotechnology	3
1.1.1 Noble metal nanoparticles	4
1.1.1.2 Synthesis and derivatisation	5
1.1.2 Noble metal nanoparticles for colorimetric detection of nucleic acids	6
1.1.2.1 Assays based on unmodified noble metal nanoparticles	6
1.1.2.2 Assays based on functionalised noble metal nanoparticles	7
1.1.3 Noble metal nanoparticles for signal enhancement	9
1.1.3.1 Fluorescence assays.....	9
1.1.3.2 Luminescence assays.....	10
1.1.3.3 Spectral labels	11
1.1.4. Noble metal nanoparticles for biomarker analysis	13
1.2 Mass Spectrometry	16
1.2.1 General concepts	17
1.2.2 Matrix-assisted laser desorption/ionisation time-of-flight (MALDI-TOF)	19
1.2.3 Surface-assisted laser desorption/ionisation time-of-flight (SALDI-TOF)	21
1.2.4 Advantages of nanoparticles for SALDI-TOF-MS	23
1.2.5 Noble metal nanoparticles for SALDI-TOF-MS analysis	24
1.3 Toxicology	28
1.3.1 General concepts	28
1.3.2 Formation of DNA adducts and chemical carcinogenesis	30
1.3.3 Methods for detection of DNA adducts	32
1.3.4 The case of acrylamide	34
1.3.4.1 Environmental risk	35
1.3.4.2 Known mechanisms of toxicity	36
1.4 Scope of thesis and main objectives	37
CHAPTER 2. MATERIALS AND METHODS	41
2.1 Materials	43

2.1.1 Chemical reagents	43
2.1.2 Solutions and buffers	45
2.1.3 Biological material.....	49
2.1.3.1 Antibodies	49
2.1.3.2 Enzymes	49
2.1.3.3 Nucleotides.....	49
2.1.3.4 DNA size markers	49
2.1.3.5 Plasmid DNA	50
2.1.3.6 Oligonucleotides.....	50
2.1.4 Equipment.....	50
2.1.5 Specialised materials	51
2.4 Methods.....	51
2.4.1 Molecular biology	51
2.4.1.1 Plasmid DNA isolation.....	51
2.4.1.2 Genomic DNA isolation from total blood.....	52
2.4.1.3 <i>In vitro</i> alkylation of nucleotides	53
2.4.2 Sample preparation.....	53
2.4.2.1 Ultrasonic procedure and agarose gel electrophoresis	53
2.4.2.2 Restriction enzyme digestion	54
2.4.2.3 Acceleration of nuclease digestion via ultrasonic energy	55
2.4.2.4 Sample treatment prior to HPLC analysis.....	55
2.4.2.5 HPLC conditions	56
2.4.2.6 Sample preparation for MS-detection: complete protocol	56
2.4.3 Nanotechnology	57
2.4.3.1 Gold nanoparticle synthesis by citrate reduction	57
2.4.3.2 Gold nanoparticle characterisation.....	57
2.4.3.3 Aptamer-gold nanoprobe synthesis	58
2.4.3.4 Stability of aptamer-gold nanoprobes	59
2.4.3.5 Colorimetric assays with aptamer-gold nanoprobes	59
2.4.4 Mass spectrometry	60
2.4.4.1 Characterisation of organic matrices.....	60
2.4.4.2 Sample deposition and MS-detection.....	60
2.4.5 Toxicity assays	62
2.4.5.1 Experimental design for acute toxicity assay on goldfish.....	62
2.4.5.2 Experimental design for acute and chronic toxicity assays on mussels	62
2.4.5.3 Genotoxicity assessment	63
2.4.5.3.1 Erythrocyte nuclear abnormality (ENA) assessment	63

2.4.5.3.2 Single-cell gel electrophoresis (comet-assay)	63
2.4.5.4 Sampling and preparation of goldfish PMS and microsomal fractions	64
2.4.5.5 Sampling and preparation of mussel whole-body homogenates	64
2.4.5.6 Analysis of CYP1A induction	65
2.4.5.7 Discontinuous ethoxyresorufin-O-deethylase (EROD) spectrophotometric assay	65
2.4.5.8 Activity of acetylcholinesterase (AChE)	66
2.4.5.9 Analysis of glutathione-S-transferase (GST) activity	66
2.4.5.10 Analysis of catalase (CAT) activity	66
2.4.5.11 Analysis of total antioxidant capacity (TAC)	67
2.4.5.12 Analysis of lipid peroxidation (LPO)	67
2.4.5.13 Histological preparations and analysis	68
2.4.6 Statistical analysis	69
2.4.6.1 Colorimetric assays with aptamer-gold nanoprobe	69
2.4.6.2 Estimation of effect concentrations	69
2.4.6.3 Analysis of biomarker data	69
CHAPTER 3. OPTIMISATION OF SAMPLE PREPARATION	71
3.1 Introduction	73
3.1.1 Ultrasonic energy and DNA fragmentation	73
3.1.2 Enzymatic hydrolysis of DNA molecules	75
3.1.3 A word on liquid chromatography	77
3.2 Results and Discussion	78
3.2.1 Development of a fast and efficient ultrasonic-based strategy for DNA fragmentation	78
3.2.1.1 Ultrasonic devices	78
3.2.1.2 Finding out the best device for DNA ultrasonic fragmentation	79
3.2.1.3 Influence of ultrasonication time	81
3.2.1.4 Influence of sample denaturation	81
3.2.1.5 Influence of sample volume	83
3.2.1.6 Influence of DNA concentration	83
3.2.1.7 Ultrasonic fragmentation versus restriction enzyme digestion	83
3.2.1.8 Ultrasonic acceleration of nuclease-mediated DNA hydrolysis	85
3.2.2 Chromatography for nucleotide separation and purification	87
3.2.2.1 Profiling different nucleotides	87
3.2.2.2 Separation of modified nucleotides via HPLC	89
3.2.2.3 Brief considerations on liquid chromatography for sample preparation	90
3.3 Conclusions	91

CHAPTER 4. GOLD NANOPARTICLES FOR IDENTIFICATION OF MODIFIED NUCLEOTIDES THROUGH MASS SPECTROMETRY AND COLORIMETRY.....	95
4.1 Introduction	97
4.2 Results and discussion.....	98
4.2.1 Matrix- and surface-assisted laser desorption/ionisation mass spectrometry for nucleotide identification.....	98
4.2.1.1 Characterisation and selection of organic matrices	98
4.2.1.2 Characterisation of gold nanoparticles	101
4.2.1.3 Profiling different nucleotides via MALDI and SALDI	101
4.2.1.4 Influence of concentration and pH for nucleotide detection	105
4.2.1.5 Identification of DNA adducts generated <i>in vitro</i>	107
4.2.1.6 Identification of DNA adducts as biomarkers in biological samples	109
4.2.2 Colorimetric detection of modified nucleotides using aptamer-gold nanoprobess... 	110
4.2.2.1 Characterisation of gold nanoparticles	110
4.2.2.2 Stability of synthesised nanoprobess	110
4.2.2.3 Colorimetric detection of glycidamide-guanine adducts.....	112
4.2.2.4 Identification of DNA adducts in solution	114
4.3 Conclusions	114
CHAPTER 5. ALTERATIONS TO AQUATIC ORGANISMS INDUCED BY ACUTE AND CHRONIC EXPOSURE TO ACRYLAMIDE	117
5.1 Introduction	119
5.2 Acute toxicity of waterborne acrylamide to goldfish	119
5.2.1 Results	120
5.2.1.1 Mortality.....	120
5.2.1.2 Genotoxicity assessment	121
5.2.1.3 CYP1A induction	121
5.2.1.4 Glutathione S-transferase activity	122
5.2.1.5 Liver histopathology	123
5.2.2 Discussion.....	124
5.3. Acute toxicity of acrylamide to Mediterranean mussel and alterations induced by chronic exposure.....	129
5.3.1 Results	129
5.3.1.1 Acute toxicity	129
5.3.1.2. Biochemical biomarkers after chronic exposure	129
5.3.1.3 Histopathology after chronic exposure.....	130
5.3.1.4 Statistical integration of biomarker results.....	131
5.3.2 Discussion.....	132

5.4. Conclusions	138
CHAPTER 6. GENERAL DISCUSSION AND CONCLUSIONS	141
REFERENCES	147
APPENDICES	169
Appendix I – Plasmid maps and sequences: pUC19 and p158.....	169
Appendix II – Calibration curves used for total protein quantification via Bradford assay and for analysis of several biomarkers.....	174
Appendix III – Characterisation of organic matrices: UV-Vis and MALDI-MS	176

FIGURE INDEX

Figure 1.1. Schematic representation of the SPR phenomenon.	5
Figure 1.2. The detection principle and colorimetric result behind the cross-linking assay developed by Mirkin and co-workers for identification of nucleotide sequences	7
Figure 1.3. The detection principle behind the non-cross-linking colorimetric assay developed by Baptista et al. for identification of nucleotide sequences.....	8
Figure 1.4. Schematic representation for a detection system based in metal-enhanced fluorescence (MEF).	10
Figure 1.5. Schematic representation for an ELISA system with AuNPs.....	16
Figure 1.6. Diagram of a mass spectrometer, including an ion source, one mass analyser, a detector and an output system for generating data (computer and printer).....	18
Figure 1.7. Schematic representation of the MALDI process	20
Figure 1.8. Schematic representation of A) linear and B) reflector mode of analysis.....	21
Figure 1.9. Some examples of sites for possible adduct formation in DNA bases.	30
Figure 1.10. Some examples of possible guanine DNA adducts with different toxicants (PAHs, mycotoxins, etc.).....	31
Figure 1.11. Epoxidation of acrylamide to glycidamide and possible interactions of these compounds with cellular components	37
Figure 2.1. Image of the four ultrasonic devices utilised in the study.	54
Figure 2.2. Solvent gradient utilised for HPLC nucleotide analysis.....	56
Figure 3.1. Generation and collapse of an acoustic cavitation microbubble.	74
Figure 3.2. A) Mechanism of hydrolysis of a phosphodiester bond between two nucleotides in a nucleic acid molecule. B) Examples of recognition sequence and restriction sites for three different restriction endonucleases.	76
Figure 3.3. Classification of chromatography modes (highlighted both ion-exchange and size-exclusion). CEC – Capillary electrochromatography.	76
Figure 3.4. Schematics of different principles of separation in liquid chromatography. A) ion-exchange chromatography; B) size-exclusion chromatography.....	77
Figure 3.5. ΔQ [J] versus time of sonication for three of the four ultrasonic devices assessed in this work.	79
Figure 3.6. DNA fragmentation potential for different sonication setups.....	80
Figure 3.7. Comparison between the sonoreactor system and restriction enzyme digestion in generating DNA fragments.	84
Figure 3.8. Electrophoretic patterns obtained for DNase I digestion of plasmid DNA with and without ultrasonication.....	85

Figure 3.9. Electrophoretic patterns obtained for DNase I digestion of plasmid DNA with increasing ultrasonic amplitude.....	86
Figure 3.10. Chromatograms of different nucleotide mixtures, for identification of different deoxynucleotides by ion-exchange HPLC	88
Figure 3.11. Chromatograms for mixtures spiked with A) glycidamide (GA); B) dGTP; C) GA-modified dGTP.....	89
Figure 3.12. Schematic representation of the complete protocol for sample preparation..	92
Figure 4.1. Characterisation of the synthesised gold nanoparticles	99
Figure 4.2. MALDI-TOF spectra of dNTPs, using CHCA as a matrix.....	101
Figure 4.3. SALDI-TOF-MS spectrum for AuNP:nucleotide mixture, in negative-ion....	102
Figure 4.4. Gold nanoparticle based ionisation of dNTPs.	104
Figure 4.5. AuNP-based SALDI-TOF spectra of equimolar mixtures of dNTPs.....	105
Figure 4.6. Variation of analyte and matrix concentration.....	106
Figure 4.7. Variation of different parameters and its influence on the relative intensity of the guanine m/z signal.....	107
Figure 4.8. AuNP-SALDI-TOF for identification nucleotide adducts.....	108
Figure 4.9. MALDI-TOF analysis of a previously reacted mixture of GA and dGTP, using CHCA as a matrix.	109
Figure 4.10. MS analysis of a previously treated DNA sample	110
Figure 4.11. Gold-aptamer nanoprobe stability against salt-induced aggregation	111
Figure 4.12. Detection assay for different dNTPs with: A) the XBA-nanoprobe, with a final MgCl ₂ concentration of 60 mM; B) His-945 nanoprobe, with a final MgCl ₂ concentration of 100 mM.....	112
Figure 4.13. Detection of glycidamide-guanine adducts using gold-aptamer nanoprobes.	113
Figure 4.14. DNA adduct detection assay with XBA-nanoprobe.....	114
Figure 5.1. Fitted dose-response curve obtained for goldfish 96-hour exposure to acrylamide	120
Figure 5.2. Reference images for the observed erythrocytes and alterations	121
Figure 5.3. Average biomarker responses and effects (±SE).....	122
Figure 5.4. Representative images observed for each class in comet-assay, scored after exposure to 150 mg/L of acrylamide in water.....	123
Figure 5.5. Example micrographs of tested <i>C. auratus</i> liver (Bouin-Hollande's, H&E)...	125
Figure 5.6. Fitted dose-response curve obtained for mussel 96-hour exposure to acrylamide.	130
Figure 5.7. Average biomarker responses and effects.....	131

Figure 5.8. Representative histological sections of tested mussels, after the 21-day exposure assay (H&E).....	133
Figure 5.9. Correlation-based principal component analysis (PCA) between biomarkers and nominal acrylamide concentration in water (as supplementary variable).....	134
Figure 5.10. Schematic model of the Nrf2–Keap1 signaling pathway	136
Figure A.1. BSA calibration curve used for quantification of total protein in goldfish samples	174
Figure A.2. BSA calibration curve used for quantification of total protein in mussel samples	174
Figure A.3. Resorufin calibration curve used for analysis of EROD in mussel samples ..	174
Figure A.4. Formaldehyde calibration curve used for analysis of catalase (CAT) in mussel samples.	175
Figure A.5. Trolox calibration curve used for analysis of total antioxidant capacity (TAC) in mussel samples.	175
Figure A.6. Malondialdehyde calibration curve used for analysis of lipid peroxidation in mussel samples.....	175
Figure A.7. Characterisation of the utilised organic matrices	176

TABLE INDEX

Table 1.1. Overview of AuNP-based colorimetric systems for nucleic acid detection.	12
Table 1.2. Protein bioassays based on noble metal NPs - a clinical perspective	14
Table 1.3. The first reported applications of inorganic surfaces for mass spectrometry ...	22
Table 1.4. Noble metal nanoparticles for SALDI-MS.....	27
Table 1.5. Different techniques employed for DNA adduct detection	32
Table 3.1. Comparison of DNA fragmentation potential for different sonication setups...	83
Table 3.2. Comparison of different conditions using the sonoreactor system and its influence on DNA fragmentation potential.	84
Table 4.1. Summary on organic matrix characterisation.....	100
Table 5.1. Mortality rate for the control group and each tested acrylamide concentration.	120
Table 5.2. Values for the correlation established between biomarker response and acrylamide concentrations, using Spearman rank-order correlation R with Bonferroni correction. (Conc: Acrylamide concentration; DNA-SB: DNA strand-breakage; ENA: erythrocytic nuclear abnormalities; CYP: Induction of CYP 1A; GST: glutathione S-transferase activity). Bold values denote significant correlations ($p < 0.01$).....	123
Table 5.3. Mussel mortality rate (by 96 h) for the control group and tested acrylamide concentrations (mg/L).	130

*To the fantastic four from Santa Marta and
Founding fathers of Abate Priscus.*

CHAPTER 1. GENERAL INTRODUCTION

Experience is not what happens to you; it's what you do with what happens to you.

Aldous Huxley

The work presented in this dissertation was accomplished at the interface of nanotechnology, mass spectrometry and toxicology. Most concepts and state-of-the art on these research areas are presented in the introduction section. However, besides these subjects, it integrates other concepts such as ultrasonic energy, chromatography and molecular biology techniques. With this in mind, the subsequent chapters may present a less extensive introduction which is included as to explain the particular concepts and subjects concerning that chapter alone. The following introduction will address nanotechnology, mass spectrometry, and toxicology directed to DNA lesions, presented in this specific order of contents merely to facilitate comprehension for the reader. It is more favourable to perceive the application of nanoparticles to mass spectrometry, if both concepts have previously been introduced in separate. As such, and despite this being a dissertation in Biology, focused in the biological subject of DNA adducts, I will firstly introduce concepts of nanotechnology and applications to biomolecular detection. Afterwards, the principles of mass spectrometry and applications of nanoparticles to mass spectrometry detection will be discussed, and only the last part will address notions about toxicology, with an emphasis on chemical carcinogenesis and the biological problem of DNA adduct formation and detection. Throughout this dissertation, some concepts may be regarded as ambiguous, such as adducts (DNA adducts or cation/mass adducts) or matrix (biological matrix or organic matrix). Whenever they appear, an adequate explanation will be provided as well as a proper context, in order to avoid confusion.

1.1 Nanotechnology

Nanotechnology involves the creation and manipulation of materials and structures on a nanometer (10^{-9} meter) scale. Several authors describe nanotechnology as the control and manipulation of materials at an atomic and molecular level, as most macromolecules present sizes comprised between 1 and 100 nm (Vo-Dinh 2005). The concept of nanotechnology was firstly introduced by Richard Feynman in 1959, in a lecture named “There’s plenty of room at the bottom” presented at CalTech (Feynman 1960). Ever since, different nanotechnology-based approaches have been developed towards an unlimited number of applications, e.g. electronics, mechanics, medicine, pharmacology, etc.

The study of nanotechnology has prompt the synthesis of novel materials and structures, and has also allowed for a more detailed comprehension of already existing materials. In terms of synthesis of nanomaterials, there are essentially two different approaches to be considered: top-down or bottom-up (Miller et al. 2005). Top-down approaches involves eroding nanomaterials from the bulk material and are mainly accomplished by diverse forms of lithography techniques, such as electron-beam lithography or soft lithography (Zhao et al. 1997, Watt et al 2005). Conversely, bottom-up approaches rely on conjugation of several molecular components, to build

nanostructures. Different techniques are utilised for bottom-up synthesis and characterisation of nanomaterials, with the most common being chemical synthesis or chemical self-assembly, where different molecules or atoms are mixed together and spontaneously organise into well-defined and stable nanostructures, due to their spatial and electronic properties (Lazzari et al. 2006). A common example of this organisation is the chemical synthesis of metallic nanoparticles, e.g. noble metal nanoparticles, from precursor salts, described in more detail in the following sections.

The field of nanotechnology draws and integrates knowledge from diverse research areas, such as physics, chemistry and material science, to develop novel applications or improve existing ones. This way, more specialised research areas have been created based in the synergy between nanotechnology and other areas, e.g. nanoelectronics, nanofluidics, nanotoxicology, nanobiotechnology. The latter, for instance is a term that defines the creation of nanostructures or nanoconjugates by using biological molecules, such as DNA or proteins as raw materials (Niemeyer and Mirkin 2004). In the last decades, there has been a massive increase in the number of nanobiotechnology-oriented platforms, namely towards biomolecular detection, with a direct application in diagnostics (Doria et al. 2007, Doria 2010, Conde et al. 2010). The following sections will address some of these systems, based on noble metal nanoparticles, for biomolecular detection of nucleic acids or biomarkers, considering a more clinical point of view.

1.1.1 Noble metal nanoparticles

The emergence of nanotechnology has prompted an intense research effort on the nanoscale properties of several materials, such as noble metal nanoparticles (NPs). These nanoparticles are usually constituted by clustered metal atoms (3 to 10^7 atoms) protected by a capping agent, and exhibit remarkable properties, such as highly tuneable spectral behaviour and an elevated surface-to-volume ratio (Liz-Marzán 2006). Other than this, noble metal NPs possess amazing optical properties, due to the localised surface plasmon resonance (LSPR), i.e. the collective oscillations of free electrons at a metal-dielectric interface when the frequency of incident light coincides with the frequency of electron oscillation (see Figure 1.1). These oscillations are influenced by the NPs' size, dispersion, shape and composition and originate the intense colours and/or very intense scattering of the colloidal dispersions of NPs (Jain et al. 2006, Liz-Marzán 2006). Particularly, gold nanoparticles (AuNPs), also referred to as colloidal gold, exhibit astounding optical, physical and catalytic properties which favour its utilisation in promising tools for biosensing, imaging or therapy applications (Boisselier and Astruc 2009, Conde 2013), such as more sensitive, faster, and simpler assays, which may also be cost-effective. Noble metal NPs have, thus, been the subject of intense research for use in biosensing, namely for low-cost high-sensitivity approaches for molecular recognition assays. Special attention has been paid to the development of systems capable of nucleic acid detection, or protein biomarker identification. These nano-based platforms may present a noteworthy alternative to already established multiplex technologies based on

fluorescence or chemiluminescence (Cai et al. 2010, Leroy and Raoult 2010), towards genome screening strategies, identification of mutations/polymorphisms associated to relevant phenotypes or characterisation of specific protein disease profiles.

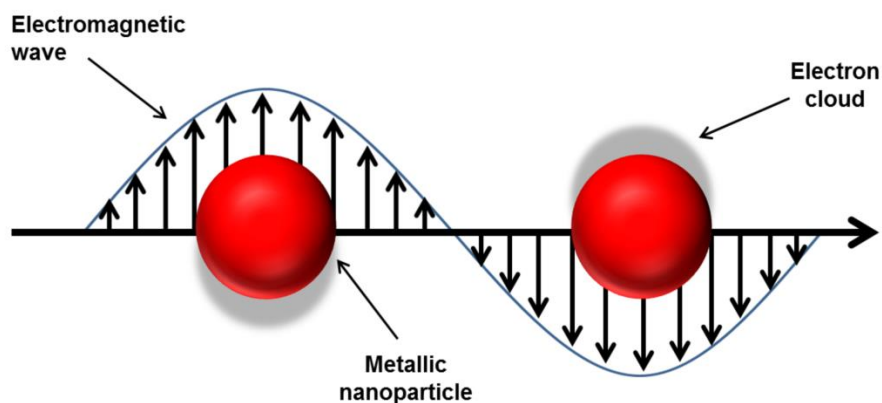


Figure 1.1. Schematic representation of the SPR phenomenon. The incident electromagnetic wave interacts with the electrons at the surface of the metal nanoparticle, generating a surface plasmon resonance.

1.1.1.2 Synthesis and derivatisation

Gold nanoparticles with sizes between 2 and 40 nm, which exhibit a typical LSPR band centred at around 520 nm, can be easily synthesised in aqueous medium via reduction of a gold salt (Baptista et al. 2008). The size dispersity of AuNPs may be tailored by altering the reduction agent (e.g. citrate, borohydride), the gold-reduction agent ratio, or temperature. These AuNPs can then be directly functionalised with thiol-containing molecules, such as antibodies or thiol-modified oligonucleotides (Mirkin et al. 1996). An oligonucleotide-gold nanoparticle conjugate is more commonly designated as a gold-nanoprobe (Au-nanoprobe) and was firstly synthesised in 1996 by Mirkin and co-workers. This remarkable contribution to the field of nanobiotechnology inspired many subsequent applications that can be used in a multitude of detection strategies for recognition of specific DNA/RNA sequences (Thaxton et al. 2006, Baptista et al. 2008) or discrimination of single-base alterations (Sato et al. 2003, Doria et al. 2007). Aside from gold-biomolecule nanoconjugates, AuNPs have also been used for several applications such as electrochemistry (Kerman et al. 2004) or mass spectrometry (Chiang et al. 2010).

There are considerably fewer reports on the use of silver NPs (AgNPs) functionalised with oligonucleotides for nucleic acid sequence detection in comparison to AuNPs. Firstly, the synthesis of AgNPs with homogeneous (normal) size distribution is considerably more difficult than that of AuNPs, and secondly, the affinity of sulphur towards silver is considerably lower, rendering functionalisation with thiolated molecules less efficient. Functionalisation with amine-modified biomolecules (Steinbrück et al. 2008) or cyclic disulphide groups (Lee et al. 2007) has been explored as an alternative to thiol-modified biomolecules. Despite exhibiting higher

scattering properties than their gold counterparts, AgNPs do not exhibit the same intense colours when in solution, and therefore their application in colorimetric assays has been residual. AgNPs have been more explored for the development of protocols involving fluorescence detection - silver enhancement (Malicka et al. 2003, Li et al. 2010), surface-enhanced Raman scattering - SERS (Moody and McCarthy 2009, Lowe et al. 2010) and in combination with gold to form bimetallic NPs, with distinct assembly concepts - core/shell and alloy (Wilcoxon 2009, Shore et al. 2011).

1.1.2 Noble metal nanoparticles for colorimetric detection of nucleic acids

1.1.2.1 Assays based on unmodified noble metal nanoparticles

As mentioned earlier, a colloidal solution of dispersed AuNPs shows an intense red colour due to the LSPR band in the visible region. Changes to the medium dielectric (such as an increase in ionic strength) cause the AuNPs to aggregate, with concomitant red-shift of the LSPR band and the solution turns blue (Baptista et al. 2008). This phenomenon has been explored for the development of detection schemes where the presence/absence of a given analyte (e.g. nucleic acid sequence) prevents or causes aggregation, thus yielding the result. The repulsion between negative charges of capping agents (e.g. citrate) at the surface of AuNPs prevents aggregation.

Based on the difference in electrostatic properties from single-strand DNA (ssDNA) to double-strand DNA (dsDNA), Li and Rothberg (2004) proposed a colorimetric detection scheme where ssDNA easily adsorbs to the AuNPs' surface and stabilises them against increasing ionic strength; conversely, dsDNA does not adsorb to the surface due to electrostatic repulsion and aggregation of AuNPs occurs. Detection of single-base mismatches was possible by de-hybridisation of previously formed dsDNA structures (perfectly matched *versus* single-base-mismatched) and observation of its influence on an AuNPs solution facing increasing ionic strength. A similar approach was used by Lee and co-workers for genotyping, where oligonucleotide probes that were perfectly complementary to the target allele sequence were hybridised to PCR products, amplified from human DNA samples, and then duplexes were denatured and mixed with AuNPs for SNP discrimination (Lee et al. 2010). A similar strategy using peptide nucleic acid (PNA) probes to control AuNPs' aggregation was proposed by Kanjanawarut and Su (2009) whereby PNA serves both as hybridisation probe and aggregating agent of citrate-capped AuNPs and AgNPs, in the absence of complementary DNA. Conversely, the presence of complementary DNA induces PNA-DNA complex formation and prevents NP aggregation. More recently, Liu and co-workers proposed an approach for discrimination of single-base mismatches localised at various positions within the target nucleotide sequence involving a probe-target hybridisation followed by a treatment with structure-selective nucleases (Liu et al. 2011). If S1 nuclease is used, when a perfect matched target hybridises with the probe, the resulting duplex will be protected from degradation; whereas a non-complementary/mismatched target will be digested to

deoxynucleotides monophosphate (dNMPs) that stabilise AuNPs against salt induced aggregation. A main drawback of this system is limited sensitivity, requiring a PCR amplification step prior to detection.

1.1.2.2 Assays based on functionalised noble metal nanoparticles

In 1996, Mirkin and co-workers described the use of oligonucleotide functionalised AuNPs for specific DNA sequence analysis, based on the change of colour of Au-nanoprobe-containing solutions, upon hybridisation to a complementary target (Mirkin et al. 1996, Elghanian et al. 1997, Storhoff et al. 1998). Upon hybridisation, the target sequences and the nanoprobe form a network, the AuNPs are brought into close vicinity and aggregation is induced, resulting in a change of colour from red to blue. The scheme in Figure 1.2 demonstrates the referred cross-linking hybridisation approach. This system has also been used in a microarray format, where a capture probe is functionalised to the surface of the array and the second probe (functionalised with an AuNP) hybridises to the captured target. Following capture and hybridisation, the Au-nanoprobe is coated with silver via a localised reduction of silver, thus amplifying detection through coupled evanescent wave-induced light scattering. This very system was used for SNP genotyping associated with thrombotic disorders on unamplified human genomic DNA (Bao et al. 2005).

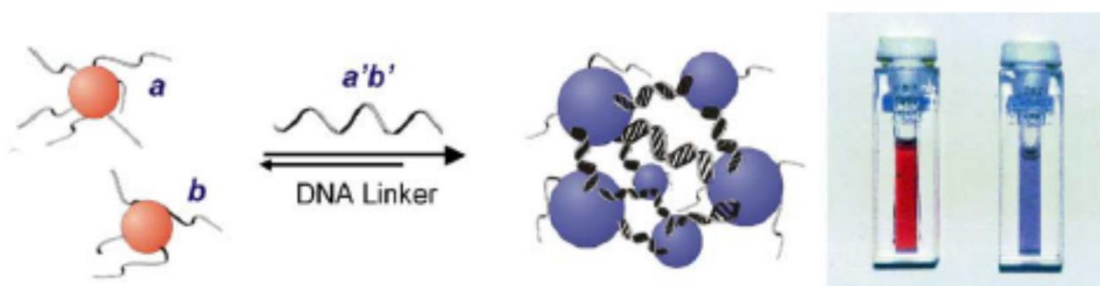


Figure 1.2. The detection principle and colorimetric result behind the cross-linking assay developed by Mirkin and co-workers for identification of nucleotide sequences. From Thaxton et al. (2006), with permission.

Using only one Au-nanoprobe in a non-cross-linking approach, Baptista and co-workers developed a sensitive method for specific identification of nucleic acids sequences (Baptista et al. 2005a,b, Conde et al. 2010). Upon mixing of the Au-nanoprobe with DNA, an increase in ionic strength will cause extensive aggregation and concomitant change of the solution from red to blue; this aggregation is prevented in case the Au-nanoprobe hybridises specifically to the complementary target (Figure 1.3). This method is capable of detecting single base mismatches (mutations or single nucleotide polymorphism, SNP) at room temperature (Doria et al. 2007), provided the following minimal conditions are met i) better discrimination is attained when the mismatch is localised at the 3' end of the nanoprobe sequence; ii) probe oligonucleotides on the AuNPs' surface strongly influences hybridisation, thus Au-nanoprobe density should not be

higher than 24 pmol/cm^2 so as not to induce repulsion of the target sequence due to the phosphate backbone (Doria et al. 2010). An overview of AuNP-based biomolecular assays for detection of single base mismatches is presented in Table 1.1.

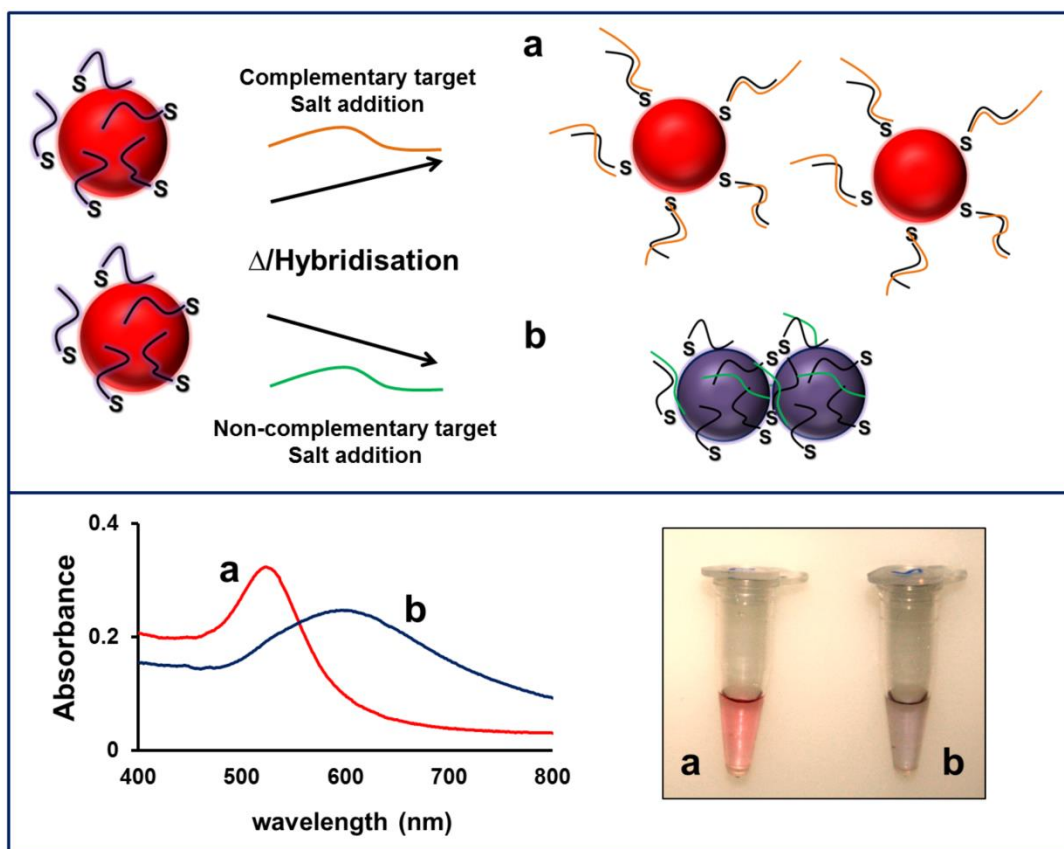


Figure 1.3. The detection principle behind the non-cross-linking colorimetric assay developed by Baptista et al. for identification of nucleotide sequences. The letters identify the possible cases and depict the mechanism, spectrum and colorimetric result for a) hybridisation with a complementary target, and b) presence of a non-complementary target.

Conversely to what has been described for AuNPs, there are only a few reports on the use of silver nanoparticles for colorimetric detection of nucleic acids, probably due to the lower efficiency of surface functionalisation provided by silver (Steinbrück 2008). AgNPs have been functionalised with oligonucleotides (Ag-nanoprobes) in an attempt to increase sensitivity due to the favourable optical properties of silver (Wilcoxon 2009). Mirkin and co-workers presented a cross-linking hybridisation colorimetric assay using AgNPs derivatised with terminal cyclic disulphide group-modified oligonucleotide probes (Lee et al. 2007). Similarly to the proposed cross-linking methods involving Au-nanoprobes, two Ag-nanoprobes, each complementary to half of the target sequence were used (Thompson et al. 2008). An interesting approach using naked AgNPs for detection of specific sequences through non-covalent interactions between oligonucleotides and AgNPs surface has been reported by Xu et al. (2009). In the presence of high ionic strength, AgNPs aggregation (and concomitant colour change of solution) can be

prevented by the unspecific adsorption of free oligonucleotides. This approach was designed mainly for poly(A) sequence analysis, benefiting from its affinity towards the coralyne ligand that binds strongly to adenine-rich regions. Recent reports have highlighted poly(A) sequences as putative new therapeutic targets for RNA-based drug design (Giri and Kumar 2009). In the absence of coralyne, poly(A) targets adsorb non-specifically to the AgNPs' surface, stabilising them against an increase in ionic strength. When coralyne is present in solution, it binds the poly(A) targets forming a duplex that prevents the oligonucleotides from interacting and stabilising the AgNPs, and aggregation occurs. Also, a colorimetric assay for characterisation of DNA:protein interactions based on DNA-AgNPs conjugates has been proposed for assessing the function of oestrogen receptor alpha ($ER\alpha$), a nuclear receptor which modulates oestrogen production through regulation of transcription. Increasing $ER\alpha$ concentration helped stabilisation of Ag-nanoprobe against high ionic strength (Tan et al. 2010). In this study, Ag-nanoprobes were shown to be more sensitive than their gold counterparts.

1.1.3 Noble metal nanoparticles for signal enhancement

1.1.3.1 Fluorescence assays

Applications of AgNPs to metal-enhanced fluorescence (MEF) for DNA hybridisation assays have also been reported, profiting from the enhancement of fluorescence when fluorophores are in the vicinity of noble metal nanostructures (Malicka et al. 2003) - see Figure 1.4 for schematic representation. AgNPs have been successfully utilised in a MEF-based system in a microarray platform to improve sensitivity (Sabanayagam and Lakowicz 2007). Li and co-workers, using a flat silicon surface (p-Chips) functionalised with AgNP-films, tested the fluorescence enhancement on four different fluorophores, demonstrating the potential of MEF-based detection for multiplex sequence analysis (Li et al. 2010). MEF-based RNA sensing has also been described using AgNP-films on glass surfaces and immobilised thiolated-oligonucleotide probes (Aslan et al. 2006a). First, a fluorophore-labelled oligonucleotide was hybridised to the RNA, and this conjugate was then hybridised to the immobilised probe on the surface, thus bringing the fluorophore and the AgNPs close together. This method presented a 100-fold improvement on RNA quantification sensitivity, in comparison to previously developed assays. Another approach has been to use microwave-accelerated metal-enhanced fluorescence (MAMEF) in DNA hybridisation assays, with high detection limits (Aslan et al. 2006b). This procedure involves the use of a MEF scheme in which low-power microwave heating is used in order to promote biomolecular recognition events.

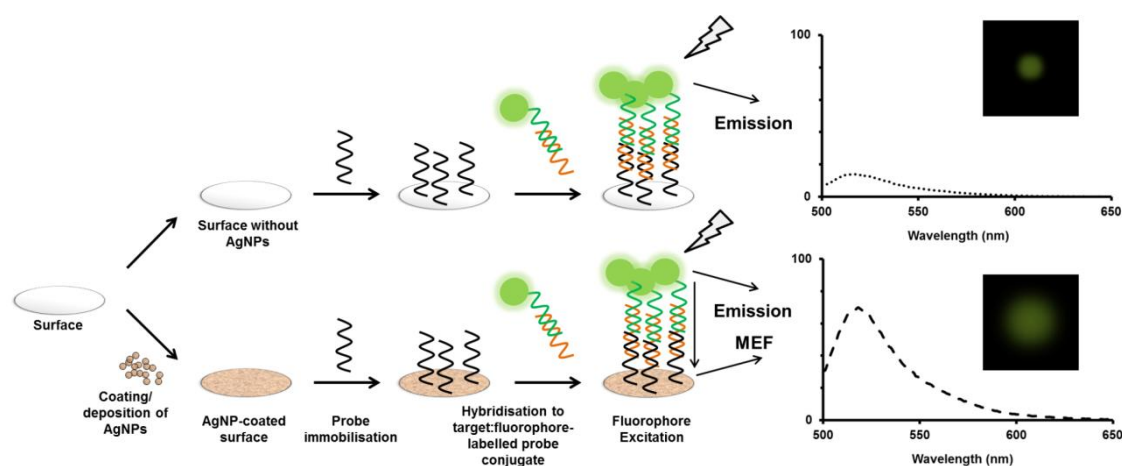


Figure 1.4. Schematic representation for a detection system based in metal-enhanced fluorescence (MEF). Fluorescence signal enhancement may be achieved by coating a surface with AgNPs prior to probe immobilisation. After hybridisation with a fluorophore labelled probe and excitation at the adequate wavelength, fluorescence intensity is potentiated by the AgNPs (MEF).

1.1.3.2 Luminescence assays

Approaches for AuNP-based labelling and chemiluminescence-based detection exhibiting good sensitivity, sequence specific discrimination and DNA target quantification have also been reported, in particular microarray platforms coupled to AuNP-catalysed silver enhancement (Li et al. 2007, Girigoswami et al. 2009). A successful genotyping approach targeting the BRCA1 gene was reported by Girigoswami and co-workers (2009), which includes two primers (primer1 and primer2), each complementary to half of the target sequence. Primer1 bears a 5' zip complementarity, necessary for analysis to be carried on a zip-code microarray platform. Primer2 is 3' thiol-modified, required to bind an AuNP for silver enhancement-based detection. Upon successful hybridisation, a ligase reaction is carried out, to seal the nick between the two primers. When the allele-specific probe is 100% complementary to the target, ligation occurs and, upon assembly on the microarray platform, the sequence binds an AuNP through 3'-thiol modification. Afterwards, the AuNP is silver-coated, for enhanced detection.

A chemiluminescent approach for DNA detection was described, whereby the Ag^+ ions arising from AgNPs dissolution act as indicators for detection (Liu et al. 2006). In this system, two different probes are used, complementary to different halves of the target, similarly to the cross-linking method previously described (see above). Following successful probe-target hybridisation, the AgNPs are dissolved using HNO_3 and Ag^+ ions determined via a coupling chemiluminescence reaction. SNPs were analysed by comparison of thermal dissociation curves for perfect complementary targets and mismatched targets, hybridised with the referred probes with very low limits-of-detection. Guo and co-workers (2010) proposed another approach for discrimination of single base alterations based on oligonucleotide probes with a cytosine loop (C6) and AgNPs' photoluminescence detection, and used this method to discriminate a single-base mutation associated to sickle-cell anaemia. Upon probe hybridisation to a perfect

complementary target, an efficient scaffold of Ag⁺ ions originates a photoluminescent AgNP, whose emissive properties potentiate the detection. Mismatched targets yielded residual luminescence emission.

1.1.3.3 Spectral labels

Noble metal NPs have also been used as signal enhancers for Raman scattering-based detection of biomolecules. AuNPs for Raman spectroscopy-based detection have also been used in combination with i) methylene blue for target labelling (Harpster et al. 2009), ii) magnetic nanoparticles for effective target capture (Zhang et al. 2011a), and iii) assembled on a multi-metal nanojunction structure for identification of single-base mismatches in an HIV-1-derived DNA sequence (Hu et al. 2010). In an effort to improve existing platforms for nucleotide sequence analysis and mismatch discrimination, Moody and McCarty (2009) proposed a proof-of-concept involving AuNPs for signal amplification of Surface-enhanced Raman Scattering (SERS). SERS detection potentiated by AuNPs was also used on cancer gene expression studies aiming at detection of multiple splice variants of human BRCA1 gene analysis (Sun and Irudayaraj 2009).

AgNPs have also been used as Raman scattering enhancers for nucleotide sequence analysis. Zhang et al. (2011b) presented an approach, using a combination of mixed Ag-nanoprobes and Raman reporter molecules, for multiplex detection of specific nucleotide sequences, through a sandwich hybridisation assay for recognition and signal amplification. Lo and co-workers (2011) used AgNPs for enhancement of the Raman scattering signal, using an Au-nanotip covered with oligonucleotide molecules and the subsequent deposition of sub~10 nm AgNPs to coat the Au-nanotip. A distinct method for SNP genotyping based on a ligation reaction coupled to Raman scattering detection and including two probes (each complementary to different halves of a target sequence) was presented by Lowe et al. (2010). A first oligonucleotide probe hybridises with the target strand downstream of a SNP and is later conjugated to an AgNP for signal amplification. The second probe, containing a Raman active fluorophore and a discriminating base at the 3' end, binds upstream of the SNP and adjacent to the first probe allowing maximum specificity. In presence of a perfect match, ligation between the two oligonucleotides is attained, bringing the fluorophore and the AgNP closer. This enhances the signal, and particular Raman signatures may be observed as different fluorophores are placed on the SNP allelic specific probes. This approach allows for flawless discrimination of SNPs occurring in the KRAS oncogene at picomolar detection levels.

Table 1.1. Overview of AuNP-based colorimetric systems for nucleic acid detection.

Detection method	Category	Principle for detection	Application	Refs
Naked AuNPs	Colorimetric	A specific probe is hybridised to a target sequence. Afterwards, AuNPs and salt are added; ssDNA stabilises AuNPs against aggregation, whilst dsDNA does not.	Detection of single-base mismatches	Li and Rothberg 2004.
		Probes 100% complementary to the target allele were hybridised to PCR products; duplexes were denatured and mixed with AuNPs; ssDNA strands resulting from dehybridisation stabilised AuNPs.	SNP genotyping of human DNA samples	Lee et al. 2010
		PNA probes are used both as hybridisation probes and as an aggregating agent for AuNPs. Probe hybridisation to a complementary target prevents PNA-induced AuNPs aggregation.	Single-base mismatch discrimination on DNA targets with different lengths	Kanjanawarut and Su 2009
		S1 nuclease is used to degrade probe:mismatch target duplexes to dNMPs, and AuNPs are added to the solution; dNMPs stabilise AuNPs against salt-induced aggregation.	Detection of point mutations in viral genomic DNA	Liu et al. 2011
Au-nanoprobes	Colorimetric Scanometric	Two Au-nanoprobes, each complementary to different halves of the sequence, are hybridised to a target; the presence of a complementary sequence induces nanoprobe aggregation.	Detection of one-base mismatch, insertion and deletion; SNP genotyping on human genomic DNA	Mirkin et al. 1996; Storhoff et al. 1998; Bao et al. 2005
	Colorimetric	Au-nanoprobe hybridisation to a complementary target results in the formation of duplexes at the nanoprobe's surface, which stabilise it against salt-induced aggregation.	Detection of single-base mutation on the β -globin gene; SNP discrimination on the DOR gene.	Baptista et al. 2005a,b; Doria et al. 2007

1.1.4. Noble metal nanoparticles for biomarker analysis

Most clinical diagnostics applications strongly rely on the identification of biomarker proteins for disease characterisation, and an enormous effort has been put into developing novel nanotechnology-based approaches for this effect (Perf ezou et al. 2012, Ray et al. 2011). Several platforms specifically designed for protein biosensing often include standard assembly concepts using antigens and antibodies for molecular recognition (e.g. sandwich immunoassay), coupled to distinct detection strategies, such as spectroscopy (Cai et al. 2009, Neely et al. 2009), electrochemistry (Mani et al. 2009, De la Escosura-Mu niz and Merko ci 2011) or imaging (Kah et al. 2007, Lee et al. 2009). Noble metal nanoparticles have brought a new dimension to such bioassays by increasing the sensitivity at lower costs (Perf ezou et al. 2012). Because most of these assays rely on previously studied and widely used biomarkers, integration into nanoparticle-based sensing platforms has been rather straightforward - Table 1.2.

Most AuNPs applications have been directed towards signal enhancement of standard protein detection assays, ranging from enzyme-linked immunosorbent assays (ELISAs) to immunoassay platforms coupled to electrochemical or SERS-based detection. Examples include increase in Rayleigh scattering intensity for Alzheimer disease diagnostics (Neely et al. 2009), nanochannel-based filtering and sensing platform for cancer biomarkers (De la Escosura-Mu niz and Merko ci 2011) and enhancement for immunochromatographic test strips (Tanaka et al. 2006). Resonance Rayleigh scattering was used in conjunction with antibody-coated AuNPs for transferrin biosensing (Cai et al. 2009) for transferrin quantification in human serum samples with a detection limit two orders of magnitude lower than ELISA. A similar concept was shown for two-photon Rayleigh spectroscopy detection of tau protein in cerebrospinal fluid (Neely et al. 2009). By using monoclonal anti-tau antibodies functionalised to AuNPs' surface, it was possible to improve scattering intensity by 16-fold, which reflects a significant increase in sensitivity (by two orders of magnitude). Femtomolar levels of prostate-specific antigen (PSA) in serum were detected using an immunoassay coupled to SERS-based detection. This was achieved by using monoclonal antibodies, with the secondary antibody being directly attached to a multifunctionalised AuNP (Grubisha et al. 2003).

A different platform using a naked-eye detection method and consisting of a AuNPs-based enhancement for immunochromatographic test strips showed promising results for clinical diagnostics purposes (Tanaka et al. 2006). In this sandwich-like assay, both the primary and the secondary antibodies are conjugated with AuNPs, increasing the limit of detection of the chorionic gonadotropin hormone (HCG) in human serum by 1 order of magnitude, to reach 10 pg/mL and of the total PSA to reach 200 pg/mL. Besides the advantage in sensitivity, this is a simple and fast method which provides results in less than 20 minutes. Self-assembled gold colloids functionalised with extractable nuclear antigens (ENAs) have also been used in combination with an optical fibre evanescent-wave sensor, for anti-nuclear antibodies (ANAs)

detection in human serum (Lai et al. 2007). This system does not require a secondary antibody and presents increased sensitivity (by an order of magnitude) when compared to traditional ELISA.

AuNPs have also been utilised as optical signal enhancers when used in conjunction with the traditional ELISA test (Ambrosi et al. 2010). The signalling antibody (secondary antibody conjugated to a reporter molecule) was attached to the surface of AuNPs and the optical signal resulting from molecular recognition was then compared in the presence and absence of the AuNP-antibody conjugates - see schematics in Figure 1.5. Besides a 2-fold increase in sensitivity, the use of AuNPs resulted in shorter incubation times when attaining a colorimetric result applied to detection of the breast tumour biomarker CA15-3 at clinically relevant levels.

Table 1.2. Protein bioassays based on noble metal NPs - a clinical perspective.

Category	Detection technique	Target / Clinical Application	Ref.
Scanometric	Light scattering measurement	Human chorionic gonadotropin (HGC), Prostate-specific antigen (PSA) and α -fetoprotein (AFP) as cancer biomarkers	Kim et al. 2009; Thaxton et al. 2009
Spectroscopy	Rayleigh scattering	Tau protein and human holotransferrin; PSA as cancer biomarker	Grubisha et al. 2003; Cai et al. 2009; Cao and Sim 2009
	SERS	Thrombin and carcinoembryonic antigen (CEA) as cancer biomarkers; prion protein PrPc	Bizzarri and Cannistraro 2009; Chon et al. 2009; Serra et al. 2011
	UV-Vis spectroscopy (naked-eye detection)	Cyclic A2 as a cancer biomarker; Glycated haemoglobin (HbA1c) as a diabetic marker	Wangoo et al. 2010; Wang et al. 2011
Immunoassay	Dynamic light scattering	CA152, CEA, CA19-9 and PAP (prostatic acid phosphatase) as cancer biomarkers	Huo 2010
	ELISA	CA15-3 cancer biomarker	Ambrosi et al. 2010
	Immunocromatography (naked-eye detection)	HCG and PSA as cancer biomarkers	Tanaka et al. 2006

Immunoassay (cont.).	Gold-modified optic fiber	Anti-nuclear antibodies (ANAs)	Lai et al. 2007
	UV-Vis spectroscopy	PSA and CEA as cancer biomarkers	Cao et al. 2009, Liu et al. 2010
Electrochemical immunoassay	Amperometry	Interleukin-6 (IL-6) and PSA as cancer biomarkers	Mani et al. 2009; Chikkaveeraiah et al. 2011
	Differential pulse voltammetry	CA15-3, tumour necrosis factor alpha (TNF- α) and Hepatitis B surface antigen	De la Escosura- Muñiz et al. 2011; Liang et al. 2011; Yin et al. 2011
	Square wave voltammetry	Human serum albumin and cardiac myoglobin as biomarkers; HIV-1 reverse transcriptase level in human serum	Omidfar et al. 2011; Suprun et al. 2011; Labib et al. 2011
	Cyclic voltammetry	CEA and human cardiac troponin I as cancer biomarkers	Ou et al. 2007; Ahammad et al. 2011
Imaging	Surface plasmon resonance imaging	Epidermal growth factor receptor (EGFR) as cancer biomarker	Kah et al. 2007
	SERS imaging	Human epidermal growth factor 2 (HER2) as cancer biomarker	Lee et al. 2009
	Reflectance imaging	Prostate-specific membrane antigen (PMSA) as a cancer biomarker	Javier et al. 2008

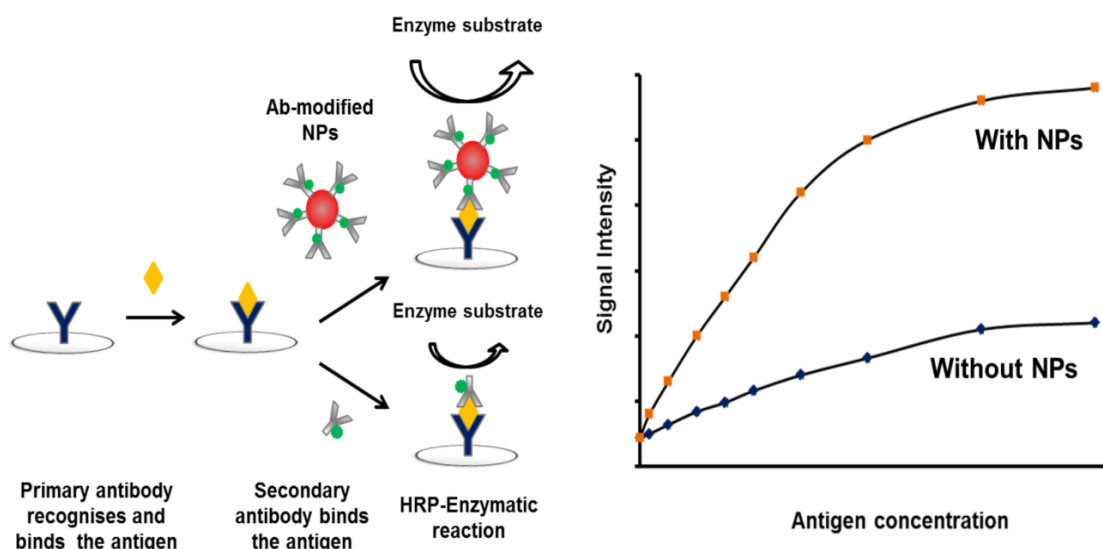


Figure 1.5. Schematic representation for an ELISA system with AuNPs. AuNPs conjugated with secondary labelled-antibodies are used for a sandwich assay. The antibody-AuNP conjugates provide an amplified response, increasing sensitivity without compromising selectivity. Adapted from Ambrosi et al (2010), with permission.

This section of the introduction addressed several concepts which are important to understand the applications of noble metal NPs. The enormous, and still growing number of systems including noble metal NPs for biomolecular detection reflects the high versatility of these nanostructures. In addition, noble metal NPs have been widely used in mass spectrometry applications, in particular for laser desorption/ionisation of small molecules. This subject however will be discussed in the mass spectrometry section, after a general introduction on mass spectrometry concepts.

1.2 Mass Spectrometry

The foundations of mass spectrometry (MS) go back to the beginning of the 20th century and the necessity to measure the mass of recently discovered charged particles. In 1897, J.J. Thompson (Nobel Prize of Physics in 1906) discovered the electron and measured its mass-to-charge ratio (Griffiths 2008). Later, in 1912, he developed the first mass spectrometer (called a parabola spectrograph) and observed the formation of positive and negative ions by experimenting on O₂, N₂, CO, CO₂ and CoCl₂. The next year he discovered the isotopes 20 and 22 of neon (De Hoffman and Stroobant 2007). The following decades during the first half of the 20th century were extremely fruitful for the mass spectrometry field, with new ionisation sources and isotopes being discovered. However, it was World War II and the “Manhattan Project” that greatly boosted the field of mass spectrometry, with the isolation of uranium-235 by A.O. Nier (1940). From here on, mass spectrometers became commercially available and throughout the

second half of the 20th century novel ionisation methods and different analysers continued to be developed (Griffiths 2008).

MS techniques present a high versatility as they can be applied to analysis of all elements and a wide range of analytes with very good sensitivities, some techniques reaching sub-attomolar detection (Dass 2007). Moreover, most MS techniques provide valuable information about structure and fragmentation of chemical compounds or biological molecules. It is therefore not surprising that MS techniques are currently being more and more employed in diverse areas of scientific research, to provide answers to problems related to physics, chemistry, biology and genetics (Baker 2010). The following sections describe the basic concepts of MS, an introduction to Matrix-Assisted Laser Desorption/Ionisation (MALDI) and the creation of Surface-Assisted Laser Desorption/Ionisation (SALDI), the incorporation of nanoparticles into mass spectrometry and applications to biomolecular detection.

1.2.1 General concepts

Mass spectrometry techniques are essentially composed by three integrated sequential events: ionisation, analysis and detection. The first phase of a MS technique consists of generating gas-phase ions from a sample of interest. Afterwards, the ionised molecules are separated according to their mass-to-charge ratio (m/z) in an analyser. Finally, the separated ions are measured in the detector and the generated signal is amplified and acquired as a mass spectrum, where information about the relative intensity (abundance) of ionised species is plotted against their m/z . The detected ions provide valuable information about the nature and structure of their precursor molecule (Dass 2007, De Hoffman and Stroobant 2007).

As previously mentioned, in MS techniques the events are sequential, despite occurring in different components of the mass spectrometer (see Figure 1.6 for a diagram of a mass spectrometer). Firstly, the sample is inserted into the ionisation source through the sample inlet. The mechanism by which the sample is introduced into the ionisation chamber varies according to the ionisation method, for example in MALDI the sample is directly introduced in the chamber, whereas other methods may include a chromatographic interface. Afterwards, the sample is ionised, either by electron ejection or capture, protonation or deprotonation, or via mass adduct formation (De Hoffman and Stroobant 2007). The first ionisation methods were electron ionisation (EI), developed in 1902 and chemical ionisation (CI), developed later in 1969. These methods were designed mainly for analysis of volatile organic compounds and were extremely energetic, causing extensive fragmentation of the analytes (Fernandes 2004). The need for new techniques suitable for analysis of liquid or solid non-volatile samples has prompted the development of more contemporary ionisation strategies, such as the soft ionisation method of MALDI, described in section 1.2.2.

After sample ionisation, the ions are accelerated into the mass analyser, where a separation occurs according to their m/z , using electric, magnetic fields or a combination of both. The choice of a given mass analyser depends on the nature of the sample, the type of analysis and the characteristics of the analyser: i) mass resolving power, i.e. how well can the analyser separate and measure ions; ii) mass accuracy, which refers to errors when measuring the m/z ratio; iii) mass range, which is the m/z range over which a mass analyser can operate; iv) ion transmission, i.e. the ratio between the number of ions that reach the detector and the number of ions that entered the analyser; v) scanning speed, which is the required period of time to produce a full mass spectrum (De Hoffman and Stroobant 2007, Carreira 2011, Hart-Smith and Blanksby 2012). For a detailed analysis and discussion on the characteristics of several mass analysers, please refer to Carreira (2011), and references therein.

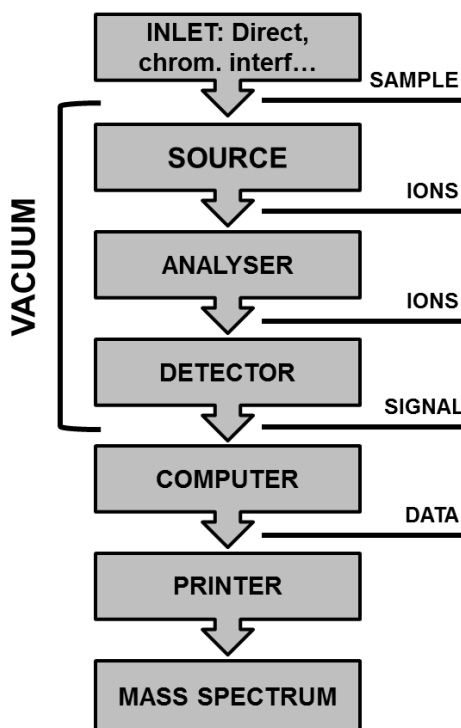


Figure 1.6. Diagram of a mass spectrometer, including an ion source, one mass analyser, a detector and an output system for generating data (computer and printer). Adapted from De Hoffman and Stroobant (2007), with permission.

The final part of a mass spectrometer is the detector, which records, amplifies and converts the ion current into an electrical signal that can readily be displayed as a count of ion pulses per time. The most important characteristics of an ion detector are sensitivity, accuracy, resolution, response time, stability, a wide dynamic range and a low noise (Dass 2007). The majority of detectors falls under two categories: i) focal-point detectors, which detects ions of a single mass at a time, and ii) focal plane detectors, that monitor ions all the time, immediately after their arrival, resulting in increased sensitivity and mass accuracy. The simplest design for a detector is

the Faraday cup, consisting in a metal box (Faraday cage) with a collector electrode to measure ion current (Koppenaar et al. 2005, Dass 2007). Nowadays, the most common ion detector is the electron multiplier (EM), or secondary ion multiplier (SEM), which can amplify the ion signal by 10^6 or more, by production of secondary electrons when the ion beam reaches an ion-sensitive dynode. The produced secondary electrons are detected by dynodes, generating a cascade signal. Other examples of detectors include photomultipliers or photographic plates, explained thoroughly by Koppenaar and co-workers (2005). The following section will introduce the basic principles of MALDI and its advantages, the relation to the creation of SALDI and applications to biomolecular detection.

1.2.2 Matrix-assisted laser desorption/ionisation time-of-flight (MALDI-TOF)

One of the most utilised and advantageous soft ionisation approaches is the MALDI technique. This term firstly appeared as “Matrix-Assisted Laser Desorption” in 1985, when Karas and co-workers published a paper about the influence of the irradiation wavelength in desorption of amino acids, and observed differences in fragmentation between amino acids alone or in a mixture (Karas et al. 1985). Some years later, in 1988, came the first application of a laser desorption/ionisation (LDI) to protein analysis, performed by Tanaka and co-workers, which dissolved the proteins in a suspension of ultra-fine cobalt powder and glycerol, for an effective ionisation. This was actually the first application of SALDI towards biomolecular analysis. At around the same time, Karas and Hillenkamp (1988) reported a method for laser desorption analysis of proteins in which the sample was mixed with a UV-absorbing organic compound in excess, acting as a matrix for ionisation. The organic matrix-based method gained momentum in the scientific community due to its advantages and is nowadays used in widespread applications (Hillenkamp and Peter-Katalinić 2007, Kafka et al. 2011, Croxatto et al. 2012).

MALDI exhibits several important characteristics that make it suitable for analysis of virtually all types of analytes: i) it is rather tolerant to buffers, salts, surfactants or chelating agents; ii) exhibits high sensitivity, usually reaching the picomolar range; iii) allows for analysis of molecules with elevated molecular weights ($> 100,000$ Da); iv) can generate whole molecule monovalent ions; v) has the capability of performing molecular imaging in complex samples (McDonnell and Heeren 2007, Reyzer and Caprioli 2007). MALDI is a discontinued ionisation technique, for ions are produced by laser pulses. In MALDI, a chemical compound known as “the matrix” is mixed in excess with the sample and the mixture is allowed to dry on an appropriate plate. During this, a “co-crystallisation” of matrix and analyte molecules occurs, i.e. the matrix forms crystals, where the sample becomes embedded and (most likely) heterogeneously distributed. After crystallisation, the plate containing the mixture is introduced into the ionisation chamber and irradiated with a pulsed laser beam (commonly used lasers are nitrogen lasers with a wavelength of 337 nm). After irradiation, the matrix absorbs the laser energy and transfers it to

the analyte, promoting a “soft ionisation” (see schematics in Figure 1.7). The ions thus formed are transported to the analyser where they are separated and then reach the detector. MALDI is regarded as a “soft ionisation” method, in contrast to other methods such as EI or CI as the inclusion of an organic matrix in excess allows for a more controlled energy transfer to the analyte and prevents extensive fragmentation, upon laser irradiation. Therefore, MALDI is of great importance when generating molecular ions with minimum fragmentation.

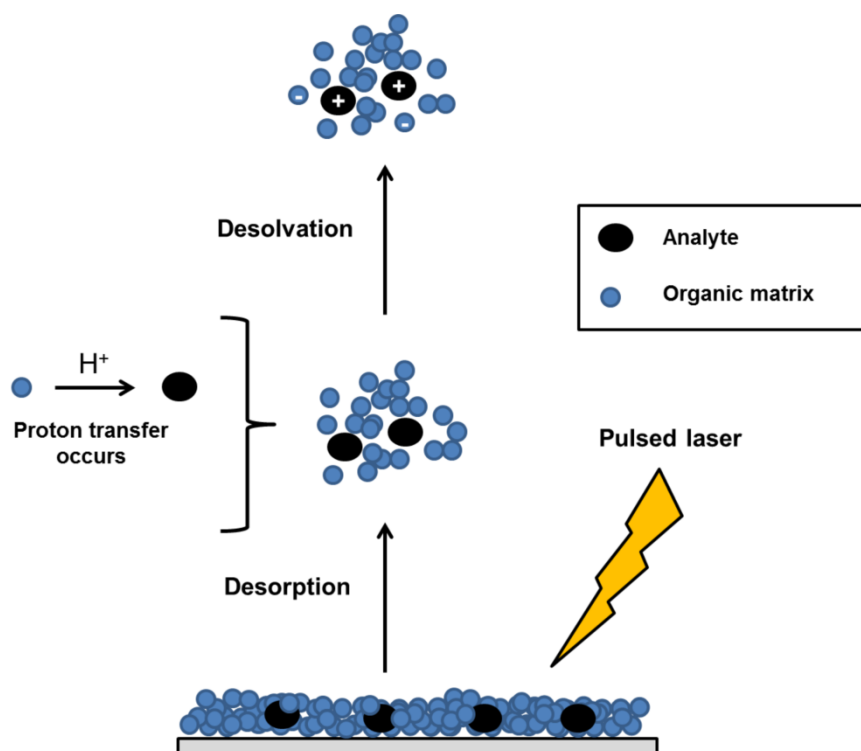


Figure 1.7. Schematic representation of the MALDI process. Adapted from De Hoffman and Stroobant (2007), with permission.

MALDI is often coupled to time-of-flight (TOF) analysers, providing a MALDI-TOF combination, suitable and most used for analysing biomolecules, such as peptides or proteins (Hillenkamp and Peter-Katalinić 2007). TOF analysers possess great mass accuracy, resolution and sensitivity and are suitable for analysis of any kind of analyte, in theory. This makes TOF mass analysers the perfect candidates to couple to a MALDI ionisation source, for analysis of singly charged, high molecular weight ions. These analysers consist of a long field-free flight tube, where ions are separated according to their velocities, i.e. the m/z is determined by measuring the time needed for the ions to travel from the source to the detector (Dass 2007). This way, smaller ions travel faster than larger ones and need less time to travel distance, from the source to the detector, however the difference in kinetic energy of ions with the same mass may affect their initial velocity and the time at which they are detected (Lane 2005). This drawback was overcome by introducing delayed-ion extraction (Brown and Lennon 1995) and reflector mode. Delayed extraction mode is achieved by introducing a time delay (in the nanosecond range)

between ionisation and acceleration into the TOF analyser. This nullifies differences in kinetic energy between ions with a same mass (although not completely), accounting for increased mass accuracy. The TOF reflector mode consists in adding a new detector and reflecting the ions to that second detector. This way, the time-of-flight path is increased without physically increasing the flight tube length, which accounts for increased resolution, through ion focusing. However, as the path length is increased, sometimes ion loss occurs mainly with high molecular weight ions, and sensitivity may be slightly compromised. This way, two distinct modes of analysis exist: linear mode and reflector mode, both depicted in Figure 1.8.

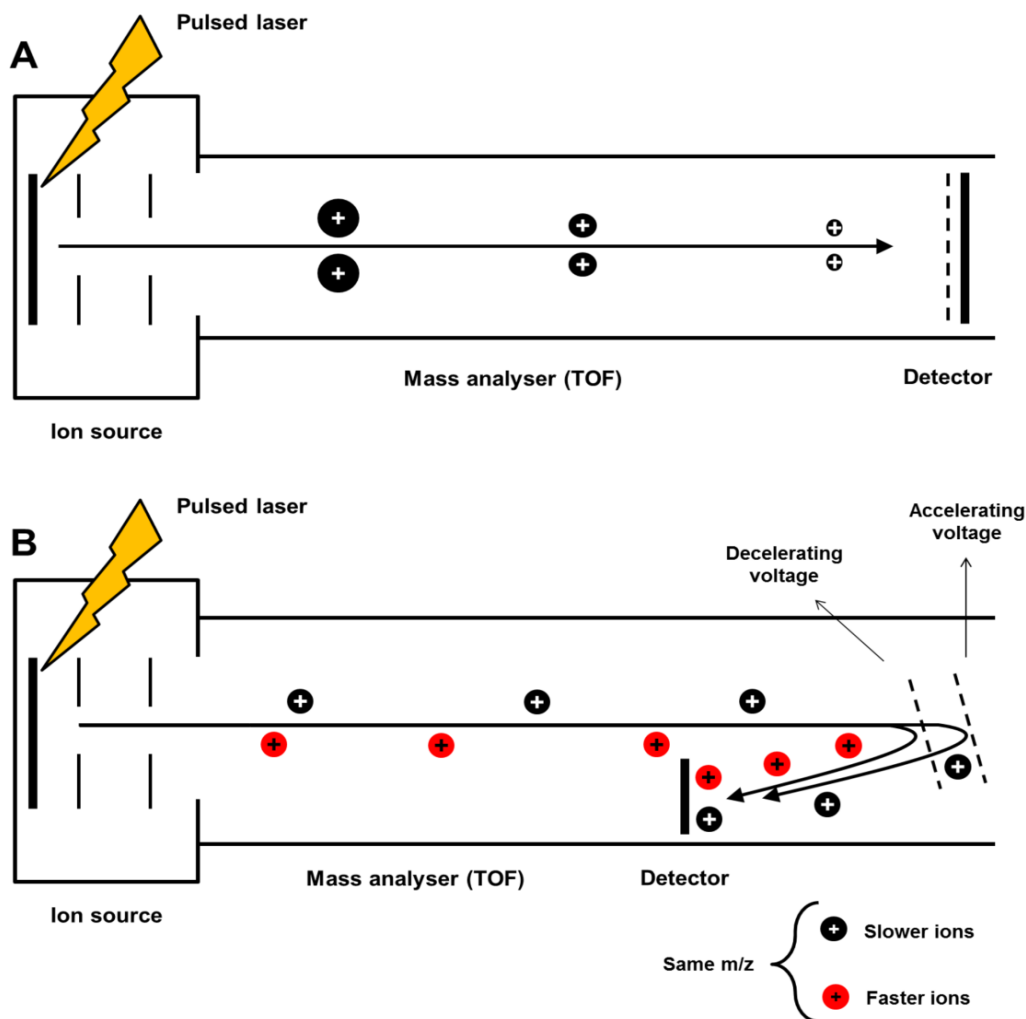


Figure 1.8. Schematic representation of A) linear and B) reflector mode of analysis. A) Linear TOF: ions are separated in a field-free drift tube, according to its velocity; smaller ions reach the detector faster than heavier ions. B) Reflector TOF: Ions are reflected by a reflectron at the end of the analyser, increasing the path length, and improving separation and resolution. Adapted from Lane (2006).

1.2.3 Surface-assisted laser desorption/ionisation time-of-flight (SALDI-TOF)

As previously mentioned, little before Karas and Hillenkamp analysed proteins via MALDI, Tanaka and co-workers (1988) developed the first application for LDI analysis of high molecular weight proteins and polymers, by using 30 nm-cobalt nanoparticles (CoNPs) dispersed in glycerol to assist in the ionisation process, instead of an organic matrix. This was the first report on LDI

using an inorganic surface other than an organic matrix to absorb and transfer energy to the analyte (see Table 1.3). Later, Sunner et al. (1995) followed a similar idea and coined the term surface-assisted laser desorption/ionisation (SALDI) for the first time applied to graphite, to distinguish desorption/ionisation performed on an inorganic surface from the organic matrix used in MALDI. Four years later, Wei et al. (1999) developed desorption/ionisation on silicon (DIOS), where the inorganic surface is composed by an array of silicon. Since then, many different nanoparticles have been employed as an inorganic surface to facilitate ionisation, instead of the traditional organic matrix (Schurenberg et al. 1999, McLean et al. 2005, Yonezawa et al. 2009). A more detailed discussion on application of nanoparticles to mass spectrometry will be presented in section 1.2.5. Different names have been used to define this approach, SALDI, nanoparticle-assisted laser desorption/ionisation (nano-PALDI), etc., but all with the common purpose of finding an organic matrix-free alternative optimal for soft ionisation of biomolecules with better sensitivity, lower background noise and reduced costs. Throughout this thesis the term SALDI will be the only one used when referring to inorganic NPs for ionisation, although it may actually comprehend other inorganic surfaces. The following sections deal with the introduction of NPs, mainly noble metal NPs, into protocols for MS biomolecular analysis. As MS techniques are composed of integrated events of ionisation, analysis and detection, with precedent protocols for sample preparation, inorganic NPs may be introduced somewhere into the system as to improve sensitivity or analytical capabilities, as discussed in the following section.

Table 1.3. The first reported applications of inorganic surfaces for mass spectrometry

Surface	Application	Analytes	Reference
30 nm cobalt NPs	LDI-TOF	Proteins, polymers	Tanaka et al. 1988
2–150 μm graphite particles	SALDI-TOF	Peptides, proteins, organic compounds	Sunner et al. 1995
Porous silicon	DIOS	Peptides, small drug molecules, glycolipids, carbohydrates	Wei et al. 1999
Several different nanoparticles	SALDI-TOF	Peptides, proteins	Schurenberg et al. 1999

1.2.4 Advantages of nanoparticles for SALDI-TOF-MS

Since the first application in 1988, NPs have been used as inorganic surfaces to overcome the main limitations of MALDI-MS, namely due to three main aspects: homogeneity in crystallisation preventing the formation of *sweet spots*, absence of matrix interference due to ionisation of matrix-derived molecular ions and efficiency of energy transfer to the analyte.

Crystal orientation heterogeneity verified during crystallisation of the matrix:analyte mixture will often originate *sweet spots* on the MALDI plate, which renders the analysis more complicated and makes quantification difficult to accomplish. The high surface area of NPs allows better sample deposition and absorption, and homogeneity in the mixture, preventing formation of *sweet spots* upon application (Black et al. 2006, Guo et al. 2006, Budimir et al. 2006). What is more, spot-to-spot and shot-to-shot variability is considerably diminished for more accurate quantification approaches (Chiang et al. 2009, Kuo et al. 2011). In contrast to what happens in commonly used organic matrices, NPs in general are not so easily ionisable upon laser irradiation (Kong et al. 2005, Vanderpuije et al. 2006, Shibamoto et al. 2009). Laser incidence may cause fragmentation and desorption of matrix-derived molecular ions producing spectra with high background signal, thus rendering analysis of low molecular weight compounds rather ineffective (Cohen and Gusev 2002, Peterson 2007). Depending on the NP composition and properties, the mass spectrum may present some signals corresponding to ionisation of metal clusters, e.g. gold nanoparticles (McLean et al. 2005). Considering that the size influences the NPs ionisation and mass signals, interference is greatly reduced when compared to conventional organic matrices.

Due to their minimum size (1~100 nm), NPs possess excellent optical properties deriving from phenomena such as surface plasmon resonance (Liz-Marzan 2006), addressed beforehand. Noble metal NPs, such as gold or silver, possess an enhanced absorptivity in the ultraviolet-visible region, which favours transformation of photothermal energy during laser irradiation and provides a more effective ionisation of analytes (Wei et al. 1999, Finkel et al. 2005). Photothermal properties and heat generation at the NP surface are directly dependent of NP volume, size and incident energy, and heat generation at a given point is related to the distance to the centre of the NP (Govorov and Richardson 2007, Maity et al. 2012). This way, ligands covalently bound to the NP surface will ionise easily as distance to the NP is minimal, but the desorption process is more difficult due to higher bond-dissociation energy. Analytes interacting weakly with NP surface will ionise differently than those covalently bound, and so NPs ought to be tailored to optimise interaction to maximise ionisation and desorption efficiency.

Most reports of nanoparticles for SALDI-MS focus on spherical nanoparticles regardless of composition. Spherical NPs seem to be the most effective for SALDI due to their high surface area and homogeneity of functionalisation with ligands. Besides this, surface heating and energy transfer from nanospheres to the vicinity occurs evenly. Of extreme relevance is the fact that the most commonly used laser for ionisation in SALDI (and MALDI) is the nitrogen laser with a

fixed wavelength at 337 nm, and nanospheres often possess high absorption values in this region of the spectrum. Other shapes, usually exhibit high absorptions in other regions of the spectrum (e.g. nanorods, 650-800 nm), which would require change of laser for optimal analysis.

Despite the advantages, a major limitation observed so far is the optimisation of the adequate NP surface according to the analyte of interest, rendering some NPs very inefficient as surface for LDI of determined analytes (Huang and Chang 2007), whereas commonly used organic matrices are often directed to a particular class or type of molecules e.g. 3-hydroxipicolinic acid (3-HPA) for long polymers and oligonucleotides, CHCA for peptides. The following section will focus on the use of noble metal NPs for laser desorption/ionisation (SALDI) analysis of a wide number of analytes.

1.2.5 Noble metal nanoparticles for SALDI-TOF-MS analysis

Noble metal NPs, functionalised or not, have been extensively used for SALDI-MS analysis of a multitude of biomolecules and elements. Besides its use as affinity probes/pre-concentrating agents, noble metal NPs have also been employed as surface for LDI (see Table 1.4). The following section considers gold, silver and platinum NPs for SALDI-MS of different analytes, with an emphasis on gold (AuNPs).

For AuNP-based SALDI-MS analysis, the most utilised AuNPs are citrate-capped 14 nm ones, most favourable for ionisation of biomolecules when compared other with smaller and larger diameter (Huang and Chang 2006). These AuNPs can be easily synthesised with a relatively fair control of size dispersion and reproducibility via the citrate reduction method developed by Turkevich (Turkevich 1985). Moreover, citrate-capped AuNPs are rather simple to derivatise with molecules containing thiol- or amino-functional groups (Mirkin et al. 1996, Duan et al. 2009). Citrate-capped AuNPs have been reported for LDI detection of melamine, ammeline and ammeline in infant formula and grain powder with detection limits in the nanomolar range (Hsieh et al. 2012). These compounds interact weakly with AuNPs, through Au-N bonds and allow easy and rapid separation through centrifugation, prior to analysis. On a different study, AuNP-based SALDI was employed towards quantification of four urinary biomarkers for carcinoid tumours in human urine samples (Kuo et al. 2011), by using an internal standard.

Aptamer-AuNP conjugates have also been used as capturing probes for ATP and glutathione molecules for SALDI analysis (Huang and Chang 2007) but unmodified 14 nm AuNPs were used as surface for LDI because the aptamer-AuNP conjugates were not effective for biomolecular ionisation. Another consideration on efficiency of AuNPs towards ionisation was recently presented by Kim and Lee (2012), where a time-of-flight secondary ion mass spectrometry (TOF-SIMS) signal amplification is promoted by enlarging AuNPs through the $\text{NH}_2\text{OH}/\text{Au}^{3+}$ seeding method. Due to an increased surface area and spherical structure, the mass signal intensity of the peptides became higher on the enlarged-AuNPs surface, when compared to bare gold surface or

submonolayer of AuNPs. AuNPs functionalised with a thrombin-binding aptamer were employed for thrombin binding and deposition on a nitrocellulose membrane (Liu et al. 2012). Upon pulsed-laser irradiation, Au cluster signals decreased proportionally to the amount of bound thrombin, and by measuring the intensity of these decreasing mass signals, very sensitive (fM) quantification of thrombin was achieved.

Antibody-modified AuNPs were used to actively interact with bacterial components, allowing for a rapid separation by centrifugation and subsequent deposition on a nitrocellulose membrane for SALDI-MS identification of bacteria (Tseng et al. 2012). Upon deposition, samples were irradiated with a pulsed-laser (LDI) and the Au cluster signals were analysed. This method was validated by analysing different samples (tap water, juice, milk, and urine) and, if the surface modification is altered it may be employed for several other analytes, such as biomarkers and viral epitopes.

Gold-silica core-shell nanoparticles (Au@SiO₂ CSNPs) for LDI-TOF-MS (Zhu et al. 2012) with different core sizes and shell thickness have been combined to attain optimal enhanced ionisation. The system was applied to a polymer (dPEG6) and results suggest that NPs with smaller core and ultrathin SiO₂ shell (2-4 nm) exhibited the best efficiency, both in signal intensity and S/N ratio. Comparing to common MALDI-TOF-MS, this approach show improved sensitivity for small molecules, but are not capable to match common organic matrices. AuNPs functionalised with dopamine dithiocarbamate were also used as a surface for SALDI-TOF-MS quantification of small molecules (Kailasa and Wu 2012), allowing cleaner mass spectra than conventional MALDI-TOF using CHCA as a matrix, and better sensitivity when analysing and quantifying small molecules such as glutathione or the drugs desipramine and enrofloxacin. Besides this, dopamine dithiocarbamate-modified AuNPs served as efficient affinity probes and ionisation surface for rapid and straightforward determination of phosphopeptides from casein proteins.

Silver nanoparticles (AgNPs) have also been employed in LDI processes. AgNPs exhibit higher scattering than AuNPs, which may be valuable when transferring absorbed energy to an analyte in the vicinity (Hua et al. 2007). For example, unmodified AgNPs were used both as affinity probes and as a surface for SALDI for determination and quantification of three different oestrogen derived molecules (Chiu et al. 2008) in the low micromolar range. Oestrogens in the urine were capable of establishing weak interactions with the AgNPs' surface, allowing for separation and pre-concentration but without notable sensitivity (0.2 μM). Recently, Niziol et al. (2013) applied monoisotopic cationic ¹⁰⁹AgNPs as a surface for LDI analysis of different low molecular weight organic compounds, including alkaloids, saccharides, amino acids, nucleosides and nucleic bases. These ¹⁰⁹AgNPs were further characterised on cationisation adducts for higher sensitivity, mass accuracy, and resolution.

SALDI-TOF using AgNPs has also been employed towards bacterial analysis of dairy products (Lee et al. 2012). By using AgNPs, bacterial identification was improved by 6-fold in yogurt samples preventing interference from milk complex proteins. In the same study, an ionic solution of CrO_4^{2-} was also used for SALDI-MS analysis and proved to be more effective than AgNPs as it improved bacteria determination by 40-fold.

AgNPs functionalised with different functional groups were employed as both affinity probes and SALDI surface for analysis of biothiol molecules such as glutathione, cysteine and homocysteine (Shrivastava and Wu 2008). A comparison between 10 and 20 nm AgNPs for LDI revealed that smaller diameters correspond to better efficiency, possibly due to a higher surface area. Unmodified AgNPs were also used as a surface for direct SALDI-MS analysis of sulphur drugs.

Platinum nanoparticles (PtNPs) have been characterised in terms of SALDI efficiency, where the elevated melting point and low heat capacity of the platinum contributed to a more effective ionisation than the one obtained with silver and copper NPs (Yonezawa et al. 2009). The use of PtNPs for SALDI analysis of amino acids, peptides, proteins and microwave digested proteins has also been reported (Shrivastava et al. 2011). PtNPs played three main roles in this approach: affinity probe, surface for LDI and acceleration of protein digestion by absorbing the microwave irradiation. Higher numbers of peptide sequences were obtained for PtNP-accelerated microwave digestion of the lysozyme protein, when compared to standard digestion of proteins for MALDI-MS.

Besides being used as surface for SALDI, PtNPs with sizes between 2-10 nm (mainly 4 nm) were used as additives with a SA matrix to enhance sensitivity when analysing cell populations of *Saccharomyces cerevisiae* and *Chlamydomonas reinhardtii* (an improvement of 125- and 5-fold, respectively) (Manikandan et al. 2012). An approach using modified PtNPs for both pre-concentration and as matrix additives for signal enhancement was described for bacterial proteomic analysis (Ahmad et al. 2012). Adding immunoglobulin G-functionalised PtNP probes to samples from rhizospheric soil and carrot plant roots proved to be an effective enrichment strategy, as the PtNP probes interact and adsorb to the bacteria surface. Together with a signal enhancement from the combination of SA with the PtNP probes, *Bacillus thuringiensis* and *B. subtilis* isolates were directly detected with low concentrations.

This section of the introduction addressed mass spectrometry and the relevance of NPs for novel MS applications for biomolecular detection. The following section will address toxicology, with an emphasis on formation, MS detection and biological relevance of DNA adducts.

Table 1.4. Noble metal nanoparticles for SALDI-MS

Nanoparticle for ionisation	Size (nm)	Detected analyte	Detection Limit	Ref
AuNPs	2-10	Peptides	100 fmol	McLean et al. 2005
	14	Melamine, ammeline, ammeline	5, 10 and 300 nM	Hsieh et al. 2012
	13	Tumour biomarkers (TRP, 5-HTP, 5-HT and 5-HIAA)	1.5 and 1.8 μ M	Kuo et al. 2011
	3.5 and 14	Glutathione, cysteine, homocysteine	2-44 nM	Chiang et al. 2009
	14	Captopropil	1 μ M	Chen et al. 2010
	9-14	Carbohydrates	82-151 nM	Su and Tseng 2007
	13.2	Carbohydrates, indolamines, peptides	46.5-5115 nM	Wu et al. 2009a
Aptamer-modified AuNPs	14	ATP, glutathione	0.48 μ M	Huang and Chang 2007
	13.3	Thrombin	50 fM	Liu et al. 2012
Antibody-modified AuNPs	5.5	<i>Escherichia coli</i>	1000 CFU/mL	Tseng et al. 2012
Au@SiO ₂ NPs	20-38	Polymers	10 fmol	Zhu et al. 2012
CHCA-modified AuNPs	14	Peptides	20 pmol	Duan et al. 2009
Dopamine dithiocarbamate-modified AuNPs	5-12	Phosphopeptides	0.01-1.6 nM	Kailasa and Wu 2012
Nile-red adsorbed AuNPs	14, 32, 56	Glutathione, cysteine, homocysteine	1-2 μ M and 25-54 nM	Huang and Chang 2006
AuNPs, AgNPs, PtNPs	20; 10-30; 20	Surfactant, peptides	N.A. ^a	Yonezawa et al. 2009
AuNPs, PtNPs	14; 37	Biomolecules, peptides, proteins	140 fmol; 23pmol	Chiang et al. 2010

1.3 Toxicology

Ever since the pre-historic times, mankind has always been aware of substances that induce adverse effects on an organism, i.e. poisons. In ancient times, i.e. Greek and Roman civilizations, countless references have been found that describe the use of poisons for hunting or assassination purposes (Gallo 2008). The study of poisons evolved throughout times, and reached its apogee during the Renaissance period in Italy. Phillip von Hohenheim, better known as Paracelsus (1493-1541) was perhaps the most significant figure in the history of toxicology (Borzelleca 2000). He was the first one to focus on the primary toxic agent, instead of the mixture or concoction it had been so far. He stated that “all substances are poisons: there is none which is not a poison. The right dose differentiates poison from a remedy”. This statement revolutionised the modern toxicological and pharmacological sciences, which continued to evolve constantly from the Middle Ages, until the 19th century. At this time, with the beginning of organic synthesis, new chemicals started to be developed, namely phosgene and mustard gas, which would later be used for warfare in World War I. Some decades later, during the World War II era, toxicology evolved rapidly, similarly to what happened with mass spectrometry. After World War II, began a fruitful period for regulatory toxicologists, marked by creation of safety programs and legislations for experimental procedures. Historical milestones of toxicological sciences are described in detail by Gallo (2008), and Hayes and Gilbert (2009).

1.3.1 General concepts

Toxicology is the study of adverse effects of a chemical or physical agent on living organisms. In order for this to be possible, toxicology is a field that integrates notions from cellular and molecular biology, biochemistry and mathematics. Toxicological research assesses the cellular, biochemical and molecular mechanisms of action as well as functional effects and their probability of occurrence. As Paracelsus defined, the study of toxicology is extremely concerned about the dose, e.g. the total amount of a certain chemical agent to which the organism has been exposed, in relation to its weight (James et al. 2000, Eaton and Gilbert 2008). Dose-response relationships allow obtaining information about potential adverse effects of a given chemical agent, lethality thresholds and simulating these effects in a population. Dose-response relationships are the domain of specialisation of descriptive toxicologists, and ultimately provide information for safety evaluation and regulatory requirements.

Other than descriptive toxicology, other sub-fields exist, such as mechanistic toxicology, regulatory toxicology, or risk assessment (James et al. 2000, Eaton and Gilbert 2008). Mechanistic toxicology, for instance, tries to understand cellular biochemical and molecular mechanisms by which chemicals exert toxic effects on living organisms. These studies are of high importance in many areas of toxicology and also pharmacology, when developing novel therapeutic agents.

Regulatory toxicologists decide if a chemical compound is safe enough to be marketed, and establish threshold levels for that chemical in society. Risk assessment draws information from all other areas of toxicology and estimates potential effects of a given chemical agent in human health or environmental, e.g. mycotoxins in food, sewage effluents in waterbodies, etc. Toxicological sciences are of extreme relevance, for human beings and animals are constantly being exposed to external agents, capable to induce damage at a tissue, and even cellular level.

In superior eukaryotic organisms, when a xenobiotic agent (i.e. a compound that is not naturally produced in the body) enters an organism it undergoes several phases: absorption, distribution, metabolism, elimination. The combination of all these phases constitutes the disposition of a chemical (Lehman-McKeeman 2008). Because the term absorption may be confounded with cellular absorption, I will refer to absorption by the organism as uptake. Uptake refers to the process by which a chemical passes the biological barriers (external tissues, body membranes) and reaches the bloodstream. There are various ways of uptake, depending on the organism, toxicant and route of exposure. In most metazoans, the liver or an analogue organ is the major organ involved in xenobiotic metabolism. Detoxification comprises two different phases: phase I and phase II. The metabolism of a xenobiotic begins with its bioactivation during phase I, which is a very important step. Phase I metabolism of organic xenobiotics (e.g. dioxins, mycotoxins) includes enzymatic complexes usually belonging to the CYP family (cytochrome P450 monooxygenases), that perform hydrolysis, reduction and oxidation reactions, which render the xenobiotic more polar and often more reactive, depending on the parent compound. Phase II enzymes perform conjugation reactions of biotransformed species with intracellular nucleophiles, e.g. glutathione. For chemicals which are mainly metabolised in the liver, the main route of excretion (i.e. elimination) is through bile (O'Flaherty 2000, Rozman and Klaasen 2003, Lehman-McKeeman 2008).

Edmond Locard (1877-1966), considered the father of forensic sciences, postulated that “every contact leaves a trace” and this became known as Locard's Exchange Principle. In toxicological sciences, this principle also applies when the xenobiotic agent establishes contact with tissues, cells or cellular components, hence the notion of biomarker. A biomarker is a reaction, behaviour or chemical compound which may indicate the interaction between a toxicant and the organism (Silins and Högberg 2011). Generally, three types of biomarkers are considered: susceptibility, exposure and effect. However, these notions are dynamic, depend on how the data is interpreted and towards what endpoint. Biomarkers of susceptibility are indicators of native (i.e. prior to exposure) characteristics of an organism/individual that render it more susceptible to the effects of certain agents, e.g. polymorphisms in DNA repair systems have been linked to increased probability of chemically-induced cancer (Goode et al. 2002). Biomarkers of exposure can be, for instance, metabolites resulting from interaction of xenobiotics with intracellular components, e.g. DNA and haemoglobin adducts as biomarkers of exposure to acrylamide (Pérez et al. 1999,

Ogawa et al. 2006, Chevolleau et al. 2007), or a broader example, the increase in activity in oxidative stress-related enzymes. Lastly, biomarkers of effect can be defined as biological consequences that constitute alterations to the basal metabolism, or structure, and may reflect adverse effects, e.g. the formation of lipid peroxides (Schrenk 1998, Sato et al. 2008). Some biomarkers, such as DNA adducts may be considered of both exposure and effect, because formation of a DNA adduct may imply a genotoxic effect, if left unrepaired (Silins and Högberg 2011). The following sections will discuss the formation and detection of DNA adducts, their biological relevance and significance as biomarkers of exposure.

1.3.2 Formation of DNA adducts and chemical carcinogenesis

The DNA molecule is susceptible to various types of damage, either physically or chemically-induced lesions. The sub-field of toxicology that studies the effects of chemical and physical agents on the DNA molecule and genetic processes of living beings is genetic toxicology (Preston and Hoffmann 2008). This field of study was pioneered in 1927 by H.J. Muller that observed mutations in *Drosophila* resulting from exposure to X-rays, constituting the first report of a DNA lesion induced by a physical agent. However, the first report of a chemically-induced DNA lesion came only in 1946, when Auerbach and Robson showed that mustard gas could induce mutations in *Drosophila* similar to those induced by X-rays. The major breakthrough on DNA adducts was presented in 1977 by Miller and Miller, who showed that chemical carcinogens could form stable, covalent bonds with macromolecules.

As previously defined, a DNA adduct results from a covalent reaction between an alkylating agent and the DNA molecule. Alkylating agents exhibit electrophilic properties, which means they are attracted to an electron-rich centre, i.e. a nucleophilic centre. Nucleotides in the DNA molecule possess several nucleophilic centres that are targeted by the alkylating agents - depicted in Figure 1.9. Specific functional groups are particularly reactive towards different nucleophilic centres, e.g. epoxide groups tend to bind positions N3 or N7 in the purine ring. In general, most abundant DNA adduct species result from alkylation of the guanine nucleobase at position N7, revealing pertinent information as biomarkers of exposure (Boysen et al. 2009).

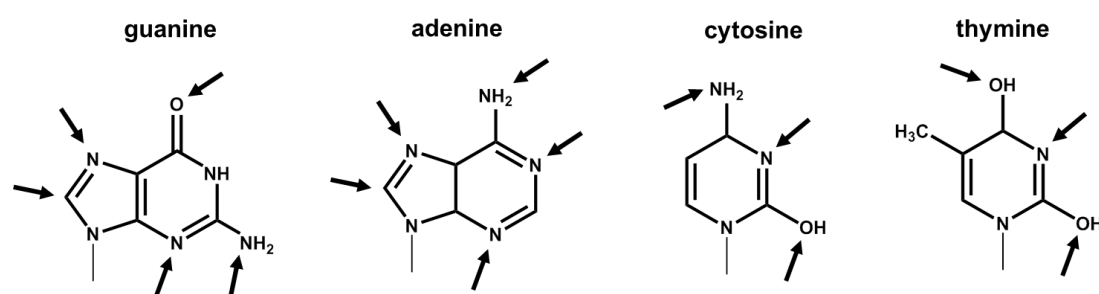


Figure 1.9. Some examples of sites for possible adduct formation in DNA bases. Purines are more targeted than pyrimidines.

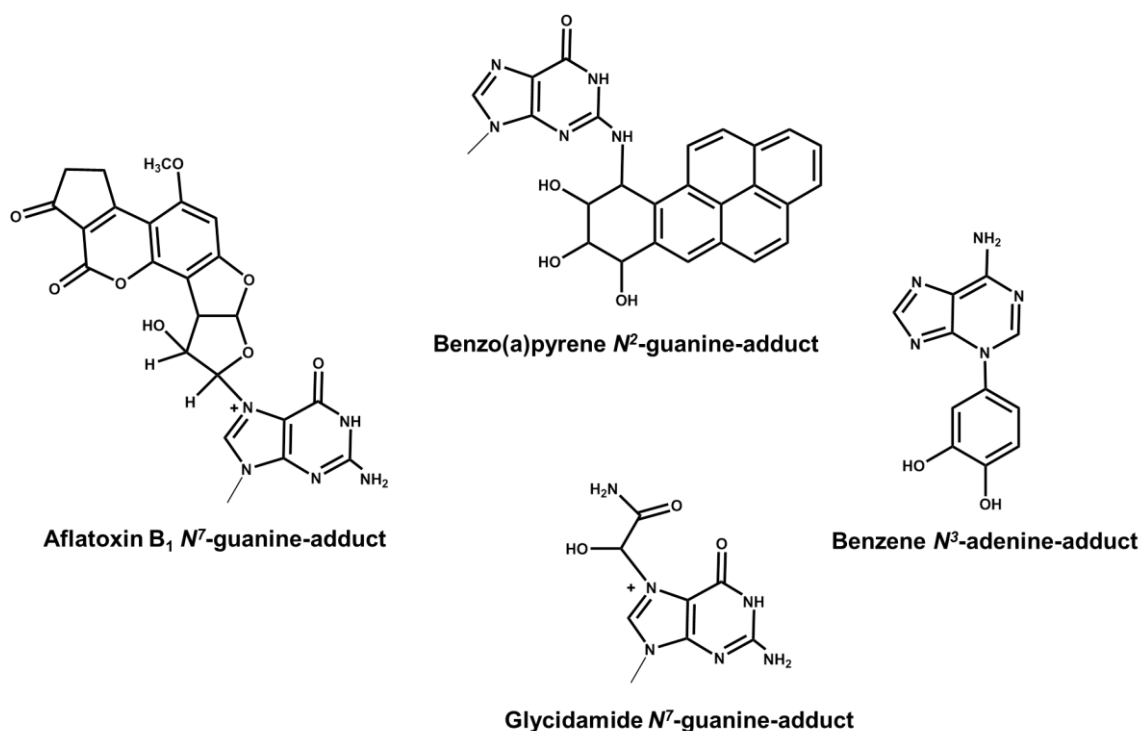


Figure 1.10. Some examples of possible guanine DNA adducts with different toxicants (PAHs, mycotoxins, etc.).

There is a wide range of substances that present the potential to alkylate nucleophilic centres in DNA, e.g. PAHs, mycotoxins, etc. (Kriek et al. 1998, Wang and Groopman 1998, Carbajal 2008) – see some examples of DNA adducts in Figure 1.10. This alkylation of the DNA molecule by exogenous agents frequently originates mutations, if not correctly repaired. These agents are called genotoxic carcinogens and play a key role in the initiation stage in the chemical carcinogenesis process (Klaunig and Kamendulis 2008). Whereas some genotoxicants are naturally reactive towards the DNA molecule (direct-acting), most agents require bioactivation beforehand (indirect-acting), which usually occurs by oxidation during phase I metabolism (Parkinson and Ogilvie 2008). The risk to the cell concerning a specific DNA adduct depends essentially of its reactivity, structure and persistence. More reactive molecules tend to overcome the competition between DNA and detoxification systems, and form an elevated number of DNA adducts, which may lead to accumulation of lesions or errors. Regarding structure, alkylating agents with a larger, less polar structure, such as PAHs, tend to originate bulky DNA adducts, which constitute a higher risk to the cell (Kriek et al. 1998, Godschalk et al. 2003, Klaunig and Kamendulis 2008). The structure also determines the main targeted sites, and consequently, the biological relevance of the DNA adduct. For instance, it has been described that smaller and more polar electrophiles binding guanine at position N7 cause instability in the purine-pentose bond, and the DNA adduct tends to be released from the DNA chain, originating an apurinic site. This lesion may be efficiently repaired by the cell, meaning this particular DNA adduct poses little carcinogenic risk, however it is extremely valuable as a biomarker of exposure (Boysen et al.

2009). Lastly, a DNA adduct persistence depends on the ability of the cell to repair the targeted site. So, for different agents, the competition between the target cellular nucleophiles (DNA, proteins) and detoxification systems comes into play, with distinct outcomes. Either way, whether as a biomarker of exposure or as a potential carcinogen, the detection of DNA adducts has provided remarkable information for mechanistic, descriptive and regulatory toxicologists.

1.3.3 Methods for detection of DNA adducts

Detection and quantification of DNA adducts in biological samples is a rather complex issue that has gained attention amongst genetic toxicologists. Different techniques have been developed and employed for identification and characterisation of DNA adducts as biomarkers of exposure to chemical agents, or cancer biomarkers (Phillips et al. 2000, Farmer et al. 2005, Brown 2012). However, there exists no perfect methodology as every described technique presents a major limitation. This way, the choice of the most adequate method for detection of a DNA adduct is closely related to the molecular structure of that DNA adduct, its abundance, and the quantity of available sample for testing. Table 1.5 depicts the different techniques employed for detection and characterisation of DNA adducts.

Table 1.5. Different techniques employed for DNA adduct detection (Farmer 2005, Brown 2012)

Method	Max. sensitivity (adducts/nucleotide)	Required DNA sample (μg)	References (examples)
HPLC/ECD or HPLC/FD	$\sim 1/10^8$	< 100	Park et al. 1989, Helbock et al. 1998
Immunoassay	$\sim 1/10^8$	< 200	Santella 1999, Divi et al. 2002
^{32}P-post-labelling	$\sim 1/10^{10}$	< 10	Reddy et al. 1989, Kotova et al. 2011
Mass spectrometry	$\sim 1/10^8$	10-100	Brown et al. 2003, Gamboa da Costa et al. 2003, Barnes and Chiu 2009
AMS	$\sim 1/10^{12}$	< 2,000	Turteltaub and Dingley 1998

ECD: electrochemical detection; **FD:** fluorescence detection; **AMS:** accelerator mass spectrometry.

Amongst all the methods employed for detection of DNA adducts, electrochemical and fluorescence detection methods are by far the simplest and exhibit reasonable sensitivity. These methods are usually used in conjunction with HPLC or capillary electrophoresis (CE) for separation (Brown 2012). Despite these advantages, such methods are only suitable to analyse fluorescent or electrochemically active adducts. Whenever the DNA adduct does not present a sufficient electrochemical or fluorescent signal, it must be derivatised to a different, more active compound, if possible (Sharma 2000).

Immunoassays may be a powerful tool in DNA adduct detection as well. These techniques rely in the use of antibodies which grants them elevated specificity, but also the risk of cross-reactivity. One other great advantage of these methods is they allow for localization of adducts in tissue, and the detection of DNA adducts in fixed preparations, by immunohistochemistry. Despite this, obtaining suitable and specific antibodies is not always simple, so immunological methods are highly dependent on the success of antibody synthesis.

³²P-post-labelling is perhaps considered as the election technique for detection of DNA adducts. This technique is of extreme versatility and sensitivity, and requires only a small sample for analysis (1-10 µg of DNA). However, it involves intensive labour and cumbersome protocols. The use of a radiolabeled compound is crucial for this technique to work and it may be seen as both an advantage and a drawback. The elevated levels of radioactivity require specialised personnel and pose a risk of exposure, but it also allows the possibility to screen a sample for DNA adduct formation without previous knowledge on the mechanisms and structures (Brown 2012). This kind of analysis is optimal for large, bulky DNA adducts, such as PAHs or mycotoxin-derived adducts, but it presents some limitations when analysing DNA adducts of low molecular weight.

From all methodologies employed for DNA adduct detection, mass spectrometry methods are those that have been more frequently used, due to its elevated specificity and the capability to provide information about the molecular structure. This is a major advantage over other techniques as it allows completely unknown DNA adducts to be analysed and characterised. Detection of DNA adducts benefits from the vast number of available instruments and the continuous evolution of mass spectrometers, with increased sensitivity (Brown 2012). For instance, liquid chromatography coupled to MS, e.g. electrospray ionisation, has been employed for DNA adduct characterisation. MS/MS data are simple to attain and provide valuable information on structure, with good sensitivity (Gamboa da Costa et al. 2003, Singh and Farmer 2006, Gaskell et al. 2007). Inductively coupled plasma mass spectrometry (ICP-MS) has also been used to analyse DNA adducts resulting from chemotherapeutic agents, such as cisplatin (Sar et al. 2008) or from toxicants, such as styrene oxide (Siethoff et al. 1999). MALDI-TOF has also been employed for characterisation of carcinogenic DNA adducts (Qiao et al. 2006, Barnes and

Chiu 2009). The major limitation of MS analysis is that it requires DNA adduct standards in order to provide an actual quantification.

Accelerator mass spectrometry (AMS) has been used since the 1980s for toxicokinetic and pharmacokinetic research (Brown et al. 2006). This technique possesses the highest sensitivity (1 adduct per 10^{12} nucleotides) and elevated specificity for DNA adduct detection. These features are closely related to the use of radiolabeled compounds (^{14}C or ^3H), an absolute requirement for the analysis (Vogel et al. 1995). Nevertheless, the most significant disadvantages are the cost of analysis and the lack of available instrumentation.

Overall, there is a need for novel methodologies for DNA adduct detection and characterisation that overcome major limitations of currently employed techniques, without compromising sensitivity and specificity. The recent advances in nanotechnology and mass spectrometry may contribute greatly for this purpose. Other than this, it is important to define procedures for sample preparation, DNA adduct enrichment or isolation, preferably simple, fast and inexpensive, to try and counter sensitivity issues during detection. The following sections focus the target molecule of study, acrylamide, its known mechanisms of toxicity and environmental risk.

1.3.4 The case of acrylamide

Acrylamide ($\text{C}_3\text{H}_5\text{NO}$) is an industrially-produced unsaturated amide with a multitude of applications in various fields. This molecule possesses extreme versatility, presenting a high solubility in water and in organic solvents (IARC 1994), which render it adequate for many different industrial applications. Its primary use is the production of polyacrylamide (co)polymers to be used as flocculants in water treatment processes (Bajdur 2008). Another relevant application is the use of acrylamide or N-methylacrylamide-based grouts in the construction of tunnels. Additional applications include agricultural processes, textile manufacturing (Myagchenkov and Kurenkov 1991) and life science research.

In 2002, acrylamide has been classified a “probable carcinogen for humans” by IARC (International Agency for Research on Cancer), following reports that showed formation of acrylamide during food processing, through the Maillard reaction (Stadler et al. 2002, Tareke et al. 2002). Until then, the main concerns were related to the ecotoxicological risk and environmental fate of acrylamide, but it readily began to turn towards human health, mostly related to the presence of acrylamide in foodstuff (Vikström et al. 2011, Watzek et al. 2012, Dobrowolski et al. 2012). Actually, ever since it was classified as a “probable carcinogen for humans”, there has been a decrease in environment-related studies of acrylamide monomers and derivatives, with most studies focusing formation of acrylamide and its metabolites *in vivo*, and corresponding dose-response effects.

1.3.4.1 Environmental risk

Employing acrylamide derivatives in water treatment processes, tunnel construction or agriculture inevitably raises the question of the environmental risk it poses. With this in mind, there has been some work about the environmental fate of acrylamide monomers after degradation of polyacrylamide (co)polymers and subsequent consequences to the biota (e.g. Brown et al. 1980a, 1980b, Friedman 2003). There are essentially two sources of acrylamide monomers which may end up in waterbodies: the contamination of polyacrylamide (co)polymer solutions with residual monomers and the eventual degradation of polymers to acrylamide molecules. Since these monomers may partition to aquatic niches, mainly freshwater systems, water contamination with acrylamide and its effects to aquatic wildlife remain a critical concern (NICNAS 2002, Badjur 2008, Weston 2009). In fact, waterbodies are acknowledged to be the main reservoirs of the substance, (Mackay model calculates that >99.9% of total acrylamide in the environment will end up in water systems) in large part owing to its high solubility in water, low vapour pressure and ability to become adsorbed to particulates (NICNAS 2002).

Acrylamide in water may suffer degradation, causing an increase in the ammonia concentration. The absence of degradation in sterilised waters suggests that the removal of acrylamide occurs via a biotic route, with abiotic removal mechanisms such as hydrolysis and photolysis being negligible (Brown et al. 1980b). Regarding biotic degradation of acrylamide at low concentrations (1 and 2 mg/L), a complete degradation by microorganisms was observed past 15 and 28 days, respectively (United States Testing Company Inc. 1991). At a concentration of 5 mg/L, approx. 50 % degradation was observed after 15 and 28 days, suggesting that, at this concentration, bacteria can no longer efficiently degrade acrylamide after 15 days of exposure. Higher acrylamide concentration denoted fewer degradation rates. Together with data from 5 mg/L, this could mean possible toxic effects to the bacteria in water.

The concerns of acrylamide monomers to aquatic wildlife led mainly to studies focusing acute toxicity to fish and crustaceans, revealing moderate to low effects (Bridié et al. 1979, Krautter et al. 1986). The effects of chronic exposure to acrylamide monomers to aquatic organisms have rarely been addressed, possibly as a consequence of reduced acute toxicity. Nonetheless, there is evidence in freshwater fish (Edwards 1975, Haasch et al. 1992) that may account for potential chronic toxicity associated to acrylamide. These findings, together with the studies *in vivo* or *in vitro* with model subjects, indicate that acrylamide monomers may indeed cause multi-level adverse effects to wildlife that require more prolonged and ecologically-realistic exposures to the xenobiotic in order to be fully comprehended. Most studies concerning acrylamide toxicity to aquatic biota targeted fish models (Woodiwiss and Fretwell 1974, Bridié et al. 1979, Krautter et al. 1986, Waddell et al. 1990) and only a few studies have focused on invertebrates, mostly model organisms like *Daphnia magna* (ABC Labs 1983a); the midge *Parathanyarsus parthenogenetica* (ABC Labs 1983b); the rotifer *Adineta vaga* (Örstan 1992), and the saltwater mysid shrimp

Mysidopsis bahia (Springborn Bionomics 1985, EG&G Bionomics 1986). Overall, invertebrates show very different sensitivities to acrylamide, as opposed to what happens in fish models, where effect concentrations typically yield little interspecific variation (see for instance Krautter et al. 1986, Walker 1991, Weston et al. 2009).

1.3.4.2 Known mechanisms of toxicity

Ever since the 80s, several studies focusing on acrylamide exposure were carried out on human and animal models (Green and Egle 1983, Howland 1985, He et al. 1989), indicating that acrylamide is metabolised in hepatocytes into a reactive epoxide by the cytochrome P450 monooxygenases (CYP2E1 in mammals), during phase I metabolism (see Figure 1.11). This bioactivation is achieved by oxidation of the double bond between α and β carbons (Carere 2006, Lineback et al. 2012). The resulting epoxide, glycidamide, is highly reactive towards nucleophilic centres in the DNA molecule, originating DNA adducts mainly at N3 and N7 in the purine ring, when in contact with DNA (Martins et al. 2007, Watzek et al. 2012). Formation of glycidamide from acrylamide during phase I metabolism is the main concern of acrylamide-induced carcinogenicity. The production of glycidamide-DNA adducts may lead to transitions, and strand breakage that, if not correctly repaired, may progress on to cancer.

Reactivity of acrylamide to cellular components is directly linked to the double bond between α and β carbons. Besides an epoxidation to glycidamide, this functional group may undergo a Michael's addition and alkylate nucleophilic centres in proteins (Mather et al. 2006, Zamora et al. 2010). For instance, acrylamide has been described to bind to neurofilaments and cytoskeletal proteins, preventing microtubule disassembly (Lapadula et al. 1989, Sickles et al. 1995). However, the major biomarkers of exposure to acrylamide found in superior organisms are haemoglobin-adducts derived from reaction of cysteine or amine groups with acrylamide or glycidamide (Pérez et al. 1999, Ogawa et al. 2006, Chevolleau et al. 2007). However it has been shown that acrylamide itself presents low reactivity towards DNA and most DNA adducts formed are a consequence of alkylation by glycidamide. The schematics in Figure 1.11 illustrates the known interactions of acrylamide and glycidamide with cellular components.

Exposure to acrylamide has been related to alterations in gene expression and oxidative stress in human cell lines and rats (Yousef and El-Demerdash 2006, Camacho et al. 2012, Sen et al. 2012), reproductive impairment (Sakamoto and Hashimoto 1986, Zenick et al. 1986, Chapin et al. 1995, Tyl and Friedman 2003, Wang et al. 2010, Camacho et al. 2012), increased formation of benign tumours in mammals and neurotoxicological effects in different organisms such as goldfish, frogs, rats and flies (Edwards 1975, Seale et al. 2012, Prasad and Muralidhara 2012), being a proven carcinogen to rodent models (see Besaratinia and Pfeifer 2007, for a review). The proposed molecular models for acrylamide toxicity have recently been reviewed by LoPachin and Gavin (2012). Acrylamide and its metabolite glycidamide are known to interact with a wide range

of biomolecules, at the cellular level, which aids in explaining the potential broad scope of its toxicological effects. For instance, evidence that acrylamide may indeed be mutagenic and clastogenic is directly linked to the binding of cytoskeletal proteins, leading to irregularities during the mytotic cycle and increased nuclear abnormalities. Chromatid gaps and breaks have also been observed in mammalian cells, previously exposed to acrylamide (Martins et al. 2007). All in all, it is believed that acrylamide and glycidamide exhibit distinct mechanisms of toxicity and different preferential targets within the cell, and to better understand the pathways adopted by each of these chemicals, their exact consequences should be analysed separately. In terms of genetic toxicology, there has been some research towards that objective, establishing comparisons between acrylamide and glycidamide (Barber et al. 2001, Doerge et al. 2005, Puppel et al. 2005, Martins et al. 2007).

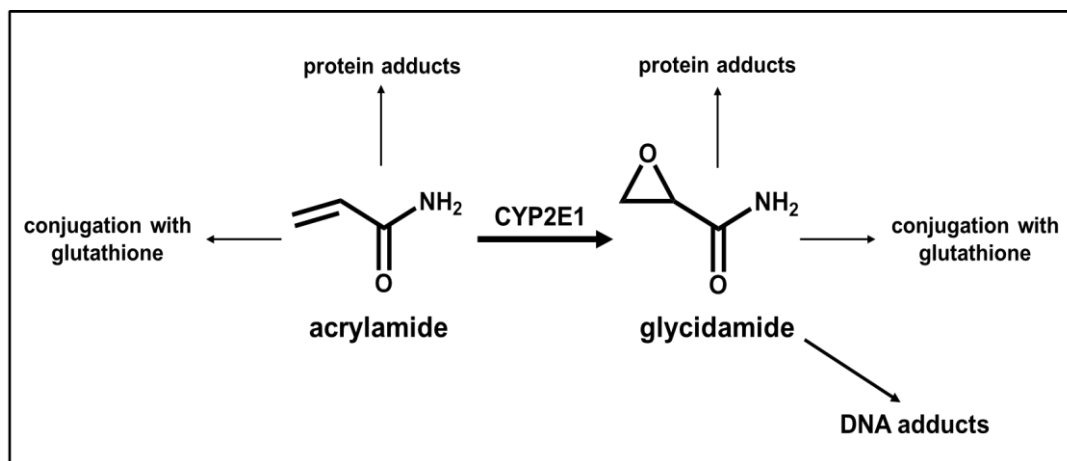


Figure 1.11. Epoxidation of acrylamide to glycidamide and possible interactions of these compounds with cellular components.

1.4 Scope of thesis and main objectives

This dissertation is centred in the biological question of DNA adducts as biomarkers of exposure to carcinogen agents, namely acrylamide. Despite being sensitive, currently employed procedures are cumbersome, time-consuming, require specialised personnel and are not risk absent for the user (the case of radiolabeled isotopes). One of the main objectives of this work is the development of an easy-to-perform gold nanoparticle-based technique suitable for identification of DNA adducts in biological samples from individuals previously exposed to a carcinogen agent. To accomplish this objective, several intermediate objectives will have to be addressed, namely at the sample preparation and the detection steps.

Regarding the sample preparation procedure, all protocols included in this section will be broken down and analysed for its utility, advantages and disadvantages. This way, a decision will be made on which protocols are the most valuable for the desired outcome and the sample

preparation procedure will be tailored according to the necessities. In particular, ultrasonic fragmentation of DNA, enzymatic hydrolysis of DNA and chromatography protocols will be addressed.

Concerning the detection step, gold nanoparticles will be employed for two distinct approaches towards DNA adduct identification: i) as an inorganic surface for laser desorption/ionisation (SALDI), to potentiate mass spectrometry detection. Gold nanoparticles will be evaluated as an inorganic surface towards nucleotide profiling, and compared to the more traditional organic matrix for laser desorption/ionisation (MALDI). After a careful analysis of SALDI vs. MALDI, and optimisation of the detection conditions, this system will ultimately be employed for identification of DNA adducts generated by exposure to acrylamide; ii) conjugated with aptamer molecules, constituting gold-aptamer nanoprobe, capable of a colorimetric identification. The stability of nanoprobe will be assessed, as well as its spectral behaviour in the presence of different nucleotides. The assay conditions will be optimised before detection of DNA adducts generated *in vitro* in different substrates (free nucleotides vs. DNA chain).

The development of a promising approach for identification of DNA adducts as exposure biomarkers would strengthen the versatility of gold nanoparticles for bioanalytical purposes, and might provide a future alternative to currently employed protocols for DNA adduct detection.

A second main objective of this work is the development of a biological model for exposure to acrylamide. This will be accomplished by a rigorous and thorough assessment of acrylamide toxicity and biomarker response in two different aquatic organisms: the goldfish and the Mediterranean mussel. Particularly, effects both at the cellular and tissue-level will be evaluated and a general overview of acrylamide mechanisms of toxicity will be explained, including genotoxicity and oxidative stress. Both acute and prolonged exposures will be assayed for a more broad comprehension of acrylamide consequences to the target organisms. To complete the toxicological study, qualitative histopathological screening will be performed and relations will be established amongst all considered biomarkers. Once the mechanisms of acrylamide toxicity in these organisms have been assessed, as well as their value as biological model for exposure, collected samples will be treated according to the developed sample preparation protocol analysed using the proposed AuNP-based approach for DNA adduct detection, as mentioned beforehand.

CHAPTER 2. MATERIALS AND METHODS

Tell me and I forget. Teach me and I remember. Involve me and I learn.

Benjamin Franklin

2.1 Materials

2.1.1 Chemical reagents

Reagents	CAS number	Distributor
1-chloro-2,4-dinitrobenzene (CDNB)	97-00-7	Sigma-Aldrich
2,4,6-trihydroxyacetophenone (THAP)	480-66-0	Sigma-Aldrich
3-(4-chloro-phenyl)-2-cyano-acrylic acid	-	Sigma-Aldrich
3-hydroxypicolinic acid (3-HPA)	874-24-8	Sigma-Aldrich
7-ethoxyresorufin	5725-91-7	Santa Cruz Biotech.
α -cyano-4-hydroxycinnamic acid (CHCA)	28166-41-8	Sigma-Aldrich
ABTS diammonium salt	30931-67-0	Alfa-Aesar
Acetonitrile	75-05-8	Carlo-Erba
Acetylcholine iodide (ACTI)	2260-50-6	Sigma-Aldrich
Acetylcholinesterase (AChE) from electric eel	9000-81-1	Sigma-Aldrich
Acridine orange	10127-02-3	Sigma-Aldrich
Acrylamide	79-06-1	Sigma-Aldrich
Albumin, from bovine serum (BSA)	9048-46-8	Sigma-Aldrich
Agarose	9012-36-6	Invitrogen
Ammonium chloride	12125-02-9	Merck
Ampicillin	69-53-4	Sigma-Aldrich
Bacteriological agar	9002-18-0	Difco
Boric acid	10043-35-3	Fluka
Bradford reagent	-	Sigma-Aldrich
Bromophenol blue	115-39-9	Merck
Catalase, from bovine liver	9001-05-2	Sigma-Aldrich
Chloroform	67-66-3	Merck
Dimethyl sulfoxide (DMSO)	67-68-5	Sigma-Aldrich
DL-Dithiothreitol (DTT) solution, 1 M	3483-12-3	Fluka
DPX mounting medium	-	BDH
Dulbecco phosphate buffered saline	-	Sigma-Aldrich
Eosin Y	15086-94-9	Sigma-Aldrich
Ethanol	64-17-5	Panreac
Ethidium bromide (EtBr)	1239-45-8	Sigma-Aldrich
Ethylenediamine tetracetic acid (EDTA)	60-00-4	Merck
Ferulic acid	537-98-4	Sigma-Aldrich

Reagents (cont.)	CAS number	Distributor
Ficoll	26873-85-8	Sigma-Aldrich
Glacial acetic acid	64-19-7	Sigma-Aldrich
Glucose	50-99-7	Sigma-Aldrich
Glycerol	56-81-5	Sigma-Aldrich
Glycine	56-40-6	Sigma-Aldrich
Glycidamide	5694-00-8	Sigma-Aldrich
Gold(III) chloride trihydrate	16961-25-4	Sigma-Aldrich
Haematoxylin	517-28-2	Sigma-Aldrich
Hydrochloric acid	7647-01-0	Sigma-Aldrich
Hydrogen peroxide	7722-84-1	Sigma-Aldrich
Low-melting point GtG agarose	39346-81-1	NuSieve
Magnesium chloride	7786-30-3	Merck
Malondialdehyde (MDA)	100683-54-3	Sigma-Aldrich
Methanol	67-56-1	Merck
Myoglobin from horse heart	100684-32-0	Sigma-Aldrich
Nicotinamide adenine dinucleotide phosphate (NADPH)	100929-71-3	Sigma-Aldrich
Nitric acid	7697-37-2	Sigma-Aldrich
Paraffin pellets, histology grade	8002-74-2	Panreac
<i>p</i> -nitrophenylphosphate (pNPP) developing solution	333338-18-4	Sigma-Aldrich
Potassium chloride	7447-40-7	Merck
Potassium hydroxide	1310-58-3	Merck
Potassium periodate	7790-21-8	Alfa Aesar
Potassium phosphate dibasic	7758-11-4	Sigma-Aldrich
Potassium phosphate monobasic	7778-77-0	Sigma-Aldrich
Proteinase K	39450-01-6	Roche
Purpald®	1750-12-5	Sigma-Aldrich
Reduced glutathione (GSH)	70-18-8	Sigma-Aldrich
Resorufin	635-78-9	Sigma-Aldrich
Sinapinic acid	530-59-6	Fluka
Sodium chloride	7647-14-5	Sigma-Aldrich
Sodium citrate tribasic hydrate	6132-04-3	Sigma-Aldrich
Sodium dodecyl sulfate (SDS)	151-21-3	Sigma-Aldrich

Reagents (cont.)	CAS number	Distributor
Sodium hydroxide	1310-73-2	Sigma-Aldrich
Sodium phosphate dibasic dihydrate	10028-24-7	Merck
Sodium phosphate monobasic monohydrate	10049-21-5	Merck
Sucrose	57-50-1	Sigma-Aldrich
Super DHB	63542-76-7	Sigma-Aldrich
TE-buffered phenol	108-95-2	Sigma-Aldrich
Thiobarbituric acid (TBA)	504-17-6	Sigma-Aldrich
\Trichloroacetic acid (TCA)	76-03-9	Merck
Trizma® base	77-86-1	Sigma-Aldrich
Triton-X 100	9002-93-1	Sigma-Aldrich
Trolox®	53188-07-1	Sigma-Aldrich
Tryptone	91079-40-2	Difco
Tween® 20	9005-64-5	Sigma-Aldrich
Xylene	1330-20-7	Sigma-Aldrich
Yeast extract	8013-01-2	USB

2.1.2 Solutions and buffers

All necessary solutions and dilutions were prepared using ultrapure (> 16.2 MΩ.cm) sterile water from a Merck Millipore Milli-Q system.

Phosphate buffer (sodium/potassium)

According to the desired pH and concentration (from Sambrook and Russel 2001)

pH	Na ₂ HPO ₄	NaH ₂ PO ₄	pH	K ₂ HPO ₄	KH ₂ PO ₄
	10 mM (mL)	10 mM (mL)		50 mM (mL)	50 mM (mL)
7.0	57.7	42.3	7.0	61.5	38.5
7.4	77.4	22.6	7.4	80.2	19.8
7.6	84.5	15.5	7.6	86.6	13.4
8.0	93.2	6.8	8.0	94.0	6.0

AL1

10 mM Tris-HCl (pH 8.0)

1 mM EDTA (pH 8.0)

50 mM glucose (Added after sterilisation in autoclave)

Store at 4 °C.

AL2

0.2 M NaOH

1 % SDS (m/v)

Prepare fresh before use.

AL3

3 M Sodium acetate (adjust pH to 4.8 with glacial acetic acid).

Store at 4 °C.

Bouin-Hollande's solution

10 % (v/v) formalin

7 % (v/v) acetic acid

Picric acid added to saturation

Store at RT.

Blocking solution

1 % BSA in 1xPBS

BM mixture

125 mM NaCl

60 mM KCl

35 mM NaH₂PO₄

50 mg/L BSA

If necessary, adjust pH to 7.0. Store at 4 °C.

Carnoy's solution

60 % (v/v) ethanol

30 % (v/v) chloroform

10 % (v/v) glacial acetic acid

Store at 4 °C.

Coating buffer

50 mM Na₂CO₃/NaHCO₃ (pH 9.6)

CS1

450 mM NaCl

3.72 % (m/v) EDTA

5 mM Tris

Sterilise by autoclaving and store at 4 °C.

Before using, add DMSO to a final concentration of 10 % (v/v) and Triton-X 100 to a final concentration of 1 % (v/v). Use within 2 hours afterwards.

CS2

1 mM EDTA

300 mM NaOH (pH 13)

Sterilise by autoclaving and store at 4 °C.

CS3

0.1 M Tris-HCl buffer (pH 7.5)

Sterilise by autoclaving and store at 4 °C.

Eluent 1

25 mM Tris-HCl (pH 8.0)

0.5 % acetonitrile

Eluent 2

25 mM Tris-HCl (pH 8.0)

800 mM NH₄Cl

0.5 % acetonitrile

ENA washing solution

Ethanol with 0.1 % (v/v) acetic acid

GST mix

100 µL of GSH 200 mM in water

100 µL of CDNB 0.1 mM in 96 % ethanol

9.8 mL of Dulbecco phosphate buffered saline

Prepare fresh before use.

LB medium (Luria-Bertani medium)

1 % (m/v) yeast extract

2 % (m/v) tryptone

2 % (m/v) NaCl

Adjust pH to 7.0 with NaOH. Sterilise by autoclaving and store at 4 °C.

LS1

0.32 M sucrose

5 mM MgCl₂

TrisHCl 10 mM (pH 7.5)

Triton-X 1 % (v/v); added after sterilization in autoclave

Store at 4 °C.

LS2

100 mM NaCl

5 mM EDTA (Na₂)

Store at RT.

MIC buffer

100 mM NaH₂PO₄ (pH 7.4)

150 mM KCl

1 mM EDTA

1 mM DTT

87 % (v/v) glycerol

Store at 4 °C.

PBS (phosphate buffered saline, pH 7.4)

8.3 mM Na₂HPO₄

1.5 mM KH₂PO₄

136 mM NaCl

2.7 mM KCl

Sterilise by autoclaving and store at 4 °C.

PMS buffer

100 mM NaH₂PO₄ (pH 7.4)

150 mM KCl

1 mM EDTA

1 mM DTT

Store at 4 °C.

TBE (5x)

446 mM Tris base

445 mM boric Acid

10 mM EDTA (pH 8.0)

Sterilise by autoclaving and store at RT. Dilute to 1xTBE working solution.

TPBS

0.05 % (v/v) Tween-20 in 1xPBS

2.1.3 Biological material**2.1.3.1 Antibodies**

- Polyclonal rabbit anti-fish CYP1A antibody (Biosense Labs, Norway)
- Alkaline phosphatase-labeled anti-rabbit antibody, produced in goat (Sigma, USA)

2.1.3.2 Enzymes

- Ribonuclease A (RNase A), DNase and protease-free (Thermo, USA)
- *Eco47I* restriction enzyme (Thermo, USA)
- *MvaI* restriction enzyme (Thermo, USA)
- DNase I, RNase-free (Thermo, USA)

2.1.3.3 Nucleotides

- dTTP solution (Thermo, USA)
- dCTP solution (Thermo, USA)
- dATP solution (Thermo, USA)
- dGTP solution (Thermo, USA)

2.1.3.4 DNA size markers

- GeneRuler DNA Ladder Mix, ready-to-use (Thermo, USA)

2.1.3.5 Plasmid DNA

- pUC19 vector (Thermo, USA) - see appendix I for additional information
- p158 plasmid (kindly provided by G. Doria) - see appendix I for additional information

2.1.3.6 Oligonucleotides

All modified-oligonucleotide were purchased from STABVida (Portugal). Sequences and specifications are displayed below.

Aptamer	Sequence (5' → 3')	Probability at 20° C (kJ/mol)
XBA-DNA	Thiol-C6-AGG GCA CGT GTA TTA CCC TAG TGG TCG ACG TCG	-19.34
His-945	Thiol-C6-TTA GGC ATC GGA AAG TGG GTT GAT GTA AGT AAC AGG CGA TGC	-33.20

2.1.4 Equipment

- Ultrasonic bath Transsonic TI-H-5 (Elma, Germany)
- Ultrasonic probe UP100H, 1 mm tip diameter (Heilscher, Germany)
- Sonoreactor UTR200 (Heilscher, Germany)
- VialTweeter (Heilscher, Germany)
- Ultrasonic bath Elmasonic S10H (Elma, Germany)
- Wide Mini-Sub Cell GT electrophoresis cell with PowerPac Basic power supply (Bio-Rad, USA)
- Sub-Cell model 96 electrophoresis cell (Bio-Rad, USA)
- Gel Doc XR+ Molecular Imager system (Bio-Rad, USA)
- HPLC pump P680 and ASI-100 autosampler, coupled to a DAD-3000RS (Dionex, USA)
- Savant SpeedVac concentrator SVC-100 (Thermo, USA)
- Thermal Cycler DNA Engine (Bio-Rad, USA)
- Thermal Cycler MyCycler (Bio-Rad, USA)
- pH 21 pH/mV meter with glass electrode (Hanna, USA)
- Orbital incubator OrbiSafe TS Netwise (Sanyo, Japan)
- Sigma 3-16K refrigerated centrifuge (Sartorius, Germany)
- Sigma 1-14 microcentrifuge (Sartorius, Germany)
- UV-Vis Spectrophotometer UV Mini-1240 (Shimadzu, Germany)
- UV-Vis Spectrophotometer Nanodrop ND-1000 (Nanodrop Technologies, USA)

- Microplate reader Infinite M200 with Absorbance module (Tecan, Switzerland)
- SZ-100 Nanoparticle Analyzer (Horiba, Japan)
- Ultraflex TOF/TOF mass spectrometer, equipped with a reflectron (Bruker, Germany)
- DMLB microscope, coupled with a DFC480 digital camera (Leica, Germany)
- EL6000 light source for DMLB microscope ((Leica, Germany)
- I3 and N2.1 filters for DMLB microscope ((Leica, Germany)

2.1.5 Specialised materials

- Quartz absorption cells (Hellma, Germany)
- 384-well small volume, microplates, black (Greiner Bio-One, Germany)
- 96-well microplates, transparent (Greiner Bio-One, Germany)
- 96-well ELISA microplates, transparent (Greiner Bio-One, Germany)
- NAP-5 columns (GE Healthcare, Sweden)
- Zeta-potential cells (Hellma, Germany)
- Glass microscope slides with ground edges (Normax, Portugal)
- Glass coverslips for microscope slides, 24x50 mm (Normax, Portugal)

2.4 Methods

2.4.1 Molecular biology

2.4.1.1 Plasmid DNA isolation

Plasmid DNA isolation was performed according to the alkaline lysis protocol described in Baptista (2000).

1. 100 mL of LB medium supplemented with 100 µg/mL ampicilin were inoculated with 100 µL of a glycerol stock, previously prepared from an isolated *E.coli* colony. The culture was grown for 14 hours, at 37 °C with constant agitation (200 rpm).
2. a) From the grown culture, a volume of 700 µL was pipetted to an eppendorf tube and 300 µL of glycerol were added. The culture stock was mixed by inversion and stored at -80°C.
 - b) The remaining culture was used for plasmid extraction via alkaline lysis protocol. Culture was transferred to 1.5 mL Eppendorf tubes and centrifuged 8 000xg and the supernatant was discarded. Two consecutive centrifugations were performed per tube, in order to maximize the number of pelleted cells. Pelleted celles were resuspended in 150 µL of AL1 solution.
3. Tubes were placed in ice for 5 min.

4. 300 μL of AL2 solution were added and the tube was gently inverted to mix and placed in ice for 5 min.
5. 225 μL of AL3 solution were added and solution was mixed by inverting the tube. Tubes were left on ice for 30 min.
6. The tubes were centrifuged for 15 min, at 15 000xg, at 4 °C.
7. After centrifugation, 630 μL (c.a. 1 vol.) from the supernatant were transferred to a clean 2 mL tube. 1 260 μL of ice-cold absolute ethanol (ca. 2 vol.) were added to each tube, and tubes were left for 2 hours in the freezer, at -20 °C.
8. Samples were centrifuged for 10 min, at 15 000xg, at 4 °C. Afterwards the supernatants were discarded, whereas the pellets were washed 2 times with ice-cold 70% ethanol and dried.
9. Pellets were resuspended in 200 μL of sterile water per tube. At this step, the number of tubes was reduced by one third, by pooling together samples from 3 tubes.
10. Afterwards, RNase A was added to a final concentration of 200 $\mu\text{g}/\text{mL}$, and digestion was carried at 37 °C for 2 hours.
11. A microextraction step followed. Firstly, 600 μL (ca. 1 vol.) of TE-buffered phenol were added, the solution was mixed by inversion for 1 min and centrifuged for 5 min, at 15 000xg, RT.
12. The aqueous (upper) phase was removed to a new tube and 600 μL of a chloroform:isoamyl alcohol (24:1) solution were added. The solution was mixed by inversion for 1 min and centrifuged for 5 min, at 15 000xg, RT.
13. The aqueous (upper) phase was removed to a new tube. To this solution, 2 volumes of ice-cold absolute ethanol (c.a. 1 100 μL) and 1/10 volumes of 3 M sodium acetate (pH 7.5) were added. The tubes were left for 2 hours in the freezer, at -20 °C.
14. The tubes were centrifuged for 15 min, at 15 000xg, at 4 °C. The supernatants were discarded and pellets were washed 3 times with ice-cold 70 % ethanol, dried and resuspended in 40 μL of sterile water.

2.4.1.2 Genomic DNA isolation from total blood

The genomic DNA isolation protocol was employed in different samples: chicken blood and goldfish hepatopancreas. The presented volumes were optimised for chicken total blood. Protocol was scaled-down when employed to DNA isolation from goldfish hepatopancreas. For blood, samples were thawed and transferred to an Eppendorf or falcon tube (depending on the volume), whereas for hepatopancreas, samples were weighted and crushed beforehand in a small volume of PBS buffer.

1. After thawing/crushing, samples were transferred to new tubes and 10 volumes of cold LS1 were added. The solution was gently mixed on ice for 10 min.
2. Tubes were centrifuged at 9 170xg, at 4° C for 10 min and the supernatant was discarded.
3. The pellet was carefully resuspended in 2 mL of LS2.

4. Afterwards, 250 μL of SDS 10 % and 50 μL of proteinase K were added. The mixture was incubated at 55° C for a minimum of 3 h with agitation.
5. A salting-out step followed, by adding 1 mL of saturated sodium chloride and mixing carefully by inverting the tube.
6. Tubes were centrifuged at 5 000xg, for 15' at 15° C and supernatant was carefully removed to a new tube.
7. Precipitation was achieved by adding 2 volumes of ice-cold absolute ethanol, mixing and leaving the tubes for 2 h in the freezer (-20° C).
8. Tubes were centrifuged at 15 000xg, for 10' at 4° C, the supernatant was discarded and the pellet was washed with 70 % cold ethanol.
9. The pellet was resuspended in 500 μL of sterile water and 10 μL of RNase (DNase free) were added to the DNA. Solution was incubated at 37° C with agitation for 2 h.
10. After incubation, 500 μL phenol were added and mixed by inverting the tube. Solution was centrifuge at 15 000 xg, for 20 min.
11. The aqueous phase was removed and 500 μL of chloroform were added. The tube was mixed by inversion and centrifuged at 15 000xg, for 10 min.
12. The aqueous phase was removed to a new tube. 2 volumes of absolute ethanol (-20°C) and 1/5 volumes of saturated sodium chloride were added to the solution, and left for 2 h in the freezer (-20° C).
13. Genomic DNA was precipitated by centrifugation at 15 000xg, for 10 min at 4° C and the pellet washed 2 times with 70 % ethanol (-20°C) and subsequently dried.
14. Ready-to-use genomic DNA was resuspended in 100 μL sterile water.

2.4.1.3 *In vitro* alkylation of nucleotides

1. Glycidamide-guanine (GA-Gua) adducts were produced by reacting 5 mM glycidamide (GA) with 1 mM dGTP at 37° C, for 72 h (pH between 7.0 and 7.5). The final volume used was 100 μL .
2. DNA adducts were produced by reacting 5 mM of GA with 500 $\mu\text{g}/\text{mL}$ of genomic DNA at 37° C, for 72 h (pH between 7.0 and 7.5). The final volume used was 100 μL .
3. After alkylation, the mixtures were heated up to 100° C for 15 min to release the alkylated guanines (Martins et al. 2007).

2.4.2 Sample preparation

2.4.2.1 Ultrasonic procedure and agarose gel electrophoresis

1. Standard ultrasonication was performed in 1.5 mL tubes with a total volume of 100 μL and final DNA concentration of 100 $\mu\text{g}/\text{mL}$, using sterile (bidistilled) water as a solvent.

2. An initial assay was performed to compare DNA fragmentation through several ultrasonic systems: probe, sonoreactor, VialTweeter and ultrasonic bath (Figure 2.1). For more information on conditions, please refer to Table 3.1 in chapter 3.
3. In parallel, an assay was performed to evaluate the temperature variation with sonication time in the sonoreactor, probe and ultrasonic bath, using bidistilled water as a solvent, with a total volume of 1 mL. For the sonoreactor and probe, temperature was measured at least once each 10 seconds, for 1.5 min. For the ultrasonic bath, temperature was measured every 10 min, for 2 hours.
4. The following assay focused the sonoreactor apparatus, at different sonication conditions (described in chapter 3 - Table 3.2).
5. After sonication, all samples were stored at 4 °C and for subsequent analysis by agarose gel electrophoresis.
6. Agarose gel electrophoresis was carried out for 300 min, at 2 V/cm, with a 1 % agarose gel in 1xTBE, using 0.1 µg/mL of GeneRuler DNA Mix Ladder (Fermentas) as a molecular weight reference.
7. Following electrophoresis, agarose gels were post-stained for 20 min in an ethidium bromide (EtBr) bath (0.5 µg/mL of EtBr in bidistilled water). A subsequent washing step with bidistilled water was used to remove excess EtBr.
8. Acquisition was carried out using a GelDoc system (hood and transilluminator) with UV excitation and the Quantity One software from Bio-Rad.

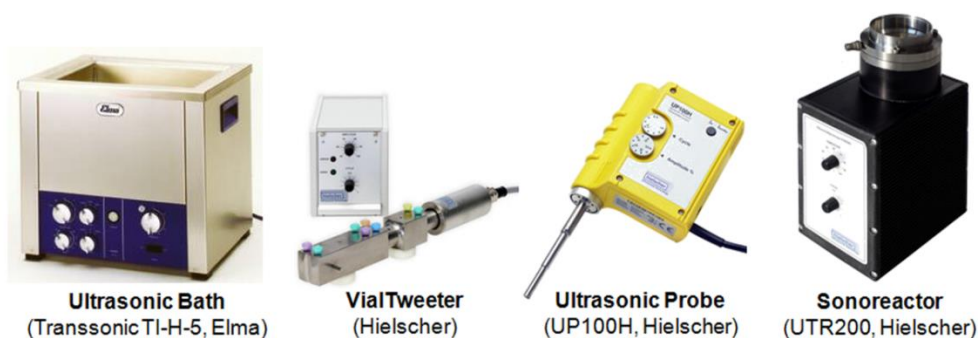


Figure 2.1. Image of the four ultrasonic devices utilised in the study.

2.4.2.2 Restriction enzyme digestion

Eco47I and *MvaI* were carefully chosen from a vast number of restriction enzymes, to produce a considerable amount of DNA fragments ranging from 100 to 1 000 bp.

1. Enzymatic digestion was carried out at 37 °C for 2 hours, in 1.5 mL tubes, with a final concentration of 1 enzyme unit/µg of DNA. Reaction buffers and mixtures were made according to the manufacturer.

2. Inactivation was performed at 65 °C, for 20 min. The digestion products were left at room temperature, to cool down, and stored at 4 °C for subsequent analysis.
3. Digestion products were analysed by agarose gel electrophoresis, following the previously mentioned experimental conditions.

2.4.2.3 Acceleration of nuclease digestion via ultrasonic energy

An unmodified pUC19 plasmid was used for this study.

1. Reaction mixtures were made in 150 µL tubes with a final volume of 20 µL, for 1 µg of plasmid DNA. DNaseI reaction buffer as present at 1x, according to the manufacturer.
2. For the first experiment, non-sonicated reactions were carried out at 37 °C, for 10 min. Sonicated reactions were treated for 10 min in a sonoreactor, with an amplitude of 50 %.
3. Afterwards, all reactions were inactivated by adding EDTA (1 mol EDTA for each mol of Mg²⁺) and incubating 15 min, at 70 °C.
4. Digestion products were analysed by agarose gel electrophoresis, following the previously mentioned experimental conditions.
5. For the second experiment, the same reaction conditions were used. The chosen final concentration of DNase I was 0.01 units, whereas the amplitude of sonication varied. Inactivation was performed as described, followed by agarose gel electrophoresis.

2.4.2.4 Sample treatment prior to HPLC analysis

1. BM mixture was divided into several 25 mL aliquots.
2. Aliquots were spiked with 100 µM of GA, dGTP or GA-Gua adducts (final concentrations), previously formed by *in vitro* alkylation. An additional aliquot spiked with bidistilled water was used as control.
3. Samples were concentrated to 1 mL by evaporation. Each sample was divided to 2 new tubes (2x500 µL).
4. A phenol:chlorophorm extraction was performed, according to the previously described procedure in section 2.4.1.2.
5. A desalting step with a NAP-5 column followed. Column was previously equilibrated with 3 volumes of bidistilled water. Afterwards, 500 µL of the sample were loaded in to the column. After adsorption was complete, the purified nucleotides were eluted with 1 mL of bidistilled water.
6. Samples were concentrated by evaporation for subsequent analysis by HPLC.

2.4.2.5 HPLC conditions

HPLC analysis of nucleotides was carried out using a DNAPac PA-100 column (4 x 250 mm), using a 4 x 50 mm guard column.

1. The whole system was washed O/N with filtered bidistilled water, at a flow of 0.1 mL/min.
2. Afterwards, mobile phase was set to a combination of Eluent 1 and Eluent 2 (90:10).
3. The entire system was washed and purged with the mobile phase.
4. Following the purge, the column was equilibrated with the mobile phase (90:10, Eluent 1:Eluent 2) for a minimum of 2 hours, at 0.2 mL/min. The backpressure was carefully monitored.
5. Afterwards, the flow was slowly increased to 1 mL/min, over 30 min. Once 1 mL/min reached, mobile phase was passed through the column for 30 min more.
6. After all preparations were made, acquisition was set to a wavelength of 254 nm. Nucleotides were analysed with a flow of 1.0 mL/min, applying the solvent gradient in Figure 2.2, with water injections between samples.

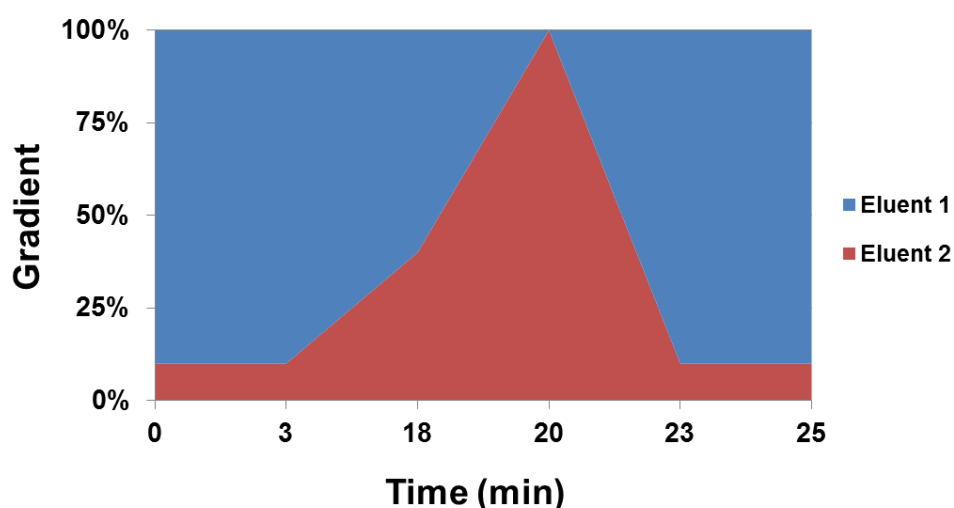


Figure 2.2. Solvent gradient utilised for HPLC nucleotide analysis.

2.4.2.6 Sample preparation for MS-detection: complete protocol

The complete protocol for sample preparation included DNA isolation, treatment with ultrasonic energy and nucleases, purification and concentration. A schematic representation of this protocol can be seen in Figure 3.11 (Chapter 3).

1. Genomic DNA isolation from goldfish hepatopancreas was performed as described in section 2.4.1.2.
2. Samples with a final volume of 100 μ L and a final DNA concentration of 100-200 μ g/mL were sonicated in a sonoreactor for 6 min, at maximum amplitude.

3. Afterwards, DNase reaction buffer and DNase I were added to final concentrations of 1x and 0.1 units per μg DNA, respectively. Reaction was carried at 37 °C, for 1 hour to ensure complete breakdown.
4. A phenol:chlorophorm microextraction followed, according to the conditions described in section 2.4.1.2.
7. The final purification step involved a NAP-5 column. Please refer to section 2.4.2.4 for the complete desalting protocol.
8. Samples were concentrated by evaporation, and quantified in a NanoDrop spectrophotometer, for subsequent MS-detection.

2.4.3 Nanotechnology

2.4.3.1 Gold nanoparticle synthesis by citrate reduction

Synthesis of gold nanoparticles via citrate reduction was performed as firstly described by Turkevich (1985) and extensively used within the Nanomedicine@FCT Research Group.

1. All glassware was previously immersed in Acqua Regia (3:1 HCl:HNO₃) overnight.
2. Glassware was washed with bidistilled water at least 5 times, and the pH inside the glassware confirmed to match the pH of the bidistilled water.
3. Using a 500 mL round bottom flask with a condenser, 250 mL of a 1 mM HAuCl₄ solution were boiled, with constant agitation.
4. While in reflux 25 mL of 38.8 mM trissodium citrate were quickly added and, upon verifying the subsequent colour change, both heat and stirring were maintained for 15 minutes.
5. After 15 minutes, the heat was turned off and stirring kept for an additional 20 minutes.
6. The solution was cooled down to room temperature and filtered using a 0.2 μm membrane filter.

2.4.3.2 Gold nanoparticle characterisation

1. An aliquot of the synthesised colloidal gold solution was diluted to reach a final concentration of ≈ 1.5 nM and UV-Vis behaviour was followed from 400 to 800 nm, on a 1240 UV-Mini spectrophotometer from Shimadzu (Japan).
2. A different aliquot was placed diluted to the same concentration in 0.1 M NaCl and UV-Vis behaviour was followed from 400 to 800 nm.
3. An aliquot of colloidal gold solution was diluted to reach a final concentration of ≈ 2.5 nM and divided into three parts.
4. The first part of this aliquot was analysed by transmission electron microscopy (TEM), as an external service, at the Microlab, Instituto Superior Técnico facilities in Lisbon, Portugal.

5. The second part was analysed by dynamic light scattering (DLS), at REQUIMTE, Faculdade de Ciências e Tecnologia, UNL. Analysis was carried out on a SZ-100 Nanoparticle Analyzer from Horiba Scientific (Japan), at a temperature of 20 °C, dispersion medium viscosity of 1 009 mPa.s and a scattering angle of 90 °C.
6. The remaining part was used for measurement of zeta-potential (ζ -potential), at REQUIMTE, Faculdade de Ciências e Tecnologia, UNL. Analysis was carried out on a SZ-100 Nanoparticle Analyzer from Horiba Scientific (Japan), at a temperature of 20 °C, dispersion medium viscosity of 1 009 mPa.s and an electrode voltage of 3.3 V.

2.4.3.3 Aptamer-gold nanoprobe synthesis

Synthesis of aptamer-gold nanoprobes was performed essentially as described by Baptista et al. (2005a) and extensively used within the Nanomedicine@FCT Research Group.

1. A solution of thiol-modified aptamers was extracted three times with 2 volumes of ethyl acetate, at 15 000xg, for 5 min each.
2. Meanwhile, a DNA grade NAP-5 column was washed and equilibrated with 3 volumes of phosphate buffer 10 mM (pH 8.0).
3. After three extractions complete, the aqueous phase was loaded into the column for the aptamer to adsorb to the resin.
4. When adsorption was complete and the first fraction washed out, the adsorbed aptamer was eluted with 1 mL of phosphate buffer 10 mM (pH 8.0), collected and immediately placed into ice.
5. The solution was analysed via UV-Vis spectrophotometry to assess OD₂₆₀ and ensure no traces of DTT were still in solution.
6. Using the OD₂₆₀ value as a reference for quantification, a theoretical ration of 50 oligos per nanoparticles was calculated.
7. According to this ratio, AuNPs and aptamers were added to react in phosphate buffer 10 mM (pH 8.0), with 0.01 % SDS (final concentration).
8. After 20 minutes, the salt-aging procedure began. Phosphate buffer 10 mM (pH 8.0) containing NaCl was added, to reach a final NaCl concentration of 0.05 M. The solution was sonicated for 10 s and incubated for an additional 20 min, at RT.
9. After 20 minutes, final NaCl concentration was raised to 0.1 M. The solution was sonicated for 10 s and incubated for an additional 20 min, at RT.
10. After 20 minutes, final NaCl concentration was raised to 0.2 M. The solution was sonicated for 10 s and incubated for an additional 20 min, at RT.
11. After 20 minutes, final NaCl concentration was raised to 0.3 M. The solution was sonicated for 10 s and incubated for 16 hours, at RT

12. After incubation, the aptamer-gold nanoprobe solution was centrifuged for 20 min, at 15000xg, at RT.
13. The supernatant was discarded, the pellet resuspended in phosphate buffer 10 mM (pH 8.0) and solution was centrifuged for 20 min, at 15 000xg, at RT.
14. Step 13 was repeated one more time.
15. The supernatant was discarded, and the pellet resuspended in phosphate buffer 10 mM (pH 8.0), with 0.1 M NaCl. The solution was centrifuged for 20 min, at 15 000xg, at RT.
16. After the final washing step, the supernatant was discarded and the pellet was resuspended in a small volume of phosphate buffer 10 mM (pH 8.0), with 0.1 M NaCl.
17. The nanoprobe solution was analysed via UV-Vis spectrophotometry to assess the redshift in the maximum absorption band and for quantification purposes.

2.4.3.4 Stability of aptamer-gold nanoprobes

All colorimetric tests with aptamer-gold nanoprobes were performed on 384-well microplates, in triplicate and spectra/absorbance values were recorded on an Infinite 2000 Microplate Reader from Tecan (Switzerland). Procedures for reaction mixtures and colorimetric assays follow those described in Baptista et al. (2005a), Doria et al. (2007), Conde et al. (2010) and Doria (2010), for instance.

1. Reaction mixtures were performed in 150 μ L tubes, to a final volume of 30 μ L, containing phosphate buffer (pH 8.0) and the aptamer-gold nanoprobes, to final concentrations of 5 mM, and 2.5 nM, respectively. Sterile water was used to adjust the final volumes, when necessary.
2. The mixtures were heated at 95 $^{\circ}$ C, for 10 min and let cool down to RT for 30 min.
3. After cooling down, MgCl₂ was added to each tube, to attain the desired final concentrations (0-120 mM).
4. The microplates were stored for 15 minutes, to for allow colour developing. Afterwards, spectrophotometric behaviour of the nanoprobes was followed from 400 to 800 nm.
5. The Areas Under the Curve ratio (AUC) between the disperse (from 500 to 550 nm) and the aggregated (from 580 to 630 nm) fractions of the nanoprobe was estimated and used as an analytical tool for evaluating stability.

2.4.3.5 Colorimetric assays with aptamer-gold nanoprobes

1. Reaction mixtures were performed in 150 μ L tubes, to a final volume of 30 μ L, containing phosphate buffer (pH 8.0) and the aptamer-gold nanoprobes to final concentrations of 5 mM, and 2.5 nM, respectively.
2. To the mixtures, the analyte was added to the desired final concentration. The analytes varied according to the test: i) dNTPs; ii) GA-alkylated and non-alkylated dGTP; iii) GA-alkylated and non-alkylated genomic DNA. Sterile water was used to adjust the final volumes, when necessary.

3. The mixtures were heated at 95 °C, for 10 min and let cool down to RT for 30 min.
4. After cooling down, MgCl₂ was added to each tube, to the threshold concentration determined beforehand (60 mM for the XBA-nanoprobe and 100 mM for the His-945 nanoprobe). Sterile water was used to adjust the final volumes, if necessary.
5. The microplates were stored for 15 minutes, to allow for colour developing. Afterwards, spectrophotometric behaviour of the nanoprobe was followed from 400 to 800 nm.
6. The Areas Under the Curve ratio (AUC) between the disperse (from 500 to 550 nm) and the aggregated (from 580 to 630 nm) fractions of the nanoprobe was estimated and used as an analytical tool for discrimination.

2.4.4 Mass spectrometry

2.4.4.1 Characterisation of organic matrices

1. Different commonly used matrices were prepared in 50:50 water:acetonitrile (by default) and consecutive dilutions were made to attain different concentrations. When necessary, organic solvent proportion was adjusted to increase solubility.
2. UV-Vis characterisation of organic matrices was carried in a NanoDrop spectrophotometer using 2 µL of solution. The Hi-Abs mode was used, considering an optical path of 0.1 mm.
3. UV-Vis spectra were analysed and a relation was established between matrix concentration and the absorbance value at 337 nm.
4. For mass spectrometry, matrix solutions were diluted to reach 3 different final concentrations (5, 2.5 and 1.25 mg/mL), and spotted on a steel plate.
5. Additional spots were prepared with matrix (same final concentrations) in the presence of 0.5 mM dGTP.
6. Analysis was carried out following the conditions described below.

2.4.4.2 Sample deposition and MS-detection

Samples were analysed as an external service at the C.A.C.T.I., Universidade de Vigo facilities in Vigo, Spain.

1. For identification of nucleotides by MALDI, the final concentrations of analyte and matrix were 500 µM and 5 mg/mL, respectively.
2. For identification of nucleotides by AuNP-SALDI, the final concentrations of analyte and AuNPs were 500 µM and 15 nM, respectively. The final concentrations of analyte and AuNPs were constant throughout the work, unless stated otherwise (*e.g.* variation of analyte concentration).
3. For analysis of GA-Guanine adducts formed by *in vitro* alkylation, AuNP and analyte final concentrations were kept at 15 nM and 500 µM, respectively.

4. Each sample was mixed 1:1 with the chosen matrix or AuNP solution. Afterwards, 1 μL of that mixture was spotted onto an AnchorChip 600/384 Target plate (Bruker, Germany) and allowed to dry at RT, protected from light. All analyses were performed in triplicate.
5. For analysis of DNA adducts in biological samples, solutions containing fragmented genomic DNA were evaporated and later resuspended in matrix or AuNP solution to attain final concentrations of 5 mg/mL or 15 nM, respectively. The volume was calculated so that each spot contained the equivalent to 1 μg of fragmented genomic DNA. All analyses were performed in triplicate.
6. Samples were analysed using an Autoflex MALDI-TOF system from Bruker (Germany) equipped with a reflectron, according to the following conditions:

	Conditions	Positive-Ion mode	Negative-Ion mode
Spectrometer	Ion source voltage 1 (kV)	19	19
	Ion source voltage 2 (kV)	16.54	16.55
	Ion source lens voltage (kV)	8.65	8.70
	Operation mode	Reflector	Reflector
	Reflector 1 (kV)	21	21
	Reflector 2 (kV)	9.7	9.7
	Ion extraction delay (ns)	0	0
	Suppression mode	Deflection	Deflection
	Suppressed up to (Da)	30	30
Detection	Detection gain reflector	6.8x	7.1x
	Sample rate (GS/s)	1	1
Laser setup	Laser frequency (Hz)	200	200
	Number of added shots	600	1200
	Laser power	45 %	45 %

7. Mass spectra were acquired using the FlexControl software from Bruker (Germany) and treated using the mMass open source Mass Spectrometry tool (Strohalm et al. 2008, 2010).

2.4.5 Toxicity assays

2.4.5.1 Experimental design for acute toxicity assay on goldfish

1. Goldfish (*Carassius auratus* L.), ≈ 6 cm standard length and ≈ 4 g average total wet weight, were obtained from national producers (Koi Park, Portugal).
2. Prior to the beginning of the experiments, fish were acclimated in 400 L polystyrene tanks for two weeks, in a closed circuit system with filtered dechlorinated tap water at a pH of 7.4 ± 0.2 , at a temperature of 19 ± 1 °C, under a 12 h light: 12 h dark photoperiod and with continuous aeration.
3. Following the acclimation period, mature fish ($n = 8$ biological replicates per treatment) were randomly distributed into 10 L volume polystyrene tanks in groups of eight fish per tank.
4. Static exposure of fish to different concentrations of acrylamide (50 to 200 mg/L) in each tank was conducted at high density (32 g fish per 10 L water) and a feeding condition of 96 hours, using an additional tank with clean tap water as control. During the experiment, fish were fed *ad libitum* with commercial feed. Exposure concentrations were chosen in accordance with the scant LC₅₀ information for other freshwater teleosts, reporting the threshold in excess of 100 mg/L (Krautter et al. 1986, Walker 1991, Weston et al. 2009).
5. Mortality and morbidity was recorded continuously to determine LC₅₀, estimated using the US EPA Probit software v3.2.

2.4.5.2 Experimental design for acute and chronic toxicity assays on mussels

1. Mediterranean mussels, *Mytilus galloprovincialis*, (c.a. 36x20 mm shell size) were collected from the intertidal zone of a clean site in NW Portuguese coast (c.a. 250 individuals).
2. Prior to the beginning of the experiments, mussels were acclimated in 50 L polystyrene tanks for one week, arranged in a closed circuit system with clean seawater (pH 7.65 ± 0.2 , temperature of 19 ± 1 °C, and salinity of 31 ± 1 ‰) under a 12 h light: 12 h dark photoperiod, with continuous aeration. The same water was used to in the bioassays.
3. Following the acclimation period, mussel individuals ($n = 15$ biological replicates per treatment) were randomly distributed to a duplicate array of 15 L polystyrene tanks. The concentrations of acrylamide ranged between 100 and 2 000 mg/L, in face of the absent information on acrylamide LC₅₀ for bivalves (all concentrations depicted in Table 5.3).
4. Static exposure of mussels to different concentrations of acrylamide (100 to 2 000 mg/L) in each tank was carried for 96 hours, using an additional tank with seawater as control. During the experiment, mussels were fed *ad libitum* with *Dunaliella salina*.
5. Mortality and morbidity was recorded continuously to determine LC₅₀, estimated using the US EPA Probit software v3.2.
6. Following acute exposure and information retrieved on LC₅₀, a chronic exposure assay was conducted. This consisted of a semi-static disposition of 15 L tanks with 39 randomly-selected mussels ($n = 13$ biological replicates per test) exposed to 1 and 10 mg/L acrylamide, with an

additional tank with seawater as control.

7. Exposure was performed during 21 days, with water changes (100 %) done every 48 hours to ensure constancy of water parameters. Feeding was provided as mentioned above.

2.4.5.3 Genotoxicity assessment

Genotoxic effects were assessed in freshly-collected whole peripheral blood cells for clastogenic and strand breakage levels through the erythrocyte nuclear abnormalities (ENA) and Comet assays, respectively.

2.4.5.3.1 Erythrocyte nuclear abnormality (ENA) assessment

ENA assessment was performed according to Costa and Costa (2007).

1. Following the experimental period, fish were collected and blood sampled from the caudal peduncle with EDTA-treated syringes as anticoagulant.
2. A drop of freshly-collected blood was smeared on a glass microscopy slide and left to dry at room temperature.
3. After drying, preparations were fixed with methanol for 15 min and left to dry, protected from light and humidity.
4. Preparations were stained with a 100 mg/L acridine orange solution for 45 min, protected from light.
5. Excess staining solution was by rinsing slides in ENA washing solution, subsequent washing in ethanol for 1 minute and dried at room temperature, protected from light.
6. After drying, preparations were mounted with DPX resin and xylene.

The frequency of cells exhibiting nuclear abnormalities was determined by observing at least 1000 mature erythrocytes per preparation. Abnormalities such as micronuclei, nuclear buds, polynucleated cells and fragmenting nuclei were considered for this analysis.

2.4.5.3.2 Single-cell gel electrophoresis (comet-assay)

The Comet assay (alkaline) was performed according to Singh et al. (1988) and adapted by Costa et al. (2008) for fish blood.

1. To ensure a successful experiment, glass microscope slides were coated beforehand with 1.5 % (w/v) agarose in 1xTAE, and left to dry in a kiln for 48 hours.
2. After sampling, blood aliquots were diluted 1:200 in cold PBS and diluted in 1 % (w/v) liquid low melting-point agarose (LMPA) in PBS.
3. 100 μ L of the dilutions was dropped on previously coated microscopy slides, covered with a

glass coverslip and immediately placed at 4 °C, for 30 min.

4. After agarose solidification, coverslips were removed and the slides were dipped into the comet Lysis solution (CS1) during 1 h, at 4 °C, protected from light.
5. Following lysis, slides were placed for 40 min into cold CS2 buffer.
6. Electrophoresis was then carried out in CS2 buffer, at 4 °C, for 30 min, at 25 V, using a Sub-Cell model 96 apparatus (Bio-Rad).
7. Slides were neutralised in CS3 solution during 15 min.
8. Staining with 20 µg/mL of ethidium bromide was performed for subsequent epifluorescence microscopy analysis.

For the analysis, approximately 100 intact comets per slide were scored, using the CometScore software (TriTek, USA). The average value of DNA percentage in tail per individual was used as direct indicator of total DNA strand breakage.

2.4.5.4 Sampling and preparation of goldfish PMS and microsomal fractions

Goldfish hepatopancreas tissue was prepared as described by Nilsen et al. (1998).

1. Following the experimental period and collection of blood samples for genotoxicity, goldfish were euthanised by cervical sectioning and hepatopancreas samples were excised and stored for further analysis (at -80 °C).
2. Previously stored samples were thawed on ice and homogenised in PMS buffer using 4 mL per g of sample.
3. Homogenates were centrifuged at 12 000xg for 20 min at 4 °C and the postmitochondrial supernatants (PMS) were collected.
4. Collected PMS were further centrifuged for 60 min at 100 000xg at 4 °C and resulting pellets (microsomal fractions) were resuspended in MIC buffer and stored at -80 °C.
5. Sub-samples of PMS fractions were collected to new tubes and also stored at -80 °C.

Total protein concentration of the samples was estimated by the Bradford assay, using BSA as standard (Bradford, 1976) and biochemical biomarker responses were normalised to total protein concentration (calibration curves are presented in Appendix II).

2.4.5.5 Sampling and preparation of mussel whole-body homogenates

1. Following the experimental period, mussel individuals were collected and dissected with the aid of a scalpel. Two similar soft-body sections were produced, one for histology, other for biochemical analysis.
2. The soft-body halves for biochemical analysis were homogenised in 600 µL of 1xPBS

(phosphate buffered saline).

3. Afterwards samples were centrifuged at 12 000xg, for 20 min, at 4 °C and the pellet discarded to obtain the cleared homogenates. All supernatants were stored at -80 °C for subsequent biomarker analysis.

Total protein in samples was determined by the Bradford assay, using BSA as standard (Bradford, 1976) and all biochemical biomarker responses were normalised to total protein concentration (calibration curves are presented in Appendix II).

2.4.5.6 Analysis of CYP1A induction

Cytochrome P4501A (CYP1A) was determined as described by Nilsen et al. (1998).

1. Previously collected microsomal fractions were diluted in ice cold coating buffer.
2. In each well of a 96-well ELISA microplate 50 µL of the sample were immobilised, with 3 replicas per sample. Microplates were incubated overnight at 4 °C.
3. Each well was washed three times with TPBS.
4. After the washing step, 100 µL of blocking solution was added to each well and microplates were incubated for two hours, at room temperature.
5. Each well was washed three times with TPBS.
6. After washing, 50 µL of the anti-CYP1A polyclonal antibody solution (diluted 1:100 in PBS) were added, with subsequent incubation at 37 °C for 1 hour.
7. Each well was washed three times with TPBS
8. After washing, 50 µL of the alkaline phosphatase (AP)-labelled secondary antibody (diluted 1:1000 in PBS) were added to each well and the microplates incubated at room temperature for 1 h.
9. Each well was washed five times with TPBS.
10. After washing, 50 µL of *p*-nitrophenylphosphate (pNPP) developing solution was added to each well, followed by 30 min incubation at room temperature.
11. To stop the reaction, 50 µL of 5 M NaOH were added to each well.
12. The absorbance was measured at 492 nm using a microplate reader and obtained results were normalised to the total protein concentration, previously estimated by the Bradford assay. Due to the absence of a commercial CYP1A standard as a reference, results were expressed as fold change relatively to the control group.

2.4.5.7 Discontinuous ethoxyresorufin-O-deethylase (EROD) spectrophotometric assay

EROD activity was measured through the discontinuous method, adapted from De Almeida et al. (2011).

1. A reaction mixture was prepared in Tris-HCl 50 mM (pH 7.4), containing 1.0 mg/mL of BSA, 5 μ M of 7-ethoxyresorufin and 0.5 mM of NADPH (final concentrations).
2. On a 96-well microplate, 20 μ L of the sample and 150 μ L of the reaction mixture were incubated for 20 min, at 37 °C, in the dark, with 3 replicas per sample.
3. Afterwards, reaction was stopped by adding 100 μ L of 2 M glycine (pH 10.4).
4. Absorbance at 572 nm was recorded, and data analysed according to a resorufin calibration curve, within the 0.78125 - 50 μ g/mL linear range (calibration curves are presented in Appendix II).

2.4.5.8 Activity of acetylcholinesterase (AChE)

Determination of AChE activity was performed via quantification of thiocholine, following Ellman et al. (1961).

1. A DTNB solution of 270 μ M in 50 mM sodium phosphate (pH 7.4) was prepared beforehand.
2. On a 96-well microplate, 50 μ L of the sample were added, with 3 replicas per sample.
3. Different wells for the positive (standard AChE from electric eel) and negative control were included, also with 3 replicas.
4. Subsequently, 150 μ L of DTNB solution were added to all wells.
5. Afterwards, 50 μ L of 3 mM ACTI were added to all wells.
6. Absorbance at 412 nm was recorded for 15 min.

2.4.5.9 Analysis of glutathione-S-transferase (GST) activity

GST activity was determined following the procedure described by Habig et al. (1974) and optimised for 96-well microplates.

1. On a 96-well microplate, 20 μ L of the PMS fraction was added, with 3 replicas per sample.
2. Different wells for the positive and negative control were included, also with 3 replicas.
3. To each well (either containing sample or control), 180 μ L of GST mix were added.
4. Mixtures were incubated for 1 minute and afterwards, the absorbance at 340 nm was measured at every minute during 10 minutes. Equine liver GST (Sigma-Aldrich) was used as positive control. The results were normalised to total protein concentration determined by the Bradford assay.

2.4.5.10 Analysis of catalase (CAT) activity

Catalase activity was assessed by measuring the concentration of formaldehyde produced from methanol in the presence of hydrogen peroxide using a spectrophotometric method described by

Johansson and Borg (1988), adapted to the microplate reader.

1. On a 96-well microplate, 20 μL of the sample were added, with 3 replicas per sample.
2. In different wells, 20 μL of bovine liver catalase were added, as a standard.
3. Subsequently, 30 μL of 100 % methanol were added to all wells.
4. Afterwards, 100 μL of 50 mM phosphate buffer (pH 7.4) were added to all wells.
5. To each well, 20 μL of hydrogen peroxide were added, to reach a final concentration of 0.035 M, and mixtures were allowed to react for 20 min.
6. The reaction was stopped by adding 30 μL of 10 M potassium hydroxide.
7. Afterwards, 30 μL of 35 mM Purpald were added to the mixture and samples allowed to incubate for 10 min.
8. Finally, 10 μL of 65.2 mM Potassium periodate were added as colour developer.
9. Absorbance was measured at 540 nm and results were quantified using a formaldehyde standard curve within the 0-75 μM range (calibration curves are presented in Appendix II).

2.4.5.11 Analysis of total antioxidant capacity (TAC)

Total antioxidant capacity of the samples was determined using a modified protocol according to the Trolox equivalent antioxidant capacity (TEAC) principle (Miller et al. 1993).

1. On a 96-well microplate, 10 μL of the sample were added, with 3 replicas per sample.
2. To each well 10 μL of myoglobin and 150 μL of ABTS were added (final concentrations of 4.5 μM and 300 μM , respectively).
3. Afterwards, 40 μL of hydrogen peroxide (final concentration of 250 μM) were added to initiate the reaction and the microplate was incubated for 5 min, RT.
4. Absorbance at 405 nm was recorded and results were analysed according to a Trolox standard curve, in the 0-1.5 mM linear range (calibration curves are presented in Appendix II).

2.4.5.12 Analysis of lipid peroxidation (LPO)

Lipid peroxidation was assessed via thiobarbituric acid-reactive species (TBARS) assay described by Uchiyama and Mihara (1978) and adapted to microplate reader by Costa et al. (2011).

1. Samples were incubated with two volumes of ice cold 10 % (m/v) trichloroacetic acid (TCA) for 15 min at 4 °C.
2. Samples were then centrifuged at 12 000xg, for 15 min.
3. Supernatants were mixed with an equal volume of 1% (m/v) thiobarbituric acid (TBA) and incubated for 15 min in a boiling water bath.

4. Samples were cooled on ice for 5 min to stop the reaction and then loaded onto a 96-well microplate.
5. Absorbance of the reddish pigment was measured at 530 nm. A malondialdehyde (MDA) standard curve was used for quantification, in the 0-0.1 μM linear range (calibration curves are presented in Appendix II).

2.4.5.13 Histological preparations and analysis

Histological preparations were obtained following essentially Martoja and Martoja (1967). Different procedures were employed for goldfish and mussels. Alterations are explained below.

1. Goldfish tissue samples were placed into a tube and fixed in Bouin-Hollande's solution over 48 h, at RT (c.a. 1 mL per 50-100 mg of tissue). As for mussels, half of an individual's soft body was fixed in Carnoy's solution over 5 h, at RT (c.a. 5 mL per g of tissue).
2. Samples were washed with distilled water (24 h for goldfish and 2 h for mussels), at RT.
3. Samples were placed into 70 % ethanol, until paraffination.
4. Paraffin pellets left in a kiln for c.a. 8 hours, at 62 °C to melt.
5. Meanwhile, samples were progressively dehydrated as follows: 2x15 min in 95% ethanol; 3x30 min in absolute ethanol.
6. Afterwards, 3x15 min in xylene was employed for intermediate impregnation.
7. After drying completely, samples were placed into liquid paraffin O/N (enough volume to cover all the sample tissue).
8. The following day, paraffin molds were cast and left to harden 15-20 min, at RT.
9. Paraffin-embedded sections were cut with a microtome (5-7 μm thick) and placed on microscopy glass slides.
10. Once preparations dried completely, deparaffination was carried out in xylene for 2x30 s.
11. Afterwards, preparations were rehydrated as follows: 30 s in absolute ethanol; 2x30 s in 95 % ethanol; 3 min in 70 % ethanol; 6 min in bidistilled water.
12. Preparations were stained with haematoxylin solution for 4 min and subsequently washed in distilled water for 2x2 min.
13. Preparations were placed 3 min in 70 % ethanol and subsequently stained with eosin for 2 min.
14. Afterwards, preparations were progressively dehydrated as follows: 30 s in 70 % ethanol; 2x30 s in 95 % ethanol; 2x30 s in absolute ethanol.
15. A final 30 s step in xylene was carried out. Preparations were let to dry O/N.
16. The following day, all slides were mounted with DPX resin and left to dry for at least 6 h.
17. Observations were carried out using a DMLB model microscope equipped with a DFC480 digital camera (Leica microsystems), on about 8 sections per slide, with at least 3 slides being prepared per specimen.

2.4.6 Statistical analysis

All statistics were performed using the Statistica10 software from Statsoft Inc. (Tulsa, USA) considering a significance value of 95 % ($\alpha = 0.05$), following Zar (1998) and Sheskin (2000). The Kolmogorov-Smirnoff and Liliefors tests were employed to verify normality of data, and the Levene's test to evaluate homogeneity of variances.

2.4.6.1 Colorimetric assays with aptamer-gold nanoprobe

1. Colorimetric assays involving Au-nanoprobes were analysed using parametric methods: ANOVA and Tukey's honest significant difference (HSD) for multiple comparisons.

2.4.6.2 Estimation of effect concentrations

1. Effect concentrations (LC_{50}) were estimated via Probit model analysis, using the EPA Probit software v3.2 (EPA, USA).

2.4.6.3 Analysis of biomarker data

Analysis of all biomarker-related data was performed using non-parametric methods, following invalidation of at least one of the assumptions needed for parametric analysis.

1. The Kruskal-Wallis H test was used for multiple comparisons and to assess significant differences within all data.
2. Subsequently, the Mann-Whitney U test was employed to assess pairwise significant differences between treatments.
3. For the goldfish data, the Spearman rank-order R with Bonferroni correction was used to establish correlations between biomarker responses and exposure concentrations.
4. For the mussel data, a correlation-based principal component analysis (PCA) was employed to integrate data on all tested biomarkers.

CHAPTER 3. OPTIMISATION OF SAMPLE PREPARATION

Some of the results presented in this chapter have been published in Larginho M, Santos HM, Doria G, Scholz H, Baptista PV, Capelo JL. 2010. Development of a fast and efficient ultrasonic-based strategy for DNA fragmentation. *Talanta* 81:881-886, where Miguel Larginho was responsible for most of the experimental work (all experiments with ultrasonic energy and DNA) and writing part of the manuscript.

It is not enough to have a good mind; the main thing is to use it well.

René Descartes

3.1 Introduction

The main objective of the work portrayed in this chapter has always been the achievement of a suitable procedure for sample treatment, beginning with DNA isolation from a biological source, up to when the sample is spotted on the MALDI plate. This chapter includes all data obtained from experiments regarding sample preparation for subsequent detection.

The first section addresses ultrasonic fragmentation of DNA as a means to attain poly-, oligo- and, ultimately, free nucleotides from heavier and more complexed DNA molecules. At the same time, several ultrasonic platforms are evaluated in terms of efficiency, to ascertain the optimal and most economic method to achieve ideal fragments for downstream applications, such as biomolecular detection, via mass spectrometry (MS) for instance. The last part of this first section evaluates the feasibility of ultrasonic platforms when compared or combined to nuclease digestion. These results have not been discussed solely in the interest of MS-based detection, but also in the context of cellular and molecular biology techniques in general (e.g. PCR amplification or enzymatic treatments). However, throughout this chapter these methods will be integrated into a more complete protocol, ending with MS-based detection, and a comprehensive discussion provided on the advantages and drawbacks of these methodologies for sample treatment.

The second section of this chapter addresses liquid chromatography, mainly high performance liquid chromatography (HPLC) of nucleotide mixtures. This section evaluates the pros and cons of including a HPLC step in the overall protocol, for additional purification/separation and discusses the decisions made regarding this technique.

The final section presents the overall protocol for sample preparation before MS detection, from the moment of DNA isolation, up to when it is spotted in the MALDI plate.

Despite these techniques being very different, all have been included in the same chapter due to the common purpose, the development and optimisation of an ideal protocol for nucleotide sample preparation for MS-based detection. With this in mind, a brief introduction is in order where the basic concepts of each technique will be explained, before heading on to the Results and Discussion section.

3.1.1 Ultrasonic energy and DNA fragmentation

The use of ultrasonic energy as fragmentation procedure for DNA samples has been gradually gathering momentum as a robust approach to attain DNA fragments susceptible of use in downstream detection protocols with minimum additional purification. The growing development of biomolecular assays (e.g. diagnostics) for biomarker analysis or nucleic acid recognition increases the concern for optimal sample preparation. This is particularly relevant when the detection depends on the specific hybridisation of oligonucleotide probes (Mehlmann et al. 2005,

Liu et al. 2007, Vinogradova et al. 2007, Baptista et al. 2008) or the decomplexation and breakdown of high molecular weight DNA, where small DNA fragments with known molecular weight and concentration are required.

Ultrasounds are described as high frequency acoustic waves (20 kHz or higher) requiring a medium in order to propagate (Luque de Castro and Capote 2007, Mason and Lorimer 2002). When passing through an aqueous solution, acoustic waves cause the formation of microbubbles filled with gas (cavities), a process known as cavitation. Two types of cavitation have been described: stable cavitation (gas body activation) and inertial cavitation (transient or vaporous). Stable cavitation occurs during low intensities of ultrasound, but inertial cavitation requires high intensities of ultrasound. The latter is responsible for high energy events, considered to be extremely destructive to biological molecules (Miller et al. 1996). During inertial sonication, the size of microbubbles varies through several cycles of compression and rarefaction: first, there is a rapid increase in size, followed by a decrease, and this cycle continues until it implodes (see Figure 3.1). The high temperatures and high pressures inside the bubble are sufficient to cause hydrolysis, sonoluminescence phenomena (Suslick et al. 1999) and shearing of biological molecules in its vicinity (Miller and Thomas 1996). Besides cavitation, two additional phenomena may lead to the damage of biological molecules: mechanical and thermal degradation; and reaction with radicals generated from water (Pritchard et al. 1966, Peacocke and Pritchard 1968, Makino et al. 1983, O'Brien Jr. 2007). Also, the use of ultrasonic waves directly in cells was shown to induce DNA fragmentation and damage (Miller et al. 1995, Miller and Thomas 1996).

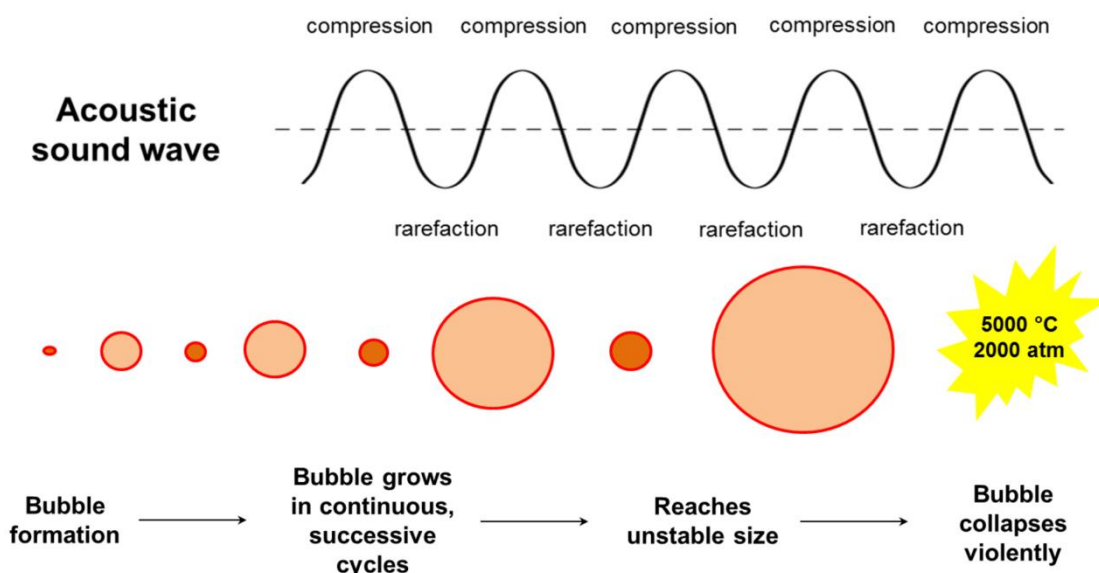


Figure 3.1. Generation and collapse of an acoustic cavitation microbubble. Adapted from Luque de Castro and Capote (2007), Mason and Lorimer (2002).

The study of the influence of acoustic shear waves in the behaviour of oligonucleotides (Cavic and Thompson 2002) has prompted the development of methodologies for DNA sample treatment relying on the use of ultrasonic probes resulting in efficient *in vitro* fragmentation of purified DNA, which can then be used in a multitude of biosensing applications (Mann and Krull 2004, Grokhovsky 2006). Several ultrasound platforms can be used towards DNA sample preparation, such as probes, sonoreactors, baths, etc., but previous studies describe only ultrasonic probes as a practical tool for DNA fragmentation (Mann and Krull 2004). Besides this, no data has yet been produced comparing these systems in terms of optimisation for ideal conditions towards DNA sample preparation.

3.1.2 Enzymatic hydrolysis of DNA molecules

In molecular biology and genetic engineering, nucleic acid cleavage is a most utilised and valuable tool by specialised enzymes, the nucleases. In terms of Enzyme Commission number, nucleases are classified as hydrolases (EC-number 3) for they catalyse the hydrolysis of a phosphodiester bond between two nucleotides in a polymeric chain (see Figure 3.2A). Nucleases may be classified into exonucleases and endonucleases. Exonucleases cleave the terminal nucleotide off the nucleic acid chain, yielding a monophosphate nucleoside and a polynucleotide, whereas endonucleases cleave the nucleic acid chain in different positions, yielding polynucleotides, oligonucleotides and free nucleotides. Considering the recognition sequence, different types of endonucleases may be distinguished. Restriction endonucleases for instance are enzymes that cleave DNA in specific recognition sequences, which vary depending on the enzyme (see Figure 3.2B for some examples).

The activity of these enzymes has firstly been verified in bacteria by Luria and Human (1952), and by Bertani and Weigle (1953), by observing differential growth of bacteriophages, depending on the host genotype. However, Arber and Linn (1969) were the first ones to propose that bacteria could protect themselves from bacteriophages by an enzymatically-mediated genetic defense mechanism. Bacteria methylate their genome in order to protect it, and these enzymes recognise and cleave a specific non-methylated DNA sequence, working as an intracellular defense mechanism against viral intrusions (Wilson and Murray 1991). The different names given to restriction enzymes are directly related to the species and strain from where they have firstly been identified (e.g. EcoRI from *E. coli*, R - strain RY13, I - first to be identified). In contrast to restriction enzymes, other endonucleases such as DNase I for instance, possess no recognition sequence, and cleave DNA molecules in a relatively nonspecific way. Digestion with nucleases is a powerful tool for sample preparation, as a means to de-complex and fragment DNA samples in a more specific, controlled way. Despite this, it is a time-consuming technique that requires optimal conditions such as pH, ionic strength and temperature in order to benefit from its full potential.

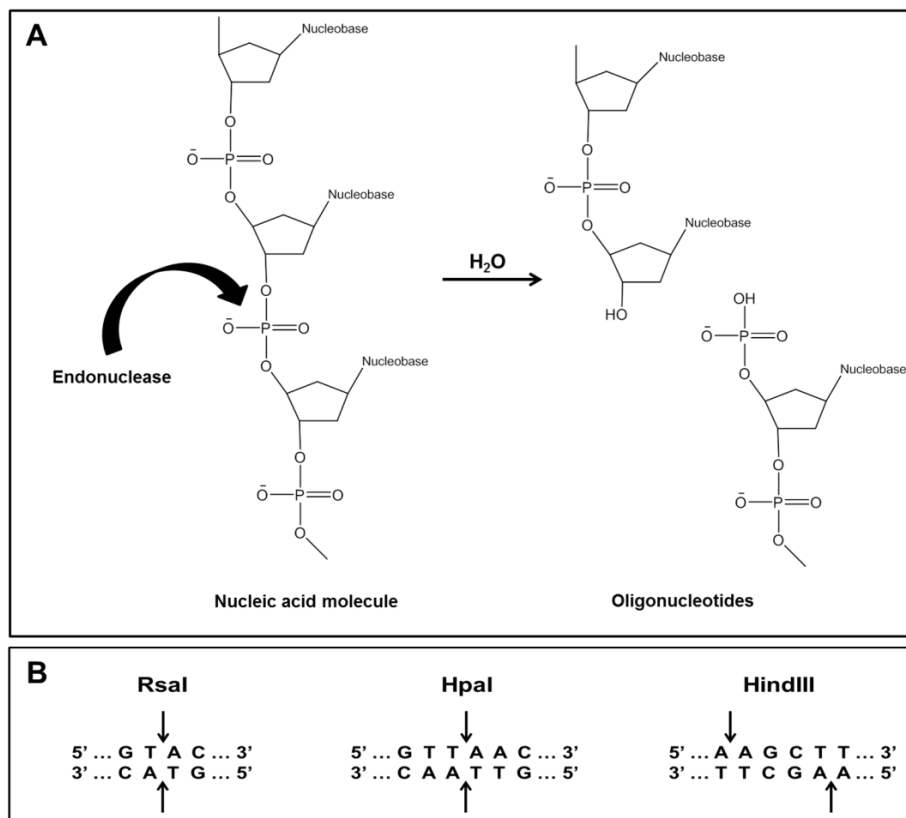


Figure 3.2. A) Mechanism of hydrolysis of a phosphodiester bond between two nucleotides in a nucleic acid molecule. B) Examples of recognition sequence and restriction sites for three different restriction endonucleases.

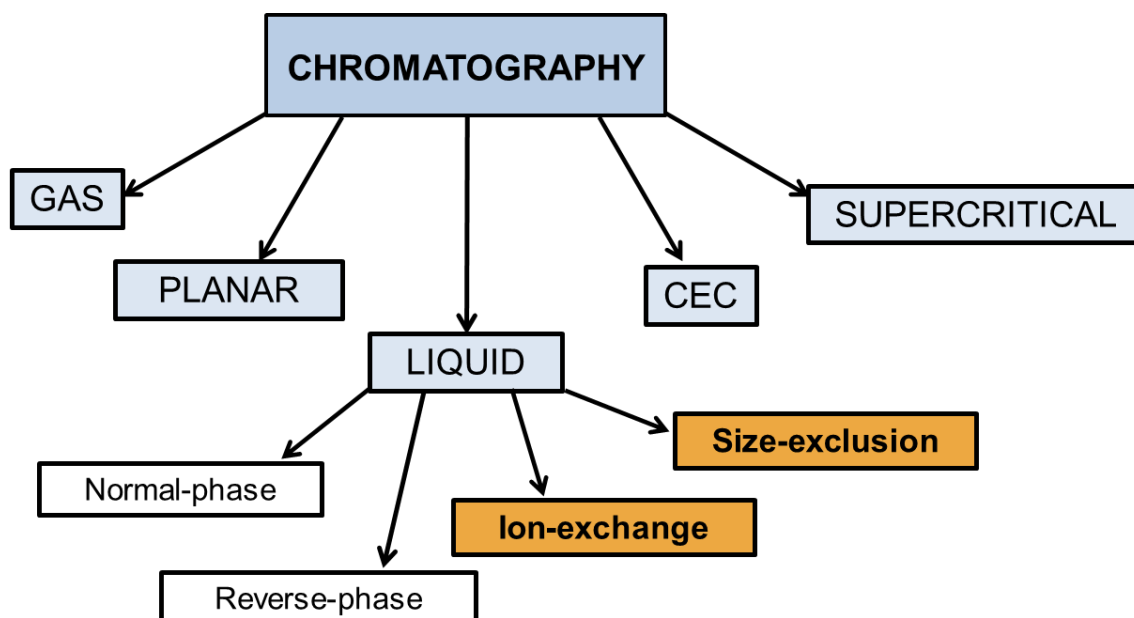


Figure 3.3. Classification of chromatography modes (highlighted both ion-exchange and size-exclusion). CEC – Capillary electrochromatography. Adapted from Kazakevich and LoBrutto (2007).

3.1.3 A word on liquid chromatography

Chromatography may be defined as a physicochemical method for separation of different components in a mixture, by selective adsorption to a specific substrate, or surface. In order to occur, this separation requires two phases: a mobile phase and a stationary phase. Chromatographic methods may be divided into liquid and gas, according to the physical state of the mobile phase (Kazakevich and LoBrutto 2007) and liquid chromatography into several different categories, according to the principle of transport through the column (see schematics in Figure 3.2). Separation by liquid chromatography is achieved by forcing the sample through a column packed with a stationary phase. The motive force is generated by the flow of mobile phase passing through the column. Depending on the separation principle, different stationary and mobile phases are selected to achieve maximum efficiency.

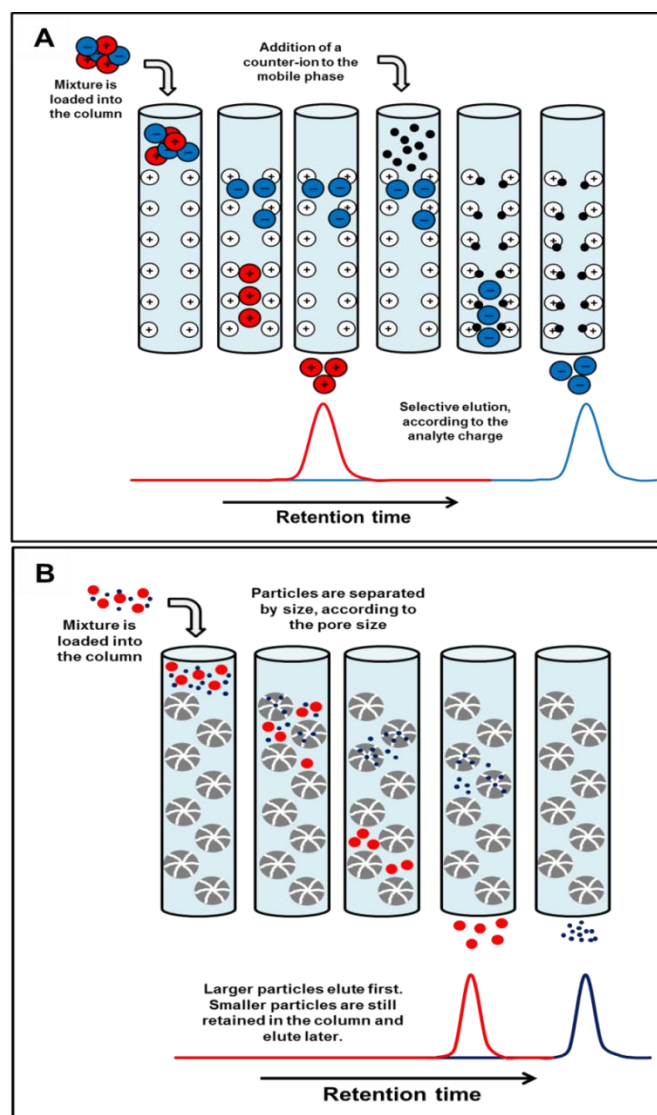


Figure 3.4. Schematics of different principles of separation in liquid chromatography. **A)** ion-exchange chromatography; **B)** size-exclusion chromatography.

In this chapter, two different principles of chromatographic separation will be addressed: ion-exchange and size-exclusion (highlighted in Figure 3.3). Separation by ion-exchange is based on the retention of differently charged analytes by a charged stationary phase (may be cationic or anionic, depending on the analytes) (Randerath and Randerath 1964, Kopaciewicz et al. 1983). This type of chromatography requires a column loaded with charged functional groups (as stationary phase) and a solvent gradient including the addition of a counter-ion to the mobile phase, in order to elute the retained compounds (see Figure 3.4A for more details). Ion-exchange columns usually attain a very good separation of components in a mixture, but require addition of salt to the mobile phase, which in some cases bring the need for desalting procedures afterwards. Besides this, ion-exchange columns are particularly sensitive to conditions such as organic solvents, pH and temperature.

In contrast to this method, size-exclusion chromatography (SEC) separates analytes by their differences in size. The SEC relies on a column packed with a porous gel, with a specific pore size, in order to slow down the elution of compound smaller than the pore (Barth et al. 1994. Sun et al. 2004). Particles larger than the pore size do not enter the gel and are excluded, eluting sooner than smaller particles (see schematics in Figure 3.4A). This kind of chromatographic separation is extremely useful for separation procedures during polymer synthesis (Moore 1964, Podzimek et al. 2001) or desalting procedures during sample preparation, for instance (Mori and Barth 1999). Despite its usefulness, this method bears a major drawback, the possibility of interaction between the mobile and stationary phases, affecting both elution and separation of components.

3.2 Results and Discussion

3.2.1 Development of a fast and efficient ultrasonic-based strategy for DNA fragmentation

3.2.1.1 Ultrasonic devices

The outcome and efficiency of ultrasonication depends on the ultrasonic device. Parameters such as frequency and intensity of ultrasonication must be carefully analysed in the implementation of this type of energy in any sample treatment workflow. To assess the differences between three ultrasonic devices, 1 mL of water was submitted to ultrasonication at different times, using 50 % of the nominal amplitude and every 5 s the temperature was measured. Figure 3.5 plots the increment in time versus the increment in Q (heat). The slope of the linear relation obtained increases according to the following: sonoreator (0.626) > UP100 probe (0.311) > Ultrasonic Bath. Since the increment in Q can be associated to cavitation effects, especially for short operation times, one may speculate that the best performance is obtained with the sonoreator.

This was subsequently confirmed with experimental data (see below). The VialTweeter was not included in this study.

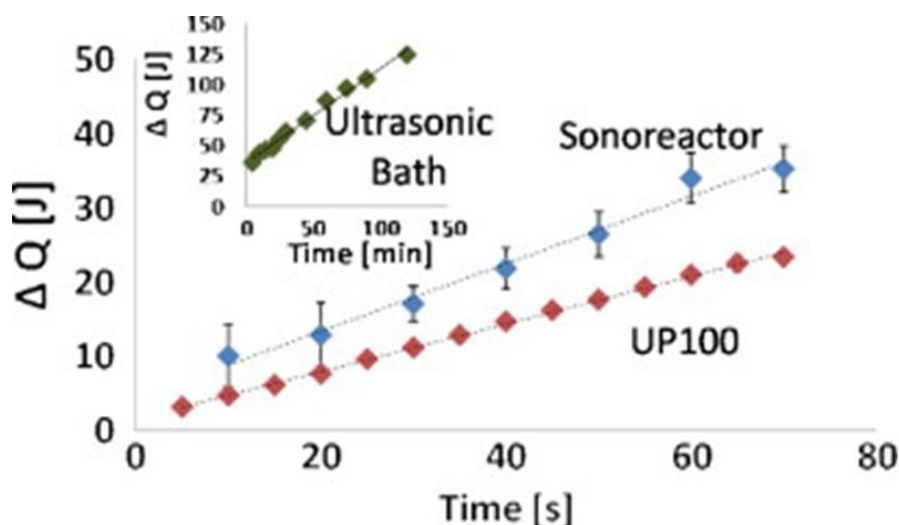


Figure 3.5. ΔQ [J] versus time of sonication for three of the four ultrasonic devices assessed in this work. The slopes of the lines (J/s) are as follows: sonoreactor, 0.453; ultrasonic probe UP100, 0.319; ultrasonic bath 0.013. The VialTweeter was not analysed in this study due to its low performance.

3.2.1.2 Finding out the best device for DNA ultrasonic fragmentation

For effective hybridisation and detection protocols, the average length of target DNA fragments should be reduced to decrease secondary structure formation (Mehlmann et al. 2005, Liu et al. 2007, Vinogradova et al. 2007). The efficiency of four different ultrasonic-based platforms to yield suitable DNA fragments was initially assessed by setting the amplitude of ultrasonication at its maximum value (100 %) and the time of treatment at 2 min. Figure 3.6 shows the electrophoretic profile of fragments originated from plasmid and genomic DNA submitted to ultrasonication. Results show that the ultrasonic bath and the VialTweeter have little effect in DNA integrity, causing only a slight disruption of some plasmid conformations - see lanes 4 and 5 for ultrasonic bath and lanes 6 and 7 for the VialTweeter. Other native conformations of the plasmid are still present after the ultrasonic treatment (red arrows in Fig. 3.6 showing the intact conformations). This can easily be explained since both systems have low intensity of sonication, and therefore cavitation efficiency is not enough to promote considerable DNA fragmentation. Conversely, the ultrasonic probe and the sonoreactor originated smaller fragments in short operation times, yielding low molecular weight fragments with total disruption of native DNA conformations (see Fig. 3.6, lanes 8–11).

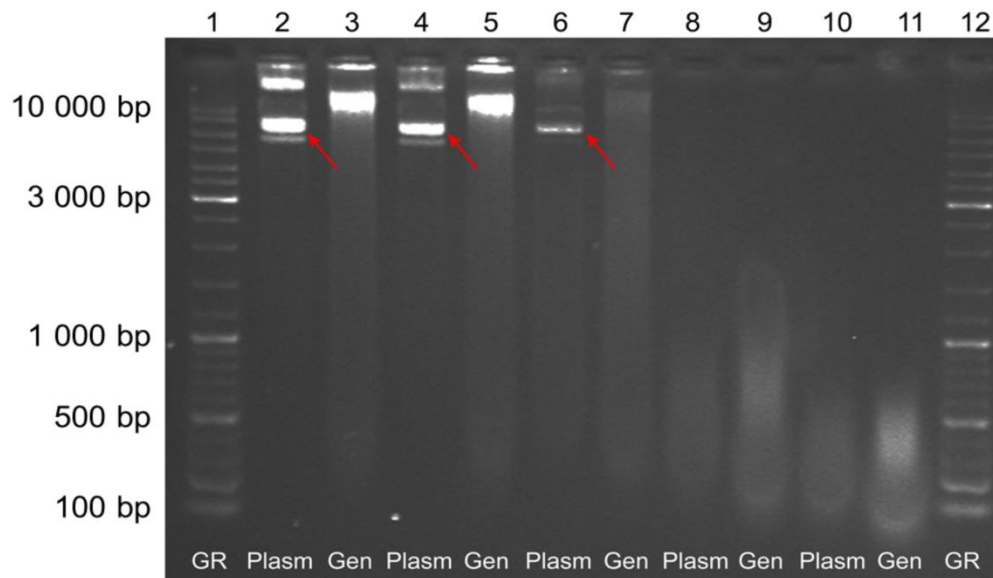


Figure 3.6. DNA fragmentation potential for different sonication setups. 1% Agarose gel (in 1x TBE) electrophoresis of plasmid and genomic DNA, respectively: lanes 2 and 3: non-sonicated; lanes 4 and 5: ultrasonic bath; lanes 6 and 7: VialTweeter; lanes 8 and 9: sonoreactor; lanes 10 and 11: UP100H probe (1 mm diameter tip). All samples were sonicated for 2 min at maximum amplitude. Lanes 1 and 12: GeneRuler DNA Mix Ladder (Fermentas). Red arrows show intact plasmid DNA conformations.

The best performance was obtained for the ultrasonic probe, where 2 min ultrasonic time and 100% ultrasonic amplitude yielded a DNA fragment distribution comprised between 600 and 100 bp – see Table 3.1. The sonoreactor also provided good results for the same experimental conditions as no native DNA conformations were observed and DNA fragments' size dispersion within the 1 500–100 bp range - see Table 3.1 and lanes 8 and 9 in Fig. 3.6. What is more, when the time of ultrasonication was increased to 8 min, the DNA fragments' size homogeneity was better, being comprised between 1 000 and 100 bp. These results are in agreement with previously reported data by Fukudome et al. (1986) and by Bankier (1993), which observed that the molecular weights of DNA fragments after ultrasound exposure were remarkably decreased when ultrasonic power was increased from 25 to 105 W. The use of an UP to fragment DNA and the evaluation of the influence of ultrasonic power and ionic strength on DNA fragmentation has already been reported (Mann and Krull 2004). More recently, it was observed that the plasmid DNA condensation affects its resistance to fragmentation caused by ultrasonic waves (Wu et al. 2009b). Despite the UP probe's potential for DNA fragmentation, this device presents two major disadvantages: aerosol formation when ultrasonication is applied to the sample, which causes loss of sample; and risk of carry over contamination, as the tip of the probe is inserted into the sample. Also, as the tip vibrates to generate ultrasonic waves, it is subjected to micro-degradation (Freitas et al. 2006), potentially leading to sample contamination with metal fragments that may hamper downstream applications (e.g. enzymatic amplification or digestion). On the other hand, the sonoreactor allows to apply indirect sonication on a sealed sample, i.e. does not enter in direct contact with the sample. Therefore, it presents the advantage of reducing the contamination risk

and possible sample losses. In addition, the formation of an aerosol is not observed. Also, the sonoreactor has been described to input 50 times less energy into the sample than the ultrasonic probe (Santos and Capelo 2007, Rial-Otero et al. 2007), reducing the risk of thermal degradation. In addition, although 2 min was enough to complete the treatment with the UP (1 sample), 4 samples can be treated at once using the sonoreactor. Therefore sample throughput is equivalent. Last but not least, the minimum sample volume that can be treated with a regular UP is 100 μ L, whilst with the sonoreactor it can be as low as 1 μ L. Based on these data, the sonoreactor-based ultrasonic treatment was selected for further studies and optimisation.

Table 3.1. Comparison of DNA fragmentation potential for different sonication setups

Conditions					Plasmid DNA		Genomic DNA	
Devices	Time (min)	Ampl (%)	Vol (μ l)	[DNA] (μ g/mL)	Peak	Homogeneity	Peak	Homogeneity
Non-sonicated	2	Max.	100	100	8 500 bp	13 000, 8 500 bp	12 000 bp	12 000-500 bp
Bath					8 500 bp	13 000, 8 500 bp	12 000 bp	12 000-500 bp
VialTweeter					8 500 bp	8 500 bp	12 000 bp	12 000-500 bp
Sonoreactor					800 bp	1 500-200 bp	700 bp	1 200-100 bp
Probe					500 bp	600-100 bp	400 bp	600-100 bp

3.2.1.3 Influence of ultrasonication time

The effect of time in ultrasonication was evaluated by applying ultrasonic energy to DNA samples at different time intervals comprised between 2 and 6 min - see Table 3.2. The ultrasonication amplitude was set at 100 %, since previous data had shown that lower amplitudes (<80 %) led to lower efficiency in the fragmentation of DNA. As may be seen in Table 3.2, the sample treatment is clearly time-dependent. For plasmid DNA, 4 min of sample treatment was enough to reach a fragment distribution comprised between 1 000 and 100 bp, whilst for genomic DNA a distribution comprised between 800 and 100 bp was obtained with 6 or 8 min of sample treatment. To guarantee the robustness of the procedure, the duration of treatment in further experiments was set to 8 min.

3.2.1.4 Influence of sample denaturation

To study the influence of the DNA conformation in the efficiency of the ultrasonic induced fragmentation, previously denatured and non-denatured DNA were submitted to the same conditions of ultrasonication. Fig. 3.3 shows that there was no improvement in the efficiency of

the treatment due to previous denaturation. This suggests that the fragmentation process caused by cavitation is mainly a physical process and not chemical, i.e. caused by the creation of radicals during the cavitation process. Ultrasonication may also cause denaturation of proteins and DNA, and therefore previous DNA denaturation maybe of little help in the fragmentation process. These findings suggest that the main contribution to DNA strands' fragmentation is due to hydrodynamic shearing forces as consequence of cavitation bubble collapse. This has been proposed by Grokhovsky (2006) to explain the influence of temperature in the breaking of DNA, where hydrodynamic forces are the main causes of ultrasonic DNA fragmentation, and that chemical processes generating radicals during cavitation play only a minor role, if any (Table 3.2).

Table 3.2. Comparison of different conditions using the sonoreactor system and its influence on DNA fragmentation potential.

Devices	Conditions				Plasmid DNA		Genomic DNA		
	Time (min)	Ampl (%)	Vol (μL)	[DNA] (μg/mL)	Peak	Homogeneity	Peak	Homogeneity	
Non-sonicated	-	-	100	100	8 500 bp	13 000, 8 500 bp	12 000 bp	12 000-500 bp	
Sonoreactor (SR)	2	100%	100	100	800 bp	1 500-200 bp	700 bp	1 200-100 bp	
	4				450 bp	1 000-100 bp	500 bp	1 100-100 bp	
	6				420 bp	1 000-100 bp	380 bp	800-100 bp	
	8				420 bp	1 000-100 bp	380 bp	800-100 bp	
	8		300	700 bp	1 500-100 bp	500 bp	1 200-100 bp		
			500	900 bp	2 100-100 bp	550 bp	1 200-100 bp		
				100	200	500	1 200-100 bp	480 bp	1 000-100 bp
					500	500	1 500-100 bp	480 bp	1 000-100 bp
SR (sample denatured beforehand)			100	420 bp	1 000-100 bp	380 bp	800-100 bp		

3.2.1.5 Influence of sample volume

For equal conditions of time and amplitude of ultrasonication, as the sample volume increases, the ultrasonication density (i.e. efficiency of treatment) is expected to decrease. This was confirmed in a set of experiments in which the ultrasonic conditions and DNA concentration were maintained, but the sample final volume was incremented from 100 to 500 μL . As shown in Fig. 3.3, the average size of the plasmid DNA fragments was 900, 700 and 420 bp whilst for genomic DNA was 550, 500 and 380 bp for sample volumes of 500, 300 and 100 μL , respectively. A volume of 100 μL was chosen as optimal for further experiments.

3.2.1.6 Influence of DNA concentration

The influence of DNA concentration was also assessed. Results suggest that for the same ultrasonication time and amplitude, the fragmentation efficiency is slightly diminished as the DNA concentration increases (Table 3.2). The size distribution of DNA fragments obtained incremented from 1 000–100 to 1 500–100 bp for plasmid DNA and from 800–100 to 1 000–100 bp for genomic DNA. However, if the time of treatment is increased, the average size of the fragments and the size distribution can be the same, regardless of the DNA concentration (range 100–500 $\mu\text{g}/\text{mL}$). After exhaustive analysis of all different conditions and setups, an optimised protocol for DNA fragmentation was set out in which the sample was sonicated by means of a sonoreactor for 6 min at 100% ultrasonication amplitude in a volume of 100 μL .

3.2.1.7 Ultrasonic fragmentation versus restriction enzyme digestion

The optimised ultrasonic protocol was compared to restriction enzyme digestion for fragmentation of DNA samples. To assure digestion, a double restriction was performed with two frequent cutters - Eco47I and MvaI. Figure 3.7 displays the electrophoretic patterns for sonicated and digested DNA samples (plasmid and total genomic DNA). The patterns corresponding to plasmid DNA samples sonicated (lane 3) and digested (lane 4) show considerable differences. The ultrasonicated sample exhibits a fragment distribution (100–500 bp), whilst the digested sample consists of numerous DNA fragments with discrete molecular weight (100–3 000 bp). This is not observed for the genomic DNA samples, where both the sonicated and digested samples (Fig. 3.7 - lanes 6 and 7, respectively) exhibit a smear corresponding to extensive fragmentation. It should be noted that, whilst ultrasonication yields fragments with low size dispersion (<500 bp), the digested sample shows a wider range of fragment distribution from high to low molecular weight fragments (from 10 000 to <100 bp).

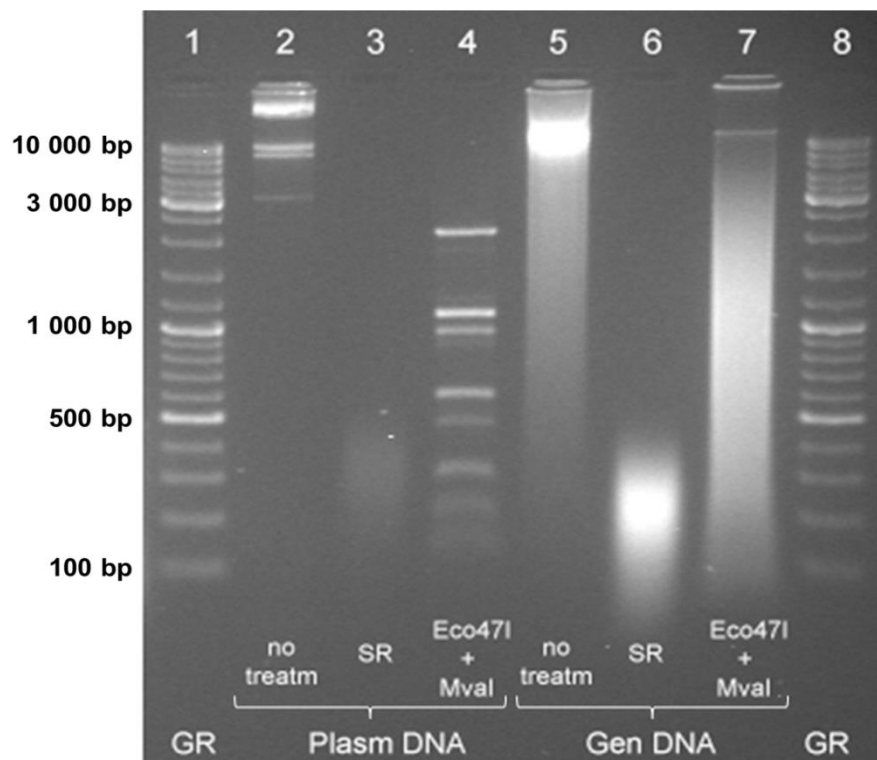


Figure 3.7. Comparison between the sonoreactor system and restriction enzyme digestion in generating DNA fragments. 1% Agarose gel (in 1x TBE) electrophoresis of plasmid DNA samples, respectively: lane 2: non-sonicated; lane 3: sonicated with the sonoreactor; lane 4: digested with restriction enzymes; and genomic DNA samples, respectively: lane 5: non-sonicated; lane 6: sonicated with the sonoreactor; lane 7: digested with restriction enzymes. Lanes 1 and 8: GeneRulerDNAMix Ladder (Fermentas). Conditions of ultrasonication: ultrasonication time 8 min, ultrasonication amplitude 100%.

The restriction enzyme treatment of genomic DNA results in a fragment profile which can be compared to that attained by simple mechanic fragmentation occurring during DNA extraction and purification (untreated sample). When compared to the untreated sample, the restriction enzyme treatment can be considered negligible as it shows a much lower capability of fragmentation than that of ultrasonication. Restriction enzyme digestion, due to the specific sequence recognition, may allow a more discrete cleavage but it is time consuming, relies on expensive reagents (e.g. enzymes, buffers) for the reaction to occur at optimum activity conditions, and requires subsequent sample purification. Contrary to what it might seem, DNA fragmentation through ultrasounds does not occur totally at random, as 5'-CpG-3' dinucleotides have been shown to be primary hotspots for double-strand breaks (Grokhovsky 2006). What is more, the ultra-sonication approach here proposed avoids any purification step, is significantly faster and less expensive than restriction enzyme methods, generating fragments of equivalent molecular weight and suitable for downstream detection applications.

3.2.1.8 Ultrasonic acceleration of nuclease-mediated DNA hydrolysis

Both ultrasonic fragmentation and nuclease digestion have been shown valuable as a means to produce DNA fragments suitable for downstream applications. However, DNA fragments may prove difficult to analyse with time-of-flight (TOF) analysers, due to its elevated molecular weight and structure. So, the ultimate objective would be a complete breakdown of the DNA molecule into free nucleotides using a rapid, inexpensive protocol. For this purpose, an experiment was performed to assess how ultrasonication would influence DNase I digestion.

The acceleration of enzymatic digestion by sonication has previously been described for trypsin proteolytic digestion in different occasions (López-Ferrer et al. 2005, Rial-Otero et al. 2007) but, no data has ever been published on ultrasonic acceleration of DNA digestion. Consequently, a simple experiment to attain whether ultrasonic energy would influence DNase I-mediated DNA hydrolysis was carried out. Contrastingly to MvaI and Eco471 (previously used), DNase I does not possess a specific recognition sequence, as it cleaves the DNA molecule preferentially next to pyrimidines, generating both oligonucleotides and free nucleotides. Results in Figure 3.8 depict electrophoretic patterns for DNase I digestions of 1 µg of plasmid DNA, for 10 minutes, with and without sonication. In both cases, down to a concentration of 0.1 units enzyme per reaction, most substrate is degraded (Figure 3.8, wells 1 to 3). A smear-like pattern is denoted in wells 4, indicating that the respective enzyme concentration (0.05 units per reaction) is not sufficient to breakdown most substrate in solution. Lower concentrations than this produce similar patterns to the non-digested DNA (Figure 3.8, wells 5 to 7).

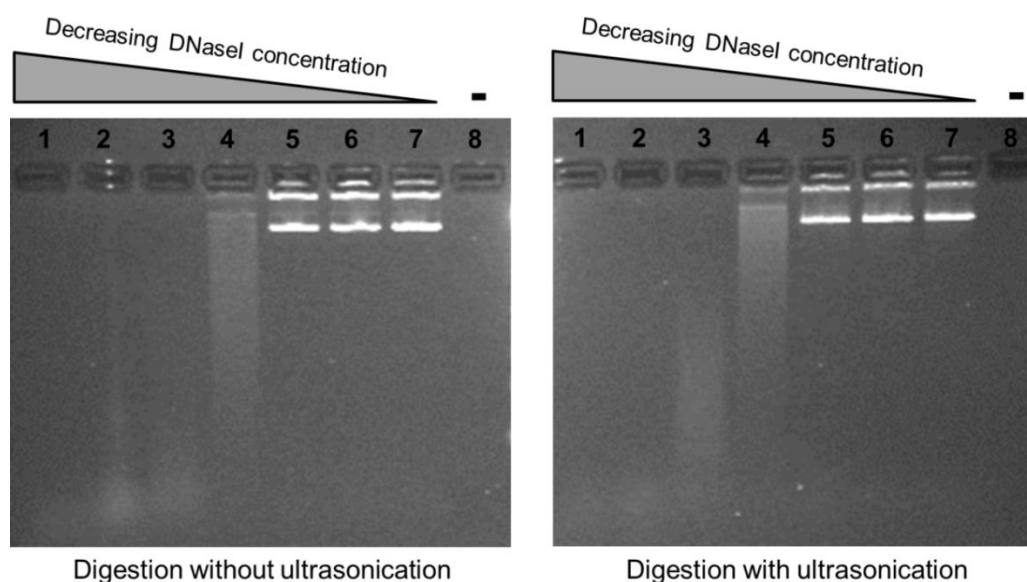


Figure 3.8. Electrophoretic patterns obtained for DNase I digestion of plasmid DNA with and without ultrasonication. Conditions: 1% agarose gel in 1xTBE; 50 V; 120 min. Lane 1: 1U DNase I; lane 2: 0.5U DNase I; lane 3: 0.1U DNase I; lane 4: 0.05U DNase I; lane 5: 0.01U DNase I; lane 6: 0.005U DNase I; lane 7: without DNase I; lane 8: without plasmid DNA.

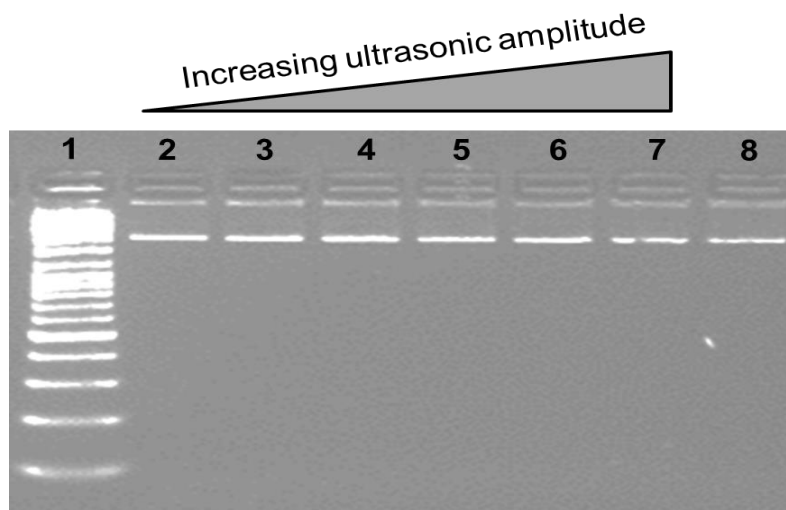


Figure 3.9. Electrophoretic patterns obtained for DNase I digestion of plasmid DNA with increasing ultrasonic amplitude. Conditions: 1% agarose gel in 1xTBE; 50 V; 120 min. Lane 1: GeneRulerDNAMix Ladder (Fermentas). Lane 2: 0% amplitude; lane 3: 10% amplitude; lane 4: 25% amplitude; lane 5: 50% amplitude; lane 6: 70% amplitude; lane 7: 80% amplitude; lane 8: without DNase I. All reactions were performed with 0.01U DNaseI, during 10 min.

Whether the digestion occurred at 37 °C in a thermo cycler, or in a sonoreactor with 50% amplitude, very similar results are observed in Figure 3.8. A slight difference in wells 3 is denoted, where ultrasonic treatment seems to have produced a seemingly longer smear, which would mean that the digestion suffered some sort of impairment, perhaps due to premature increased enzyme denaturation via acoustic cavitation. Results in Figure 3.8 seem to indict that 10 minutes of ultrasonic treatment at 50% amplitude did not accelerate DNase I digestion. In comparison to proteins, the DNA molecule presents a higher resistance to unfolding and denaturation. This may be why treatment of DNA samples proves more of a challenge. Nevertheless, an additional experiment was performed, to assess whether ultrasonic amplitude would produce differences. Data in Figure 3.9 depicts electrophoretic patterns of plasmid DNA reacted with DNase I, for 10 min, at different ultrasonic amplitudes. A remarkable resemblance can be observed in electrophoretic patterns in lanes 2 to 8, from 0 to 80% amplitude, primarily indicating that, at the tested conditions, ultrasonic energy did not effectively accelerated DNase I digestion of plasmid DNA. The maximum established amplitude for this experiment was 80% because previous knowledge on fragmentation of DNA showed that above this amplitude, plasmid DNA may fragment due to action of ultrasonic energy alone, and if that occurred, results would be rendered inconclusive. Also, the period of sonication/digestion was kept constant at 10 minutes in all digestion-related experiments with a specific purpose. Based on previous experiments, this sonication period may be considered a long time for continuous sonication of a DNA/protein solution. However, if an ultrasonic acceleration of digestion would have been denoted at 2, 5 or 7 minutes, it would be seen in the electrophoretic pattern. Thus, considering there is no spontaneous re-ligation of DNA fragments in solution (phosphodiester bond), by action of

ultrasonic energy or DNase I, a maximum time limit was set at 10 minutes. As both experiments carried out showed no significant influence of ultrasonic energy on DNA-mediated hydrolysis, the variation of sonication period (reaction time) was found of little relevance and was therefore not investigated.

Considering all data discussed beforehand, to improve DNA breakdown to free nucleotides the most successful option would be a combined protocol involving a first, rapid DNA fragmentation step with ultrasonic energy and a subsequent digestion step with DNase I.

3.2.2 Chromatography for nucleotide separation and purification

Liquid chromatography (LC) was procured to achieve efficient separation of nucleotides from the remainder molecules in a solution. This technique would be preceded by DNA fragmentation and breakdown to nucleotides, which would mean that enzymatic components and saline buffers might still remain in solution. To rid the solution of these contaminants, the first suggestions would be to perform a phenol:chlorophorm extraction for protein removal, followed by a desalting step using a DNA-grade size-exclusion column (NAP-5). This protocol possesses some advantages, such as low cost, easiness and time-efficiency, however it presents a major disadvantage: it pools together all nucleotides in a given mixture and cannot effectively separate each one from the next. Since this separation may be important, the incorporation of a high performance liquid chromatography (HPLC) step in the protocol was evaluated. It would present a considerable increase in time and cost, however, depending on the results, it could prove extremely valuable for subsequent analysis. For better results, a DNA-grade anion exchange column was tested, which would efficiently retain the nucleotides, separating them from other components.

3.2.2.1 Profiling different nucleotides

Preliminary results indicated that reverse-phase and normal-phase chromatography were not adequate for elution of phosphate nucleotides. The similar affinity of all nucleotides towards the stationary phase rendered these methodologies unable to efficiently resolve its separation. After some experimenting with ion-exchange chromatography (using a HPLC system), the best conditions for nucleotide elution were found (described in Methods section 2.4.2.5). The first step would be the identification each nucleotide's elution peak, as well as its characteristic retention time, according to the experimental chromatography conditions. In order to accomplish this, different mixtures of 3 nucleotides were analysed by ion-exchange HPLC (Figure 3.10). The retention times vary according to the nucleotide in question. Pyrimidine nucleotides present lower retention times than purines with thymine being the nucleotide which elutes sooner (retention time ≈ 7.54 min). Also, guanine seems to be the nucleotide more effectively retained by the column, possibly due to lower affinity towards the mobile phase (retention time ≈ 9.36 min). As

the used principle was ion-exchange, when a nucleotide passes through the column, it would mainly be retained by trapping the phosphate groups, and the observed shifts in retention times are possibly due to the chemistry of the nucleobase and its interaction with the mobile phase. After acquiring the retention times and chromatographic profile of all 4 nucleotides, the next step included the analysis of modified nucleotides and the alkylating agent, glycidamide.

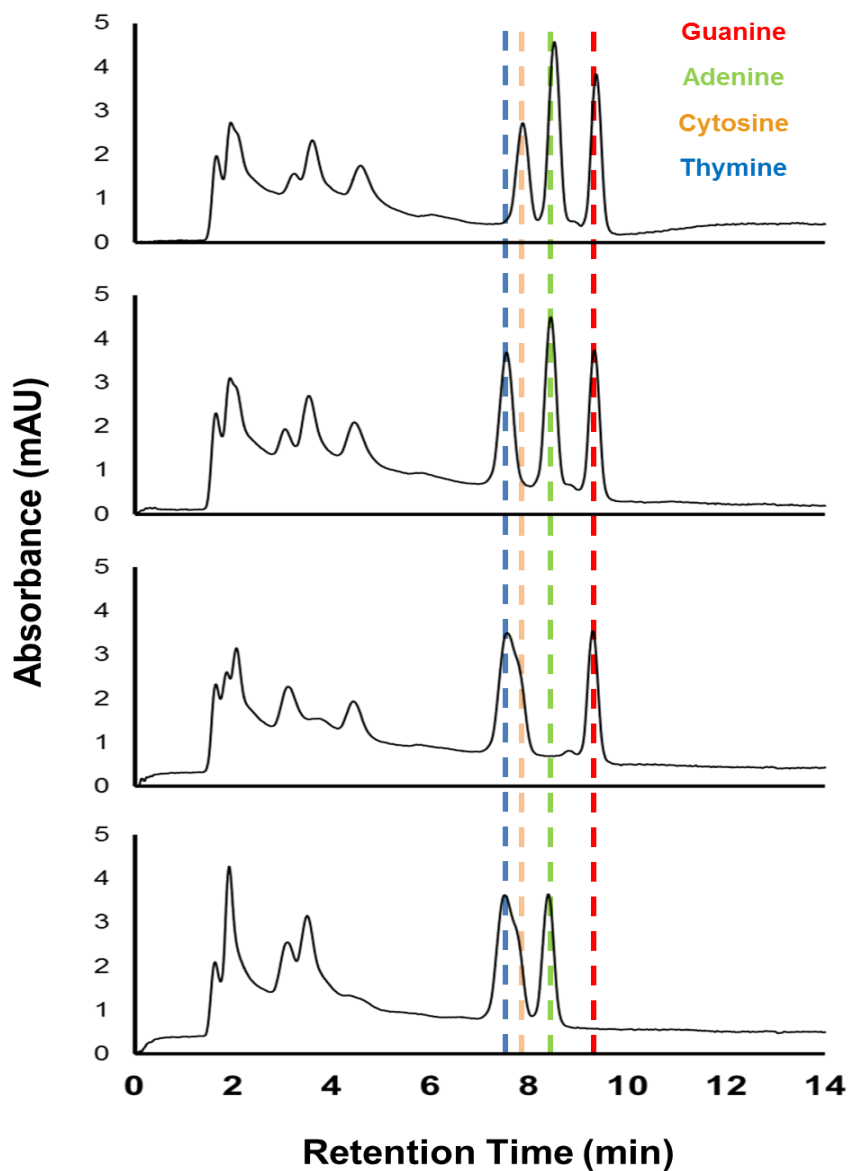


Figure 3.10. Chromatograms of different nucleotide mixtures, for identification of different deoxynucleotides by ion-exchange HPLC. Lines of different colours highlight different nucleotide elution peaks. Measured retention times, thymine \approx 7.54 min; cytosine \approx 7.87 min; adenine \approx 8.51 min; guanine \approx 9.36 min.

3.2.2.2 Separation of modified nucleotides via HPLC

When inserted in a more complete protocol, the separation of modified nucleotides would not be performed in treated, contaminant-free samples, but rather in mixtures containing the remainder of nuclease digestions (saline buffers, enzymatic fractions, etc.) and possibly molecular radicals generated during the ultrasonication step (Milowska and Gabryelak 2007). So, to simulate such conditions and contaminants, a mixture containing these components was made (see Methods section 2.4.2.4), and spiked with i) glycidamide (GA), ii) dGTP, and iii) GA-modified dGTP (GA-guanine adduct). Mixtures were desalted, filtered and analysed by ion-exchange HPLC, employing previously described conditions.

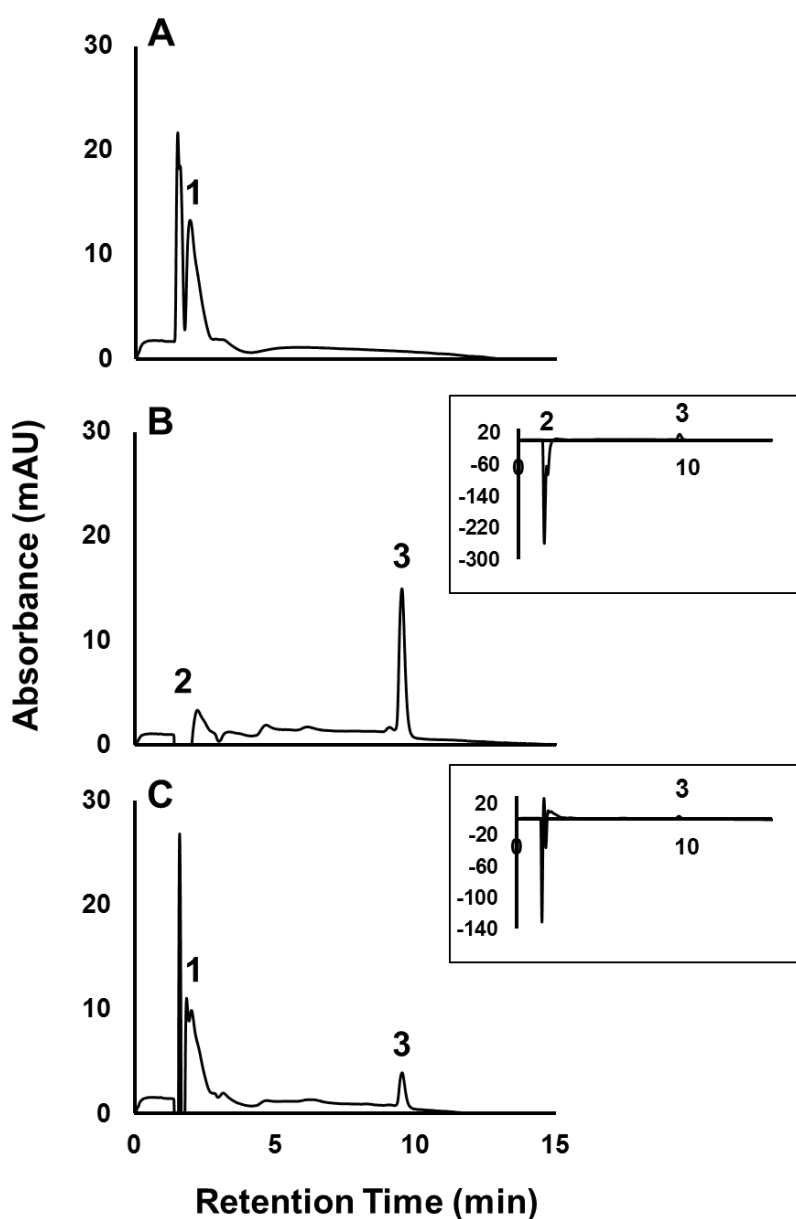


Figure 3.11. Chromatograms for mixtures spiked with A) glycidamide (GA); B) dGTP; C) GA-modified dGTP. Insets represent an overview of the chromatogram, with a broader scale on the Y-axis. Different numbers correspond to different chromatographic signals.

Considering all chromatograms in Figure 3.11, immediate differences are denoted amongst them. The signal marked with 1 (Fig. 3.11 A and C) appears only in samples containing GA, at relatively low retention times, which may be related to the elevated hydrophilic nature of GA, as well as low interactions with positively charged groups (in the column). The chromatographic signal of dGTP appears later in the chromatograms and can easily be identified as 3, in Fig. 3.11B,C. Its intensity appears lower in 3.11C, possibly due to the consumption of guanines, during the previous alkylation reaction with GA. The visible signal of dGTP in Fig. 3.11C (marked with 3) indicates a reaction yield below 100%, so unreacted (non-alkylated) guanine molecules still remained in solution. Other than this, a sharp negative peak is also denoted in Fig. 3.11B,C (marked with 2), which can possibly be linked to differences in absorbance between the mobile phase and saline components in the sample. The chromatogram in Fig. 3.11 C presents no visible chromatographic signals that can be attributed to a GA-guanine adduct. Considering the chemistry of both guanine and GA, a signal corresponding to the GA-Gua adduct might appear at low retention times, in case the alkylated guanine would be released from the pentose and phosphate groups. Otherwise, it would be trapped in the column and should elute in close proximity to the dGTP signal. The fact that a GA-Gua adduct elution peak is not visible in the chromatogram may indicate that either GA greatly increased its hydrophilicity and lowered retention, or its concentration is too little to be analysed by a UV-Vis diode-array detector, at 254 nm. Both these hypotheses are regarded as a disadvantage of this method for separation of modified nucleotides. Nevertheless, fractions corresponding to low retention times were collected and subsequently analysed by MALDI-TOF, using CHCA as a matrix. The analysis revealed no mass signals corresponding to GA-guanine adducts.

3.2.2.3 Brief considerations on liquid chromatography for sample preparation

The incorporation of an ion-exchange HPLC step in the protocol for sample preparation and detection of DNA adducts possessed the main advantage of isolating the desired analyte (GA-Guanine adduct) removing additional contaminations and possibly increasing sensitivity and resolution. However, this protocol required the addition of two desalting steps, before and after HPLC separation. Besides this, the HPLC technique is time-consuming and did not bring a significant advantage to the protocol. Considering this scenario, it was decided to employ a phenol:chloroform microextraction, followed by a size-exclusion chromatography step by using a NAP-5 DNA-grade column and subsequent sample concentration. Phenol:chloroform microextractions are commonly used in DNA isolation protocols and effectively remove contaminant proteins from solution. By using this combined approach, a contaminant-free solution of nucleotides may be attained, without additional treatment. The elution step was performed using sterile water, in order to prevent an elevated content in salt when concentrating

the sample. Previous experience within the research group with microextraction procedures and NAP-5 columns for DNA and oligonucleotide purification contributed greatly for this decision.

3.3 Conclusions

This chapter firstly described a simple, fast, high-throughput and inexpensive sonoreactor-based method for DNA fragmentation. Four ultrasonic devices were compared in terms of fragmentation efficiency, and only the sonoreactor and the ultrasonic probe were found suitable for efficient DNA fragmentation. Despite this, the sonoreactor (cup horn) shows several advantages when compared to an ultrasonic probe: (i) allows for processing of smaller sample volumes, down to 1 μL ; (ii) prevents extensive sample overheating, reducing the degradation of analytes in solution; and (iii) avoids cross-contamination between samples and contamination with metal fragments resulting from vibration of immersed ultrasonic probes. When comparing methodologies for DNA fragmentation, the proposed sonoreactor approach shows some advantages when compared to restriction enzyme digestion, namely a larger extent of DNA fragmentation with smaller size dispersion is attained in less time at smaller costs. This data was published in Larginho et al. 2010 (Talanta 81:881-886).

Restriction enzyme digestion exhibits a greater control on DNA fragmentation, as it is entirely sequence-dependent. However, both methodologies are valuable and noteworthy tools to consider when preparing DNA samples. For this reason, an attempt to accelerate nuclease digestion via ultrasonic energy was further presented and discussed. No major differences were denoted between electrophoretic patterns from DNA solutions digested in the same conditions, with and without sonication. Also, ultrasonic amplitude did not seem to considerably affect nuclease digestion of DNA samples.

The second part of this chapter consisted on an assessment of chromatographic methods for nucleotide separation, prior to the detection step. An ion-exchange HPLC method was evaluated for nucleotide profiling and separation, showing that the desired analyte (GA-modified guanine nucleotides) cannot be efficiently isolated, under the tested conditions. An alternative was presented, consisting on a microextraction and size-exclusion chromatography for contaminant and salt removal, followed by sample concentration. The final result would be a clean, contaminant-free mixture of nucleotides (both modified and unmodified) ready for detection.

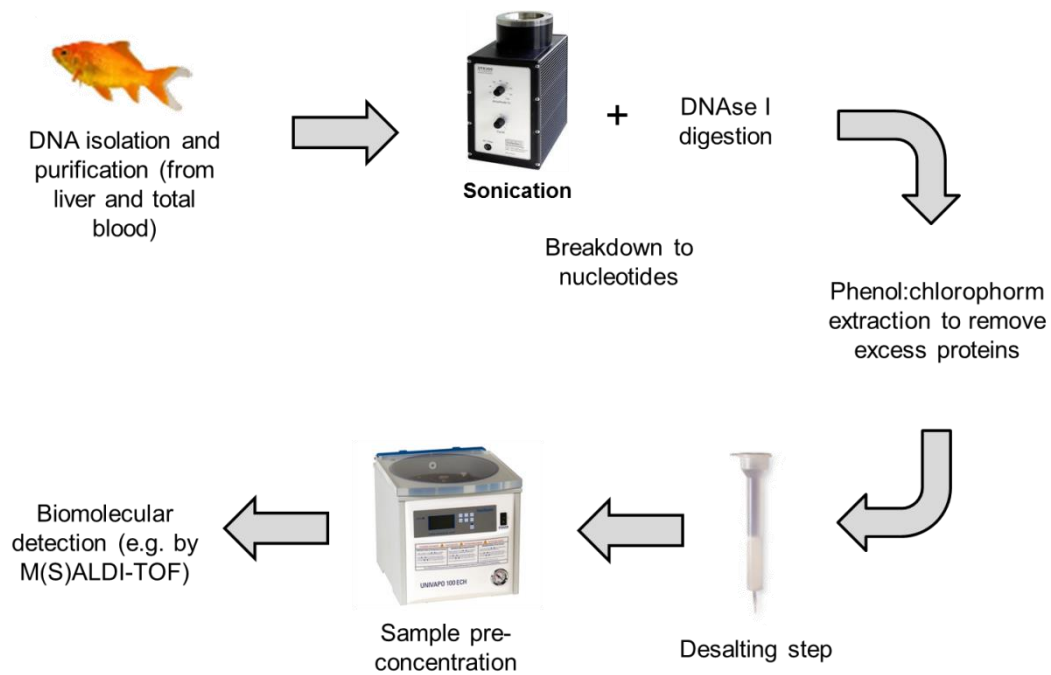


Figure 3.12. Schematic representation of the complete protocol for sample preparation.

The main objective pertaining the work presented in this chapter is represented in Figure 3.12. The devised protocol considers all steps between the initial preparation of tissues or cell lysates, down to the detection. Figure 3.12 highlights the main phases of the protocol for sample preparation. The procedure initiates with genomic DNA isolation and purification from the target tissue or cell lysate. Afterwards, DNA breakdown to free nucleotides is achieved by a 2-step method: ultrasonic fragmentation of DNA followed by a DNase I treatment of DNA fragments in solution. Subsequently, a micro-extraction with phenol and chlorophorm is carried out, before the desalting and concentration steps. In summary, the proposed procedure for sample treatment is rather fast, simple and inexpensive, and generates contaminant-free free nucleotide solutions, suitable for subsequent MS-detection.

CHAPTER 4. GOLD NANOPARTICLES FOR IDENTIFICATION OF MODIFIED NUCLEOTIDES THROUGH MASS SPECTROMETRY AND COLORIMETRY

Some of the results presented in this chapter have been published in Larginho M, Capelo JL, Baptista PV. 2013. Fast nucleotide identification through fingerprinting using gold nanoparticle-based surface-assisted laser desorption/ionisation. *Talanta* 105:417-421, where Miguel Larginho was responsible for the experimental work and writing part of the manuscript.

Some of the results presented in this chapter have been published in Larginho M, Santos S, Almeida J, Baptista PV. 2014. DNA adduct identification using gold-aptamer nanoprobe. *IET Nanobiotechnology*, where Miguel Larginho was responsible for part of the experimental work (choosing the probe, synthesis and characterisation of nanoparticles and nanoprobe, and statistics), and writing part of the manuscript.

Success is a science: if you have the conditions, you get the result.

Oscar Wilde

4.1 Introduction

Research on biomolecular detection has greatly benefitted from the advances on nanotechnology, namely synthesis, characterisation and conjugation of nanomaterials, such as gold nanoparticles (Baptista et al. 2008). Gold nanoparticles (AuNPs) exhibit remarkable physico-chemical and optical properties, which allow for procedures of derivatisation with biomolecules (Mirkin et al. 1996) and colorimetric strategies of detection (Baptista et al. 2005a, 2005b, Thaxton et al. 2006, Veigas et al. 2012). Different studies have described the incorporation of AuNPs in already existing techniques, improving sensitivity and specificity (Zhang et al. 2011a,b, Ambrosi et al. 2010), with strong impact in diagnostics, biomedicine and other related fields (Jain et al. 2006, Baptista et al. 2008). In addition, AuNPs have been proposed as substituents of organic matrices for SALDI-MS analysis of biomolecules, and these methodologies using have been effectively employed for the analysis of peptides and proteins (McLean et al. 2005, Huang and Chang 2006, Chiang et al. 2010). SALDI-TOF analysis of nucleic acid molecules and nucleotides has also been proposed (Huang and Chang 2007), overcoming issues related to the difficulty of detection of DNA molecules using time-of-flight (TOF) analysers due to the high molecular weight, while allowing identification of nucleotides and nucleosides. Furthermore, synthesis and application of AuNP bioconjugates has been described for different biomolecules, such as proteins, fluorophores (Rosa et al. 2011) or aptamers (Chen et al. 2008, Zhang et al. 2013).

Aptamers are short polymeric molecules (e.g. nucleic acid, peptides) that adopt a particular secondary structure depending on their sequence and possess the capability of binding different ligands, according to sequence specificity and particular chemical interactions amongst them (Mairal et al. 2008). Aptamer molecules are usually generated by Systematic Evolution of Ligands by EXponential enrichment (SELEX), a combinatorial chemistry technique which has evolved to select specific aptamers by affinity (Ellington and Szostak 1990, Tuerk and Gold 1990) and consists in the synthesis of an oligonucleotide library, subsequent mixture with the target ligand and separation by affinity. Production of new, specific aptamer sequences and its compilation into a database allows for a subsequent search and utilisation of aptamer molecules already characterised and described. Due to their elevated affinity towards specific ligands, aptamers have been widely used in biosensing protocols, either for recognition and detection (Chen et al. 2008, Wang and Liu 2008) or in affinity probes for ligand enrichment. Thrombin-binding aptamers (TBA) for instance, have been combined with different nanoparticles and widely used towards detection of thrombin in biological fluids (Wang et al. 2008, Zhang et al. 2012). A distinct aptamer, specific for ATP binding, has been functionalised to AuNPs, creating ATP-binding probes used both for colorimetric detection (Chen et al. 2008) and ligand enrichment (Huang and Chang 2007). Still on nucleotide-binding aptamers, a different ATP-binding sequence has been

successfully employed on a label-free fluorescence assay for ATP detection (Wang and Liu 2008) and, on a different study, an RNA aptamer selective for both guanine and xanthine binding has been characterised (Kiga et al. 1998). Despite the described aptamer-based approaches for nucleotide binding, so far no attempts have been made for detection of modified nucleotides, e.g. DNA adducts derived from nucleobase alkylation.

One of the major objectives of this thesis is the AuNP-based detection of DNA adducts (modified nucleotides) as biomarkers of exposure to an alkylating agent. Perhaps the main complication of using DNA adducts as biomarkers of DNA damage is their low abundance in tissues/fluids, after exposure. This situation leads to the use of radiolabelled isotopes (Gupta 1985, Coldwell et al. 2008) and cumbersome, expensive protocols when detecting DNA adducts, to guarantee suitable and sensitive approaches. Therefore, simple, sensitive and safer novel approaches for detection of DNA adducts as toxicological biomarkers are necessary, to prevent the use of procedures that present in itself, a considerable toxicological risk (e.g. radiolabeled isotopes).

With this in mind, the following chapter emphasises the use of AuNPs in two distinct based approaches for nucleotide identification. Firstly, matrix- and surface- assisted laser desorption/ionisation (MALDI/SALDI) using gold nanoparticles (AuNPs) will be evaluated as an approach for identification of modified and unmodified nucleotides. Subsequently, a second section in this chapter will describe an alternative method, based on aptamer-gold nanoprobe, for colorimetric identification of modified nucleotides in solution. The chosen analyte of study will be the DNA adduct resulting from alkylation of guanines by glycidamide (GA-Gua), upon biotransformation of acrylamide by the CYP monooxygenase pathway (Settels et al. 2008, Watzek et al. 2012), which is regarded as a biomarker of exposure to acrylamide (Carere 2006). These methods may be viewed as relevant contributions towards identification of DNA adducts in solution in a rather fast and straightforward way, allowing for a quick biomarker screening and subsequent correlation to other biomarkers, in the context of genetic toxicology studies.

4.2 Results and discussion

4.2.1 Matrix- and surface-assisted laser desorption/ionisation mass spectrometry for nucleotide identification

4.2.1.1 Characterisation and selection of organic matrices

The main advantage of MALDI is the use of an organic matrix, which aids in ionisation and prevents extensive fragmentation of the analyte, however for optimal analysis of different analytes, a suitable matrix should be chosen in each case. With this in mind, some commercially available matrices, namely α -cyano-4-hydroxycinnamic acid (CHCA), ferulic acid, 2',4',6'-

trihydroxyacetophenone (THAP), 3-hydroxypicolinic acid (3-HPA), super-dihydroxybenzoic acid (Super DHB), sinapinic acid (SA), 3-(4-chloro-phenyl)-2-cyano acrylic acid (Cl-Ph-AA) and 2-(4'-hydroxybenzeneazo) benzoic acid (HABA), were characterised via UV-Vis spectrophotometry and tested for its efficiency in nucleotide ionisation. Nucleotide analysis with MALDI-TOF is usually carried out in negative-ion mode due to the analyte affinity towards the formation of negative molecular ions in the gas-phase (Huang and Chang 2006). In addition, and despite MALDI being classified as a soft ionisation technique, there is still the risk of fragmenting the nucleotide during ionisation, due to its molecular structure. Results are summarised in Table 4.1 (for more information and mass spectra, see Appendix III) and show that m/z signals corresponding to dGTP molecular structure, i.e. identification of dGTP molecular ion peaks, appeared only when CHCA or ferulic acid were mixed with the sample, whereas the remaining organic matrices failed to yield conclusive identification signals. Moreover, when CHCA was employed, more intense (relative) m/z signals were denoted in positive and negative-ion mode (Table 4.1). Thus, CHCA was chosen as a matrix for subsequent experimentation.

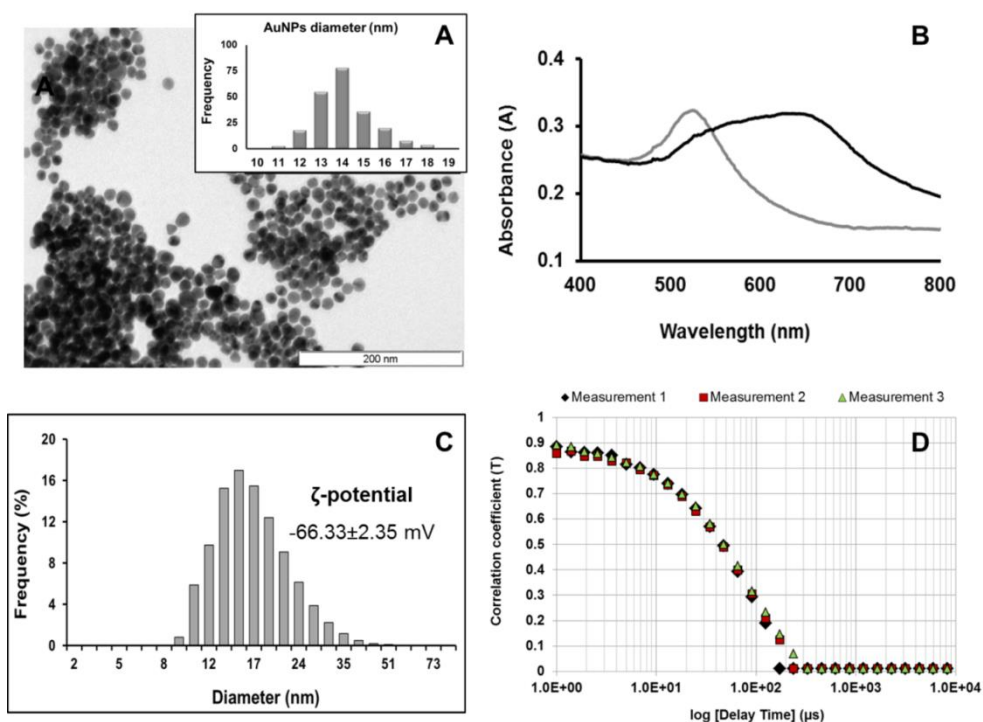
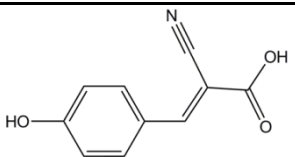
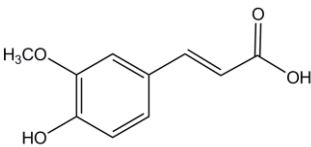
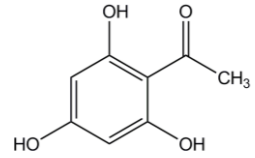
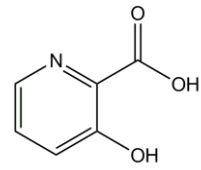
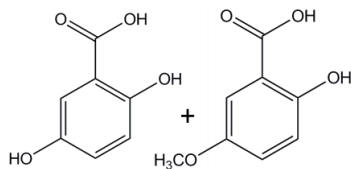
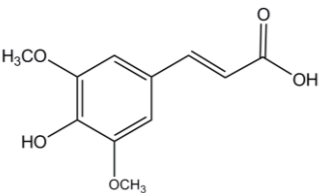
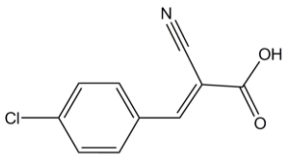
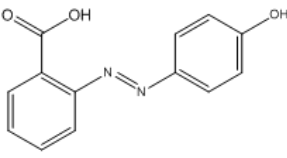


Figure 4.1. Characterisation of the synthesised gold nanoparticles: A) Transmission electron microscopy (TEM) imaging - inset presenting the size distribution from counting 250 particles; B) UV-Vis spectrum of the dispersed gold nanoparticle solution, with a maximum absorption centred at 519 nm (grey line), and the same solution, in the presence of 0.1 M NaCl (black line). C) Dynamic light scattering (DLS) measurements to determine the hydrodynamic radius of the AuNPs ($PI = 0.37 \pm 0.02$; z -average = 17.7 ± 0.1 nm), including the zeta-potential (ζ -potential) measurement as an indicator of colloid. D) Correlation curves obtained for three independent measurements of a AuNP solution by DLS.

Table 4.1. Summary on organic matrix characterisation

Name	Chemical structure	Max Absorption	dGTP mass signal	
			Positive	Negative
CHCA		337 nm	YES	YES
Ferulic acid		325 nm	NO	YES
THAP		286 nm	NO	NO
3-HPA		304 nm	NO	NO
Super DHB		328 nm	NO	NO
Sinapinic acid		325 nm	NO	NO
Cl-Ph-AA		304 nm	NO	NO
HABA		361 nm	NO	NO

4.2.1.2 Characterisation of gold nanoparticles

Synthesised AuNPs were characterised by TEM, DLS, ζ -potential and UV-Vis spectroscopy. TEM imaging revealed a spherical NP population following a roughly normal distribution, with an average diameter of 14 ± 1.6 nm (see Figure 4.1A). The attained AuNP dispersion exhibited a bright red colour and a maximum plasmon band around 519 nm, which shifts to higher wavelengths (≈ 650 nm) in the presence of NaCl (Figure 4.1B). DLS measurements showed a higher frequency of NPs with diameter values around 15-17 nm, with a z-average of 17.7 ± 0.1 nm and a polydispersion index (PI) of 0.37 ± 0.025 (Figure 4.1C,D). Measurement of ζ -potential showed a value of -66.33 ± 2.35 mV indicated a very stable colloidal solution.

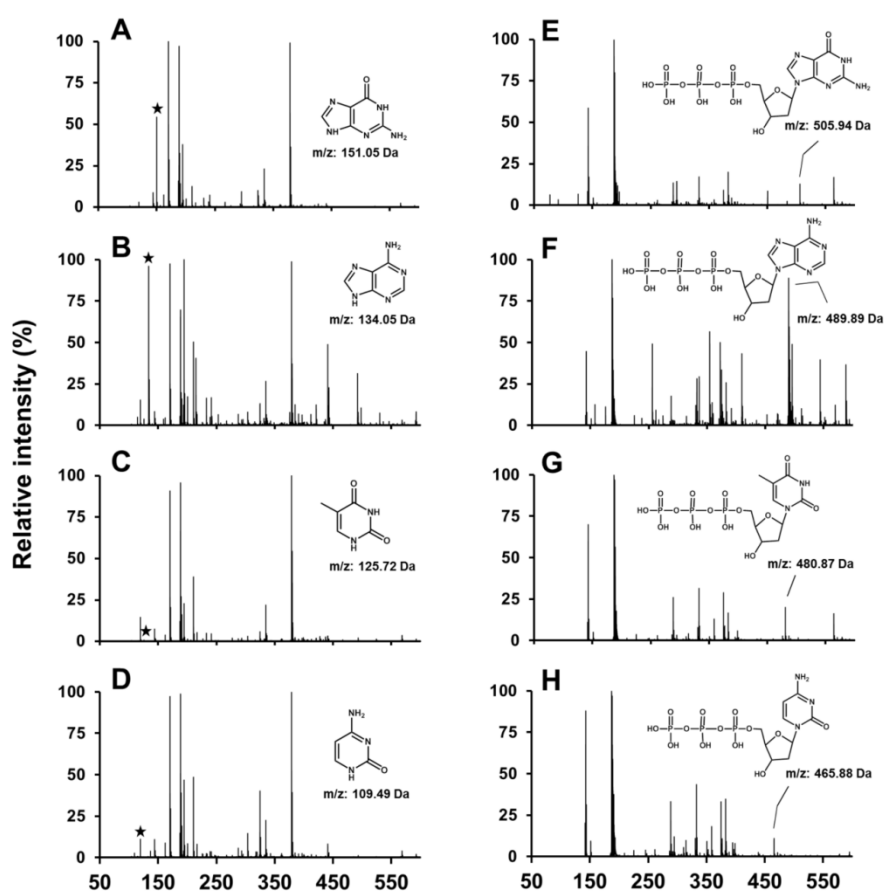


Figure 4.2. MALDI-TOF spectra of dNTPs, using CHCA as a matrix. A-D) acquisition in positive-ion mode: A) matrix+dGTP; B) matrix+dATP; C) matrix+TTP; D) matrix+dCTP. E-H) acquisition in negative-ion mode: E) matrix+dGTP; F) matrix+dATP; G) matrix+TTP; H) matrix+dCTP; Mass signals of nucleobases marked with a black star (A-D). Molecular ion peaks highlighted in the mass spectra (E-H). Structural information on nucleobases and nucleotides is included on each spectrum. Final concentrations: analyte = 500 μ M; matrix = 5 mg/mL.

4.2.1.3 Profiling different nucleotides via MALDI and SALDI

Profiling of diverse deoxynucleotides with CHCA matrix in both positive and negative-ion mode showed different ionisation patterns, revealing a variety of possible molecular rearrangements in the ion plume (Knochenmuss and Zenobi 2003, Knochenmuss and Zhigilei

2012). In positive-ion mode, m/z signals that could be attributed to different nucleobases appeared in lower mass regions of the spectrum (100-200 Da), and molecular ion signals from the whole structure were not detected (Figure 4.2A-D). However, in negative-ion mode m/z signals corresponding to the complete, intact structure of the nucleotides were denoted in the 450-550 Da range (see Figure 4.2E-H), depending on the nucleotide: 505.94 Da for dGTP; 489.89 Da for dATP; 480.87 Da for dTTP; 465.88 Da for dCTP. These results suggest that the analytes fragment during the MALDI process, i.e. the presence of a matrix is not sufficient in protecting this particular type of analytes from fragmentation. Furthermore, mass signals were obtained at relatively close m/z values to those resulting from fragmentation and rearrangement of matrix ions. Therefore, matrix ions constitute an important source in the analysis.

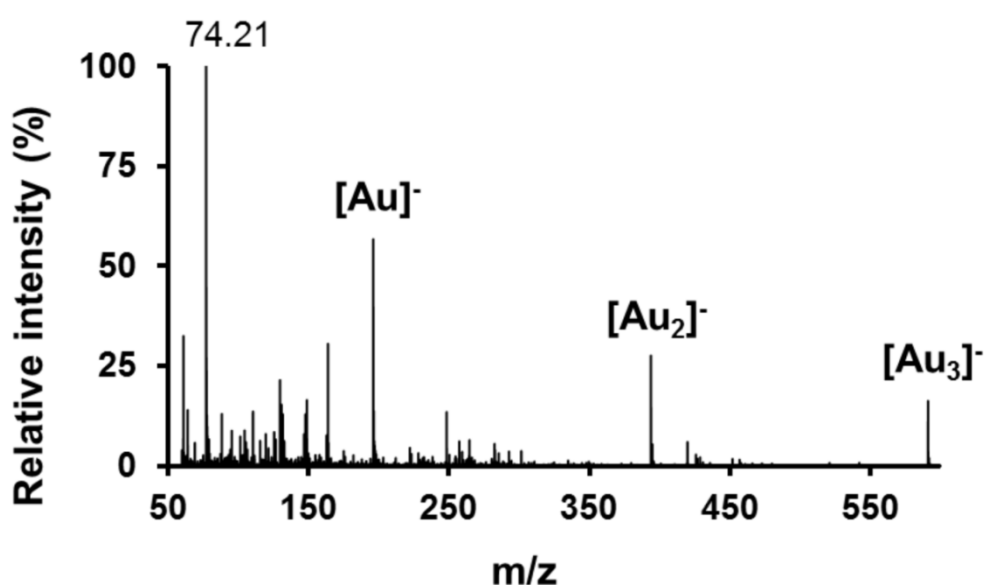


Figure 4.3. SALDI-TOF-MS spectrum for AuNP:nucleotide mixture, acquired in negative-ion mode: m/z signals for gold clusters are visible, as well as an unknown intense signal at 74.21 Da.

In contrast to CHCA, using AuNPs to assist in ionisation do not allow to unequivocally attribute an existing m/z signal to a given nucleotide when acquiring in negative-ion mode. The resulting spectra for any of the different dNTPs are very similar, presenting characteristic signals attributed to gold clusters and a high intensity peak at 74.21 Da, which cannot be associated to the mass/charge (m/z) ratio of any known structures that might have been present in the sample (see Figure 4.3). Conversely, when acquiring in positive-ion mode, specific patterns are observed for each of the analysed nucleotides. Figure 4.4 shows the mass spectra for different deoxynucleotides, when using AuNPs to assist in the ionisation process. Fig. 4.4A presents the mass spectrum for the AuNP solution, where the characteristic signals at 196.96 Da, 236.44 Da, 393.93 Da and 590.89 Da attributed to gold clusters may be observed (McLean et al. 2005). When AuNPs are mixed with the deoxynucleotide sample, the intensity of these characteristic peaks

often plummets, resulting in clearer spectra, allowing identification of specific nucleobase signals with low background noise. This way, identification of deoxynucleotides in positive-ion mode is accomplished in a rather straightforward and rapid manner, as signature peaks that may mask the nucleotide fingerprint are removed from the spectrum. Further analysis of Fig. 4.4B–E reveals common m/z signals in all spectra (337.54 Da, 365.55 Da, 377.55 Da, 421.40 Da, 603.36 Da, 631.30 Da - highlighted with a black asterisk) with variable relative intensities, which may be related to structural similarities between all analytes, i.e. the pentose (deoxyribose) and the phosphate groups. In addition to these signals, some specific signature peaks for each nucleobase can also be easily attributed as the related peak differs according to the analysed nucleotide (Fig. 4.4B: 157.66 Da for guanine; C: 141.65 Da for adenine; D: 132.64 Da for thymine; E: 117.24 Da for cytosine).

In the previous chapter, it was discussed how it was not possible to efficiently separate modified nucleotides from unmodified ones, via chromatography, during sample preparation. For this reason, a final, contaminant-free mixture of nucleotides was obtained, for subsequent MS analysis. With this in mind, and to evaluate specific nucleotide identification via fingerprinting using AuNP-assisted desorption/ionisation, different nucleotides were mixed in equimolar proportions and ionised using AuNPs - see Fig. 4.5. For each case, the specific patterns can be visualised (highlighted in Fig. 4.5 with black asterisks), depending on the presence of distinct nucleobases in the mixture (Fig. 4.5A–D). Regarding ion formation, guanine and cytosine bases are clearly favoured (Fig. 4.5C), as they present a considerably more intense signal. Thymine shows the lowest relative intensity of the analysed nucleotides (see Fig. 4.5B and D). These results support the association between m/z signals in the mass spectra and the presence of different nucleobases in the sample. Despite this association, these signals present a deviation, when in comparison to the molecular weights of different nucleobases. These differences are too great to be explained by calibration errors of the apparatus, but are too low to be considered as cation adducts. At present there is no data in the literature that could help clarifying the underlying reason for this deviation, but this might be somehow related to the AuNPs used for assisting ionisation, whose energy transfer to the sample may induce different ion combinations that have, thus far, not been characterised.

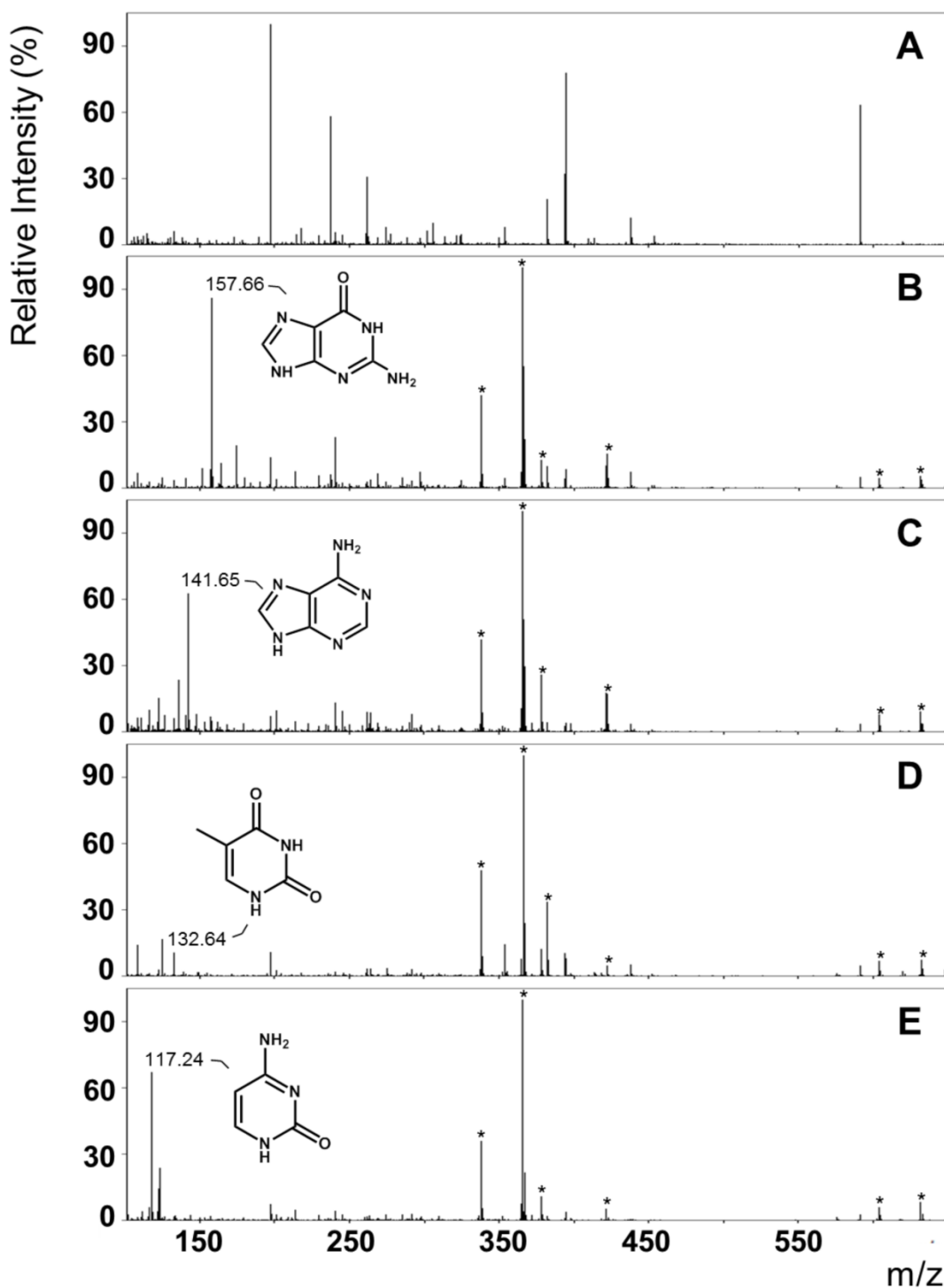


Figure 4.4. Gold nanoparticle based ionisation of dNTPs. The SALDI-TOF spectra of dNTPs obtained using AuNPs for ionisation. A) AuNPs with a final concentration of 15 nM; B) mass spectrum for dGTP; C) mass spectrum for dATP; D) mass spectrum for TTP; E) mass spectrum for dCTP. Black asterisks highlight signature peaks common to all nucleotides. Specific peaks for each nucleotide indicated with the mass value (Da) and structural information displayed next to the label. Final concentration of dNTPs = 500 μ M; AuNPs = 15 nM.

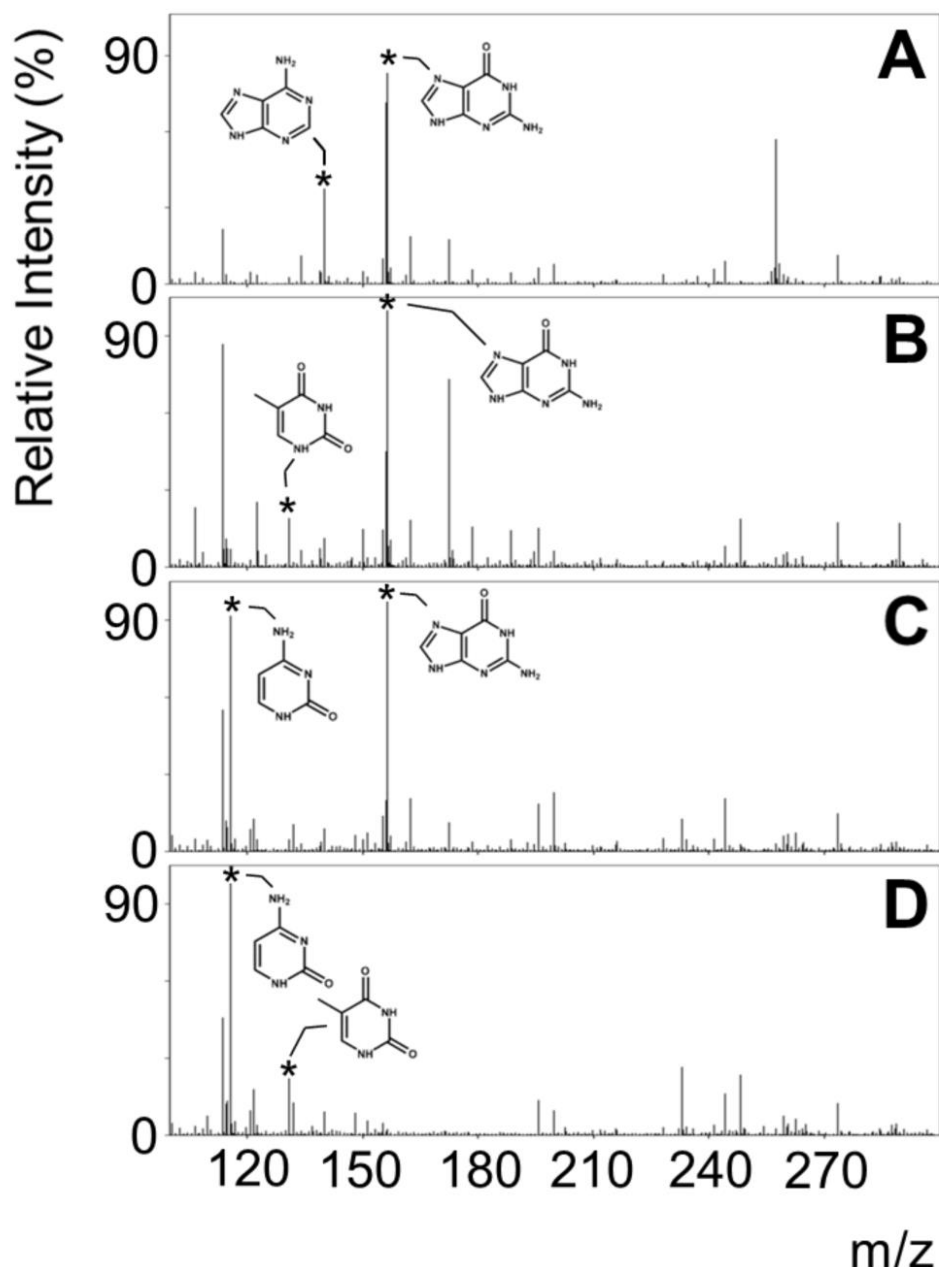


Figure 4.5. AuNP-based SALDI-TOF spectra of equimolar mixtures of dNTPs. A) dATP and dGTP; B) TTP and dGTP; C) dCTP and dGTP; D) dCTP and TTP; Specific peaks for each nucleotide are highlighted in the mass spectra with black stars and chemical information of the various nucleotides displayed next to it. Final concentration of dNTPs = 500 μ M; AuNPs = 15 nM.

4.2.1.4 Influence of concentration and pH for nucleotide detection

Because laser desorption/ionisation is a destructive ionisation technique with some instrumental variability, the influence of analyte and matrix/AuNP concentration on the signal intensity was assessed, together with spot-to-spot variability. All MALDI-TOF and SALDI-TOF analyses were performed considering the most intense m/z signal in the spectrum as 100%, and the relative intensities of the desired signals calculated accordingly. This would provide an analysis of the variation of relative intensity in m/z signals corresponding to the analyte, without however providing any kind of information on quantification. Varying the matrix concentration has not

produced major alterations in relative intensity of dGTP signal, in negative-ion mode (see Figure 4.6A), apart from variability. As for the relation between analyte concentration and relative intensity, it follows a hyperbolic tendency, with an initial increase and subsequent stabilisation, from a dGTP concentration of 100 μM on (Figure 4.6B).

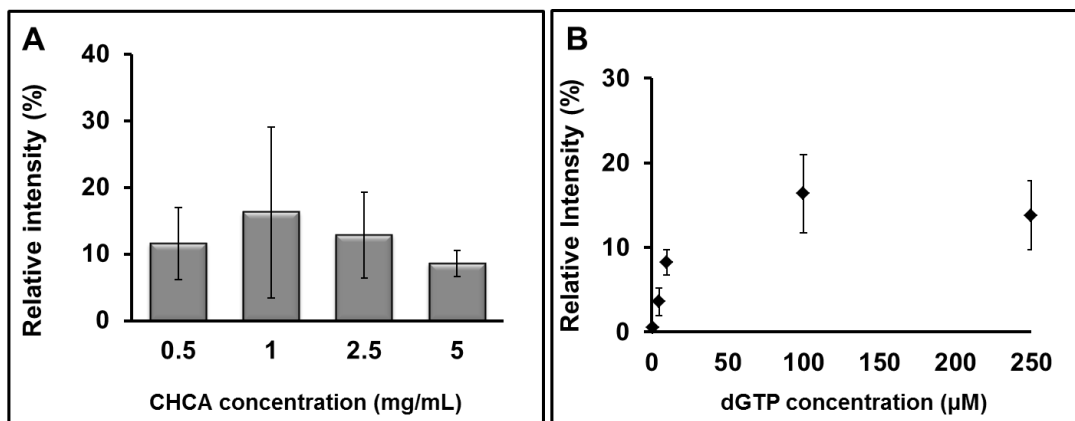


Figure 4.6. Variation of analyte and matrix concentration. A) The relative intensity of the dGTP peak is plotted against the dGTP concentration from data attained for the observed mass peak at 507.9 Da, in negative-ion mode. B) Variation of relative intensity with concentration of CHCA in the mixture. All data was collected from 5 independent replicates.

Regarding SALDI-TOF analysis, the analyte (dGTP) concentration was varied from 0 to 250 μM in the presence of AuNPs, and the relative intensities of the identified peak (157.66 Da) have been analysed. Data depicted in Figure 4.7A shows an increase in the intensity of m/z signals for an increasing analyte concentration up to 50 μM , where the signal intensity starts to stabilise up to the maximum concentration of analyte used (250 μM). The inset shows a closer look into the first concentrations, until 50 μM , where there appears to be a linear relation between the signal relative intensity and analyte concentration. This relation between relative intensity and analyte concentration shows that, after optimisation of the procedure and calibration of the detection set-up, an actual quantification assay might be possible (using a standard with different isotopes). The 0–50 μM concentration range was chosen to further analyse glycidamide–guanine adducts. The influence of AuNP concentration was also evaluated. Figure 4.7B shows that 15 nM appears to favour both relative intensity and little variability of the mass signal. Other authors have also reported this concentration as being suitable for analysis of other small organic molecules via AuNP-based SALDI-TOF (Chiang et al. 2010). All in all, this concentration also seems to be suitable for nucleotide analysis. Subsequently, a rapid evaluation of the influence of pH was performed, as well as the differences when using buffer or water as a solvent (Figure 4.7C). Data in Figure 4.7C indicates that, if standard deviations are considered, there is no considerable variation in relative intensity according to the pH of the sample. Using water as a solvent promotes both elevated intensity in the analyte signals, as well as low spot-to-spot variability, similarly to ammonium citrate at a pH close to neutral (6 or 7).

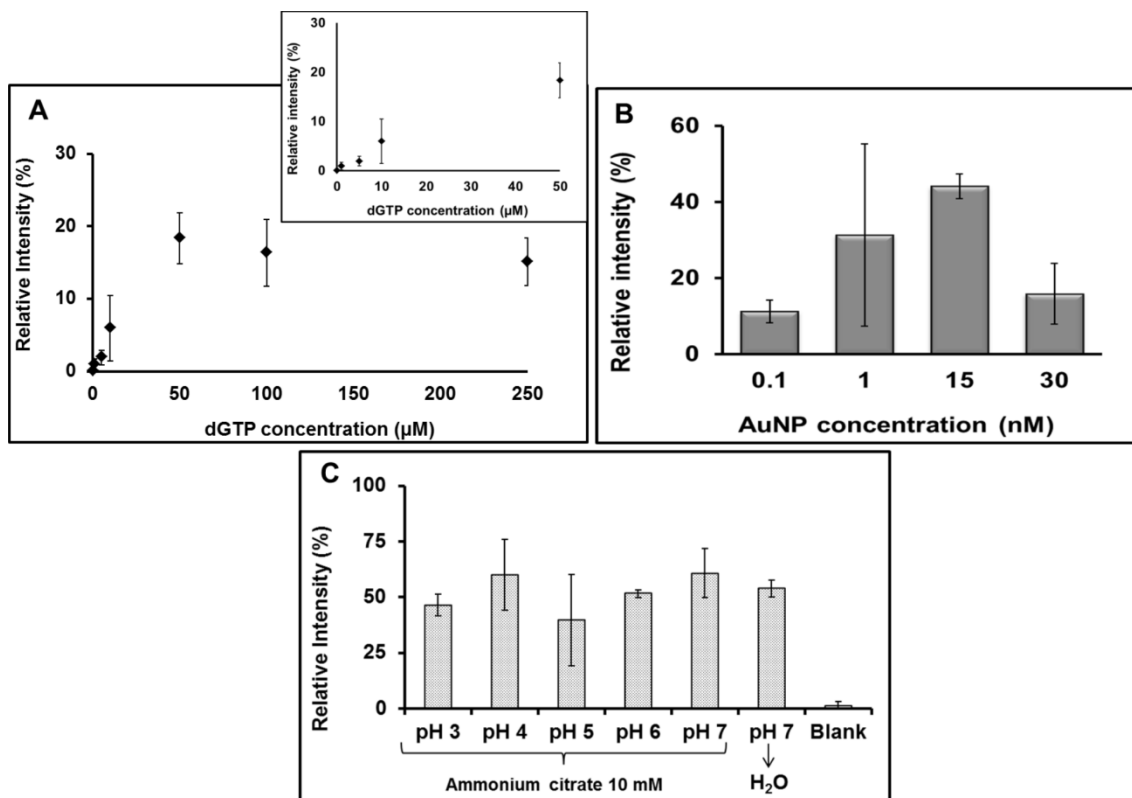


Figure 4.7. Variation of different parameters and its influence on the relative intensity of the guanine m/z signal. A) Semi-quantification of dGTP via AuNP-SALDI: relative intensity of the signal is plotted against the dGTP concentration from data attained for the observed mass peak at 157.66 Da, as an indicator to the presence of guanine (inset highlights a linear tendency between 0 and 50 µM). B) Influence of AuNP concentration on spot-to-spot variability and relative intensity. C) Alterations in relative intensity according to variations in the pH of the mixture.

4.2.1.5 Identification of DNA adducts generated *in vitro*

Upon a successful identification of deoxynucleotides in positive-ion mode using AuNPs for ionisation, the described AuNP-SALDI approach was applied to enhance detection of a most relevant analyte that can be used as exposure biomarker. Glycidamide (GA) is a well-known alkylating agent capable of generating guanine derived DNA adducts. GA is an epoxide derived from acrylamide (AA) biotransformation via cytochrome P450 monooxygenase pathway. Genotoxicity induced by AA has been reported that has been frequently associated to the N7-GA-Gua adduct resulting from a nucleophilic attack of GA to the guanine nitrogen centres on DNA molecule (Segerbäck et al. 1995, Gamboa da Costa et al. 2003, Besaratinia and Pfeifer 2004, Martins et al. 2007).

In vitro alkylation reaction and sample spotting on the MALDI plate were performed as described in chapter 2, sections 2.4.1.3 and 2.4.4.2, respectively. Based on the GA molecular weight (87 Da) and previously described structures for GA-DNA adducts (Gamboa da Costa et al. 2003, Backman et al. 2004), the GA-Gua adduct ought to present a specific peak in the 244–245 Da mass range (considering the guanine’s characteristic signature of 157.66 Da attained

beforehand plus 87 Da). Fig. 4.8 shows the obtained AuNP-based SALDI spectra for GA, in Fig. 4.8A; dGTP, in Fig. 4.8B; and dGTP+GA, in Fig. 4.8C. All spectra present a considerably intense mass peak at 236.44 Da, associated to AuNPs. Fig. 4.8C shows a mass peak at 244.62 Da, which is not present in any other sample and can be attributed to the presence of guanine adducts. A similar mass deviation is denoted, such as the one discussed for nucleotide identification, as GA-Gua adducts have been analysed via MALDI-TOF with CHCA, and found to possess a m/z signal of 239.97 Da (see Figure 4.6). No formation of sodium cationic species was observed when AuNPs were used, in contrast to what happened with CHCA (Figure 4.9). Fig. 4.8D reveals a linear trend within the 0–50 mM concentration range for dGTP+GA. The proposed AuNP-based SALDI approach allows identification of GA-Gua adducts through fingerprinting down to 5 μM , which corresponds to 5 pmol on the MALDI plate. However, this concentration may not correspond to the actual GA-Gua adduct final concentration as this is directly related to the alkylation reaction yield.

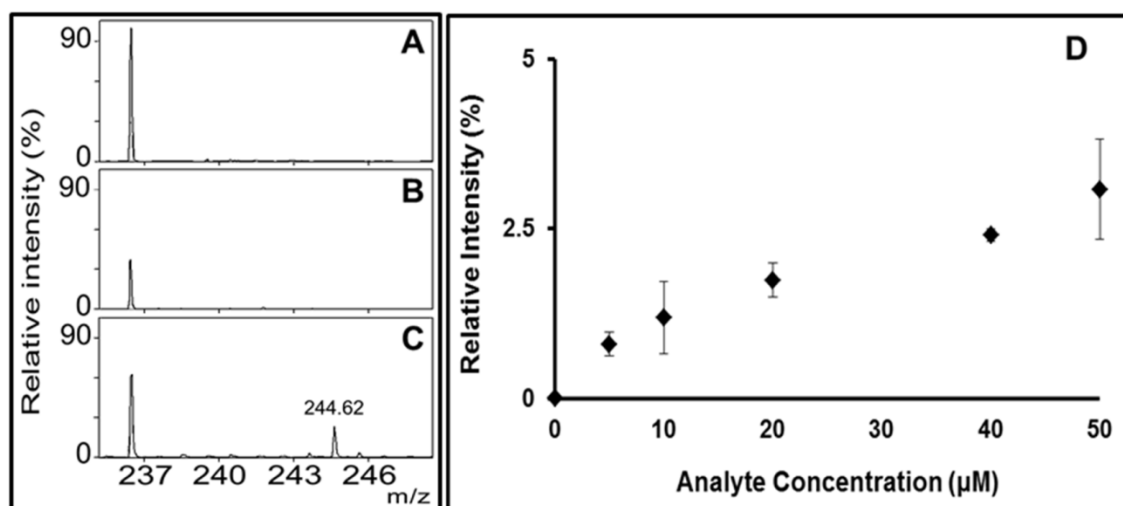


Figure 4.8. AuNP-SALDI-TOF for identification nucleotide adducts. AuNPs based SALDI approach was used to identify a glycidamide-guanine DNA adduct. Mass spectra attained within the considered mass range for A) AuNPs and glycidamide; B) AuNPs and dGTP; C) AuNPs and dGTP, previously reacted with glycidamide. A specific signature peak only observed in spectrum C, at 244.62 Da associated to the presence of GA-Gua DNA adduct. D) Plot of relative intensity vs. analyte concentration for the observed mass peak at 244.62 Da.

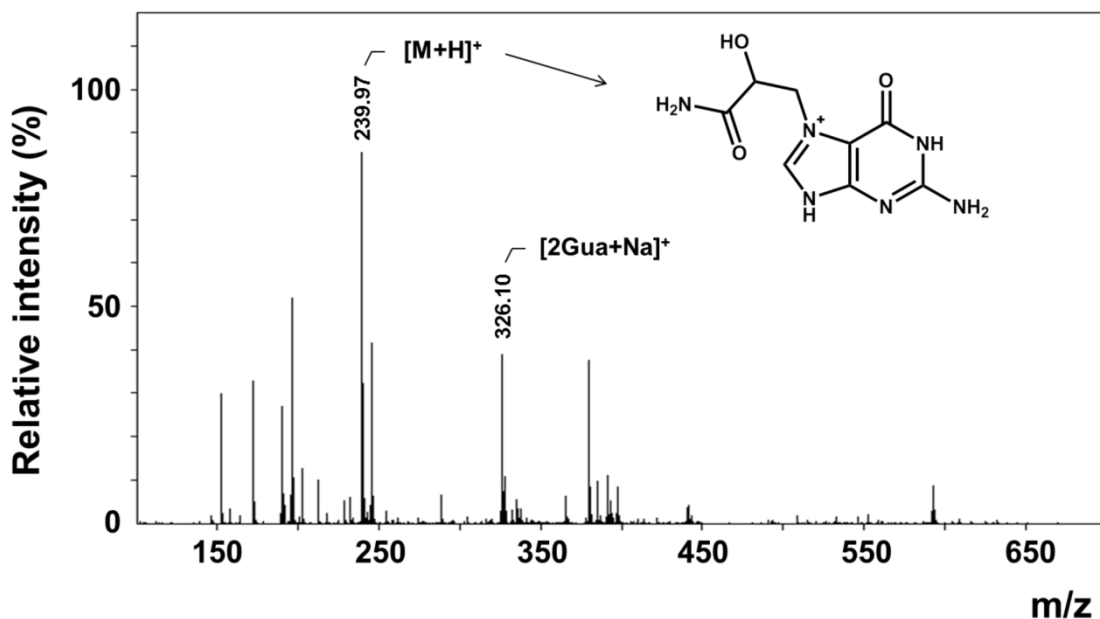


Figure 4.9. MALDI-TOF analysis of a previously reacted mixture of GA and dGTP, using CHCA as a matrix. A specific signal corresponding to a GA-guanine adduct can be denoted. Structural information on the GA-Gua adduct is also depicted on the spectrum.

4.2.1.6 Identification of DNA adducts as biomarkers in biological samples

The proposed AuNP-SALDI approach was applied to detection of glycidamide-DNA adducts in biological samples from goldfish hepatopancreas. *Carassius auratus* (goldfish) individuals were exposed to 150 mg/L of acrylamide in water during 96 hours, then euthanised and the organs removed for further testing, as indicated in chapter 2, section 2.4.5.4. Hepatopancreas samples were treated as previously described in chapter 3 and subsequently spotted in a stainless steel plate with CHCA (for MALDI) or AuNPs (for SALDI). MALDI-TOF with CHCA allowed the identification of a m/z signal at 239.97 Da, with a S/N of 103, which may correspond to a GA-guanine DNA adduct (marked with a black star in Figure 4.10A). No combinations with cations or other molecular rearrangements that may have occurred after ionisation were observed. The identified m/z signal does not appear in mass spectra from control samples (Figure 4.10B), i.e. individuals not exposed to acrylamide, so it must identify a by-product from acrylamide metabolism or cellular damage. In contrast, no similar m/z signals have been observed when AuNPs were employed for SALDI-TOF analysis (Figure 4.10C). These results seem to indicate that the AuNP-based SALDI-TOF approach for analysis of modified nucleotides does not yield comparable results to MALDI-TOF, when employing an adequate organic matrix, e.g. CHCA.

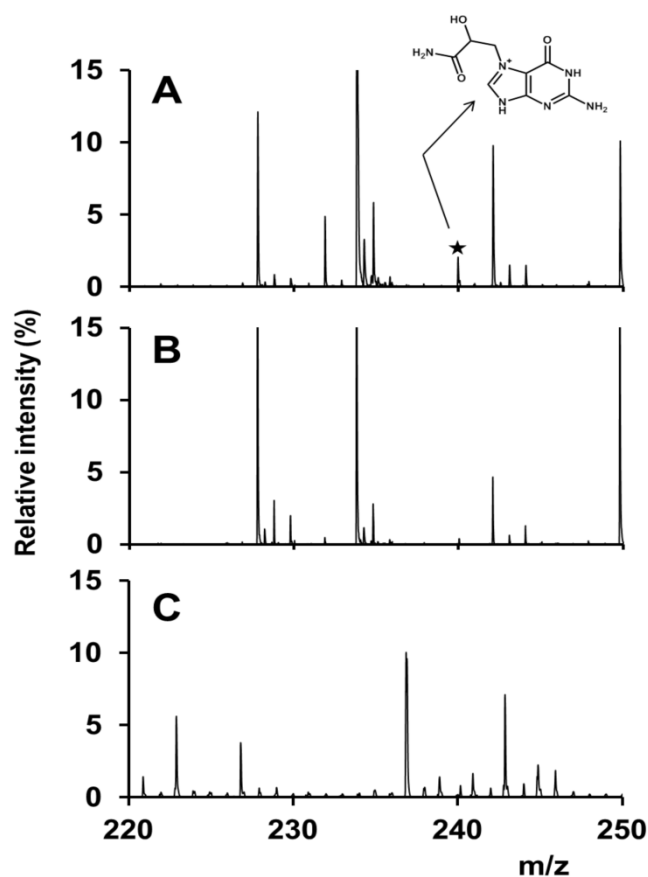


Figure 4.10. MS analysis of a previously treated DNA sample: A) MALDI-TOF analysis of a sample from goldfish, previously exposed to 150 mg/L acrylamide; B) MALDI-TOF analysis of a sample from control goldfish, not exposed to acrylamide; C) AuNP-SALDI-TOF analysis of a sample from goldfish, previously exposed to 150 mg/L acrylamide. Black star marks the molecular ion signal for a DNA adduct (structural information included).

4.2.2 Colorimetric detection of modified nucleotides using aptamer-gold nanoprobe

4.2.2.1 Characterisation of gold nanoparticles

Characterisation of synthesised gold nanoparticles is equivalent to that depicted in Figure 4.1. Synthesis yielded spherical AuNPs with an average diameter of 14 nm. The NP population followed a normal distribution, with a maximum absorption band centred at 519 nm. For additional information, please refer to section 4.2.1.2 and Figure 4.1 in this chapter.

4.2.2.2 Stability of synthesised nanoprobe

Functionalisation with the DNA aptamers causes the plasmon band to shift 6 nm to the right (maximum absorption at 525 nm) – see spectral profiles of disperse and aggregated nanoprobe in Figure 4.11A,B. Au-aptamer nanoprobe stability against increasing MgCl_2 concentrations was assessed and the areas under the curve ($\text{AUC}_{500-550}/\text{AUC}_{580-630}$) were used as an analytical tool to evaluate nanoprobe stability (see progressive de-stabilisation in Figure 4.11C,D). XBA-nanoprobe de-stabilisation is observed for MgCl_2 concentrations above 50 mM (Figure 4.11A,C).

Contrastingly, His-945 nanoprobe shows a more elevated stability, up to a concentration on 90 mM of MgCl_2 (Figure 4.11B,D). To ensure maximum efficiency and discrimination in the subsequent detection assays, the chosen MgCl_2 concentrations for the XBA and His-945 nanoprobe were 60 and 100 mM, respectively.

Afterwards, the Au-aptamer nanoprobe behaviour in the presence of dNTPs was assessed. The presence of dNTPs appears to differently influence nanoprobe stabilisation as different tendencies can be denoted for both nanoprobe. In the presence of different dNTPs, the AUC ratio of XBA-nanoprobe increases progressively with purine nucleotide (dATP and dGTP) concentration, whereas pyrimidines do not appear to efficiently stabilise the nanoprobe (Figure 4.12A). On the other hand, His-945 nanoprobe does not appear to efficiently stabilise with increasing dNTP concentration, regardless of the nucleotide (Figure 4.12B), and exhibits increased variability than XBA nanoprobe. From this test, the different specificity from each aptamer towards nucleotides can clearly be denoted. The XBA-aptamer has been described for specific binding of guanine and xanthine (Kiga et al. 1998), and according to this result, purine nucleotides better succeed in stabilising the XBA-nanoprobe, so it would appear that a ligand with a higher affinity stabilises the Au-nanoprobe against salt-induced aggregation.

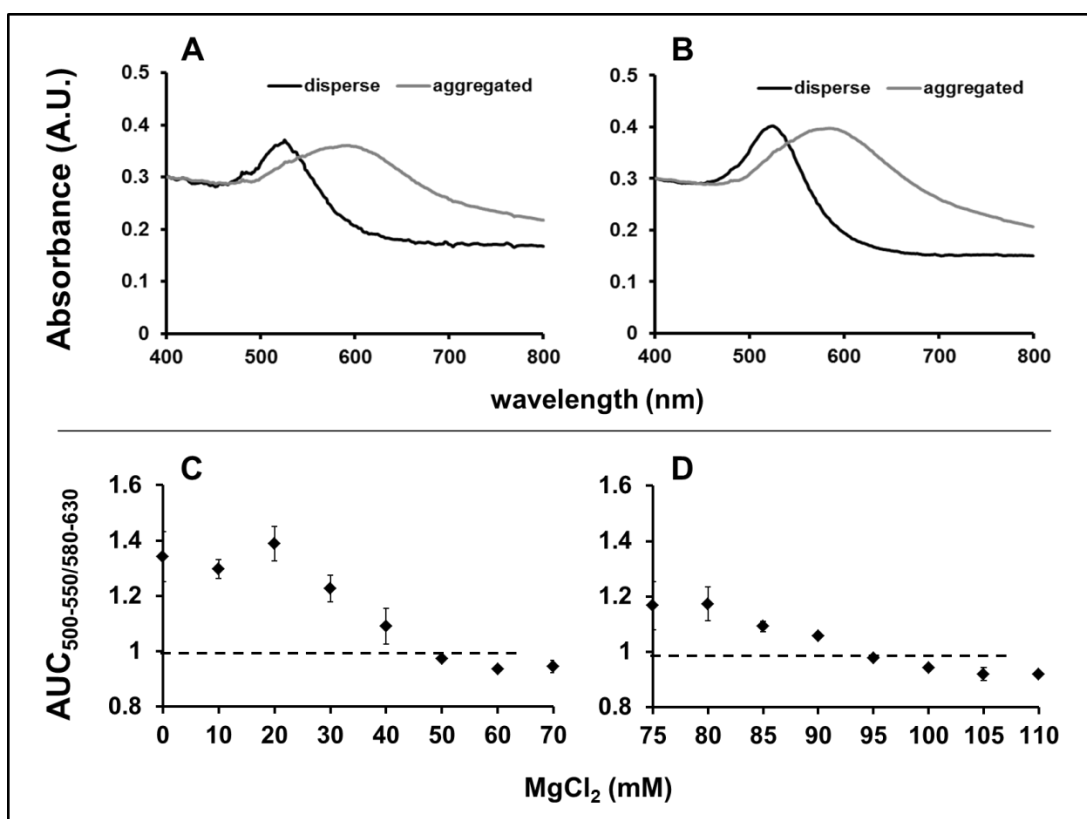


Figure 4.11. Gold-aptamer nanoprobe stability against salt-induced aggregation. Spectral profiles of disperse and aggregated nanoprobe for A) XBA-nanoprobe, and B) His-945 nanoprobe. Progressive destabilisation with increasing MgCl_2 concentration for C) XBA-nanoprobe, threshold set at 60 mM MgCl_2 ; and D) His-945 nanoprobe, threshold set at 100 mM MgCl_2 .

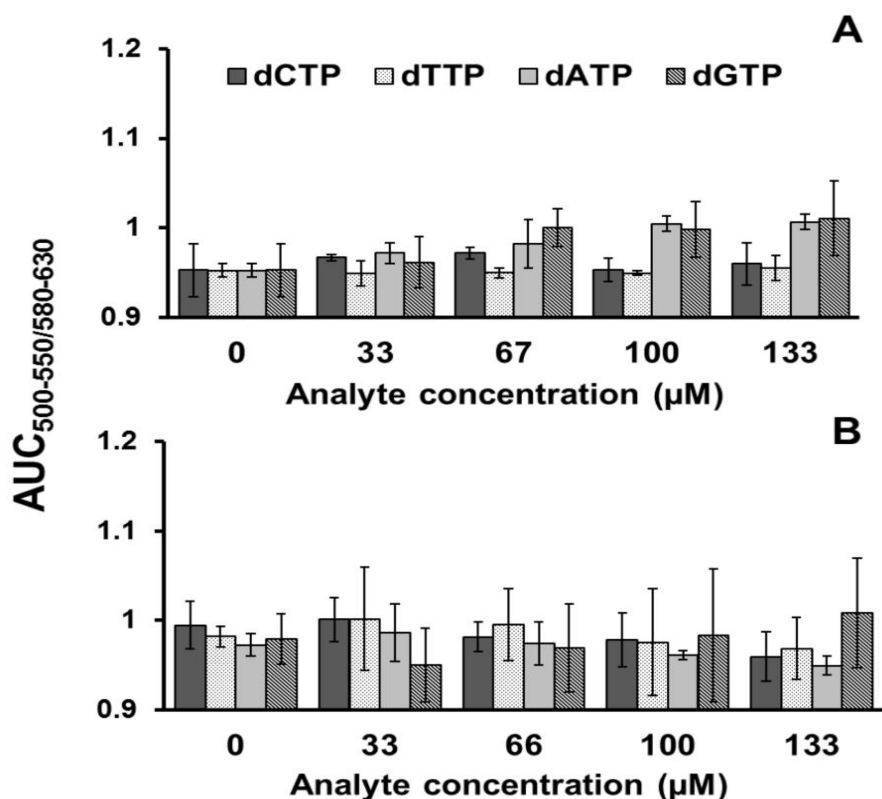


Figure 4.12. Detection assay for different dNTPs with: A) the XBA-nanoprobe, with a final MgCl₂ concentration of 60 mM; B) His-945 nanoprobe, with a final MgCl₂ concentration of 100 mM. Presented values and error bars correspond to average \pm SD.

4.2.2.3 Colorimetric detection of glycidamide-guanine adducts

Both nanoprobes were evaluated for its capability to efficiently discriminate GA-alkylated guanines from GA and dGTP. A discrimination assay between dGTP, GA and modified guanine (GA-Gua adduct) is highlighted in Figure 4.13A, where both the AUC ratio and the spectral behaviour are shown. Regarding the spectra, in both dGTP and GA assays a plasmon shift occurs to higher wavelengths (\sim 600 nm) which translates into Au-nanoprobe de-stabilisation and subsequent aggregation, whereas in the presence of GA-Gua adduct, the maximum plasmon band remains at 525 nm indicating higher stabilisation against ionic strength. The presence of an analyte with affinity is believed to bind the aptamer, inducing the formation of a secondary structure that increases Au-nanoprobe stabilisation against salt-induced aggregation. Rising concentrations of these analytes were tested and verified both spectral behaviour and AUC ratio.

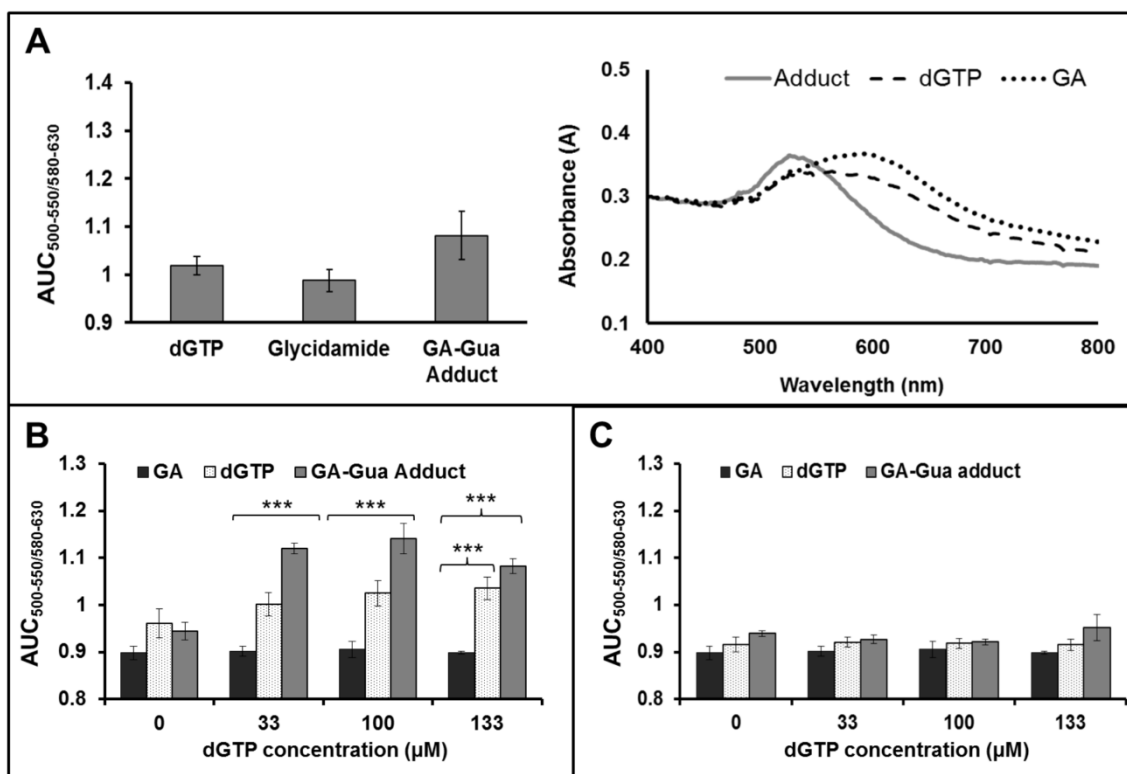


Figure 4.13. Detection of glycidamide-guanine adducts using gold-aptamer nanoprobcs. A) Discrimination of glycidamide-guanine adducts by AUC analysis (left) and spectral behaviour (right) in a final nucleotide concentration of 67 μM . Areas under the curve (AUC) for B) the XBA-nanoprobe and C) the His-945 nanoprobe, in the presence of the three different analytes. AUC values and error bars correspond to average \pm SD. *** highlight statistical significant differences ($p < 0.001$). Square brackets indicate comparisons between the three different conditions (GA, dGTP and GA-Gua adduct). Curly brackets indicate comparison between two conditions.

Results in Figure 4.13B present similar AUC ratios for increasing concentration of GA, which means the nanoprobe stability is not altered, for the tested concentrations. Rising concentration of guanine nucleotides however, both unmodified and alkylated, progressively stabilise the XBA-nanoprobe against salt-induced aggregation. Nevertheless, for all tested concentrations, the AUC ratio is considerably higher in the case of the latter, which allows the identification of modified guanines in a dGTP:adduct mixture, for guanine concentrations higher than 33 μM . Multiple comparisons using the Tukey's HSD test found significant differences ($p < 0.001$) between all AUC ratio mean values, at concentrations of 33 and 100 μM (square brackets and asterisks in Figure 4.13B). At a superior concentration, no significant differences were found between dGTP and GA-Gua adduct ($p > 0.05$), however both significantly differ from GA ($p < 0.001$) – curly brackets in Figure 4.13B. Regarding the His-945 nanoprobe, throughout the studied concentrations, the AUC ratio is slightly more elevated than both dGTP and GA, however with similar values, none of them reaching the threshold value of 1 (Figure 4.13C). For the His-945 probe, no significant differences were found between the obtained values of AUC ($p > 0.05$). This indicates that the His-945 nanoprobe is not efficiently stabilised against salt-induced aggregation, which may indicate this sequence possesses reduced affinity for the tested analytes.

4.2.2.4 Identification of DNA adducts in solution

Considering the previously obtained results where the XBA-nanoprobe seems to efficiently identify alkylated guanines, this nanoprobe was tested with rising concentrations of both alkylated and unmodified genomic DNA. Both samples were heated to 95 °C to ensure complete release of the alkylated guanines from the DNA chain. Increasing concentrations of genomic DNA increase the AUC ratio i.e. progressively stabilise the nanoprobe against aggregation. The values for AUC ratio are very similar and only from 150 µg/mL differences can be denoted, although both values remain above the threshold (Figure 4.14), and a clear discrimination between treated and untreated genomic DNA is more troublesome to attain. This is in accordance with statistical analysis, which found no significant differences ($p > 0.05$) between the mean values of AUC ratios, for colorimetric detection in genomic DNA. These differences are possibly related to fewer DNA adducts being generated *in vitro* when GA is reacted with genomic DNA, rather than dGTP alone. Moreover, the sample complexity is considerably higher than before, when only dGTP was present as a monomer, instead of all four nucleotides as a polymer chain.

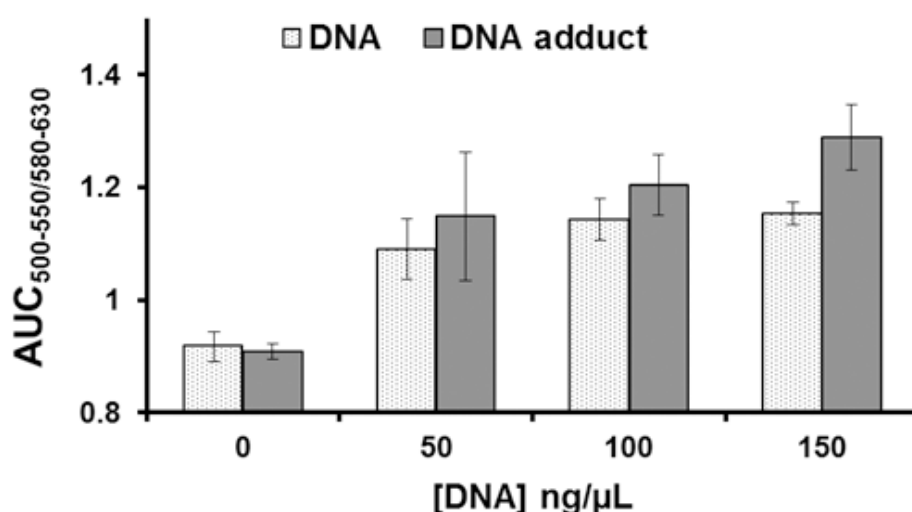


Figure 4.14. DNA adduct detection assay with XBA-nanoprobe. Below 150 µg/mL genomic DNA, no differences are denoted; final MgCl₂ concentration = 60 mM. AC values and error bars correspond to average ± SD.

4.3 Conclusions

The first section of this chapter described a rapid and easy methodology for identification of deoxynucleotides through specific nucleotide fingerprint by using gold nanoparticles for SALDI-TOF-MS. The use of gold nanoparticles greatly contributes to lower background noise generally associated with fragmentation of organic matrices used in MALDI-TOF analysis of molecules in the low mass range (<600 Da). However, MALDI-TOF using CHCA as a matrix has proved more

flexible, as it can identify nucleotides in both positive and negative-ion mode. The AuNP-SALDI approach was subsequently applied to the successful identification of a biologically relevant DNA adduct resulting from glycidamide alkylation of guanine. *In vivo* formation of glycidamide-alkylated guanines may be regarded as a biomarker of acrylamide-induced genotoxicity, and its detection is therefore of paramount importance for toxicity studies. However, the proposed concept was not enough to ensure an efficient detection of DNA adducts in biological samples from individuals exposed to acrylamide possibly due to a low abundance of DNA adducts being generated *in vivo*. To increase the probability of a successful identification, further work before detection is required, namely the development of optimal preparation strategies including isolation of the DNA adduct in study. MALDI-TOF with CHCA, on the other hand produced a low intensity signal, albeit with very good S/N, accounting for identification of glycidamide-guanine DNA adducts in biological samples. All data considered it would appear that, in terms of sensitivity, AuNP-SALDI-TOF still does not yield comparable results to MALDI-TOF with a suitable organic matrix. This data was published in Larginho et al. 2013 (Talanta 105:417-421).

In the second section of this chapter, a colorimetric detection assay using Au-aptamer nanoprobe for the detection of modified nucleotides was shown. This approach was inspired on the non-cross-linking hybridisation system developed by Baptista et al. (2005) and optimised for discrimination of nucleotide sequences and point mutations (Doria et al. 2007, Doria 2010; Conde et al. 2010). The reported concept was employed to identify glycidamide-alkylated guanines, firstly in a nucleotide solution, with statistical significance ($p < 0.001$), and afterwards in a genomic DNA sample. This methodology may reveal itself very valuable for its capability to detect DNA adducts in solution in a rather fast, simple and inexpensive way, with results as rewarding as currently used techniques. However, there is still the need for future studies on quantification capability together with characterisation of the limit of detection when using real biological samples. This data was published in Larginho et al. 2014 (IET Nanobiotechnology).

CHAPTER 5. ALTERATIONS TO AQUATIC ORGANISMS INDUCED BY ACUTE AND CHRONIC EXPOSURE TO ACRYLAMIDE

Some of the results presented in this chapter have been published in Larguinho M, Costa PM, Sousa G, Costa MH, Diniz MS, Baptista PV. 2014. Histopathological findings on *Carassius auratus* hepatopancreas upon exposure to acrylamide: correlation with genotoxicity and metabolic alterations. *Journal of Applied Toxicology*, 34:1293-302, where Miguel Larguinho was responsible for the part of the experimental work (exposure assay, effect concentrations, comet-assay and phase I/phase II biomarkers), and writing part of the manuscript.

Some of the results presented in this chapter have been published in Larguinho M, Cordeiro A, Diniz MS, Costa PM, Baptista PV. 2014. Metabolic and histopathological alterations in the marine bivalve *Mytilus galloprovincialis* induced by chronic exposure to acrylamide, *Environmental Research*, 135:55-62, where Miguel Larguinho was responsible for part of the experimental work (exposure assays, effect concentrations, oxidative stress biomarkers and part of the histology), and writing part of the manuscript.

If you only read the books that everyone else is reading, you can only think what everyone else is thinking.

Haruki Murakami

5.1 Introduction

In order to fully understand the toxicological challenge pertaining a specific toxicant, it is paramount to possess a well characterised biological model of exposure. The previous chapter addressed the detection of DNA adducts as biomarkers of exposure to acrylamide. Apart from adducts generated *in vitro*, it was necessary to test the AuNP-based methods in biological samples from individuals previously exposed to acrylamide. With this in mind, this chapter describes toxicity studies in biological organisms, to establish a model of exposure to acrylamide in water. Exposure assays will be carried out to evaluate molecular and cellular consequences in aquatic organisms, triggered after acute or chronic exposure to waterborne acrylamide, to mimetise a “real exposure” and its consequences.

Acrylamide is widely used for the production of polyacrylamide (co)polymers for agricultural applications (Myagchenkov and Kurenkov 1991) and water treatment processes (Bajdur 2008). The presence of acrylamide in water courses, mainly freshwater, is somewhat inevitable, in part due to the degradation chemistry of polyacrylamide polymers to acrylamide monomers, but also due the proximity of agricultural crop fields or manufacturing plants to freshwater systems. In brackish or seawater, however it is more ecologically relevant to assess the prolonged effects of exposure to low acrylamide concentrations, since it is very difficult to reach elevated toxic concentrations in marine ecosystems due to its wide surface area and depth. The environmental risk associated with the presence of acrylamide in water ecosystems has led to the work here presented.

Due to their ecological and biological relevance, two different models of study will be used. The first section addresses the effects of acrylamide to a teleost freshwater fish (*Carassius auratus*), commonly known as goldfish. The second section will address the putative chronic effects of acrylamide in aquatic wildlife, using a marine bivalve (*Mytilus galloprovincialis*), commonly known as Mediterranean mussel, as a model. For a more clear comprehension and cohesive discussion integrating all obtained data, each of the sections in the following chapter is divided into separate Results and Discussion sections.

5.2 Acute toxicity of waterborne acrylamide to goldfish

Teleosts constitute almost 50% of the subphylum Vertebrata, comprising an immense variety of habitats and possess several advantages towards the research of toxicological issues such as relatively short life cycles, high reproduction rate, rather easy manipulation and low cost maintenance, which renders these organisms as appealing surrogates for higher-order vertebrates, such as mammals (reviewed in Bolis et al. 2001). In addition, these fish present biological

similarity with higher vertebrates, including the ability to metabolise xenobiotics and bioaccumulate toxicants and their by-products (Bolis et al. 2001, van der Oost et al. 2003). *Carassius* sp. in particular have been used for a multitude of studies concerning toxicity effects (Diniz et al. 2009, Cavas 2011, Kubrak et al. 2012) including exposure to different pollutants in water, e.g. heavy metal ions. This first section shall evaluate the effects of acrylamide at several levels of biological organisation and try to establish a vertebrate biological model of study for acrylamide deleterious effects. Particularly, the extent of genotoxic and mutagenic effects of acrylamide will be evaluated, and its correlation to deployment of biochemical defences that are recognised mechanisms for other organic toxicants (c.a. CYP1A and glutathione S-transferases). In addition, a qualitative histopathological analysis in liver and pancreatic tissues will also be subject of study.

5.2.1 Results

5.2.1.1 Mortality

The determined LC_{50} for acrylamide in water was estimated as 119.5 mg/L as shown in Figure 5.1. The highest tested concentration of acrylamide (200 mg/L) resulted in a mortality index of 100 % (see Table 5.1).

Table 5.1. Mortality rate for the control group and each tested acrylamide concentration (Conc.).

Conc. (mg/L)	Control	50	100	150	200
Individuals	8	8	8	8	8
Total Dead	0	1	1	5	8
Mortality (%)	0	12.5	12.5	62.5	100

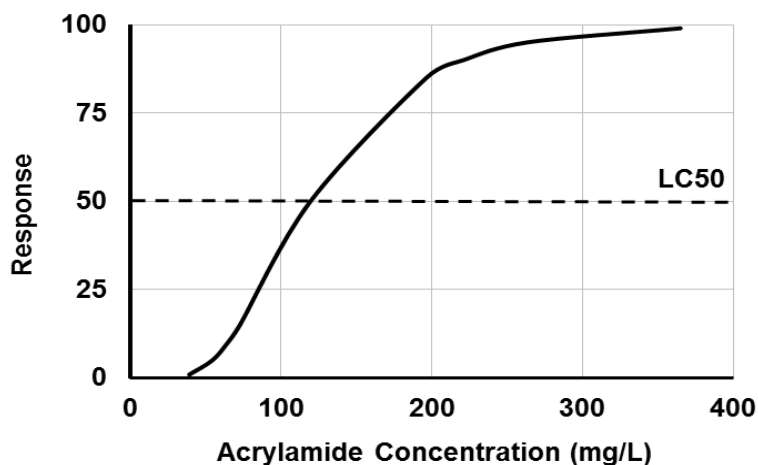


Figure 5.1. Fitted dose-response curve obtained for goldfish 96-hour exposure to acrylamide. Estimated LC_{50} = 119.5 mg/L.

5.2.1.2 Genotoxicity assessment

Fig. 5.2 illustrates representative examples of erythrocytic nuclei, from normal-shaped (Fig. 5.2A) to distinct classes of ENAs (Figs. 5.2B to 5.2I). Lobed nuclei (Fig. 5.2B) and nuclear buds (Fig. 5.2E) were the most frequently observed abnormalities. Fig. 5.3A summarises the average frequency of ENA-exhibiting cells observed for each acrylamide test. The control group shows an ENA frequency of $4.09 \pm 0.39\%$, which tends to increase significantly - Mann-Whitney U ($p < 0.05$) - with acrylamide concentration, reaching a value of $17.14 \pm 0.93\%$ for the highest tested concentration (150 mg/L).

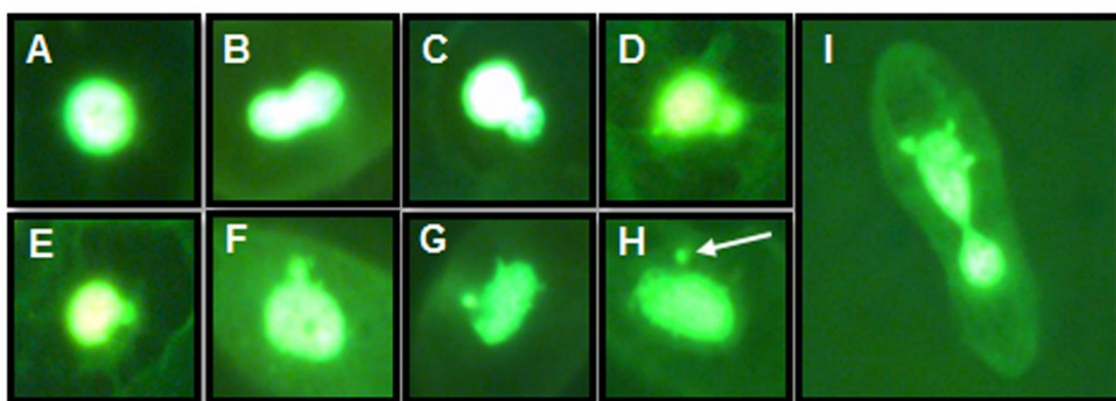


Figure 5.2. Reference images for the observed erythrocytes and alterations. A) mature goldfish erythrocytes; B) bilobed (fragmenting) nucleus; C,D) budding nuclei; E-G) nuclear buds, towards formation of a micronucleus; H) erythrocyte exhibiting evidenced micronuclei (highlighted with a white arrow); I) polynucleated cell (full fragmentation) exhibiting micronuclei.

Peripheral blood cell comets were assigned to five different classes, according to the % of DNA in tail: class I - 0 to 20% DNA, class II - 20 to 40%, class III - 40 to 60%, class IV - 60 to 80% and class V - 80 to 100% (Fig. 5.4). No comets were found belonging to class V in any experimental condition. The control group shows an average $32.35 \pm 10.68\%$ of DNA in tail (Fig. 5.3B) that tends to increase with acrylamide concentration. The most significant increase, comparative to control, was observed in fish exposed to 150 mg/L, where the average value of DNA percentage in tail reached $59.61 \pm 9.23\%$ (Fig. 5.3B). Significant positive correlations ($p < 0.01$) were found between acrylamide concentration and both ENA frequency and DNA-strand breakage ($R = 0.961$ and 0.636 respectively), and between individual ENA frequencies and total DNA-strand breakage ($R = 0.676$) – see Table 5.2, extrapolated from the % of DNA in the nucleoids' tail.

5.2.1.3 CYP1A induction

Figure 5.3C shows a progressive increase in hepatic CYP1A according to the different acrylamide concentrations. Data show a similar behaviour to that of the Comet assay, i.e. a dose-dependent increase is observed, steeper towards exposure to 150 mg/L acrylamide, where the

induction of CYP1A reached 1.67-fold in comparison to control (Fig. 5.3C). CYP1A induction yielded significant, positive correlations ($p < 0.01$) with ENA frequency, total DNA strand breakage and acrylamide concentrations ($R = 0.745, 0.670$ and 0.678 , respectively) – Table 5.2.

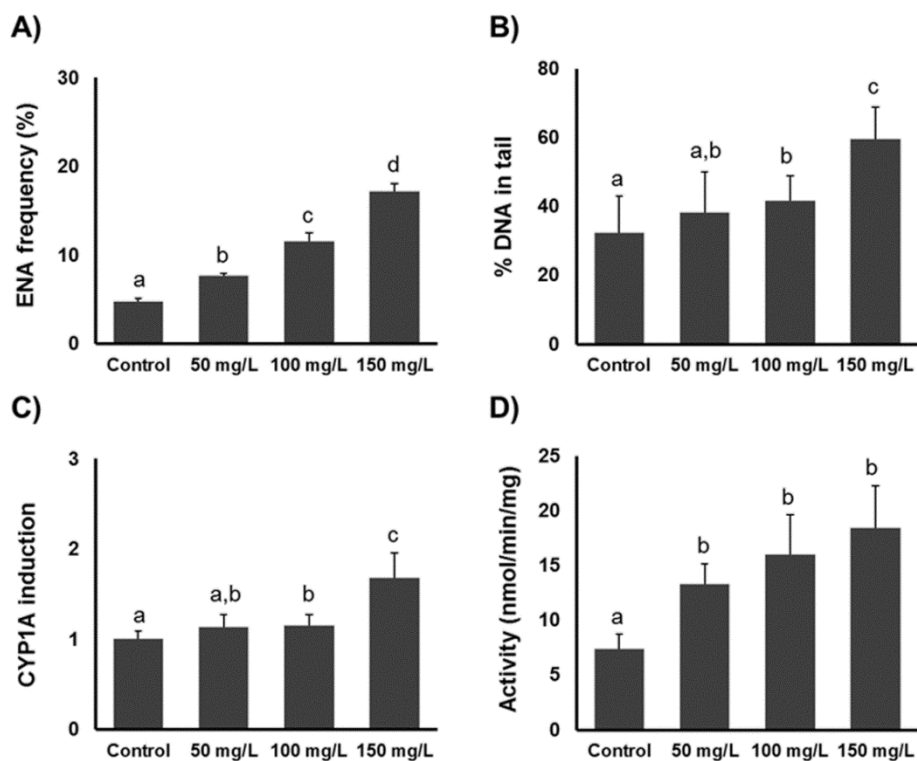


Figure 5.3. Average biomarker responses and effects (\pm SE). A) Observed ENA frequencies (Kruskal-Wallis $H = 22.15$, $p < 0.01$); B) DNA strand-breakage assessed from the % DNA in tail (Kruskal-Wallis $H = 10.44$, $p < 0.02$); C) Induction of CYP 1A [-fold increase, relatively to the control group] (Kruskal-Wallis $H = 11.21$, $p < 0.02$); D) Assessment of GST activity (Kruskal-Wallis $H = 13.75$, $p < 0.01$). Different letters indicate pairwise significant differences detected using the Mann-Whitney U test for *post-hoc* comparisons ($p < 0.05$).

5.2.1.4 Glutathione S-transferase activity

A significant increase in hepatic GST activity when comparing acrylamide exposed and controls was detected [Mann-Whitney U test ($p < 0.05$)], even though no differences were detected between different concentrations of exposure (Fig. 5.3D). Significant differences were only denoted when comparing the control group with different exposure concentrations. Significant positive correlations ($p < 0.01$) were found between GST activity and acrylamide concentration ($R = 0.859$), ENA frequency ($R = 0.791$) and DNA-strand breakage ($R = 0.739$) – Table 5.2.

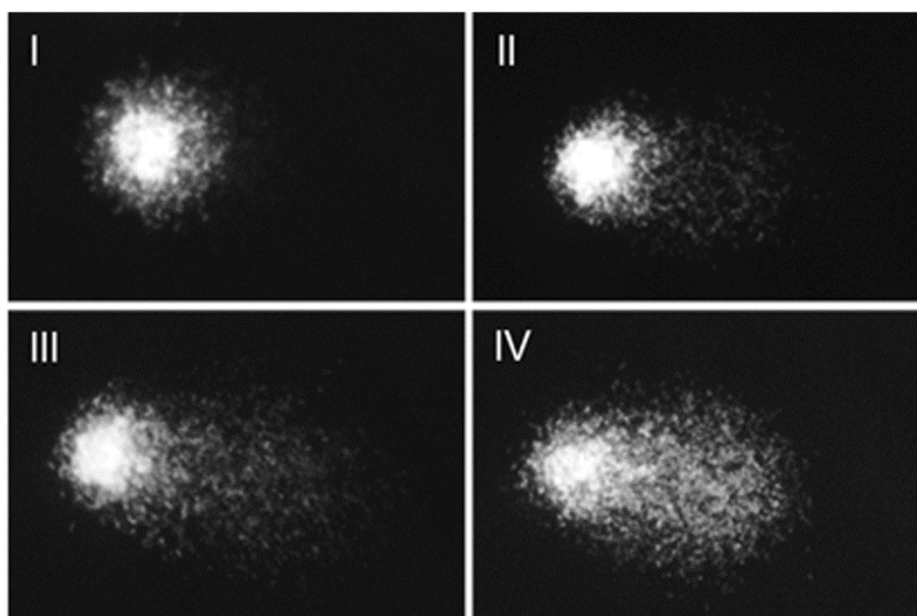


Figure 5.4. Representative images observed for each class in comet-assay, scored after exposure to 150 mg/L of acrylamide in water. I) <20% DNA in tail; II) 21-40% DNA in tail; III) 41-60% DNA in tail; IV) 61-80% DNA in tail.

Table 5.2. Values for the correlation established between biomarker response and acrylamide concentrations, using Spearman rank-order correlation R with Bonferroni correction. (Conc: Acrylamide concentration; DNA-SB: DNA strand-breakage; ENA: erythrocytic nuclear abnormalities; CYP: Induction of CYP 1A; GST: glutathione S-transferase activity). Bold values denote significant correlations ($p < 0.01$).

	Conc	DNA-SB	ENA	CYP	GST
Conc	1.000	0.636	0.961	0.678	0.859
DNA-SB	0.636	1.000	0.676	0.670	0.739
ENA	0.961	0.676	1.000	0.745	0.791
CYP	0.678	0.670	0.745	1.000	0.528
GST	0.859	0.739	0.791	0.528	1.000

5.2.1.5 Liver histopathology

Control animals presented the typical/normal structure of the hepatic parenchyma (Fig. 5.5A), consisting of polygonal regular-sized hepatocytes containing a central spherical nucleus, densely packed around sinusoids, with pancreatic tissue intrusions thus forming a hepatopancreas (Takashima and Hibya 1995, Akiyoshi and Inoue 2004).

Fish exposed to 50 mg/L acrylamide yielded no distinctive lesions and alterations to tissue, however, the pancreatic acini were considerably affected, consistent with chronic pancreatitis, exhibiting acinar cell necrosis and diffuse intrusion of macrophages containing irregular-sized bodies of lipofuscin-like pigments, which should indicate a response to increased cell death likely apoptosis (Fig. 5.5B). Affected acinar cells also revealed pronounced decolouration, likely due to a reduction in zymogen granules and endoplasmic reticula.

The same degree of pancreatic alterations occurred in animals exposed to 100 and 150 mg/L acrylamide. Additionally, significant hepatic tissue alterations occurred from 100 mg/L onwards, mostly comprising of diffuse eosinophilic hepatocellular alteration, a histopathological trait often regarded as pre-neoplastic (e.g. Vethaak and Wester 1996), with evidence of focal cell death and intrusion of macrophages but scant or absent hyperaemia (Fig. 5.5C). Nuclear morphological alterations (pleomorphisms) like pyknosis were observed focally, albeit infrequently. Evidence of pancreatic disease persisted at higher concentrations of exposure, still with an unclear dose-effect relationship (Fig. 5.5D). Animals exposed to the highest concentration of acrylamide (150 mg/L) also endured diffuse eosinophilic hepatocellular alteration but the inflammatory response was more evident than in the previous treatments, even though not diffuse (Fig. 5.5E). Additionally, hepatocytes revealed degeneration, either lipidic or eosinophilic, the latter consisting of intraplasmatic reddish inclusions, presumably caused by an accumulation of actin or its degradation products, similar in aspect (but not size) to the Mallory-Denk bodies found in mammalian hepatocytes (Strnad et al. 2008, Costa et al. 2009, 2011). Pancreatic intrusions into the hepatic parenchyma were seemingly reduced in size and number and the remaining acini were severely altered, as previous, evidencing also considerable intrusion by macrophages and focal cell death (Fig. 5.5F).

5.2.2 Discussion

The present study showed that a freshwater fish, although able to deploy biochemical defences towards waterborne acrylamide-induced challenge (namely boosting CYP1A biosynthesis and GST activity), is still susceptible to severe deleterious effects in the liver and, moreover, in pancreatic acini. Still, the histopathological appraisal failed to reveal endpoints consistent with a general systemic failure (e.g. acute inflammation in the hepatopancreas), indicating that the substance is in fact primarily toxic to pancreatic cells and that the organ failure may be the critical factor involved in acrylamide-induced mortality.

In order to ensure that acrylamide degradation in water would not condition this study, existing reports on the subject were analysed. The biotic and abiotic degradation of the acrylamide monomer in aquatic environments has previously been addressed: Brown et al. (1980a) have studied this subject and concluded that abiotic factors such as hydrolysis or photolysis are negligible, upon verifying the absence of acrylamide degradation in sterilised water after 2000 hours. Microorganism-derived degradation however was verified after 15 days in non-sterilised river water, up to an acrylamide concentration of 2 mg/L, according to the OECD 301D “Ready Biodegradability Closed Bottle Test” (United States Testing Company Inc. 1991). Concentrations above this threshold (comparable to the ones used in our work) were deemed too toxic for microorganisms, thus leading to the assumption that biodegradation should not be a confounding factor for this study.

Acrylamide lethality thresholds have been surveyed in several freshwater vertebrates and invertebrates. The LC₅₀ (96 h) determined for freshwater fish ranged between 100 mg/L (bluegill), 110 mg/L (rainbow trout) and 120 mg/L (fathead minnow) (Krautter et al. 1986; Walker 1991; Weston et al. 2009).

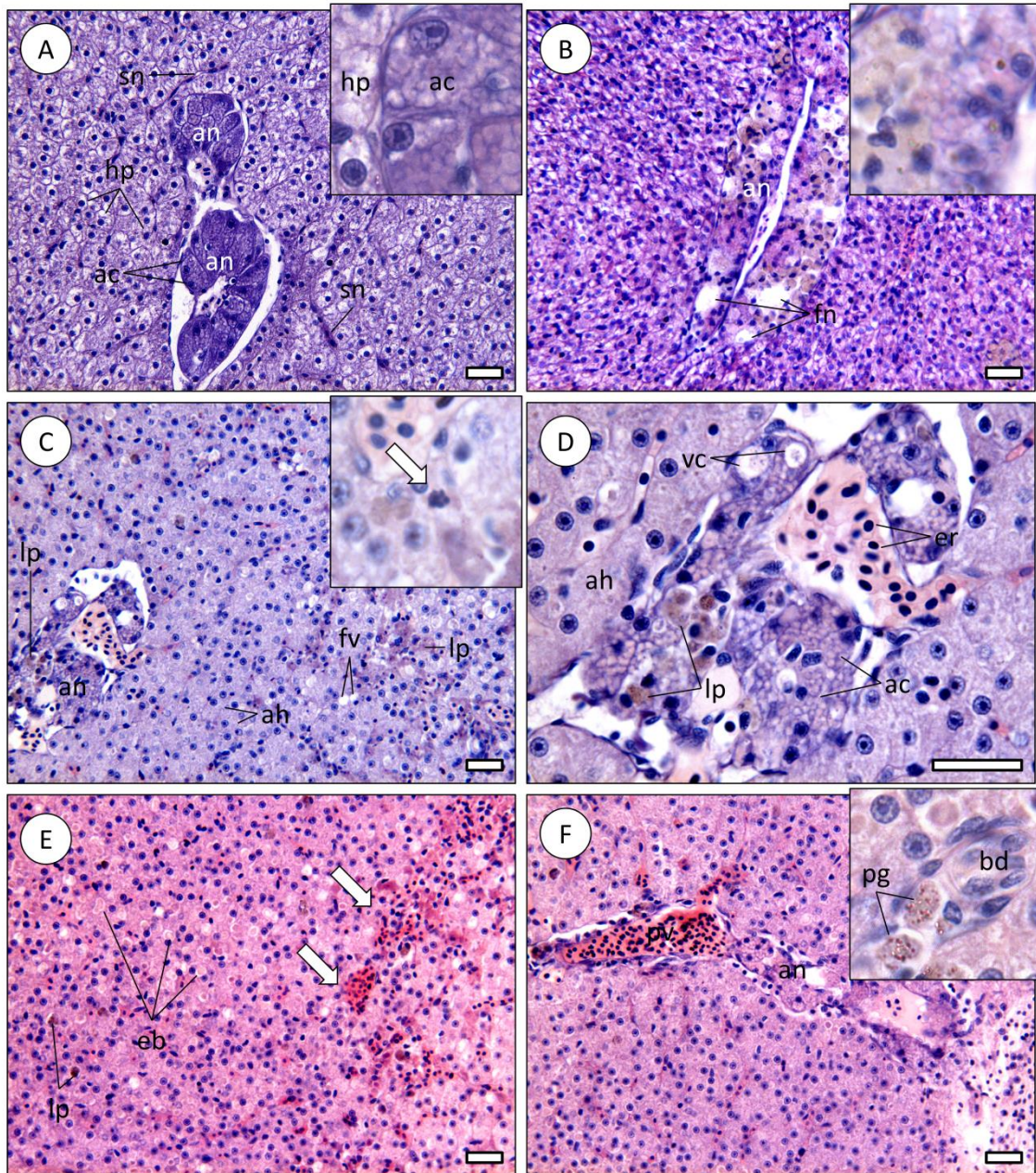


Figure 5.5. Example micrographs of tested *C. auratus* liver (Bouin-Hollande's, H&E). A) Normal liver architecture from control fish. Hepatocytes (hp) are regular in size, roughly polyhedric in shape and are arranged into a compact parenchyma with few sinusoids (sn). Pancreatic acini (an) intrude into the parenchyma, each comprised of reticulate, highly basophilic cells (i.e. with high affinity to haematoxylin), indicating a highly active cytoplasm with a dense rough endoplasmatic reticulum. Inset: detail of normal hepatic (hp) and acinar (an) cells. B) Severe atrophy of pancreatic acini in a fish exposed to 50 mg/L acrylamide. The acinus reveals focal necrosis (fn) and diffuse intrusion of macrophages containing lipofuscin-like material, brownish-yellow in colour (inset). Normal acinar cells are almost absent from the samples whereas the hepatic parenchyma appears to be essentially unaltered. C) Liver of a fish exposed to 100 mg/L acrylamide, revealing alterations to pancreatic acini located in an area of hepatocellular alteration

consisting of enlarged, slightly eosinophilic cells that lost the common polyhedral shape (ah). Fat vacuoles (potentially) are also present (fv), as well as (melano)macrophages containing lipofuscin-like granules (lp) in small foci of necrotic tissue. Inset: a hepatocyte of the same specimen undergoing early-stage apoptosis beside a macrophage containing lipofuscin-like substances. The cell's dense, highly basophilic nucleus reveals the typical "blebbing" of apoptosis (arrow). D) Same as previous, at high-power magnification, highlighting the altered pancreatic acini between altered hepatocytes (ah). Note the lipofuscin-containing bodies, likely inside macrophages (lp) and the vacuoles inside acinar cells containing undifferentiated cellular debris (vc). The blood vessel connecting the acini is engorged by erythrocytes (er), confirming local inflammatory processes, together with macrophage intrusion. E) Hepatocellular and inflammation-related changes in the liver of a fish exposed to 150 mg/L acrylamide. The hepatic parenchyma is almost entirely formed by eosinophilic cells, occasionally presenting lipofuscin-containing bodies (lp) and eosinophilic bodies (eb). There are no evident signs of necrosis; however focal hyperaemia denounces inflammation (arrows). F) Same as previous, showing altered pancreatic acini (an) adjacent to a congested branch of the hepatic portal vein (pv). Inset: detail of melanomacrophages containing pigment (melanin- or lipofuscin-like) vesicles (pg) near a bile duct (bd). Scale bars: 25 μ m.

Therefore, the 96-hour LC₅₀ hereby estimated for *C. auratus* (119.5 mg/L) is consistent with previous findings. However, information regarding the lesions elicited by exposure to aquatic animals is essentially absent. The present study revealed that sub-lethal exposures to acrylamide in *C. auratus* are genotoxic and toxic to both liver and pancreas, in an apparent dose-dependent disposition, however clearly more severe to the pancreatic acini at all concentrations, which combined with the residual mortality occurring at the lowest concentration of exposure (50 mg/L), likely indicates a specific toxicological mechanism rather than a general physiological failure. Furthermore, both CYP1A and GST activity induction were correlated to acrylamide concentrations in water both the genotoxicity biomarkers. Altogether, these findings suggest that responses are triggered, albeit insufficient to avoid direct tissue- and organ-level damage to the surveyed organs.

Genotoxicity analysis revealed a similar trend between clastogenesis (given by the frequency of ENA) and total DNA-strand breakage (derives from the Comet assay), meaning a dose-dependent increase with rising concentrations of waterborne acrylamide (Figs. 5.3A and 5.3B). Additionally, the two effects were linked, and correlated to CYP1A induction which should mean a similar pattern between *in vivo* metabolism of acrylamide and *in vivo* metabolism of other CYP-activated xenobiotics such as polycyclic aromatic hydrocarbons (PAHs) and dioxins. These xenobiotics, when bioactivated via CYP1A produce highly genotoxic compounds and reactive oxygen species (ROS) as by-products, equally genotoxic. Although both the Comet assay and ENA analysis have extensively been used in fish to assess genotoxicity of single or combined toxicants (Lee and Steinert 2003, Costa et al. 2008, Cavas 2011), few studies have been designed to understand the mechanisms of acrylamide-induced genotoxicity on these organisms. Much work made on acrylamide genotoxicity in vertebrates (i.e., rats, mice and humans) focuses on its biotransformation to glycidamide and establishes a comparison between effects caused by the two molecules at equivalent concentrations (e.g. Martins et al. 2007). For instance, El-Assouli (2009) demonstrated, through the Comet assay performed on rat leukocytes, that oral administration of acrylamide increased DNA damage. The same study also showed that *in vitro* incubation with

acrylamide does not result in increased DNA damage, which supports the fact that acrylamide *per se* has low reactivity to DNA, prior to CYP bioactivation. Several other Comet assay experiments have also revealed dose-dependent DNA damage in different tissues (e.g. liver, leukocytes, spleen) from mice and rats (Dobrzynska 2007, El-Bohi et al. 2011), with more extensive damage in mice. According to Lee and Steinert (2003), chemicals associated with DNA damage in fish may be grouped in four classes: genotoxicants acting directly on DNA, chemicals whose metabolites alkylate DNA; substances that increase production of ROS; chemicals that inhibit DNA repair systems and substances that induce DNA damage by multiple mechanisms, which could be the case of acrylamide, as suspected from the occurrence of dose-dependent CYP1A induction. Additionally, the present findings show a significant increase in GST activity in liver cells at higher acrylamide concentrations (Fig. 5.3D) and a positive significant correlation between DNA strand breakage and GST activity. This enzyme, in fish inclusively, plays a major role as an antioxidant, involved in the detoxification of ROS and hydrophilic toxicants, e.g. CYP-activated hydrophobic substances, by conjugating them with reduced glutathione (see Salinas and Wong 1999, Schlenk et al. 2008). In fact, different reports have suggested that acrylamide may potentiate intracellular ROS production (Yousef and El-Demerdash 2006) with genotoxic consequences, increased GST activity as response and with subsequent depletion of the free radical scavenger glutathione (Awad et al. 1998, Jiang et al. 2007). Studies with human lymphocytes have also shown that acrylamide-derived DNA damage may arise from increased free radicals in the cell and that, in addition, acrylamide may interfere with the DNA repair process (Blasiak et al. 2004). It is thus possible that acrylamide induces CYP1A, which in turn metabolises acrylamide to glycidamide (leading to the formation of DNA adducts, being directly genotoxic) with ROS as by-products. Ultimately it may boost GST, whose transcription is Keap1-mediated and therefore dependent of intracellular ROS (see Kobayashi and Yamamoto 2005) activity, impairing DNA repair. Research on this specific mechanism is still lacking. In addition, there is yet the need to provide conclusive evidence that (or which) CYP isoforms are able to metabolise acrylamide in fish. Still, caution is mandatory here, since CYP1A in fish is known to be induced by several classes of environmental toxicants (Haasch et al. 1992, Bucheli and Font 1995, Buhler and Wang-Buhler 1998, Oh et al. 2009), including non CYP-activatable (e.g. Diniz et al. 2009, Olsvik et al. 2011).

Besides DNA-strand breakage, it has been verified that DNA frequencies increase with acrylamide concentrations, and a positive correlation has been found between the two effects, even though the two biomarkers reflect different levels of damage to the DNA molecule. Acrylamide has already been described to be clastogenic and mutagenic to animals (Friedman 2003) and to arrest the mitotic cycle in human HT 1080 cells (Sickles et al. 1995). This is confirmed by evidence that acrylamide directly binds to neurofilaments and cytoskeletal proteins, namely microtubule-associated proteins (Lapadula et al. 1989) and inhibits kinesin proteins

preventing microtubule binding and disassembly (Sickles et al. 2007). These interactions may lead to deficiencies in the formation of the mitotic spindle, which would in turn result in increased nuclear abnormalities. In point of fact, it has been shown that acrylamide increases chromatid gaps and chromatid breaks in mammalian cells (Martins et al. 2007). Also, Jiang et al. (2007) verified increased micronuclei frequency in human HepG2 cells treated with acrylamide, which is in concordance with the current results. Given the similarity between phases I and II responses following exposure to acrylamide and potentially carcinogenic environmental toxicants (e.g. some PAHs), it is probable that pro-mutagenic effects of acrylamide in fish, as shown for murine models (see Besaratinia and Pfeifer 2007), are likely to occur.

There is no information on hepatic or pancreatic histopathological lesions caused by acrylamide. However, both organs are well known to be involved in the storage and detoxification of xenobiotics. Although pancreatic toxicity is much less studied than the liver, in mammals chronic or acute pancreatitis (as observed in the present study) is long known to occur by action of pharmaceuticals and their metabolites (Scarpelli 1989). Still, there is some evidence from mammalian studies (including human epidemiology results) that acrylamide causes tumour and non-tumour alterations in several organs, including liver and pancreas, with some potential evidence of malignancies in the latter (Shipp et al. 2006). Interestingly, eosinophilic hepatocellular alteration, a recurrent alteration in the livers of fish exposed to 150 mg/L of acrylamide, has been considered pre-neoplastic in fish (Koehler et al. 2004), and has inclusively been associated (as in the present study) with the occurrences of eosinophilic bodies in the severely impacted livers of fish exposed to complex mixtures of environmental contaminants, especially by CYP-activatable PAHs (Costa et al. 2009). Lipofuscin on the other hand (the “age pigment”), is thought to result from the oxidation of lipids and proteins (Terman and Brunk 1998), which should indicate oxidative stress occurring in the tissues, especially in the pancreatic acini, leading to cell death and organ loss-of-function, thus another evidence of critical organ failure as a result from exposure to this substance. Moreover, since more severe lesions were verified in pancreatic acini than in hepatocytes, CYP1A induction in the liver may have not been considerably hampered at lower acrylamide concentrations of exposure. However, it is possible that the CYP1A response in fish exposed to concentrations higher than 100 mg/L acrylamide may have been directly influenced by occurring lesions in the hepatocytes, resulting in hindered production of CYP1A.

5.3. Acute toxicity of acrylamide to Mediterranean mussel and alterations induced by chronic exposure

Bivalve molluscs, in particular mussels (*Mytilus* spp.) are widely surveyed within the field of environmental toxicology, whether to test the hazards of pollutants ex-situ or in biomonitoring (Fernandéz et al. 2010). Their ecological and economic importance, sensitivity to toxicants, relative simplicity of the mollusc body plan and easy handling render these organisms as key targets to address the effects of traditional and novel, so-called “emerging” pollutants, from endocrine disruptors to nanotoxicants (see for instance Aarab et al. 2006, Tedesco et al. 2010, Canesi et al. 2012). In terms of metabolic activity, the key organ to analyse is the bivalve digestive gland, which is the analogue of the vertebrate liver, in the sense that it is a major metabolic and excretion organ that plays an important role in bioaccumulation and detoxification. The second section of this chapter presents data obtained when determining the chronic and acute effects of waterborne acrylamide, at the cellular and subcellular levels, in the marine bivalve *Mytilus galloprovincialis* through a whole-organisms screening approach.

5.3.1 Results

5.3.1.1 Acute toxicity

The LC₅₀ (96 h) for acrylamide in water was estimated as 411 mg/L (95 % CI: 364.9 – 416.8 mg/L) as shown in Fig. 5.6. The highest tested concentration of acrylamide (2000 mg/L) resulted in a mortality index of 87 %. The control test and exposure to 100 mg/L yielded no mortality (Table 5.3). Similarly, no mortality occurred during the chronic assay.

5.3.1.2. Biochemical biomarkers after chronic exposure

The biomarker results retrieved from the chronic assay are summarised in Fig. 5.7. The chronic bioassay yielded significant differences among treatments (Kruskall-Wallis H, $p < 0.05$) only for EROD activity, lipid peroxidation and GST activity. Specifically, the most significant differences in EROD were observed between mussels exposed to 1 mg/L acrylamide and the controls (Mann-Whitney U, $p < 0.05$). However, no significant differences were found between individuals exposed to 1 and 10 mg/L (Fig. 5.7A). Conversely, no significant differences were found in either AChE or catalase activities between any experimental group (Figs. 5.7B and 5.7C, respectively). Lipid peroxidation and GST activity depicted a similar trend, with significant differences to control being found in animals exposed to 10 mg/L, albeit not between the two acrylamide treatments (Figs. 5.7D and 5.7E). Similarly to the activities of AChE, and catalase, no significant differences were found between treatments regarding TAC (Fig. 5.7F). The highest increment in biomarker responses was observed for lipid peroxidation in animals exposed to the highest concentration of the substance (up to ≈ 2 -fold).

Table 5.3. Mussel mortality rate (by 96 h) for the control group and tested acrylamide concentrations (mg/L).

	Control	100	250	500	1000	2000
Individuals	15	15	15	15	15	15
Total dead	0	0	5	12	12	13
Mortality (%)	0	0	33	80	80	87

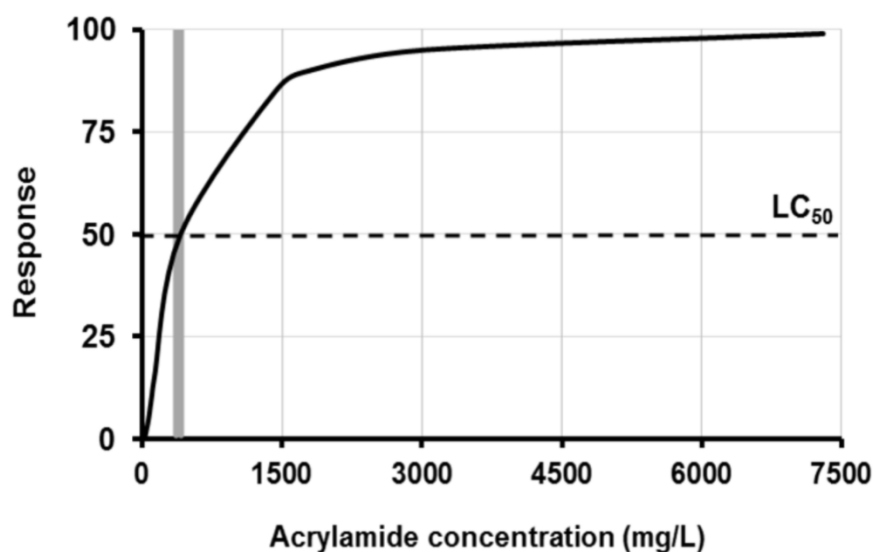


Figure 5.6. Fitted dose-response curve obtained for mussel 96-hour exposure to acrylamide. Estimated LC₅₀ = 411 mg/L. Grey area represents the 95 % confidence interval: 364.9 – 416.8 mg/L.

5.3.1.3 Histopathology after chronic exposure

No significant lesions were observed in the digestive glands of mussels exposed to either concentration of acrylamide during the chronic bioassay. However, all animals exposed to 10 mg/L of the toxicant, when compared to control animals, presented few, scattered foci of haemocytic infiltration in the connective tissue that have nonetheless retained the normal structure (Fig. 5.8A). Similarly, no significant alterations were observed in gills (Fig. 5.8B) or male gonads (Fig. 5.8C) in any of the tested animals. The most significant alterations were observed in female gonads of animals exposed to 1 and 10 mg/L acrylamide, in a seemingly dose-response disposition. While control animals retained the typical microanatomy of maturing bivalve ovaries (Fig. 5.8D), all female mussels exposed to 1 mg/L acrylamide consistently revealed increased numbers of oocytes with signs of atresia (degenerating oocytes evidencing autolytic process) with few necrotic oocytes (Fig. 5.8E). The most severe lesions were observed in mussels exposed to 10 mg/L acrylamide (Fig. 5.8F), where necrotic oocytes became common, which resulted in fully atrophied follicles. Inflammation-related alterations (namely intrusion of haemocytes) within the adipogranular tissue were also common.

5.3.1.4 Statistical integration of biomarker results

Correlation-based principal component analysis (PCA) comprising tested concentrations and the individual data of all surveyed biomarkers yielded two main factors that, when combined, explained over 70% of the total variance (71.56%). Acrylamide nominal concentration in water was included as supplementary variable. The PCA data revealed GST and lipid peroxidation yielded a similar trend to the concentration of acrylamide in water, when compared to remaining biomarker responses (Fig. 5.9). Acetylcholine esterase and antioxidant capacity (TAC) appeared strongly linked, however not directly to acrylamide concentration. Contrastingly, EROD and catalase were set apart from the other responses and not directly correlated to each other or other biomarkers, although, comparatively, EROD activity exhibited a more similar trend to acrylamide concentration in water.

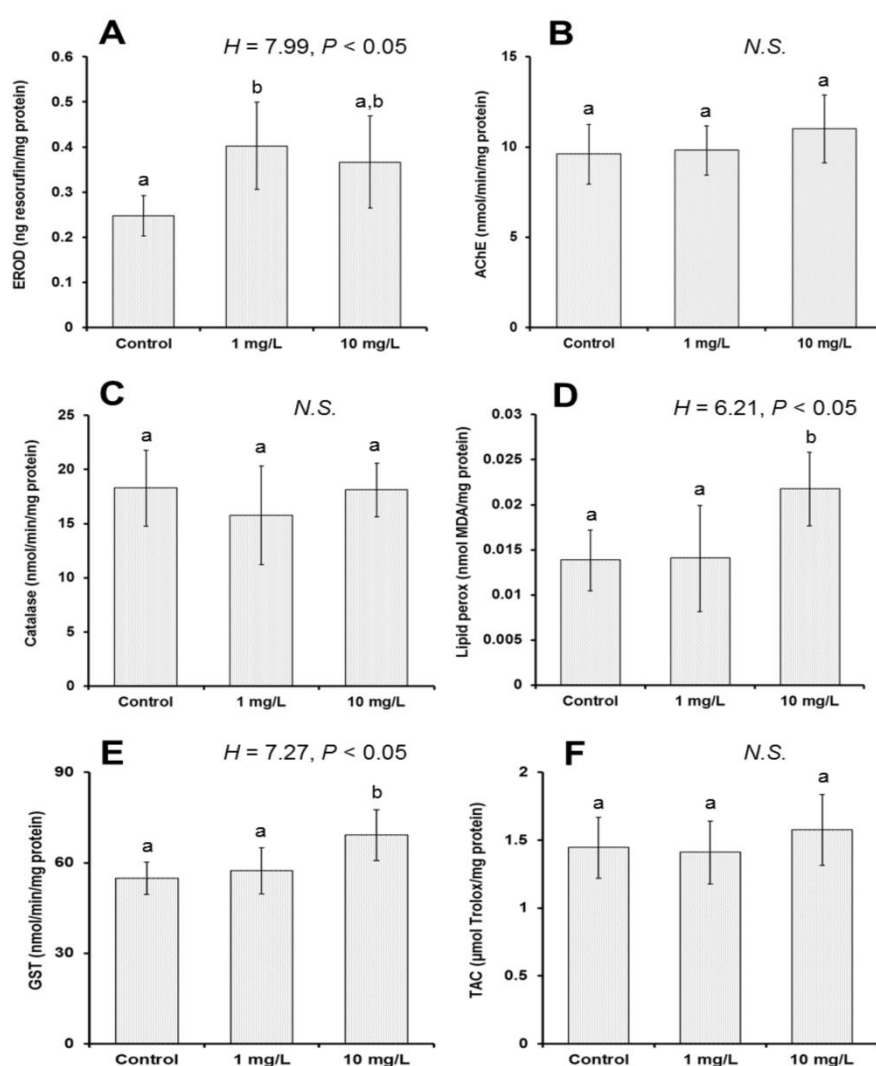


Figure 5.7. Average biomarker responses determined from whole soft-body samples of mussels exposed for 21 days to waterborne acrylamide (1 and 10 mg/L) plus controls. A) ethoxyresorufin-O-deethylase (EROD) activity; B) acetylcholine esterase (AChE) activity; C) catalase activity; D) lipid peroxidation; E) glutathione-s-transferase (GST) activity; F) total anti-oxidant capacity. Error bars denote 95 % confidence intervals. Multiple comparison statistics were obtained with the Kruskal-Wallis ANOVA by ranks H-test (N.S. means not significant). Different letters indicate significant differences between specific pairs of experimental treatments (Mann-Whitney U test, $p < 0.05$).

5.3.2 Discussion

To date, most information on acrylamide toxicity and effector concentrations to aquatic organisms has been retrieved from freshwater species, particularly teleosts (Krautter et al. 1986, Walker 1991, Weston et al. 2009). As such, there is only scant information on bivalves and seawater species in general. The current results show rather elevated effect concentrations for acrylamide in mussels ($LC_{50} = 411$ mg/L). This relatively high LC_{50} , indicating low acute toxicity, compared to (freshwater) fish, typically ≈ 100 mg/L (see section 5.2 in this chapter) indicates, a priori, that the substance is of little toxicity to marine bivalves. Considering that the highest concentrations of acrylamide found in aquatic (freshwater) ecosystems range within the μg scale up to few mg/L in sewage effluents, according to aged studies (Croll et al. 1974, Brown et al. 1980a), this information appears to substantiate the common notion that acrylamide poses little risk to aquatic fauna. Nonetheless, the findings from the chronic exposure assay (1 - 10 mg/L) indicate that acrylamide is able to induce responses to exposure in mussels, with respect to EROD and GST activities. Nonetheless, where the increase in lipid peroxides indicates the formation of oxidative radicals, the unchanged levels of TAC indicate that the overall ability to cope with oxidative stress remained unaltered, suggesting, thus, low-moderate oxidative challenge occurring at the present conditions of exposure. Also, severe lesions to female gonads in mussels (according to the observed individuals) were observed, which may imply a very significant risk for populations following prolonged exposure. Moreover, Croll et al. (1974) noticed that microbial degradation of acrylamide, judged to be fast in freshwater systems (within few days to reach half-life), tends to become extended in marine and brackish waters. It must be noted, though, that predicting acrylamide dispersion using level I and level III fugacity models showed that $\approx 99\%$ of acrylamide in the environment partitions to aquatic systems (NICNAS, 2002). Due to its elevated water solubility it is highly probable that the substance is washed away from atmosphere in rain water. A main source of acrylamide to environment is the presence of acrylamide monomers (around 0.1 %) in polyacrylamide polymers used for e.g. grouting applications, drinking water, paper manufacture and flocculants in mineral processing. Degradation tests made on acrylamide in water showed that its half-life varies greatly and that concentrations above 2 mg/L are not efficiently and quickly degraded by biotic or abiotic factors (Brown et al. 1980a). With this in mind, the possibility of acrylamide accumulation in aquatic niches or washing out to seawater/estuarine systems has to be considered, where it may contaminate the biota directly or become deposited in sediments (Brown et al. 1980b), hence the importance of understanding the effects of the substance in a wide array of organisms. On the other hand, if degradation of acrylamide may be relatively inefficient, it is possible that biomagnification events occur, as well as trapping in sediments, rendering concentrations of the substance higher than could be expected off pollution hotspots, a subject that needs yet further research. As such, the relatively high

concentrations tested in the present study (which resemble those near effluent discharge sites) may not be so far astray of what could be found in highly impacted coastal waterbodies such as lagoons, rias and estuaries.

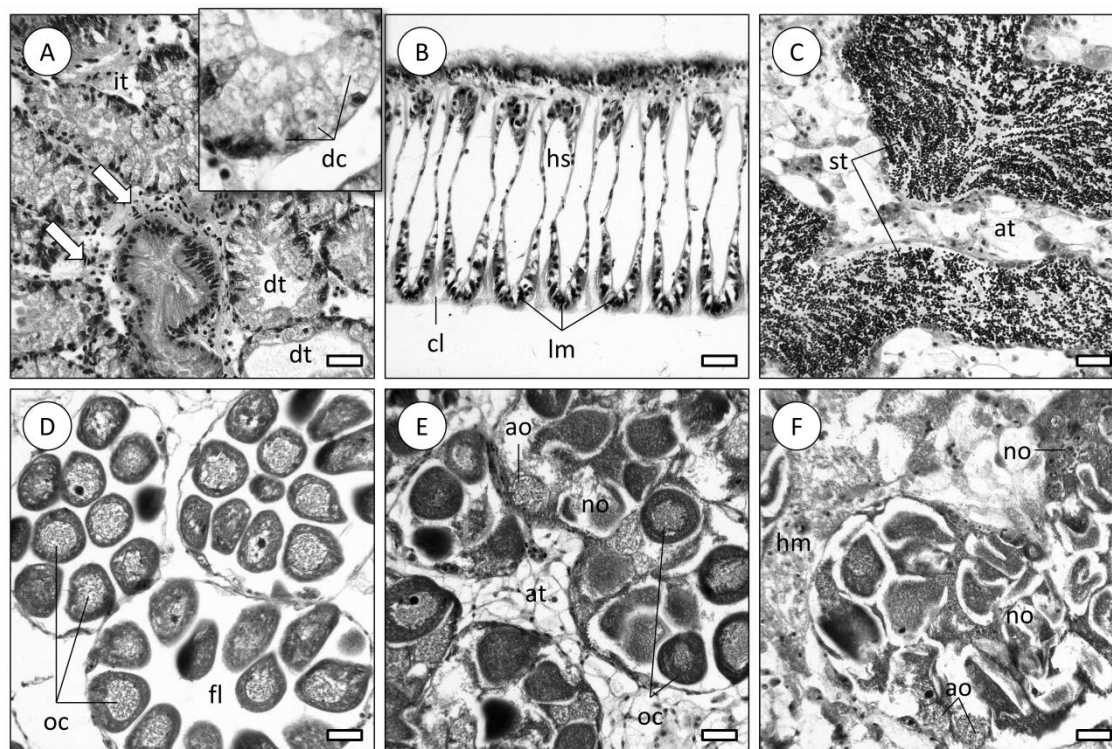


Figure 5.8. Representative histological sections of tested mussels, after the 21-day exposure assay (H&E). A) Digestive gland of a mussel exposed to 10 ppm acrylamide. The digestive tubules (dt) present normal structure, consisting of a single-cell layer epithelium. Moderate haemocytic infiltration (arrow) is found in intertubular tissue (it). Inset: Detail of a digestive tubule of an animal exposed to 10 ppm acrylamide, revealing highly vacuolised digestive cells (dc). B) Normal gills of a control mussel, showing well-defined ciliary plates (cl) between lamellae (lm), similarly to animals exposed to 1 or 10 ppm acrylamide. Notice the haemal space devoid of any significant presence of haemocytes. C) Testes of a mussel exposed to 10 ppm acrylamide, revealing normal microanatomy of maturing seminiferous tubules (st) and adipogranular tissue (at). D–E) Progressive series of ovarian atrophy of mussels exposed to acrylamide, compared to control animals. Control mussels (D) exhibited normal ovarian follicles (fl) containing maturing oocytes (oc). E) Atrophied follicles of a female mussel exposed to 1 ppm acrylamide, revealing many atresic (degenerating) oocytes (ao) and a few necrotic oocytes (no) amidst normal oocytes. The overall structure of the ovary remains intact, with no evident signs of alterations in the adipogranular connective tissue (at). F) Highly affected ovarian follicles in a mussel exposed to 10 ppm acrylamide, with many necrotic oocytes (no) and fewer atresic oocytes. Haemocytic infiltration (hm) can be observed in the adipogranular tissue. Scale bars: 25 µm.

Many authors report mussels to be particularly well adapted to respond to environmental stressors (including toxicological challenge) due to their natural ability to cope with extreme variations in temperature and anoxia (owing to the intertidal habitat) and ability to interrupt filter-feeding in face of sub-optimal environmental parameters (e.g. Davenport and Manley 1978, Sloof et al. 1983, Kramer et al. 1989, Santovito et al. 2005, Braby and Somero 2009). However, if these defence mechanisms could, at least in part, explain low acute toxicity of acrylamide to these organisms (and moderate biochemical responses), they are not consistent with the severe

histopathological lesions encountered in ovaries but not in other organs, indicating a specific toxicological target of the substance (i.e. gonadotoxic) rather than general systemic failure.

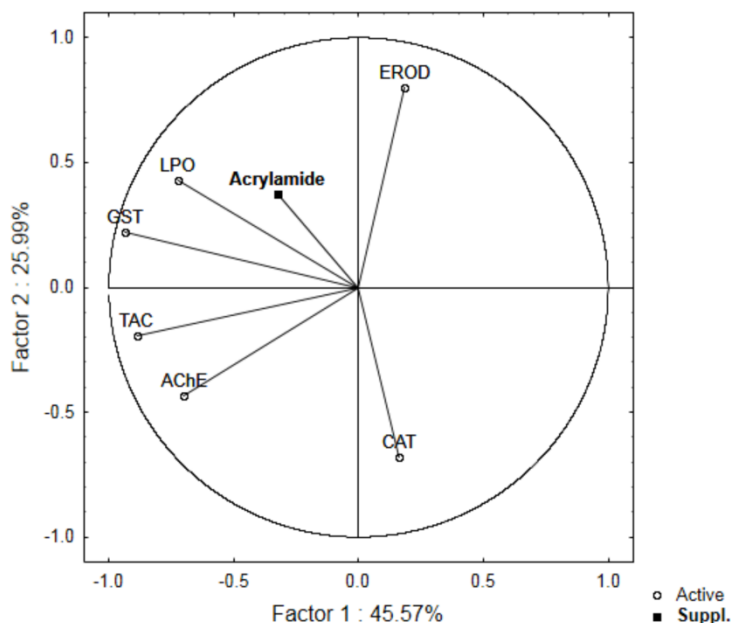


Figure 5.9. Correlation-based principal component analysis (PCA) between biomarkers and nominal acrylamide concentration in water (as supplementary variable). The percentage of explained variance per PCA factor is indicated. Factor 1 eigenvalue = 2.73 and Factor 2 eigenvalue = 1.56. EROD: ethoxyresorufin-O-deethylase (EROD) activity; AChE: acetylcholine esterase activity; TAC: total antioxidant capacity; LPO: lipid peroxidation; CAT: catalase activity; GST: glutathione-s-transferase (GST) activity.

Overall, results from the biochemical analyses show modest responses and effects to waterborne acrylamide, although the increase in lipid peroxidation, GST and EROD activities suggest some degree of metabolic activation of the xenobiotic, since EROD is Ahr-dependent (reviewed by Tompkins and Wallace 2007). In fact, similarly to other organic xenobiotics, acrylamide bioactivation by CYP mixed function oxidases (MFOs) produces reactive oxygen species as by-products which explains, at least in part, an elevated lipid peroxidation, whereas GST mediates the conjugation of hazardous metabolites to glutathione in an attempt to inactivate them. However, to date, no research has been published regarding the role of MFOs in the detoxification of acrylamide monomers in molluscs. There is evidence that molluscan MFOs may be less efficient than their vertebrate counterparts (Peters et al. 202), which may partially explain the overall moderate, albeit accountable biochemical responses of mussels to the substance, as well as reduced acute toxicity in mussels, when compared to fish. In fact, mussels tend to yield reduced acute toxicity effects in face of Ahr-mediated toxicants (as some PAHs and dioxins), which is accordant with the high LC_{50} (96 h) threshold obtained in this work. In spite of the scarce research on the chronic effects and responses triggered by the substance, acrylamide has been found to induce GST and EROD *in vitro* in human HepG2 cells (Sen et al. 2012) and to increase CYP1A levels in goldfish liver, as previously discussed in section 5.2.

The findings also indicate low or null neurotoxic effects of acrylamide via inhibition of AChE

activity in *M. galloprovincialis*. Although acrylamide is often linked to neurotoxic effects in humans and other mammals (Howland 1985, He et al. 1989, LoPachin and Gavin 2012, Pennisi et al. 2013), literature reporting its effects on esterase enzymes is essentially missing. Moreover, no previous information on invertebrates was found. From the current state-of-the art, it is clear that the neurotoxic effects of acrylamide to these organisms need further research. Conversely, the most significant adverse effects endured by mussels in the present study were detected in female gonads (Fig. 5.8). The results thus suggest that in mussels, acrylamide targets primarily female gonads, which indicates that the substance holds a more important ecological impact than it could be expected. In fact, there are indications that acrylamide is indeed gonadotoxic, e.g. to male rats, with alteration in epididymal sperm reserves and possible induction of Leydig cell hyperplasia (Wang 2010).

Oxidative stress is one of the main consequences of toxicological challenge, with multiple causes, mechanisms and effects. Organisms typically possess a broad array of defences against the formation of ROS. The increase in lipid peroxidation following exposure to acrylamide without a significant change in total anti-oxidant capacity (as well as catalase activity) should indicate that antioxidant defences were not fully depleted. It must be noticed, however, that the TAC assay measures the global antioxidant potential of the cell, including enzymatic and non-enzymatic anti-oxidants (e.g. glutathione, tocopherol, ascorbic acid, etc.), therefore providing a generalist perspective of the anti-oxidant machinery, since responses to oxidative stress are not equally triggered by acrylamide. Catalase and GST for instance, yielded contrasting results (Fig. 5.7C and E) despite being part of the enzymatic antioxidant machinery and being regulated by the same pathway. Both catalase and GST expression is mediated by the Nrf2-Keap1 pathway through which, electrophiles such as ROS will cause the release of the transcription factor Nrf2 from its repressor, Keap1 (see schematics in Figure 5.10). The transcription factor will then bind to the antioxidant response element (ARE) of specific genes (such as catalase and GST), promoting transcription (reviewed by Kobayashi and Yamamoto 2005). Still, there are very significant species- and organ-specific variations in the activities of anti-oxidant enzymes. The activity of catalase, for instance, a phase II peroxisomal enzyme chiefly involved in H₂O₂ catabolism, has been found to be especially responsive in the digestive gland of wild *M. galloprovincialis* from impacted sites, whereas GST activity was more responsive in gills (Vidal-Liñan and Bellas 2013). Although no significant histopathological lesions were found in either organ, this information additionally highlights the need for caution when interpreting data from anti-oxidant enzymes, as noted by many researchers in the field (van der Oost et al. 2003), especially when retrieving data from whole-organism samples. On its turn, the similar pattern between lipid peroxidation and GST (Fig. 5.7) is accordant with the function of the latter in conjugating lipid peroxides during phase II processes, and thus assisted in the reduction of intracellular ROS formed during acrylamide bioactivation. Altogether, the ability to deploy anti-

oxidant defences most likely contributed to the low or null histopathological alterations observed in most mussel tissues, with emphasis to the digestive gland, which is the analogue to the vertebrate liver and, therefore, the primary organ for detoxification. The link between lipid peroxidation, GST activity and acrylamide concentration in water (Fig. 5.9) agree with the notion that exposure to acrylamide induces the formation of ROS and likely the deployment of glutathione-related responses to deal with these by-products, and eventual acrylamide metabolites.

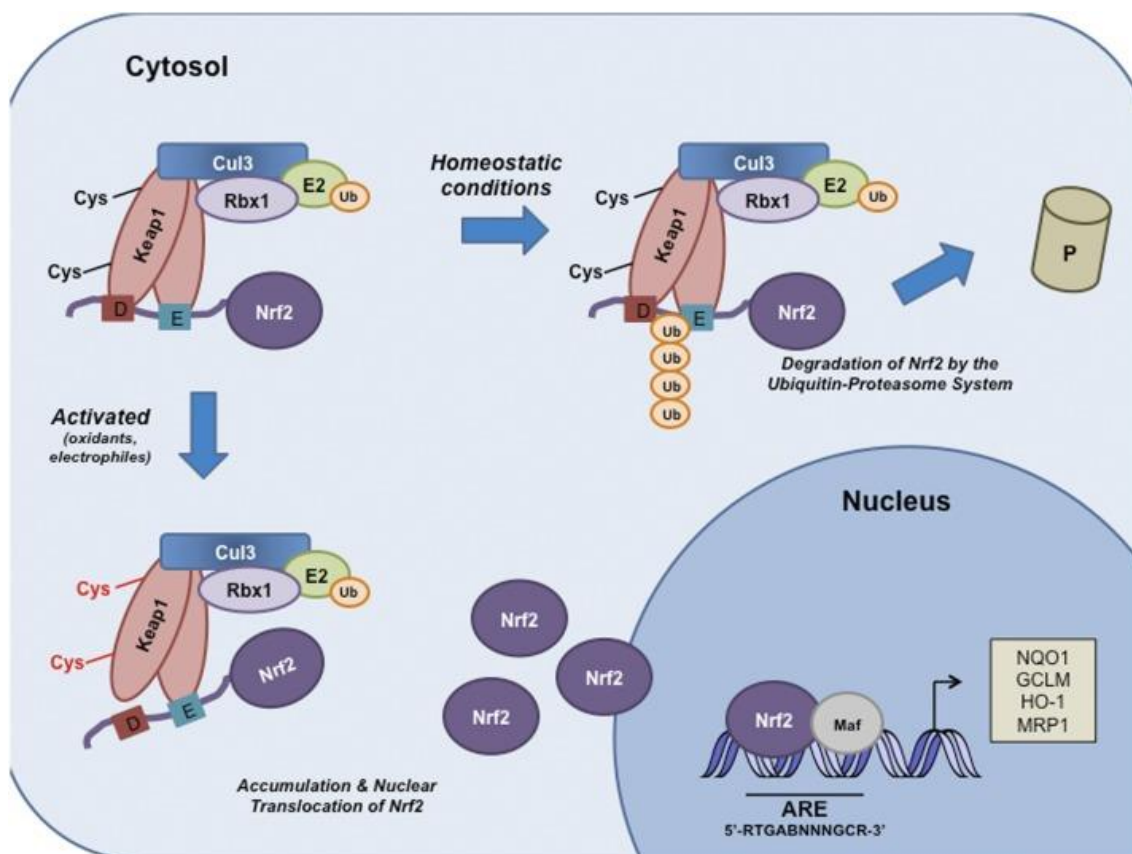


Figure 5.10. Schematic model of the Nrf2–Keap1 signaling pathway. Under basal conditions, Keap1 binds to the ETGE and DLG motifs on Nrf2 and brings Nrf2 into Keap1–Cul3–E3 ubiquitin ligase complex, leading to ubiquitination and subsequent degradation of Nrf2. Oxidative stress or electrophiles can cause a conformational change in the Keap1–Cul3–E3 ubiquitin ligase by acting on specific cysteine residues in Keap1. These changes disrupt Nrf2–Keap1 binding at the DLG domain. Nrf2 is stabilized, and free Nrf2 translocates to the nucleus, where it dimerizes with members of the small Maf family and binds to AREs (5'-RTGABNNNGCR-3') within regulatory regions of a wide variety of cell defense genes, including NQO1, GCLM, HO-1, and MRP1. (E) ETGE; (D) DLG. Reprinted with permission, from Jaramillo and Zhang (2013). Copyright 2013 Cold Spring Harbor Laboratory Press.

There are only a few references on histopathological alterations elicited by acrylamide. Among the few studies, there is evidence for testicular alterations in mice (Wang et al. 2010) and hepatopancreas lesions in goldfish (section 5.2 in this chapter). The lack of histopathological approaches to acrylamide toxicity renders difficult to pinpoint specific alterations induced by the substance. Although the present study, which intended to be a ground-breaking screening

assessment on the effects of acrylamide in mussels, surveyed a reduced number of organisms, it shows that chronic exposure to acrylamide may cause severe deleterious effects to mussel female gonads. Specifically, a reduction in number of oocytes per ovarian follicle and caused oocyte atresia and necrosis in mussels exposed to acrylamide from 1 mg/L (Fig. 5.8). These findings, although seemingly preliminary, should point to a new direction in research. Interestingly, these alterations resemble those observed in mussels exposed to endocrine disruptors (Aarab et al. 2006). However, despite similar histological alterations it is not clear that acrylamide actually impairs hormonal functions and ought to be regarded as a potential endocrine disruptor. In fact, acrylamide has been found to de-regulate basal cellular functions and structures, inclusively by inducing deficiencies in the formation of the mitotic spindle, either by binding neurofilaments and cytoskeletal proteins (Lapadula et al. 1989) or by inhibiting kinesin proteins, consequently preventing microtubule binding and disassembly (Sickles et al. 2007). Although this information should imply that virtually all cell types and tissues are susceptible to acrylamide-induced damage, the present findings suggest that reproductive tissue may be particularly sensitive to the substance, suggesting a specific toxicological pathway and indicate that further research is needed to fully disclose the potential gonadotoxic effects of acrylamide in marine molluscs. Still, acrylamide-induced reproductive toxicity has been also reported in mice, for both male and female gonads and gametes (Sakamoto and Hashimoto 1986, Zenick et al. 1986, Chapin et al. 1995, Wang et al. 2010), even though most of the studies do not consider histopathology as an endpoint. Still, male mice exposed to acrylamide in drinking water yielded alterations in Sertoli cells and epididymis, ultimately influencing spermatogenesis and the normal reproductive function (Wang et al. 2010). Overall, the specific mechanisms why acrylamide was notoriously gonadotoxic in female gonads following chronic exposure, whereas the digestive gland and gills (the main organ of apical entry of the xenobiotic) were less affected, remain elusive. Nevertheless, it is likely that, in spite the moderate biochemical responses and effects (and low acute toxicity as well), chronic exposure to acrylamide may seriously compromise the reproductive effort of mussels. As such, caution is mandatory when interpreting biomarker data from animals exposed to this substance. It must also be noticed that the bivalve gonads, especially testis, are relatively undifferentiated, comparative to vertebrates and even other molluscs, which hinders histopathological appraisals focusing mostly on structural alterations. Thus, more detailed microscopic, biochemical and fertility studies ought to be conducted with this and other species of bivalves in order to ascertain the full extent of gonadotoxicity of this aquatic pollutant.

5.4 Conclusions

In summary, acrylamide is genotoxic by promoting both chromosomal clastogenesis and DNA-strand breakage. The results are in accordance with the expected alterations imposed by CYP-activated organic toxicants, which could mean DNA damage via ROS and epoxide adducts (generating strand breakage) and spindle malformations (causing clastogenesis due to faulty mitosis). On the other hand, ROS and mutations may easily explain the acute damage endured by the hepatic parenchyma and moreover by the pancreatic acini, both involved in toxicant metabolism and bioaccumulation. It should be noted though that the mechanisms by which acrylamide is biotransformed to glycidamide *in vivo* are not yet fully known, neither is the pathway of CYP induction by the substance (for instance, if the aryl hydrocarbon receptor is involved, as for known CYP-inducers). Also, the present study showed that acrylamide, at least in freshwater fish, owes a significant part of its toxicity to severe pancreatic tissue lesions, regardless of biochemical defences being deployed, which sustains the inherent physiological hazard of the toxicant, to which is added a most probable effect as a genotoxicant and probable mutagenic agent in fish. This data was published in Larguinho et al. 2014 (Journal of Applied Toxicology 34:1293-302).

In accordance with the general notion that acrylamide holds reduced environmental hazards, the verified acute toxicity to *M. galloprovincialis* is low, attaining $LC_{50} \approx 4$ fold higher than for freshwater fish. However, chronic exposure to the xenobiotic indicated some degree of metabolic activation by mussels, with subsequent formation of ROS and toxic metabolites but without overwhelming the organisms' anti-oxidant capacity, which clearly indicates the substance is toxicological active to these marine bivalves. However, probably the most significant findings were retrieved from the whole-organism histopathological screening, which revealed female gonads to be the most affected organ. As such, although posing little threat with respect to mortality, the chronic effects of acrylamide may be underestimated by the current state-of-the-art, especially concerning the deleterious effects to the species reproductive effort, therefore compromising populational equilibrium. This data was published in Larguinho et al. 2014 (Environmental Research 135:55-62).

CHAPTER 6. GENERAL DISCUSSION AND CONCLUSIONS

Believe you can and you're halfway there.

Theodore Roosevelt

The biological problem concerning the formation of DNA adducts and their role as biomarkers of exposure to carcinogen agents is of great importance and it has been growing within the scientific community. Analysis and quantification of DNA adducts provide valuable information not only about specific toxicants and the associated risk, but also about the susceptibility of a genome to a particular kind of carcinogen. The central objective portrayed in this thesis is the development of a nanotechnology-based method for detection of DNA adducts. With the emergence of nanotechnology as a scientific field of study, new and improved methods and materials arose, with advantages in terms of biomolecular detection. With this in mind, gold nanoparticles were incorporated into different systems to try and enhance their capabilities and render the suitable for DNA adduct detection. To accomplish this objective, a simultaneous three-way strategy was devised consisting of: 1. optimisation of sample preparation for analysis; 2. the use of AuNPs to improve existing techniques for DNA adduct detection: a robust MS-based laser desorption technique, and a simpler colorimetric test; 3. the development of a biological model of exposure to acrylamide, including a toxicity assessment to better grasp the biological consequences of the toxicant. A workflow and timeline were properly set in order to address these several aspects i.e. procedures for sample preparation preceding detection, development of a AuNP-based method for rapid detection of DNA adduct in solution, *in vitro* production of DNA adducts from reaction with an alkylating agent and *in vivo* production of DNA adducts by exposure of a model organism to the toxicant.

Regarding sample preparation, ultrasonic energy was found extremely valuable to produce DNA fragments suitable for downstream applications, via fragmentation of a highly complex genomic DNA sample. Enzymatic hydrolysis of DNA samples was compared with ultrasonic energy for fragmentation of DNA samples, and both techniques were found adequate, each with its own advantages, depending on the final purpose. Data concerning these experiments was published in Larginho et al. 2010 (Talanta 81:881-886). Additionally, an attempt was made to accelerate nuclease digestion with ultrasonic energy, similarly to what has been described for proteolytic enzymes (Lopéz-Ferrer et al. 2005, Rial-Otero et al. 2007). This was believed to be an interesting concept however no major differences were denoted from using ultrasonic energy during digestion, at the tested conditions of study. The attempt to use ion-exchange HPLC to profile nucleotides and separate DNA adducts from remainder sample constituents revealed no visible elution signals of the DNA adduct in the chromatograms. Detection by UV-Vis is possibly not sensitive enough to identify trace amounts of DNA adducts in solution. On the other hand, the continuous desalting and purification procedures before and after HPLC separation may have resulted in sample loss. All things considered, ion-exchange HPLC proved valuable information when profiling different nucleotides in solution, but proved inconclusive for DNA adduct separation. With this in mind, a NAP-5 DNA-grade column for desalting and purification was used. The setup was less elaborated, there was no DNA adduct separation from other nucleotides,

but prevented extensive sample loss. Ultimately, by putting together all experiments concerning sample preparation, a complete protocol was devised for DNA adduct analysis by mass spectrometry, since DNA extraction and isolation from a biological model, down to detection via AuNP-based SALDI-TOF.

About the proposed methodology for detection of DNA adducts, an attempted was made to introduce AuNPs into an already existing MS technique, to assess its potential for nucleotide analysis. Citrate-capped 14 nm AuNPs proved noteworthy in nucleotide profiling by SALDI-TOF-MS, although the specific mass signals generated present some deviations to the expected molecular ion signals. These differences are too little to be due to formation of cation-adducts (no relation to DNA adducts) during gas-phase rearrangements, and no literature has been found that described such discrepancies. The method of AuNP-SALDI for nucleotide profiling was published in Larginho et al. 2013 (Talanta 105:417-421). AuNPs have also accounted for identification of DNA adducts generated *in vitro* (GA-guanine adducts), but when biological samples were analysed, no mass signal could be identified. This may be related to the low abundance of DNA adducts *in vivo*, which possibly calls for alternative and elaborate methods for sample preparation and more importantly, isolation of DNA adduct from the remainder components in the sample (as mentioned before). Nevertheless, MALDI-TOF analysis of the same biological samples with an adequate organic matrix (CHCA) produced a mass signal corresponding to the DNA adduct molecular ion, which means that CHCA as a MALDI matrix is still capable of more sensitive detection than AuNPs. Future work may involve nucleotides labelled with different isotopes, e.g. ^{15}C , ^{18}O , to allow for both nucleotide and DNA adduct quantification in samples. An alternative colorimetric method based on AuNP and inspired in the non-cross-linking assay developed by Baptista and co-workers (2005a) was also presented. This method accounted for a positive identification of modified nucleotides in solution with statistical significance. Moreover, differences were observed, albeit not significant, for detection of DNA adducts in samples generated by *in vitro* alkylation of high complexity genomic DNA, with minimal sample preparation. All data concerning the colorimetric tests was recently published in Larginho et al. 2014 (IET Nanobiotechnology). The approach shows enormous potential for rapid, simple and cost-effective detection of DNA adducts in solution, however there is still the need for further testing, namely in real biological samples, from organisms exposed to the carcinogen.

The exposure assays performed during this thesis have provided valuable information on mechanistic and descriptive toxicology of acrylamide to aquatic organisms. The first exposure assay targeted a freshwater fish, focusing mainly on genotoxicity and induction of phase I and phase II metabolism enzymes, to evaluate biotransformation of acrylamide to glycidamide and correlate that with DNA and chromosomal damage. In addition, it was intended to evaluate the goldfish as a biological model for acrylamide toxicity, as well as correlate the detection of DNA

adducts in tissues with the other biomarkers, but since DNA adducts have only been detected by MALDI at the highest tested concentration (150 mg/L), this was not possible. Nevertheless, evaluation of genotoxicity via Comet assay and ENA analysis in peripheral blood samples constitutes a relatively rapid and simple approach which may prove worthy when screening for biomarkers of induced DNA damage in superior vertebrates. All data concerning acrylamide toxicity to goldfish was published in Larginho et al. 2014 (*Journal of Applied Toxicology* 34:1293-302). The second assay consisted of acute and chronic toxicity of waterborne acrylamide to a bivalve, and targeted mainly histopathological lesions and cell biochemical defences deployed in response to acrylamide-induced damage, namely oxidative stress. This was intended to be a study about acrylamide itself, its consequences to the cell, e.g. Michael's addition to bind proteins, conjugation with glutathione, triggered antioxidant response, because most studies on acrylamide turn out to be a comparison between its toxicity and glycidamide, usually in terms of genotoxicity. All data concerning acrylamide toxicity to mussels was recently published in Larginho et al. 2014 (*Environmental Research* 135:55-62).

In terms of acute toxicity, waterborne acrylamide is low or mildly toxic to the organisms tested, as they presented relatively high effect concentrations (from 100 to 500 mg/L). It is very unlikely for the aquatic niche to reach this order of concentrations, unless a chemical disaster occurs. Aquatic vertebrates were shown to be less tolerant than invertebrates to short exposures to elevated acrylamide concentrations. This could be related to the feeding strategies and metabolic adaptations of each organism, revealing different susceptibilities in terms of internal organs and defence mechanisms activated to counter the xenobiotic. Nevertheless, from all obtained data, it seems that acrylamide effects become notorious when a more prolonged exposure to environmentally relevant concentrations comes into play.

The most surprising results in both vertebrates and invertebrates were the histopathological lesions induced by acrylamide in different tissues. In fish, it targeted mostly pancreatic intrusions in the hepatopancreas, whilst in mussels the gonads were the main affected organ. Acrylamide provoked histopathological lesions similar to other classes of chemical toxicants, in both fish and mussels. This may suggest that aquatic organisms possess non-specific defence mechanisms which are triggered in the presence of a wide array of toxicants, e.g. PAHs, dioxins. Importantly, prolonged exposure to acrylamide has revealed to be extensively damaging to gonads from female mussels, despite these organisms exhibit a certain resilience to environmental toxicants and stresses. As such, despite the seemingly low mortality index, the adverse effects this substance has on the biota should not be underestimated and, both in terms of biological consequences to the organism and ecotoxicology, there is still much to be unravelled.

REFERENCES

- Aarab N, Lemaire-Gony S, Unruh E, Hansen PD, Larsen BK, Andersen OK, Narbonne JF. 2006. Preliminary study of responses in mussel (*Mytilus edulis*) exposed to bisphenol A, diallyl phthalate and tetrabromodiphenyl ether. *Aquat Toxicol.* 78S:S86-92.
- ABC Labs. 1983a. Dynamic 96 hour acute toxicity of acrylamide monomer to water fleas (*Daphnia magna*). Test Report #29736.
- ABC Labs. 1983b. Dynamic 96 hour acute toxicity of acrylamide monomer to midge larvae (*Parathanyarsus parthenogenetica*). Test Report #29736.
- Ahammad AJ, Choi Y, Koh K, Kim J, Lee J, Lee M. 2011. Electrochemical detection of cardiac biomarker troponin I at gold nanoparticle-modified ITO electrode by using open circuit potential. *Int J Electrochem Sci.* 6:1906-1916.
- Ahmad F, Siddiqui MA, Babalola OO, Wu H. 2012. Biofunctionalization of nanoparticle assisted mass spectrometry as biosensors for rapid detection of plant associated bacteria. *Biosens Bioelectron.* 35:235-242.
- Akiyoshi H and Inoue A. 2004. Comparative histological study of teleost livers in relation to phylogeny. *Zool Sci.* 21:841-850.
- Ambrosi A, Airò F, Merkoçi A. 2010. Enhanced gold nanoparticle based ELISA for a breast cancer biomarker. *Anal Chem.* 82: 1151-1156.
- Arber W and Linn S. 1969. DNA modification and restriction. *Annu Rev Biochem.* 38:467-500.
- Aslan K, Huang J, Wilson GM, Geddes CD. 2006a. Metal-enhanced fluorescence-based RNA sensing. *J Am Chem Soc.* 128:4206-4207.
- Aslan K, Malyn SN, Geddes CD. 2006b. Fast and sensitive DNA hybridization assays using microwave-accelerated metal-enhanced fluorescence. *Biochem Biophys Res Commun.* 348:612-617.
- Awad ME, Abdel-Rahman MS, Hassan SA. 1998. Acrylamide toxicity in isolated rat hepatocytes. *Toxicol in Vitro* 12:699-704.
- Backman J, Sjöholm R, Kronberg L. 2004. Characterization of the adducts formed in the reactions of glycidamide with thymidine and cytidine. *Chem Res Toxicol.* 17:1652-1658.
- Bajdur WM. 2008. Application of acrylamide polymers as flocculants in sewage coagulation process. *Proc ECOpole.* 2:291-297.
- Baker M. 2010. Mass spectrometry for biologists. *Nat Methods.* 7:157-161.
- Bankier AT. 1993. Generation of random fragments by sonication. In: Griffin HG and Griffin AM, editors. *Methods in molecular biology*, vol. 23. DNA sequencing: laboratory protocols. Totowa (USA). Humana Press, Inc. p. 47-50.
- Bao YP, Huber M, Wei T, Marla SS, Storhoff JJ, Müller UR. 2005. SNP identification in unamplified human genomic DNA with gold nanoparticle probes. *Nucl Acid Res.* 33:e15.
- Baptista P, Doria G, Henriques D, Pereira E, Franco R. 2005a. Colorimetric detection of eukaryotic gene expression with DNA-derivatized gold nanoparticles. *J Biotechnol.* 119:111-7.
- Baptista P, Koziol-Montewka M, Paluch-Oles J, Doria G, Franco R. 2005b. Gold-nanoparticle-probe-based assay for rapid and direct detection of *Mycobacterium Tuberculosis* DNA in clinical samples. *Clin Chem.* 52:1433.

- Baptista P, Pereira E, Eaton P, Doria G, Miranda A, Gomes I, Quaresma P, Franco R. 2008. Gold nanoparticles for the development of clinical diagnosis methods. *Anal Bioanal Chem.* 391:943-950.
- Baptista P. 2000. Integrated mapping and gene analysis in regions showing loss of heterozygosity in human breast cancer in the short arm of Chromosome 1 [dissertation]. University of London.
- Barber DS, Hunt J, LoPachin RM, Ehrich M. 2001. Determination of acrylamide and glycidamide in rat plasma by reversed-phase high performance liquid chromatography. *J Chromatogr B* 758:289-293.
- Barnes CA and Chiu NHL. 2009. Accurate characterization of carcinogenic DNA adducts using MALDI tandem time-of-flight mass spectrometry. *Int J Mass Spectrom* 279:170-175.
- Barth HG, Jackson C, Boyes BE. 1994. Size exclusion chromatography. *Anal Chem.* 66:595R-620R.
- Bertani G and Weigle JJ. 1953. Host controlled variation in bacterial viruses. *J Bacteriol.* 65:113-121.
- Besaratinia A and Pfeifer GP. 2004. Genotoxicity of acrylamide and glycidamide. *J Natl Cancer Inst.* 96:1023-1029.
- Besaratinia A and Pfeifer PG. 2007. A review of mechanisms of acrylamide carcinogenicity. *Carcinogenesis* 28:519-528.
- Bizzarri AR and Cannistraro S. 2009. Surface-enhanced Raman spectroscopy combined with atomic force microscopy for ultrasensitive detection of thrombin. *Anal Biochem.* 393:149-154.
- Black C, Poile C, Langley J, Herniman J. 2006. The use of pencil lead as a matrix and calibrant for matrix-assisted laser desorption/ionization. *Rapid Commun Mass Spectrom.* 20:1053-1060.
- Blasiak J, Gloc E, Wozniak K, Czechowska A. 2004. Genotoxicity of acrylamide in human lymphocytes. *Chem-Biol Interact.* 149:137-149.
- Boisselier E and Astruc D. 2009. Gold nanoparticles in nanomedicine: preparations, imaging, diagnostics, therapies and toxicity. *Chem Soc Rev.* 38:1759-1782.
- Bolis CL, Piccolella M, Dalla Valle AZ, Rankin JC. 2001. Fish as models in pharmacological and biological research. *Pharmacol Res.* 44:265-280.
- Borzelleca JF. 2000. Paracelsus: Herald of Modern Toxicology. *Toxicol Sci.* 53:2-4.
- Boysen G, Pachkowski BF, Nakamura J, Swenberg JA. 2009. The formation and biological significance of N7-guanine adducts. *Mutat Res.* 678:76-94.
- Braby CE and Somero GN. 2009. Following the heart: temperature and salinity effects on heart rate in native and invasive species of blue mussels (genus *Mytilus*). *J Exp Biol.* 209:2554-2566.
- Bradford MM. 1976. A rapid and sensitive method for the quantitation of microgram quantities of protein utilizing the principle of protein-dye binding. *Anal Biochem.* 72:248-254.
- Bridié AL, Wolff CJM, Winter M. 1979. The acute toxicity of some petrochemicals to goldfish. *Water Res.* 13:623-626.
- Brown K, Harvey CA, Turteltaub KW, Shields SJ. 2003. Structural characterization of carcinogen-modified oligodeoxynucleotide adducts using matrix-assisted laser desorption/ionization mass spectrometry. *J Mass Spectrom* 38:68-79.
- Brown K, Tompkins EM, White INH. 2006. Applications of accelerator mass spectrometry for pharmacological and toxicological research. *Mass Spec Rev.* 25:127-145.
- Brown K. 2012. Methods for the detection of DNA adducts. In: Parry JM and Parry EM, editors. *Genetic toxicology: principles and methods.* New York (USA). Humana Press. p. 207-230.

- Brown L, Bancroft KCC, Rhead MM. 1980b. Laboratory studies on the adsorption of acrylamide monomer by sludge, sediments, clays, peat and synthetic resins. *Water Res.* 14:779-781.
- Brown L, Rhead MM, Bancroft KCC, Allen N. 1980a. Model studies of the degradation of acrylamide monomer. *Water Res.* 14:775-778.
- Brown RS and Lennon JJ. 1995. Mass resolution improvement by incorporation of pulsed ion extraction in a matrix-assisted laser desorption/ionization linear time-of-flight mass spectrometer. *Anal Chem.* 67:1998-2003.
- Bucheli TD and Font K. 1995. Induction of cytochrome-450 as a biomarker for environmental contamination in aquatic ecosystems. *Crit Rev Environ Sci Technol.* 25:201-268.
- Budimir N, Blais JC, Fournier F, Tabet JC. 2006. The use of desorption/ionization on porous silicon mass spectrometry for the detection of negative ions for fatty acids. *Rapid Commun Mass Spectrom.* 20:680-684.
- Buhler D and Wang-Buhler J. 1998. Rainbow trout cytochrome P450s: purification, molecular aspects, metabolic activity, induction and role in environmental monitoring. *Comp Biochem Physiol C.* 121:107-137.
- Cai H, Yang P, Feng J, Cai J. 2009. Immunoassay detection using functionalized gold nanoparticle probes coupled with resonance Rayleigh scattering. *Sensor Actuat B-Chem.* 135:603-609.
- Cai S, Lau C, Lu J. 2010. Sequence-specific detection of short-length DNA via template-dependent surface-hybridization events. *Anal Chem.* 82:7178-7184.
- Camacho L, Latendresse JR, Muskhelishvili L, Patton R, Bowyer JF, Thomas M, Doerge DR. 2012. Effects of acrylamide exposure on serum hormones, gene expression, cell proliferation, and histopathology in male reproductive tissues of Fischer 344 rats. *Toxicol Lett.* 211:135-43.
- Canesi L, Ciacci C, Fabbri R. 2012. Bivalve molluscs as a unique target group for nanoparticle toxicity. *Mar Environ Res.* 76:16-21.
- Cao C and Sim SJ. 2009. Resonant Rayleigh light scattering response of individual Au nanoparticles to antigen-antibody interaction. *Lab Chip.* 9:1836-1839.
- Cao C, LiX, Lee J, Sim SJ. 2009. Homogenous growth of gold nanocrystals for quantification of PSA protein biomarker. *Biosens Bioelectron.* 24:1292-1297.
- Carbajal M. 2008. Aflatoxin-DNA adducts as biomarkers of cancer: nature, formation, kinds of AF-DNA adducts, methodology, effects, and control. In: Siantar DP, Trucksess MW, Scott PM, Herman EM, editors. *Food contaminants: mycotoxins and food allergens.* Washington DC (USA). American Chemical Society. p. 13-55.
- Carere A. 2006. Genotoxicity and carcinogenicity of acrylamide: a critical review. *Ann Ist Super Sanità* 42:144-155.
- Carreira RJ. 2011. Development of new methodologies in sample treatment for proteomics workflow based on enzymatic probe sonication technology and mass spectrometry [dissertation]. Universidade NOVA de Lisboa. 188 p.
- Cavas T. 2011. In vivo genotoxicity evaluation of atrazine and atrazine-based herbicide on fish *Carassius auratus* using the micronucleus test and the comet assay. *Food Chem Toxicol.* 49:1431-1435.
- Cavic BA and Thompson M. 2002. Interfacial nucleic acid chemistry studied by acoustic shear wave propagation. *Anal Chim Acta* 469:101-113.
- Chapin RE, Fail PA, George JD, Grizzle TB, Heindel JJ, Harry GJ, Collins BJ, Teague J. 1995. The reproductive and neural toxicities of acrylamide and three analogues in swiss mice, evaluated using the continuous breeding protocol. *Toxicol Sci.* 27:9-24.

Chen SJ, Huang YF, Huang CC, Lee KH, Lin ZH, Chang HT. 2008. Colorimetric determination of urinary adenosine using aptamer-modified gold nanoparticles. *Biosens Bioelectron.* 23:1749-1753.

Chen W, Chiang C, Lin Y, Chang H. 2010. Quantification of captopril in urine through surface-assisted laser desorption/ionization mass spectrometry using 4-mercaptobenzoic acid-capped gold nanoparticles as an internal standard. *J Am Soc Mass Spectrom.* 21:864-867.

Chevolleau S, Jacques C, Canlet C, Tulliez J, Debrauwer L. 2007. Analysis of hemoglobin adducts of acrylamide and glycidamide by liquid chromatography–electrospray ionization tandem mass spectrometry, as exposure biomarkers in French population. *J Chromatogr A.* 1167:125-134.

Chiang C, Chen W, Chang H. 2010. Nanoparticle-based mass spectrometry for the analysis of biomolecules. *Chem Soc Rev.* 40:1269-1281.

Chiang N, Chiang C, Lin Z, Chiu T, Chang H. 2009. Detection of aminothiols through surface-assisted laser desorption/ionization mass spectrometry using mixed gold nanoparticles. *Rapid Commun Mass Spectrom.* 23:3063–3068.

Chikkaveeraiah BV, Mani V, Patel V, Gutkind JS, Rusling JF. 2011. Microfluidic electrochemical immunoarray for ultrasensitive detection of two cancer biomarker proteins in serum. *Biosens Bioelectron.* 26:4477-4483.

Chiu T, Chang L, Chiang C, Chang H. 2008. Determining estrogens using surface-assisted laser desorption/ionization mass spectrometry with silver nanoparticles as the matrix. *J Am Soc Mass Spectrom.* 19:1343-1346.

Chon H, Lee S, Son SW, Oh CH, Choo J. 2009. Highly sensitive immunoassay of lung cancer marker carcinoembryonic antigen using surface-enhanced Raman scattering of hollow gold nanospheres. *Anal Chem.* 81:3029-3034.

Cohen LH and Gusev AI. 2002. Small molecule analysis by MALDI mass spectrometry. *Anal Bioanal Chem.* 373:571-586.

Coldwell KE, Cutts SM, Ognibene TJ, Henderson PT, Phillips DR. 2008. Detection of adriamycin–DNA adducts by accelerator mass spectrometry at clinically relevant adriamycin concentrations. *Nucl Acids Res.* 36:e100.

Conde J, de la Fuente J, Baptista P. 2010. RNA quantification using gold nanoprobe, application to cancer detection. *J Nanobiotechnol.* 8:5.

Conde J. 2013. Cancer theranostics: multifunctional gold nanoparticles for diagnostics and therapy [dissertation]. Universidade NOVA de Lisboa. 362 p.

Costa PM and Costa MH. 2007. Genotoxicity assessment in fish peripheral blood: a method for a more efficient analysis of micronuclei. *J Fish Biol.* 71(Supplement A):148-151.

Costa PM, Diniz MS, Caeiro S, Lobo J, Martins M, Ferreira AM, Caetano M, Vale C, DelValls TA, Costa MH. 2009. Histological biomarkers in liver and gills of juvenile *Solea senegalensis* exposed to contaminated estuarine sediments: a weighted indices approach. *Aquat Toxicol.* 92:202-12.

Costa PM, Lobo J, Caeiro S, Martins M, Ferreira AM, Caetano M, Vale C, DelValls TA, Costa MH. 2008. Genotoxic damage in *Solea senegalensis* exposed to sediments from the Sado Estuary (Portugal): Effects of metallic and organic contaminants. *Mutat. Res.* 654:29-37.

Costa PM, Neuparth T, Caeiro S, Lobo J, Martins M, Ferreira AM, Caetano M, Vale C, DelValls TA, Costa MH. 2011. Assessment of the genotoxic potential of contaminated estuarine sediments in fish peripheral blood: laboratory versus in situ studies. *Environ Res.* 111:25-36.

Croll BT, Arkell GM, Hodge RPJ. 1974. Residues of acrylamide in water. *Water Res.* 8:989-993.

- Croxatto A, Prod'hom G, Greub G. 2012. Applications of MALDI-TOF mass spectrometry in clinical diagnostic microbiology. *FEMS Microbiol Rev.* 36:380-407.
- Dass C. 2007. *Fundamentals of contemporary mass spectrometry*, 1st edition. New Jersey (USA). John Wiley & Sons, Inc.
- Davenport J and Manley A. 1978. The detection of heightened sea-water copper concentrations by the mussel *Mytilus edulis*. *J Mar Biol Assoc UK.* 58:843-850.
- De Almeida L, Froneman W, Pletschke B. 2011. Optimization of a cytochrome-P450-monoxygenase-1A-mediated EROD assay in the cape hake species *Merluccius capensis* and *Merluccius paradoxus* (Pisces). *Enzyme Res.* 2011:ID 108395.
- De Hoffman E and Stroobant V. 2007. *Mass spectrometry: Principles and applications*, 3rd edition. Chichester (UK). John Wiley & Sons, Inc.
- De la Escosura-Muñiz A and Merkoçi A. 2011. A Nanochannel-Nanoparticle-Based Filtering and Sensing Platform for Direct Detection of a Cancer Biomarker in Blood. *Small.* 7:675-682.
- Diniz MS, Peres I, Castro L, Freitas AC, Rocha-Santos TAP, Costa PM, Pereira R, Duarte AC. 2009. Effects of ECF-Kraft pulp mill effluent treated with fungi (*Rhizopus oryzae*) on reproductive steroids and liver CYP1A of exposed goldfish (*Carassius auratus*). *Ecotoxicology* 18:1011-1017.
- Divi RL, Beland FA, Fu PP, Von Tungeln LS, Schoket B, Camara JE, Ghei M, Rothman N, Sinha R, Poirier MC. 2002. Highly sensitive chemiluminescence immunoassay for benzo[a]pyrene-DNA adducts: validation by comparison with other methods, and use in human biomonitoring. *Carcinogenesis.* 23:2043-2049.
- Dobrowolski P, Huet P, Karlsson P, Eriksson S, Tomaszewka E, Gawron A, Pierzynowski SG. 2012. Potato fiber protects the small intestinal wall against the toxic influence of acrylamide. *Nutrition* 28:428-435.
- Dobrzynska MM. 2007. Assessment of DNA damage in multiple organs from mice exposed to x-rays or acrylamide or a combination of both using the comet assay. *In Vivo* 21:657-662.
- Doerge DR, Gamboa da Costa G, McDaniel LP, Churchwell MI, Twaddle NC, Beland FA. 2005. DNA adducts derived from administration of acrylamide and glycidamide to mice and rats. *Mutat Res* 580:131-141.
- Doria G, Baumgartner B, Franco R, Baptista P. 2010. Optimizing Au-nanoprobes for specific sequence discrimination. *Col Surf B.* 77:122-124.
- Doria G, Franco R, Baptista P. 2007. Nanodiagnosics: fast colorimetric method for single nucleotide polymorphism/mutation detection. *IET Nanobiotechnol.* 1:53-57.
- Doria G. 2010. DNA nanoprobes for molecular detection [dissertation]. Universidade NOVA de Lisboa. 177 p.
- Duan J, Linman MJ, Chen CY, Cheng QJ. 2009. CHCA-modified Au nanoparticles for laser desorption ionization mass spectrometric analysis of peptides. *J Am Soc Mass Spectrom.* 20:1530-1539.
- Eaton DL and Gilbert SG. 2008. Principles of toxicology. In: Klaasen CD, editor. *Casarett and Doull's Toxicology: the basic science of poisons*, 7th edition. New York (USA). McGraw-Hill Medical. p. 11-43.
- Edwards PM. 1975. Neurotoxicity of acrylamide and its analogues and effects of these analogues and other agents on acrylamide neuropathy. *Br J Ind Med.* 32:31-38.
- EG&G Bionomics. 1986. Acute toxicity of acrylamide to mysid shrimp (*Mysidopsis bahia*). Report No. BP-83-5-58-R.

- El-Assouli SM. 2009. Acrylamide in selected foods and genotoxicity of their extracts. *J Egypt Public Health Assoc.* 84:369-390.
- El-Bohi KM, Moustafa GG, El sharkawi NI, Sabik LME. 2011. Genotoxic effects of acrylamide in adult male albino rats liver. *J Am Sci.* 7:1097-1108.
- Elghanian R, Storhoff J, Mucic R, Letsinger R, Mirkin C. 1997. Selective Colorimetric Detection of Polynucleotides Based on the Distance-Dependent Optical Properties of Gold Nanoparticles. *Science.* 277:1078-1081.
- Ellington AD and Szostak JW. 1990. In vitro selection of RNA molecules that bind specific ligands. *Nature.* 346:818–822.
- Ellman GL, Courtney KD, Andres jr V, Featherstone RM. 1961. A new and rapid colorimetric determination of acetylcholinesterase activity. *Biochem Pharmacol.* 7:88-90, IN1, 91-95.
- Farmer PB, Brown K, Tompkins E, Emms VL, Jones DJL, Singh R, Phillips DH. 2005. DNA adducts: mass spectrometry methods and future prospects. *Toxicol Appl Pharmacol.* 207:S293–S301.
- Fernandes AM. 2004. Métodos de ionização em espectrometria de massa. Departamento de Química, Universidade de Aveiro (Portugal).
- Fernández B, Campillo JA, Martínez-Gómez C, Benedicto J. 2010. Antioxidant responses in gills of mussel (*Mytilus galloprovincialis*) as biomarkers of environmental stress along the Spanish Mediterranean coast. *Aquat Toxicol.* 99:186-197.
- Feynman RP. 1960. There's plenty of room at the bottom. *Engineering and Science.* 23:22-36.
- Finkel NH, Prevo BG, Velez OD, He L. 2005. Ordered silicon nanocavity arrays in surface-assisted desorption/ionization mass spectrometry. *Anal Chem.* 77:1088-1095.
- Freitas S, Heilscher G, Merkle HP, Gander B. 2006. Continuous contact-and contamination-free ultrasonic emulsification-a useful tool for pharmaceutical development and production. *Ultrason Sonochem.* 13:76-85.
- Friedman M. 2003. Chemistry, biochemistry, and safety of acrylamide. A review. *J Agric Food Chem.* 51:4504-4526.
- Fukudome K, Yamaoka K, Nishikori K, Tatehata H, Yamamoto O. 1986. Ultrasonic scission of deoxyribonucleic acid in aqueous solution II. Precipitacional fractionation and molecular weights of sonicated samples. *Polym J.* 18:81-88.
- Gallo MA. 2008. History and scope of toxicology. In: Klaasen CD, editor. *Casarett and Doull's Toxicology: the basic science of poisons*, 7th edition. New York (USA). McGraw-Hill Medical. p. 3-10.
- Gamboa da Costa G, Churchwell MI, Hamilton LP, von Tungeln LS, Beland FA, Marques MM, Doerge DR. 2003. DNA adduct formation from acrylamide via conversion to glycidamide in adult and neonatal mice. *Chem Res Toxicol.* 16:1328-1337.
- Gaskell M, Kaur B, Farmer PB, Singh R. 2007. Detection of phosphodiester adducts formed by the reaction of benzo[a]pyrene diol epoxide with 2'-deoxynucleotides using collision-induced dissociation electrospray ionization tandem mass spectrometry. *Nucl Acid Res* 35:5014-5027.
- Giri P and Kumar GS. 2009. Molecular aspects of small molecules-poly(A) interaction: an approach to RNA based drug design. *Curr Med Chem.* 16:965-987.
- Girigoswami A, Li T, Jung C, Mun H, Park H. 2009. Gold nanoparticle-based label-free detection of BRCA1 mutations utilizing DNA ligation on DNA microarray. *J Nanosci Nanotechnol.* 9:1019-1024.

- Godschalk RW, Van Schooten FJ, Bartsch H. 2003. A critical evaluation of DNA adducts as biological markers for human exposure to polycyclic aromatic compounds. *J Biochem Mol Biol.* 36:1-11.
- Goode EL, Ulrich CM, Potter JD. 2002. Polymorphisms in DNA repair genes and associations with cancer risk. *Cancer Epidemiol Biomarkers Prev.* 11:1513-30.
- Govorov AO and Richardson HH. 2007. Generating heat with metal nanoparticles. *Nano Today.* 2:30-38.
- Green MA, Egle JL. 1983. The effects of acetaldehyde and acrolein on blood pressure in guanethidine-pretreated hypertensive rats. *Toxicol Appl Pharmacol.* 69:29-36.
- Griffiths J. 2008. A brief history of mass spectrometry. *Anal Chem.* 80:5678-5683.
- Grokhovsky SL. 2006. Specificity of DNA cleavage by ultrasound. *Mol Biol.* 40:317-325.
- Grubisha DS, Lipert RJ, Park H, Driskell J, Porter MD. 2003. Femtomolar detection of prostate-specific antigen, an immunoassay based on surface-enhanced Raman scattering and immunogold labels. *Anal Chem.* 75:5936-5943.
- Guo W, Yuan J, Dong Q, Wang E. 2010. Highly Sequence-Dependent Formation of Fluorescent Silver Nanoclusters in Hybridized DNA Duplexes for Single Nucleotide Mutation Identification. *J Am Chem Soc.* 132:932-934.
- Guo Z, Ganawi AAA, Liu Q, He L. 2006. Nanomaterials in mass spectrometry ionization and prospects for biological application. *Anal Bioanal Chem.* 384: 584–592.
- Gupta RC. 1985. Enhanced sensitivity of ³²P-postlabeling analysis of aromatic carcinogen:DNA adducts. *Cancer Res.* 45:5656.
- Haasch ML, Sutherland LA, Wejksnora PJ, Lech JL. 1992. Effect of acrylamide monomer on hepatic CYP1A1 monooxygenase induction in rainbow trout. *Comp Biochem Physiol C.* 102:281-286.
- Habig WH, Pabst MJ, Jacoby WB. 1974. Glutathione S-transferases: the first enzymatic step in mercapturic acid formation. *J Biol Chem.* 249:7130-7139.
- Harpster MH, Zhang H, Sankara-Warrier A, Ray BH, Ward TR, Kollmar JP, Carron KT, Mecham JO, Corcoran RC, Wilson WC, Johnson PA. 2009. SERS detection of indirect viral DNA capture using colloidal gold and methylene blue as a Raman label. *Biosens Bioelectron.* 25:674-681.
- Hart-Smith G and Blanksby SJ. 2012. Mass analysis. In: Barner-Kowollik C, Gruending T, Falkenhagen J, Weidner S, editors. *Mass spectrometry in polymer chemistry*, 1st edition. Weinheim (Germany). Wiley-VCH Verlag. p. 5-32.
- Hayes AN and Gilbert SG. 2009. Historical milestones and discoveries that shaped the toxicology sciences. In: Luch A, editor. *Molecular, clinical and environmental toxicology*, vol 1: *Molecular toxicology*. Basel (Switzerland). Birkhäuser Verlag AG. p. 1-35.
- He F, Zhang S, Wang H. 1989. Neurological and electropneuromyographic assessment of the adverse effects of acrylamide on occupationally exposed workers. *Scand J Work Environ Health* 15:125-129.
- Helbock HJ, Beckman KB, Shigenaga MK, Walter PB, Woodall AA, Yeo HC, Ames BN. 1998. DNA oxidation matters: The HPLC-electrochemical detection assay of 8-oxo-deoxyguanosine and 8-oxo-guanine. *P Natl Acad Sci USA.* 95:288-293.
- Hillenkamp F and Peter-Katalinić J. 2007. *MALDI MS: a practical guide to instrumentation, methods and applications*. Weinheim (Germany). Wiley-VCH Verlag.
- Howland RD. 1985. Biochemical studies of acrylamide neuropathy. *Neurotoxicology* 6:7-16.

Hsieh Y, Chen W, Tomalová I, Preisler J, Chang H. 2012. Detection of melamine in infant formula and grain powder by surface-assisted laser desorption/ionization mass spectrometry. *Rapid Commun Mass Spectrom.* 26:1393-1398.

Hu J, Zheng P, Jiang J, Shen G, Yu R, Liu G. 2010. Sub-attomolar HIV-1 DNA detection using surface-enhanced Raman spectroscopy. *Analyst.* 135:1084-1089.

Hua L, Chen J, Liya G, Tan SN. 2007. Silver nanoparticles as matrix for laser desorption/ionization mass spectrometry of peptides. *J Nanopart Res.* 9:1133-1138.

Huang Y and Chang H. 2007. Analysis of adenosine triphosphate and glutathione through gold nanoparticles assisted laser desorption/ionization mass spectrometry. *Anal Chem.* 79:4852-4859.

Huang YF and Chang HT. 2006. Nile red-adsorbed gold nanoparticle matrixes for determining amino thiols through surface-assisted laser desorption/ionization mass spectrometry. *Anal Chem.* 78:1485-1493.

Huo Q. 2010. Protein complexes/aggregates as potential cancer biomarkers revealed by a nanoparticle aggregation immunoassay. *Col Surf B.* 78:259-265.

IARC. 1994. Acrylamide. IARC Monographs. Volume 60:389-433.

Jain P, Lee K, El-Sayed I, El-Sayed M. 2006. Calculated absorption and scattering properties of gold nanoparticles of different size, shape, and composition: applications in biological imaging and biomedicine. *J Phys Chem B.* 110:7238-7248.

James RC, Roberts SM, Williams PL. 2000. General principles of toxicology. In: James RC, Roberts SM, Williams PL, editors. *Principles of toxicology: environmental and industrial applications*, 2nd edition. New York (USA). John Wiley & Sons, Inc. p. 3-34.

Jaramillo MC and Zhang DD. 2013. The emerging role of the Nrf2-Keap1 signaling pathway in cancer. *Genes Dev.* 27:2179-2191.

Javier DJ, Nitin N, Levy M, Ellington A, Richards-Kortum R. 2008. Aptamer-targeted gold nanoparticles as molecular-specific contrast agents for reflectance imaging. *Bioconjugate Chem.* 19:1309-1312.

Jiang L, Cao J, An Y, Geng C, Qu S, Jiang L, Zhong L. 2007. Genotoxicity of acrylamide in human hepatoma G2 (HepG2) cells. *Toxicol in Vitro* 21:1486-1492.

Johansson LH and Borg LA. 1988. A spectrophotometric method for determination of catalase activity in small tissue samples. *Anal Biochem.* 174:331-336.

Kafka AP, Kleffman T, Rades T, McDowell A. 2011. The application of MALDI TOF MS in biopharmaceutical research. *Int J Pharm.* 417:70-82.

Kah JC, Kho CG, Sheppard CJ, Shen ZX, Soo KC, Olivo MC. 2007. Early diagnosis of oral cancer based on the surface plasmon resonance of gold nanoparticles. *Int J Nanomed.* 2:785-798.

Kailasa SK and Wu H. 2012. One-pot synthesis of dopamine dithiocarbamate functionalized gold nanoparticles for quantitative analysis of small molecules and phosphopeptides in SALDI- and MALDI-MS. *Analyst.* 137:1629-1638.

Kanjanawarut R and Su X. 2009. Colorimetric detection of DNA using unmodified metallic nanoparticles and peptide nucleic acid probes. *Anal Chem.* 81:6122-6129.

Karas M and Hillenkamp F. 1988. Laser desorption ionization of proteins with molecular masses exceeding 10,000 daltons. *Anal Chem.* 60:2299-2301.

Karas M, Bachmann D, Hillenkamp F. 1985. Influence of the wavelength in high-irradiance ultraviolet laser desorption mass spectrometry of organic molecules. *Anal Chem.* 57:2935-2939.

Kazakevich Y and LoBrutto R. 2007. *HPLC for pharmaceutical scientists*. Hoboken (USA). John Wiley & Sons, Inc.

Kerman K, Saito M, Morita Y, Takamura Y, Ozsoz M, Tamiya E. 2004. Electrochemical coding of single-nucleotide polymorphisms by monobase-modified gold nanoparticles. *Anal Chem.* 76:1877-1884.

Kiga D, Futamura Y, Sakamoto K, Yokoyama S. 1998. An RNA aptamer to the xanthine/guanine base with a distinctive mode of purine recognition. *Nucl. Acids Res.* 26:1755-1760.

Kim D, Daniel WL, Mirkin CA. 2009. Microarray-based multiplexed scanometric immunoassay for protein cancer markers using gold nanoparticle probes. *Anal Chem.* 81:9183-9187.

Kim Y and Lee TG. 2012. Secondary ions mass spectrometric signal enhancement of peptides on enlarged-gold nanoparticle surfaces. *Anal Chem.* 84:4784-4788.

Klaunig JE and Kamendulis LM. 2008. Chemical carcinogenesis. In: Klaasen CD, editor. *Casarett and Doull's Toxicology: the basic science of poisons*, 7th edition. New York (USA). McGraw-Hill Medical. p. 381-413.

Knochenmuss R and Zenobi R. 2003. MALDI ionization: the role of in-plume processes. *Chem Rev.* 103:441-452.

Knochenmuss R and Zhigilei LV. 2012. What determines MALDI ion yields? A molecular dynamics study of ion loss mechanisms. *Anal Bioanal Chem.* 402:2511-2519.

Kobayashi M and Yamamoto M. 2005. Molecular mechanisms activating the Nrf2-Keap1 pathway of antioxidant gene regulation. *Antioxid Redox Signal.* 7:385-394.

Koehler A, Alpermann T, Lauritzen B, van Noorden JF. 2004. Clonal xenobiotic resistance during pollution-induced toxic injury and hepatocellular carcinogenesis in liver of female flounder (*Platichthys flesus (L.)*). *Acta Histochem.* 106:155-170.

Kong XL, Huang LCL, Hsu C, Chen W, Han C, and Chang H. 2005. High-affinity capture of proteins by diamond nanoparticles for mass spectrometric analysis. *Anal Chem.* 77:259-265.

Kopaciewicz W, Rounds MA, Fausnaugh J, Reigner FE. 1983. Retention model for high-performance ion-exchange chromatography. *J Chromatogr A.* 26:3-21.

Koppelaar DW, Barinaga CJ, Denton MB, Sperline RP, Hieftje GM, Schilling GD, Andrade FJ, Barnes JH. 2005. MS detectors. *Anal Chem.* 77:418A-427A.

Kotova N, Jurén T, Myöhänen K, Cornelius M, Abramsson-Zetterberg L, Backman J, Menzel U, Rydberg P, Kronberg L, Vähäkangas K, Segerbäck D. 2011. ³²P-HPLC analysis of N1-(2-carboxy-2-hydroxyethyl)deoxyadenosine: A DNA adduct of the acrylamide-derived epoxide glycidamide. *Toxicol Lett* 207:18-24.

Kramer KJM, Jenner HA, de Zwart D. 1989. The valve movement response of mussels: a tool in biological monitoring. *Dev Hydrob.* 54:433-443.

Krautter GR, Mast RW, Alexander HC, Wolf CH, Friedman MA, Koschier FJ, Thompson CM. 1986. Acute toxicity tests with acrylamide monomer and macroinvertebrates and fish. *Environ Toxicol Chem.* 5:373-371.

Kriek E, Rojas M, Alexandrov K, Bartsch H. 1998. Polycyclic aromatic hydrocarbon-DNA adducts in humans: relevance as biomarkers for exposure and cancer risk. *Mutat Res.* 400:215-31.

Kubrak OI, Husak VV, Rovenko BM, Poigner H, Mazepa MA, Kriews M, Abele D, Lushchak VI. 2012. Tissue specificity in nickel uptake and induction of oxidative stress in kidney and spleen of goldfish *Carassius auratus*, exposed to waterborne nickel. *Aquat Toxicol.* 118-119:88-96.

Kuo T, Chen J, Chiu Y, Tsai C, Hu C, Chen C. 2011. Quantitative analysis of multiple urinary biomarkers of carcinoid tumors through gold-nanoparticle-assisted laser desorption/ionization time-of-flight mass spectrometry. *Anal Chim Acta.* 699:81-86.

- Labib M, Martić S, Shipman PO, Kraatz H. 2011. Electrochemical analysis of HIV-1 reverse transcriptase serum level: Exploiting protein binding to a functionalized nanostructured surface. *Talanta*. 85:770-778.
- Lai N, Wang C, Chiang H, Chau L. 2007. Detection of antinuclear antibodies by a colloidal gold modified optic fiber: comparison with ELISA. *Anal Bioanal Chem*. 388:901-907.
- Lane CS. 2005. Mass spectrometry-based proteomics in the life sciences. *Cell Mol Life Sci*. 62:848-869.
- Lapadula DM, Bowe M, Carrington CD, Dulak L, Friedman M, Abou-Donia MB. 1989. In vitro binding of [¹⁴C] acrylamide to neurofilament and microtubule proteins of rats. *Brain Res*. 481:157-161.
- Lazzari M, Rodríguez-Abreu C, Rivas J, López-Quintela MA. 2006. Self-assembly: a minimalist route to the fabrication of nanomaterials. *J Nanosci Nanotechnol*. 6:892-905.
- Lee C, Gopal J, Wu H. 2012. Ionic solution and nanoparticle assisted MALDI-MS as bacterial biosensors for rapid analysis of yogurt. *Biosens Bioelectron*. 31:77-83.
- Lee H, Joo S, Lee S, Lee C, Yoon K, Lee K. 2010. Colorimetric genotyping of single nucleotide polymorphism based on selective aggregation of unmodified gold nanoparticles. *Biosens Bioelectron*. 26:730-735.
- Lee J, Lytton-Jean A, Hurst S, Mirkin C. 2007. Silver Nanoparticle-Oligonucleotide Conjugates Based on DNA with Triple Cyclic Disulfide Moieties. *NanoLett*. 7:2112-2115.
- Lee RF and Steinert S. 2003. Use of the single cell gel electrophoresis/comet assay for detecting DNA damage in aquatic (marine and freshwater) animals. *Mutat Res*. 544:43-64.
- Lee S, Chon H, Lee M, Choo J, Shin SY, Lee YH, Rhyu IJ, Son SW, Oh CH. 2009. Surface-enhanced Raman scattering imaging of HER2 cancer markers overexpressed in single MCF7 cells using antibody conjugated hollow gold nanospheres. *Biosens Bioelectron*. 24:2260-2263.
- Lehman-McKeeman LD. 2008. Absorption, distribution and excretion of toxicants. In: Klaasen CD, editor. *Casarett and Doull's Toxicology: the basic science of poisons*, 7th edition. New York (USA). McGraw-Hill Medical. p. 131-159.
- Leroy Q and Raoult D. 2010. Review of microarray studies for host–intracellular pathogen interactions. *J Microbiol Met*. 81: 81-95.
- Li H and Rothberg L. 2004. Colorimetric detection of DNA sequences based on electrostatic interactions with unmodified gold nanoparticles. *Proc Natl Acad Sci USA*. 101:14036-14039.
- Li J, Wang Z, Gryczynski I, Mandrecki W. 2010. Silver nanoparticle-enhanced fluorescence in microtransponder-based immuno- and DNA hybridization assays. *Anal Bioanal Chem*. 398:1993-2001.
- Li Z, Liu C, Fan Y, Duan X. 2007. Chemiluminescent detection of DNA hybridization using gold nanoparticles as labels. *Anal Bioanal Chem*. 387:613-618.
- Liang R, Chen Y, Qiu J. 2011. A sensitive amperometric immunosensor for hepatitis B surface antigen based on biocompatible redox-active chitosan–toluidine blue/gold nanoparticles composite film. *Anal Methods*. 3:1338-1343.
- Lineback DR, Coughlin JR, Stadler RH. 2012. Acrylamide in foods: a review of the science and future considerations. *Annu Rev Food Sci Technol*. 3:15-35.
- Liu C, Li Z, Du B, Duan X, Wang Y. 2006. Silver nanoparticle-based ultrasensitive chemiluminescent detection of DNA hybridization and single-nucleotide polymorphisms. *Anal Chem*. 76:3738-3744.
- Liu M, Jia C, Huang Y, Lou X, Yao S, Jin Q, Zhao J, Xiang J. 2010. Highly sensitive protein detection using enzyme-labeled gold nanoparticle probes. *Analyst*. 135:327-331.

Liu M, Yuan M, Lou X, Mao H, Zheng D, Zou R, Zou N, Tang X, Zhao J. 2011. Label-free optical detection of single-base mismatches by the combination of nuclease and gold nanoparticles. *Biosens Bioelectron.* 26:4294-4300.

Liu W, Guo H, Wu J. 2007. Effects of target length on the hybridization efficiency and specificity of rRNA-based oligonucleotide microarrays. *Appl Environ Microbiol.* 73:73-82.

Liu Y, Chang H, Chiang C, Huang C. 2012. Pulsed-laser desorption/ionization of clusters from biofunctional gold nanoparticles: implications for protein detections. *Appl Mater Interfaces.* 4:5241-5248.

Liz-Marzán L. 2006. Tailoring surface plasmons through the morphology and assembly of metal nanoparticles. *Langmuir* 22:32-41.

Lo H, Hsiung H, Chattopadhyay S, Han H, Chen C, Leu J, Chen K, Chen L. 2011. Label free sub-picomole level DNA detection with Ag nanoparticle decorated Au nanotip arrays as surface enhanced Raman spectroscopy platform. *Biosens Bioelectron.* 26:2413-2418.

LoPachin RM and Gavin T. 2012. Molecular mechanism of acrylamide neurotoxicity: lessons learned from organic chemistry. *Environ Health Perspect.* 120:1650-1657.

Lopéz-Ferrer D, Capelo JL, Vásquez J. 2005. Ultra fast trypsin digestion of proteins by high intensity focused ultrasound. *J Prot Res* 4:1569-1574.

Lowe AJ, Huh YS, Strickland AD, Erickson D, Batt CA. 2010. Multiplex single nucleotide polymorphism genotyping utilizing ligase detection reaction coupled surface enhanced Raman spectroscopy. *Anal Chem.* 82:5810-5814.

Luque de Castro MD and Capote FP. 2007. Analytical applications of ultrasound. Amsterdam (The Netherlands). Elsevier.

Luria SE and Human ML. 1952. A nonhereditary, host-induced variation of bacterial viruses. *J Bacteriol.* 64:557-569.

Mairal T, Ozalp VC, Lozano Sánchez P, Mir M, Katakis I, O'Sullivan CK. 2008. Aptamers: molecular tools for analytical applications. *Anal Bioanal Chem.* 390:989-1007.

Maity S, Bochinski JR, Clarke LI. 2012. Metal nanoparticles acting as light-activated heating elements within composite materials. *Adv Funct Mater.* 22:5259-5270.

Makino K, Mossoba MM, Riesz P. 1983. Chemical effects of ultrasound on aqueous solutions. Formation of hydroxyl radicals and hydrogen atoms. *J Phys Chem.* 87:1369-1377.

Malicka J, Gryczynski I, Lakowicz JR. 2003. DNA hybridization assays using metal-enhanced fluorescence. *Bioch Biophys Res Commun.* 306:213-218.

Mani V, Chikkaveeraiah BV, Patel V, Gutkind JS, Rusling JF. 2009. Ultrasensitive immunosensor for cancer biomarker proteins using gold nanoparticle film electrodes and multienzyme-particle amplification. *ACS Nano* 3:585-594.

Manikandan M, Wu H, Hasan N. 2012. Cell population based mass spectrometry using platinum nanodots for algal and fungal studies. *Biosens Bioelectron* 35:493-497.

Mann LT and Krull UJ. 2004. The application of ultrasound as a rapid method to provide DNA fragments suitable for detection by DNA biosensors. *Biosens Bioelectr.* 20:945-955.

Martins C, Oliveira NG, Pingarilho M, Gamboa da Costa G, Martins V, Marques MM, Beland F, Churchwell MI, Doerge DR, Rueff J, Gaspar JF. 2007. Cytogenetic damage induced by acrylamide and glycidamide in mammalian cells: correlation with specific glycidamide-DNA adducts. *Toxicol Sci.* 95:383-390.

Martoja R and Martoja M. 1967. *Initiation aux Techniques de l'Histologie Animal.* Paris (France). Masson & Cie.

- Mason TJ and Lorimer JP. 2002. Applied sonochemistry: uses of power ultrasound in chemistry and processing. Weinheim (Germany). Wiley-VCH Verlag.
- Mather BD, Viswanathan K, Miller KM, Long TE. 2006. Michael addition reactions in macromolecular design for emerging technologies. *Prog Polym Sci.* 31:487-531.
- McDonnell LA and Heeren RM. 2007. Imaging mass spectrometry. *Mass spectrom rev.* 26:606-643.
- McLean JA, Stumpo KA, Russel DH. 2005. Size-Selected (2-10 nm) Gold Nanoparticles for Matrix Assisted Laser Desorption Ionization of Peptides. *J Am Chem Soc.* 127:5304-5305.
- Mehlmann M, Townsend MB, Stears RL, Kuchta RD, Rowlen KL. 2005. Optimization of fragmentation conditions for microarray analysis of viral RNA. *Anal Biochem.* 347:316-323.
- Miller DL and Thomas RM. 1996. The role of cavitation in the induction of cellular DNA damage by ultrasound and lithotripter shock waves in vitro. *Ultrasound Med Biol.* 22:681-687.
- Miller DL, Thomas RM, Buschbom RH. 1995. Comet assay reveals DNA strand breaks induced by ultrasonic cavitation in vitro. *Ultrasound Med Biol.* 21:841-848.
- Miller JC, Serrato R, Represas-Cardenas JM, Kundahl G. 2005. The handbook of nanotechnology: business, policy and intellectual property law. Hoboken (USA). John Wiley & Sons, Inc.
- Miller MW, Miller DL, Brayman AA. 1996. A review of in vitro bioeffects of inertial ultrasonic cavitation from a mechanistic perspective. *Ultrasound Med Biol.* 22:1131-1154.
- Miller NJ, Rice-Evans C, Davies MJ. 1993. A new method for measuring antioxidant activity. *Biochem Soc Trans.* 21:95S.
- Milowska K and Gabryelak T. 2007. Reactive oxygen species and DNA damage after ultrasound exposure. *Biomol Engineer.* 24:263-267.
- Mirkin C, Letsinger R, Mucic R, Storhoff J. 1996. A DNA-Based Method for Rationally Assembling Nanoparticles into Macroscopic Materials. *Nature.* 382:607-609.
- Moody B and McCarty G. 2009. Statistically significant Raman detection of midsequence single nucleotide polymorphisms. *Anal Chem.* 81:2013-2016.
- Moore JC. 1964. Gel permeation chromatography. 1. A new method for molecular weight distribution of high polymers. *J Polym Sci Part A.* 2:835-843
- Mori S and Barth HG. 1999. Size exclusion chromatography. Heidelberg (Germany). Springer Verlag.
- Myagchenkov VA and Kurenkov VF. 1991. Applications of acrylamide polymers and copolymers: a review. *Polym-Plast Tech.* 30:109-135.
- Neely A, Perry C, Varisli B, Singh AK, Arbneshi T, Senapati D, Kalluri JR, Ray PC. 2009. Ultrasensitive and highly selective detection of Alzheimer's disease biomarker using two-photon Rayleigh scattering properties of gold nanoparticle. *ACS Nano.* 3:2834-2840.
- NICNAS. 2002. Acrylamide. National Industrial Chemicals Notification and Assessment Scheme. Priority Existing Chemical Assessment Report N° 23.
- Niemeyer CM and Mirkin CA. 2004. Nanobiotechnology: concepts, applications and perspectives. Weinheim (Germany). Wiley-VCH Verlag.
- Nier AO. 1940. A mass spectrometer for routine isotope abundance measurements. *Rev Sci Instrum.* 11:212-216.
- Nilsen BM, Berg K, Goksøyr A. 1998. Induction of cytochrome P450 1A (CYP1A) in fish. A Biomarker for environmental pollution. *Method Mol Biol.* 107:423-38.

- Niziol J, Rode W, Laskowska B, Ruman T. 2013. Novel monoisotopic ^{109}Ag NPET for laser desorption/ionization mass spectrometry. *Anal Chem.* 85:1926–1931.
- O'Brien Jr WD. 2007. Ultrasound–biophysics mechanisms. *Progr Biophys Mol Biol.* 93:212-255.
- O'Flaherty EJ. 2000. Absorption, distribution and elimination of toxic agents In: James RC, Roberts SM, Williams PL, editors. *Principles of toxicology: environmental and industrial applications*, 2nd edition. New York (USA). John Wiley & Sons, Inc. p. 35-55.
- Ogawa M, Oyama T, Isse T, Yamaguchi T, Murakami T, Endo Y, Kawamoto T. 2006. Hemoglobin adducts as a marker of exposure to chemical substances, especially PRTR class I designated chemical substances. *J Occup Health.* 48:314-328.
- Oh S, Ryu BT, Kim HR, Choi K, Chung K. 2009. Molecular cloning of CYP1A gene and its expression by benzo(a)pyrene from goldfish (*Carassius auratus*). *Environ Toxicol.* 24:225-234.
- Olsvik PA, Brattås M, Lie KK, Goksøyr A. 2011. Transcriptional responses in juvenile Atlantic cod (*Gadus morhua*) after exposure to mercury-contaminated sediments obtained near the wreck of the German WW2 submarine U-864, and from Bergen Harbor, Western Norway. *Chemosphere* 83:552-563.
- Omidfar K, Dehdast A, Zarei H, Sourkahi BK, Larijani B. 2011. Development of urinary albumin immunosensor based on colloidal AuNP and PVA. *Biosens Bioelectron.* 26:4177-4183.
- Örstan A. 1992. Toxicity of acrylamide derivatives to embryos of the rotifer *Adineta vaga*. *Bull Environ Contam Toxicol.* 48:901-906.
- Ou C, Yuan R, Chai Y, Tang M, Chai R, He X. 2007. A novel amperometric immunosensor based on layer-by-layer assembly of gold nanoparticles-multi-walled carbon nanotubes-thionine multilayer films on polyelectrolyte surface. *Anal Chim Acta.* 603:205-213.
- Park JW, Cundy KC, Ames BN. 1989. Detection of DNA adducts by high-performance liquid chromatography with electrochemical detection. *Carcinogenesis* 10:827-832.
- Parkinson A and Ogilvie BW. 2008. Biotransformation of xenobiotics. In: Klaasen CD, editor. *Casarett and Doull's Toxicology: the basic science of poisons*, 7th edition. New York (USA). McGraw-Hill Medical. p. 161-304.
- Peacocke AR and Pritchard NJ. 1968. The ultrasonic degradation of biological macromolecules under conditions of stable cavitation. II. Degradation of deoxyribonucleic acid. *Biopolymers.* 6:605-623.
- Pennisi M, Malaguarnera G, Puglisi V, Vinciguerra L, Vacante M, Malaguerna M. 2013. Neurotoxicity of acrylamide in exposed workers. *Int J Environ Res Public Health* 10:3843-3854.
- Pérez HL, Cheong HK, Yang JS, Osterman-Golkar S. 1999. Simultaneous analysis of hemoglobin adducts of acrylamide and glycidamide by gas chromatography-mass spectrometry. *Anal Biochem.* 274:59-68.
- Perfézou M, Turner A, Merkoçi A. 2012. Cancer detection using nanoparticle-based sensors. *Chem Soc Rev.* 41:2606-2622.
- Peters LD, Telli-Karakoç F, Hewer A, Phillips DH. 2002. In vitro mechanistic differences in benzo[a]pyrene-DNA adduct formation using fish liver and mussel digestive gland microsomal activating systems. *Mar Environ Res.* 54:499-503.
- Peterson DS. 2007. Matrix-free methods for laser desorption/ionization mass spectrometry. *Mass Spectrom Rev.* 26:19-34.
- Phillips DH, Farmer PB, Beland FA, Nath RG, Poirier MC, Reddy MV, Turtletaub KW. 2000. Methods of DNA adduct determination and their application to testing compounds for genotoxicity. *Environ Mol Mutagen* 35:222-233.

Podzimek S, Vlcek T, Johann C. 2001. Characterization of branched polymers by size exclusion chromatography coupled with multiangle light scattering detector. I. Size exclusion chromatography elution behavior of branched polymers. *J Appl Polym Sci* 81:1588-1594.

Prasad SN and Muralidhara. 2012. Evidence of acrylamide induced oxidative stress and neurotoxicity in *Drosophila melanogaster* - Its amelioration with spice active enrichment: Relevance to neuropathy. *Neurotoxicology* 33:1254-1264.

Preston RJ and Hoffmann GR. 2008. Genetic toxicology. In: Klaasen CD, editor. Casarett and Doull's Toxicology: the basic science of poisons, 7th edition. New York (USA). McGraw-Hill Medical. p. 329-379.

Pritchard NJ, Hughes DE, Peacocke AR. 1966. The ultrasonic degradation of biological macromolecules under conditions of stable cavitation. I. Theory, methods, and application to deoxyribonucleic acid. *Biopolymers* 4:259-273.

Puppel N, Tjaden Z, Fueller F, Marko D. 2005. DNA strand breaking capacity of acrylamide and glycidamide in mammalian cells. *Mutat Res* 580:71-80.

Qiao Z, Udeochu U, Jimerson T, Fletcher M, Bakare O, Hosten CM. 2006. Detection of benzyopyrene-deoxyguanosine adducts by matrix-assisted laser desorption/ionization time-of-flight mass spectrometry. *Rapid Commun Mass Spectrom* 20:487-492.

Randerath K and Randerath E. 1964. Ion-exchange chromatography of nucleotides on poly-(ethyleneimine)-cellulose thin layers. *J Chromatogr A*. 16:111-125.

Ray S, Reddy PJ, Choudhary S, Raghu D, Srivastava S. 2011. Emerging nanoproteomics approaches for disease biomarker detection: A current perspective. *J Prot.* 18:2660-2681.

Reddy MV, Blackburn GR, Schreiner CA, Mehlman MA, Mackerer CR. 1989. ³²P analysis of DNA adducts in tissues of benzene-treated rats. *Environ Health Persp* 82:253-257.

Reyzer ML and Caprioli RM. 2007. MALDI-MS-based imaging of small molecules and proteins in tissues. *Curr Opin Chem Biol*. 11:29-35.

Rial-Otero R, Carreira RJ, Cordeiro FM, Moro AJ, Santos HM, Vale G, Moura I, Capelo JL. 2007. Ultrasonic assisted protein enzymatic digestion for fast protein identification by matrix-assisted laser desorption/ionization time-of-flight mass spectrometry Sonoreactor versus ultrasonic probe. *J Chromatogr A*. 1166:101-107.

Rosa JP, Lima JC, Baptista PV. 2011. Experimental photophysical characterization of fluorophores in the vicinity of gold nanoparticles. *Nanotechnology*. 22:415202.

Rozman KK and Klaasen CD. 2003. Absorption, distribution and excretion of toxicants. In: Klaasen CD and Watkins III JB, editors. Casarett and Doull's essentials of toxicology. New York (USA). McGraw-Hill Medical. p. 59-70.

Sabanayagam R and Lakowicz J. 2007. Increasing the sensitivity of DNA microarrays by metal-enhanced fluorescence using surface-bound silver nanoparticles. *Nucl Acid Res*. 35.

Sakamoto J and Hashimoto K. 1986. Reproductive toxicity of acrylamide and related compounds in mice - effects on fertility and sperm morphology. *Arch Toxicol*. 59:201-205.

Salinas AE and Wong MG. 1999. Glutathione S-transferases-a review. *Curr Med Chem*. 6:279-309.

Sambrook J and Russel DW. 2001. *Molecular Cloning: a laboratory manual*, 3rd edition. New York (USA). Cold Spring Harbor Laboratory Press.

Santella RM. 1999. Immunological methods for detection of carcinogen-DNA damage in humans. *Cancer Epidemiol Biomarkers Prev* 8:733-739.

Santos HM and Capelo JL. 2007. Trends in ultrasonic-based equipment for analytical sample treatment. *Talanta* 73:795-802.

- Santovito G, Piccinni E, Cassini A, Irato P, Albergoni V. 2005. Antioxidant responses of the Mediterranean mussel, *Mytilus galloprovincialis*, to environmental variability of dissolved oxygen. *Comp Biochem Physiol C*. 140:321-329.
- Sar DG, Montes-Bayón M, Ortiz LA, Blanco-González E, Sierra LM, Sanz-Medel A. 2008. In vivo detection of DNA adducts induced by cisplatin using capillary HPLC–ICP-MS and their correlation with genotoxic damage in *Drosophila melanogaster*. *Anal Bioanal Chem* 390:37-44.
- Sato K, Hosokawa K, Maeda M. 2003. Rapid aggregation of gold nanoparticles induced by non-cross-linking DNA hybridization. *J Am Chem Soc*. 125:8102-8103.
- Sato S, Shirakawa H, Tomita S, Ohsaki Y, Haketa K, Tooi O, Santo N, Tohkin M, Furukawa Y, Gonzalez FJ, Komai M. 2008. Low-dose dioxins alter gene expression related to cholesterol biosynthesis, lipogenesis, and glucose metabolism through the aryl hydrocarbon receptor-mediated pathway in mouse liver. *Toxicol Appl Pharmacol*. 229:10-19.
- Scarpelli DG. 1989. Toxicology of the pancreas. *Toxicol Appl Pharmacol*. 101:543-54.
- Schlenk D, Celander M, Gallagher EP, George S, James M, Kullman SW, van der Hurk P, Willett K. 2008. Biotransformation in fishes. In: Di Giulio RT and Hinton DE, editors. *The Toxicology of Fishes*. Boca Raton (USA). Taylor and Francis. p. 153-234.
- Schrenk D. 1998. Impact of dioxin-type induction of drug-metabolizing enzymes on the metabolism of endo- and xenobiotics. *Biochem Pharmacol*. 55:1155-1162.
- Schurenberg M, Dreisewerd K, Hillenkamp F. 1999. Laser desorption/ionization mass spectrometry of peptides and proteins with particle suspension matrixes. *Anal Chem*. 71:221–229.
- Seale SM, Feng Q, Agarwal AK, El-Alfy AT. 2012. Neurobehavioral and transcriptional effects of acrylamide in juvenile rats. *Pharmacol Biochem Behav*. 101:77-84.
- Segerbäck D, Calleman CJ, Schroeder JL, Costa LG, Faustman EM. 1995. Formation of N-7-(2-carbamoyl-2-hydroxyethyl)guanine in DNA of the mouse and the rat following intraperitoneal administration of [¹⁴C]acrylamide. *Carcinogenesis* 16:1161-1165.
- Sen A, Ozgun O, Arinç E, Arslan S. 2012. Diverse action of acrylamide on cytochrome P450 and glutathione S-transferase isozyme activities, mRNA levels and protein levels in human hepatocarcinoma cells. *Cell Biol Toxicol*. 28:175-86.
- Serra A, Manno D, Filippo E, Buccolieri A, Urso E, Rizzello A, Maffia M. 2011. SERS based optical sensor to detect prion protein in neurodegenerate living cells. *Sensor Actuat B-Chem*. 156:479-485.
- Settels E, Bernauer U, Palavinskas R, Klaffke HS, Gundert-Remy U, Appel KE. 2008. Human CYP2E1 mediates the formation of glycidamide from acrylamide. *Arch Toxicol*. 2008:717-727.
- Sharma M. 2000. Analysis of tamoxifen-DNA adducts by high-performance liquid chromatography using postcolumn online photochemical activation. *Biochem Biophys Res Commun* 273:40-44.
- Sheskin FJ. 2000. *Handbook of Parametric and Nonparametric Statistical Procedures*, 2nd edition. Boca Raton (USA). Chapman & Hall.
- Shibamoto K, Sakata K, Nagoshi K, Korenaga T. 2009. Laser desorption ionization mass spectrometry by using surface plasmon excitation on gold nanoparticle. *J Phys Chem C*. 113:17774–17779.
- Shipp A, Lawrence G, Gentry R, McDonald T, Bartow H, Bound J, Macdonald N, Clewell H, Allen B, Van Landingham C. 2006. Acrylamide: review of toxicity data and dose-response analyses for cancer and noncancer. *Effects Crit Rev Toxicol*. 36:481-608.
- Shore M, Wang J, Johnston-Peck A, Oldenburg A, Tracy J. 2011. Synthesis of Au(Core)-Ag(Shell) nanoparticles and their conversion to AuAg alloy nanoparticles. *Small*. 7:230-234.

Shrivastava K and Wu H. 2008. Applications of silver nanoparticles capped with different functional groups as the matrix and affinity probes in surface-assisted laser desorption/ionization time-of-flight and atmospheric pressure matrix-assisted laser desorption/ionization ion trap mass spectrometry for rapid analysis of sulfur drugs and biothiols in human urine. *Rapid Commun Mass Spectrom.* 22:2863–2872.

Shrivastava K, Agrawal K, Wu H. 2011. Application of platinum nanoparticles as affinity probe and matrix for direct analysis of small biomolecules and microwave digested proteins using matrix-assisted laser desorption/ionization mass spectrometry. *Analyst.* 136:2852–2857.

Sickles DW, Sperry AO, Testino A, Friedman M. 2007. Acrylamide effects on kinesin-related proteins of the mitotic/meiotic spindle. *Toxicol Appl Pharm.* 222:111-121.

Sickles DW, Welter DA, Friedman MA. 1995. Acrylamide arrests mitosis and prevents chromosome migration in the absence of changes in spindle microtubules. *J Toxicol Env Health* 44:73-86.

Siethoff C, Feldmann I, Jakubowski N, Linscheid M. 1999. Quantitative determination of DNA adducts using liquid chromatography/electrospray ionization mass spectrometry and liquid chromatography/high-resolution inductively coupled plasma mass spectrometry. *J Mass Spectrom.* 34:421–426.

Silins I and Högberg J. 2011. Combined toxic exposures and human health: biomarkers of exposure and effect. *Int J Environ Res Public Health.* 8:629-647

Singh NP, McCoy MT, Tice RR, Schneider EL. 1988. A simple technique for quantitation of low levels of DNA damage in individual cells. *Exp Cell Res.* 175:184-191.

Singh R and Farmer PB. 2006. Liquid chromatography-electrospray ionization-mass spectrometry: the future of DNA adduct detection. *Carcinogenesis* 27:178-196.

Sloof W, de Zwart D, Marquenie JM. 1983. Detection limits of a biological monitoring system for chemical water pollution based on mussel activity. *Bull Environ Contam Toxicol.* 30:400-405.

Springborn Bionomics. 1985. Toxicity test report – Chronic toxicity of acrylamide monomer to mysid. NTIS/OTS Order No. 0510508. Doc # 40-8631565.

Stadler RH, Blank I, Varga N, Robert F, Hau J, Guy PA, Robert MC, Riediker S. 2002. Acrylamide from Maillard reaction products. *Nature* 419:449-450.

Steinbrück A, Csaki A, Ritter K, Leich M, Köhler JM, Fritzsche W. 2008. Gold-silver and silver-silver nanoparticle constructs based on DNA hybridization of thiol- and amino-functionalized oligonucleotides. *J Biophoton.* 1:104-113.

Storhoff J, Elghanian R, Mucic R, Mirkin C, Letsinger R. 1998. One-Pot Colorimetric Differentiation of Polynucleotides with Single Base Imperfections Using Gold Nanoparticle Probes. *J Am Chem Soc.* 120:1959-1964.

Strnad P, Stumptner C, Zatloukal K, Denk H. 2008. Intermediate filament cytoskeleton of the liver in health and disease. *Histochem. Cell Biol.* 129:735-749.

Strohalm M, Hassman M, Košata B, Koldíček M. 2008. mMass data miner: an open source alternative for mass spectrometric data analysis. *Rapid Commun Mass Spec* 22:905-908.

Strohalm M, Kavan D, Novák P, Volný M, Havlíček V. 2010. mMass 3: a cross-platform software environment for precise analysis of mass spectrometric data. *Anal Chem* 82:4648-4651.

Su CL and Tseng WL. 2007. Gold nanoparticles as assisted matrix for determining neutral small carbohydrates through laser desorption/ionization time-of-flight mass spectrometry. *Anal Chem.* 79:1626-33.

Sun L and Irudayaraj J. 2009. PCR-free quantification of multiple splice variants in a cancer gene by surface-enhanced Raman spectroscopy. *J Phys Chem B.* 113:14021-14025.

- Sun T, Chance RR, Graessley WW, Lohse DJ. 2004. A study of the separation principle in size exclusion chromatography. *Macromolecules* 37: 4304-4312.
- Sunner J, Dratz E, Chen Y. 1995. Graphite surface-assisted laser desorption/ionization time-of-flight mass spectrometry of peptides and proteins from liquid solutions. *Anal Chem.* 67:4335-4342.
- Suprun EV, Shilovskaya AL, Lisitsa AV, Bulko TV, Shumyantseva VV, Archakov AI. 2011. Electrochemical Immunosensor Based on Metal Nanoparticles for Cardiac Myoglobin Detection in Human Blood Plasma. *Electroanal.* 23:1051-1057.
- Suslick KS, Didenko Y, Fang MM, Hyeon T, Kolbeck KJ, McNamara III WB, Mdeleni MM, Wong M. 1999. Acoustic cavitation and its chemical consequences *Phil Trans R Soc Lond A.* 357:335-353.
- Takashima F and Hibiya T. 1995. An atlas of fish histology. Normal and pathological features, 2nd edition. Tokyo (Japan). Kodansha.
- Tan Y, Su X, Zhu Y, Lee J. 2010. Sensing of transcription factor through controlled-assembly of metal nanoparticles modified with segmented DNA elements. *ACS Nano.* 4:5101-5110.
- Tanaka K, Waki H, Ido W, Akita S, Yoshida Y, Yoshida T. 1988. Protein and polymer analyses up to m/z 100 000 by laser ionization time-of flight mass spectrometry. *Rapid Commun Mass Spectrom.* 2:151-153.
- Tanaka R, Yuhi T, Nagatani N, Endo T, Kerman K, Takamura Y, Tamiya E. 2006. A novel enhancement assay for immunochromatographic test strips using gold nanoparticles. *Anal Bioanal Chem.* 385:1414-1420.
- Tareke E, Rydberg P, Karlsson P, Eriksson S, Törnqvist M. 2002. Analysis of acrylamide, a carcinogen formed in heated foodstuffs. *J Agric Food Chem.* 50:4998-5006.
- Tedesco S, Doyle H, Blasco J, Redmond G, Sheehan D. 2010. Oxidative stress and toxicity of gold nanoparticles in *Mytilus edulis*. *Aquat Toxicol.* 100:178-186.
- Terman A and Brunk U. 1998. Lipofuscin: mechanisms of formation and increase with age. *APMIS* 106:265-276.
- Thaxton C, Georganopoulou D, Mirkin C. 2006. Gold nanoparticle probes for the detection of nucleic acid targets. *Clin Chim Acta.* 363:120-126.
- Thaxton CS, Elghanian R, Thomas AD, Stoeva SI, Lee J, Smith ND, Schaeffer AJ, Klocker H, Horninger W, Bartsch G, Mirkin CA. 2009. Nanoparticle-based bio-barcode assay redefines “undetectable” PSA and biochemical recurrence after radical prostatectomy. *P Natl Acad Sci USA.* 106:18437-18442.
- Thompson D, Enright A, Faulds K, Smith W, Graham D. 2008. Ultrasensitive DNA detection using oligonucleotide-silver nanoparticle conjugates. *Anal Chem.* 80:2805-2810.
- Tompkins LM and Wallace AD. 2007. Mechanisms of cytochrome P450 induction. *J Biochem Mol Toxicol.* 21:176-181.
- Tseng Y, Chang H, Huang C. 2012. A mass spectrometry-based immunosensor for bacteria using antibody-conjugated gold nanoparticles. *Chem Commun.* 48:8712–8714.
- Tuerk C and Gold L. 1990. Systematic evolution of ligands by exponential enrichment: RNA ligands to bacteriophage T4 DNA polymerase. *Science.* 249:505–510.
- Turkevich J. 1985. Colloidal Gold. Part I. *Gold Bull.* 18:86-91.
- Turteltaub KW and Dingley KH. 1998. Application of accelerated mass spectrometry AMS in DNA adduct quantification and identification. *Toxicol Lett* 102-103:435-439.
- Tyl RW, Friedman MA. 2003. Effects of acrylamide on rodent reproductive performance. *Reprod Toxicol.* 17:1-13.

- Uchiyama M and Mihara M. 1978. Determination of malonaldehyde precursor in tissues by thiobarbituric acid test. *Anal Biochem.* 86:271-278.
- United States Testing Company Inc. 1991. Modified OECD test for ready biodegradability. Test Report 063102-4.
- van der Oost R, Beyer J, Vermeulen N.P.E. 2003. Fish bioaccumulation and biomarkers in environmental risk assessment: a review. *Environ Toxicol Phar.* 13:57-149.
- Vanderpuije BNY, Han G, Rotello VM, Vachet RW. 2006. Mixed monolayer-protected gold nanoclusters as selective peptide extraction agents for MALDI-MS analysis. *Anal Chem.* 78:5491-5496.
- Veigas B, Jacob JM, Costa MN, Santos DS, Viveiros M, Inácio J, Martins R, Barquinha P, Fortunato E, Baptista PV. 2012. Gold on paper–paper platform for Au-nanoprobe TB detection. *Lab Chip.* 12:4802-4808.
- Vethaak AD and Wester PW. 1996. Diseases of flounder *Platichthys flesus* in dutch coastal and estuarine waters, with particular reference to environmental stress factors. II. Liver histopathology. *Dis Aquat Org.* 26:99-116.
- Vidal-Liñán L and Bellas J. 2013. Practical procedures for selected biomarkers in mussels, *Mytilus galloprovincialis* - Implications for marine pollution monitoring. *Sci Total Environ.* 461-462:56-64.
- Vikström AC, Abramsson-Zetterberg L, Naruszewicz M, Athanassiadis I, Granath FN, Törnqvist MÅ. 2011. In vivo doses of acrylamide and glycidamide in humans after intake of acrylamide-rich food. *Toxicol Sci.* 119:41-49.
- Vinogradova OA, Physnaya IA, Zarytova VF, Ivanova EM, Pyshnyi DV. 2007. Enhancement of a hybridization analysis efficiency by the controlled DNA fragmentation. *Appl Mol Biol.* 41:148-156.
- Vo-Dinh T. 2005. Protein nanotechnology: protocols, instrumentation and applications. Totowa (USA). Humana Press, Inc.
- Vogel JS, Turteltaub KW, Finkel R, Nelson DE. 1995. Accelerator mass spectrometry. *Anal Chem* 67:353A-359A.
- Waddell WJ, Lech JJ, Marlowe C, Kleinow KM, Friedman MA. 1990. The distribution of [¹⁴C]acrylamide in rainbow trout studied by whole-body autoradiography. *Fundam Appl Toxicol.* 14:84-87.
- Walker JD. 1991. Ecological effects testing under the toxic substances control act: acrylamide. *Environ Toxic Water* 6:363-369.
- Wang H, Huang P, Lie T, Li J, Hutz RJ, Li K, Shi F. 2010. Reproductive toxicity of acrylamide-treated male rats. *Reprod Toxicol.* 29:225-230.
- Wang JS and Groopman JD. 1998. DNA damage by mycotoxins. *Mutat Res.* 424:167-181.
- Wang W, Chen C, Qian M, Zhao XS. 2008. Aptamer biosensor for protein detection using gold nanoparticles. *Anal Biochem.* 373:21321-9.
- Wang X, Wu L, Ren J, Miyoshi D, Sugimoto N, Qu X. 2011. Label-free colorimetric and quantitative detection of cancer marker protein using noncrosslinking aggregation of Au/Ag nanoparticles induced by target-specific peptide probe. *Biosens Bioelectron.* 21:4804-4809.
- Wang Y and Liu B. 2008. ATP detection using a label-free DNA aptamer and a cationic tetrahedralfluorene. *Analyst.* 133:1593-1598.
- Wangoo N, Kaushal J, Bhasin KK, Mehta SK, Suri CR. 2010. Zeta potential based colorimetric immunoassay for the direct detection of diabetic marker HbA1c using gold nanoprobe. *Chem Commun.* 46:5755-5757.

- Watt F, Bettiol AA, Van Kan JA, Teo EJ, Breese MBH. 2005. Ion beam lithography and nanofabrication: a review. *Int J Nanosci.* 4:269-286.
- Watzek N, Böhm N, Feld J, Scherbl D, Berger F, Merz KH, Lampen A, Reemtsma T, Tannenbaum SR, Skipper PL, Baum M, Richling E, Eisenbrand G. 2012. N7-glycidamide-guanine DNA adduct formation by orally ingested acrylamide in rats: a dose-response study encompassing human diet-related exposure levels. *Chem Res Toxicol.* 25:381-390.
- Wei J, Buriak JM, Siuzdak G. 1999. Desorption-ionization mass spectrometry on porous silicon. *Nature.* 399:243-246.
- Weston D, Lentz RD, Cahn MD, Ogle RS, Rothert AK, Lydy MJ. 2009. Toxicity of anionic polyacrylamide formulations when used for erosion control in agriculture. *J Environ Qual* 38:238-247.
- Wilcoxon J. 2009. Optical Absorption Properties of Dispersed Gold and Silver Alloy Nanoparticles. *J Phys Chem B.* 113:2647-2656.
- Wilson GG and Murray NE. 1991. Restriction and modification. *Annu Rev Genet.* 25:585-627.
- Woodiwiss FS, Fretwell G. 1974. The toxicities of sewage effluents, industrial discharges and some chemical substances to brown trout (*Salmo trutta*) in the Trent river authority area. *Water Pollut Control* 73:396-405.
- Wu HP, Yu CJ, Lin CY, Lin YH, Tseng WL. 2009a. Gold nanoparticles as assisted matrices for the detection of biomolecules in a high-salt solution through laser desorption/ionization mass spectrometry. *J Am Soc Mass Spectrom.* 20:875-82.
- Wu M, Freitas S, Monteiro G, Prazeres D, Santos J. 2009b. Stabilization of naked and condensed plasmid DNA against degradation induced by ultrasounds and high-shear vortices. *Biotechnol Appl Biochem.* 53:237-246.
- Xu X, Wang J, Yang F, Jiao K, Yang X. 2009. Label-free colorimetric detection of small molecules utilizing DNA oligonucleotides and silver nanoparticles. *Small.* 5:2669-2672.
- Yin Z, Liu Y, Jiang L, Zhu J. 2011. Electrochemical immunosensor of tumor necrosis factor α based on alkaline phosphatase functionalized nanospheres. *Biosens Bioelectron.* 26:1890-1894.
- Yonezawa T, Kawasaki H, Tarui A, Watanabe T, Arakawa R, Shimada T, Mafuné F. 2009. Detailed investigation on the possibility of nanoparticles of various metal elements for surface-assisted laser desorption/ionization mass spectrometry. *Anal Sci.* 25:339-346.
- Yousef MI and El-Demerdash FM. 2006. Acrylamide-induced oxidative stress and biochemical perturbations in rats. *Toxicology* 219:133-141.
- Zamora R, Delgado RM, Hidalgo FJ. 2010. Model reactions of acrylamide with selected amino compounds. *J Agric Food Chem.* 58:1708-13.
- Zar JH. 1998. *Biostatistical Analysis*, 4th edition. Upper Saddle River (USA). Prentice Hall.
- Zenick H, Hope E, Smith MK. 1986. Reproductive toxicity associated with acrylamide treatment in male and female rats. *J Toxicol Environ Health* 17:457-72.
- Zhang H, Harpster MH, Park HJ, Johnson PA. 2011a. Surface-enhanced Raman scattering detection of DNA derived from the west Nile virus genome using magnetic capture of Raman-active gold nanoparticles. *Anal Chem.* 83:254-260.
- Zhang J, Liu B, Liu H, Zhang X, Tan W. 2013. Aptamer-conjugated gold nanoparticles for bioanalysis. *Nanomedicine.* 8:983-993.
- Zhang X, Zhu S, Deng C, Zhang X. 2012. Highly sensitive thrombin detection by matrix assisted laser desorption ionization-time of flight mass spectrometry with aptamer functionalized core-shell Fe₃O₄@C@Au magnetic microspheres. *Talanta.* 88:295-302.

Zhang Z, Wen Y, Ma Y, Luo J, Jiang L, Song Y. 2011b. Mixed DNA-functionalized nanoparticle probes for surface-enhanced Raman scattering-based multiplex DNA detection. *Chem Commun.* 47:7407-7409.

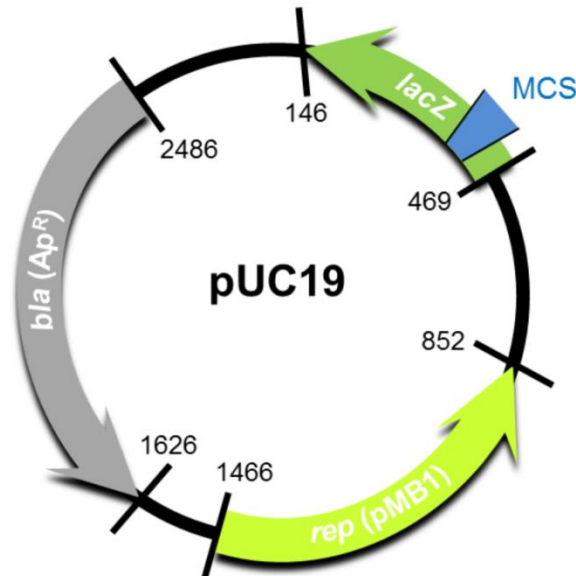
Zhao XM, Xia Y, Whitesides GM. 1997. Soft lithographic methods for nano-fabrication. *J Mater Chem.* 7:1069-1074.

Zhu X, Wu L, Mungra DC, Xia S, Zhu J. 2012. Au@SiO₂ core-shell nanoparticles for laser desorption/ionization time of flight mass spectrometry. *Analyst.* 137:2454-2458.

APPENDICES

Appendix I – Plasmid maps and sequences: pUC19 and p158

pUC19



```

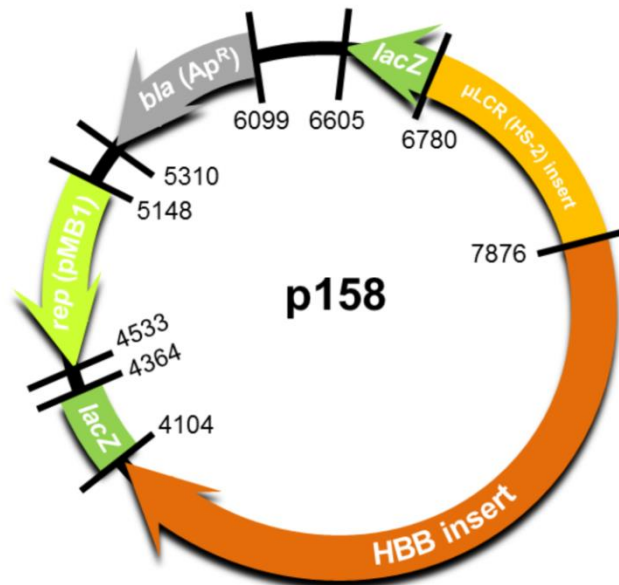
1  TCGCGCGTTT  CGGTGATGAC  GGTGAAAACC  TCTGACACAT  GCAGCTCCCG
51  GAGACGGTCA  CAGCTTGTCT  GTAAGCGGAT  GCCGGGAGCA  GACAAGCCCG
101 TCAGGGCGCG  TCAGCGGGTG  TTGGCGGGTG  TCGGGGCTGG  CTTAACTATG
151 CGGCATCAGA  GCAGATTGTA  CTGAGAGTGC  ACCATATGCG  GTGTGAAATA
201 CCGCACAGAT  GCGTAAGGAG  AAAATACCGC  ATCAGGCGCC  ATTCGCCATT
251 CAGGCTGCGC  AACTGTTGGG  AAGGGCGATC  GGTGCGGGCC  TCTTCGCTAT
301 TACGCCAGCT  GGC GAAAGG  GGATGTGCTG  CAAGGCGATT  AAGTTGGGTA
351 ACGCCAGGGT  TTTCCAGTC  ACGACGTTGT  AAAACGACGG  CCAGTGAATT
401 CGAGCTCGGT  ATCCGGGAT  CCTCTAGAGT  CGACCTGCAG  CCATGCAAGC
451 TTGGCGTAAT  CATGGTCATA  GCTGTTTCCT  GTGTGAAATT  GTTATCCGCT
501 CACAATTCCA  CACAACATAC  GAGCCGGAAG  CATAAAGTGT  AAAGCCTGGG
551 GTGCCTAATG  AGTGAGCTAA  CTCACATTAA  TTGCGTTGCG  CTCACTGCCC
601 GCTTTCAGT  CGGGAAAACCT  GTCGTGCCAG  CTGCATTAAT  GAATCGGCCA
651 ACGCGCGGGG  AGAGGCGGTT  TGCGTATTGG  GCGCTCTTCC  GCTTCCTCGC
701 TCACTGACTC  GCTGCGCTCG  GTCGTTCCGC  TCGGCGGAGC  GGTATCAGCT
751 CACTCAAAGG  CGGTAATACG  GTTATCCACA  GAATCAGGGG  ATAACGCAGG
801 AAAGAACATG  TGAGCAAAAAG  GCCAGCAAAA  GGCCAGGAAC  CGTAAAAAGG
851 CCGCGTTGCT  GCGTTTTTTC  CATAGGCTCC  GCCCCCCTGA  CGAGCATCAC
901 AAAAAATCGAC  GCTCAAGTCA  GAGGTGGCGA  AACCCGACAG  GACTATAAAG
951 ATACCAGGCG  TTTCCCCCTG  GAAGCTCCCT  CGTGCGCTCT  CCTGTTCCGA
1001 CCCTGCCGCT  TACCGGATAC  CTGTCCGCCT  TTCTCCCTTC  GGAAGCGTG
1051 GCGCTTTC  ATAGCTCACG  CTGTAGGTAT  CTCAGTTCGG  TGTAGGTCGT
1101 TCGCTCCAAG  CTGGGCTGTG  TGCACGAACC  CCCCCTTCAG  CCCGACCGCT
1151 GCGCCTTATC  CGGTAACTAT  CGTCTTGAGT  CCAACCCGGT  AAGACACGAC
1201 TTATCGCCAC  TGGCAGCAGC  CACTGGTAAC  AGGATTAGCA  GAGCGAGGTA
1251 TGATAGCGGT  GCTACAGAGT  TCTTGAAGTG  GTGGCCTAAC  TACGGCTACA
1301 CTAGAAGAAC  AGTATTTGGT  ATCTGCGCTC  TGCTGAAGCC  AGTTACCTTC
1351 GAAAAAAGAG  TTGGTAGCTC  TTGATCCGGC  AAACAAACCA  CCGCTGGTAG
1401 CGGTGGTTTT  TTTGTTTGCA  AGCAGCAGAT  TACGCGCAGA  AAAAAAGGAT
1451 CTCAAGAAGA  TCCTTTGATC  TTTTCTACGG  GGTCTGACGC  TCAGTGGAAC
1501 GAAAATCAC  GTTAAGGGAT  TTTGGTCATG  AGATTATCAA  AAAGGATCTT
1551 CACCTAGATC  CTTTTAAATT  AAAAAATGAAG  TTTTAAATCA  ATCTAAAGTA
1601 TATATGAGTA  AACTTGGTCT  GACAGTTACC  AATGCTTAAT  CAGTGAGGCA
  
```

```

1651 CCTATCTCAG CGATCTGTCT ATTTTCGTTCA TCCATAGTTG CCTGACTCCC
1701 CGTCGTGTAG ATAACCTACGA TACGGGAGGG CTTACCATCT GGCCCCAGTG
1751 CTGCAATGAT ACCGCGAGAC CCACGCTCAC CGGCTCCAGA TTTATCAGCA
1801 ATAAACCAGC CAGCCGGAAG GGCCGAGCGC AGAAGTGGTC CTGCAACTTT
1851 ATCCGCCTCC ATCCAGTCTA TTAATTGTTG CCGGGAAGCT AGAGTAAGTA
1901 GTTCGCCAGT TAATAGTTTG CGCAACGTTG TTGCCATTGC TACAGGCATC
1951 GTGGTGTAC GCTCGTCGTT TGGTATGGCT TCATTCAGCT CCGGTTCCCA
2001 ACGATCAAGG CGAGTTACAT GATCCCCCAT GTTGTGCAAA AAAGCGGTTA
2051 GCTCCTTCGG TCCTCCGATC GTTGTGAGAA GTAAGTTGGC CGCAGTGTTA
2101 TCACTCATGG TTATGGCAGC ACTGCATAAT TCTCTTACTG TCATGCCATC
2151 CGTAAGATGC TTTTCTGTGA CTGGTGAGTA CTCAACCAAG TCATTCTGAG
2201 AATAGTGTAT GCGGCGACCG AGTTGCTCTT GCCCGGCGTC AATACGGGAT
2251 AATACCGCGC CACATAGCAG AACTTTAAAA GTGCTCATCA TTGGAAAACG
2301 TTCTTCGGGG CGAAAACCTCT CAAGGATCTT ACCGCTGTTG AGATCCAGTT
2351 CGATGTAACC CACTCGTGCA CCCAACTGAT CTTCAGCATC TTTTACTTTC
2401 ACCAGCGTTT CTGGGTGAGC AAAAACAGGA AGGCAAAATG CCGCAAAAAA
2451 GGAATAAAG GCGACACGGA AATGTTGAAT ACTCATACTC TTCCTTTTTTC
2501 AATATTATTG AAGCATTAT CAGGGTTATT GTCTCATGAG CGGATACATA
2551 TTTGAATGTA TTTAGAAAAA TAAACAAATA GGGGTTCCGC GCACATTTCC
2601 CCGAAAAGTG CCACCTGACG TCTAAGAAAC CATTATTATC ATGACATTAA
2651 CCTATAAAAA TAGGCGTATC ACGAGGCCCT TTCGTC

```

p158



```

1 GTTAACCTCC TATTTGACAC CACTGATTAC CCCATTGATA GTCACACTTT
51 GGGTTGTAAG TGACTTTTTTA TTTATTTGTA TTTTGTACTG CATTAAGAGG
101 TCTCTAGTTT TTTATCTCTT GTTTCCTAAA ACCTAATAAG TAACATAATGC
151 ACAGAGCACA TTGATTTGTA TTTATTTCTAT TTTTAGACAT AATTTATTAG
201 CATGCATGAG CAAATTAAGA AAAACAACAA CAAATGAATG CATATATATG
251 TATATGTATG TGTGTATATA TACACACATA TATATATATA TTTTTTCTTT
301 TCTTACCAGA AGGTTTTAAT CCAAATAAGG AGAAGATATG CTTAGAACCG
351 AGGTAGAGTT TTCATCCATT CTGTCTGTA AGTATTTTGC ATATTTCTGGA
401 GACGCAGGAA GAGATCCATC TACATATCCC AAAGCTGAAT TATGGTAGAC
451 AAAACTCTTC CACTTTTAGT GCATCAACTT CTTATTTGTG TAATAAGAAA
501 ATTGGGAAAA CGATCTTCAA TATGCTTACC AAGCTGTGAT TCCAAATATT
551 ACGTAAATAC ACTTGCAAAG GAGGATGTTT TTAGTAGCAA TTTGTACTGA
601 TGGTATGGGG CCAAGAGATA TATCTTAGAG GGAGGGCTGA GGGTTTGAAG
651 TCCAACCTCT AAGCCAGTGC CAGAAGAGCC AAGGACAGGT ACGGCTGTCA

```

170

701 TCACTTAGAC CTCACCTGT GGAGCCACAC CCTAGGGTTG GCCAATCTAC
751 TCCCAGGAGC AGGGAGGGCA GGAGCCAGGG CTGGGCATAA AAGTCAGGGC
801 AGAGCCATCT ATTGCTTACA TTTGCTTCTG ACACAACCTGT GTTCACTAGC
851 AACCTCAAAC AGACACCATG GTGCATCTGA CTCCTGAGGA GAAGTCTGCC
901 GTTACTGCCC TGTGGGGCAA GGTGAACGTG GATGAAGTTG GTGGTGAGGC
951 CCTGGGCAGG TTGGTATCAA GGTTACAAGA CAGGTTTAAG GAGACCAATA
1001 GAAACTGGGC ATGTGGAGAC AGAGAAGACT CTTGGGTTTC TGATAGGCAC
1051 TGACTCTCTC TGCCTATTGG TCTATTTTCC CACCTTAGG CTGTGGTGG
1101 TCTACCTTG GACCCAGAGG TTCTTTGAGT CCTTTGGGGA TCTGTCCACT
1151 CCTGATGCTG TTATGGGCAA CCTAAGGTG AAGGTCATG GCAAGAAAGT
1201 GCTCGGTGCC TTTAGTGATG GCCTGGCTCA CCTGGACAAC CTCAAGGGCA
1251 CCTTTGCCAC ACTGAGTGAG CTGCACTGTG ACAAGCTGCA CGTGGATCCT
1301 GAGAACTTCA GGGTGAGTCT ATGGGACGCT TGATGTTTTT TTTCCCTTC
1351 TTTTCTATGG TTAAGTTCAT GTCATAGGAA GGGGATAAGT AACAGGGTAC
1401 AGTTTAGAAT GGGAAACAGA CGAATGATTG CATCAGTGTG GAAGTCTCAG
1451 GATCGTTTTA GTTCTTTTTA TTTGCTGTTC ATAACAATTG TTTTCTTTTG
1501 TTTAATTCTT GCTTCTTTT TTTTCTTCT CCGCAATTTT TACTATTATA
1551 CTTAATGCCT TAACATTGTG TATAACAAA GGAAATATCT CTGAGATACA
1601 TTAAGTAACT TAAAAAATAA CTTTACACAG TCTGCCTAGT ACATTACTAT
1651 TTGGAATATA TGTGTGCTTA TTTGCATATT CATAATCTCC CTACTTTATT
1701 TTCTTTTATT TTTAATTGAT ACATAATCAT TATACATATT TATGGGTTAA
1751 AGTGTAATGT TTTAATATGT GTACACATAT TGACCAAATC AGGGTAATTT
1801 TGCATTTGTA ATTTTAAAAA ATGCTTCTCT CTTTTAATAT ACTTTTTTGT
1851 TTATCTTATT TCTAATACTT TCCCTAATCT CTTTCTTTCA GGGCAATAAT
1901 GATACAATGT ATCATGCCTC TTTGCACCAT TCTAAAGAA AACAGTGATA
1951 ATTTCTGGGT TAAGGCAATA GCAATATCTC TGCATATAAA TATTCTGCA
2001 TATAAATTGT AACTGATGTA AGAGGTTTCA TATTGCTAAT AGCAGCTACA
2051 ATCCAGCTAC CATTCTGCTT TTATTTTATG GTTGGGATAA GGCTGGATTA
2101 TTCTGAGTCC AAGCTAGGCC CTTTTGCTAA TCATGTTTAT ACCTCTTATC
2151 TTCTCCCAC AGCTCCTGGG CAACGTGCTG GTCTGTGTGC TGGCCCATCA
2201 CTTTGGCAA GAATTCACCC CACCAGTGCA GGCTGCCTAT CAGAAAGTGG
2251 TGGCTGGTGT GGCTAATGCC CTGGCCACA AGTATCACTA AGCTCGCTTT
2301 CTTGCTGTCC AATTTCTATT AAAGGTTCCCT TTGTTCCCTA AGTCCAACTA
2351 CTAAACTGGG GGATATTATG AAGGGCCTTG AGCATCTGGA TTCTGCCTAA
2401 TAAAAAACAT TTATTTTCAT TGCAATGATG TATTTAAATT ATTTCTGAAT
2451 ATTTTACTAA AAAGGGAATG TGGGAGGTCA GTGCATTTAA AACATAAAGA
2501 AATGAAGAGC TAGTTCAAAC CTGGGAAAA TACACTATAT CTTAAACTCC
2551 ATGAAAGAAG GTGAGGCTGC AAACAGCTAA TGCACATTGG CAACAGCCCC
2601 TGATGCATAT GCCTTATFCA TCCCTCAGAA AAGGATTCAA GTAGAGGCTT
2651 GATTTGGAGG TTAAAGTTTT GCTATGCTGT ATTTTACATT ACTTATTGTT
2701 TTAGCTGTCC TCAATGAATG CTTTTCACTA CCCATTTGCT TATCCTGCAT
2751 CTCTCAGCCT TGACTCCACT CAGTTCTCTT GCTTAGAGAT ACCACCTTTC
2801 CCCTGAAGTG TTCCTTCCAT GTTTTACGGC GAGATGGTTT CTCCTCGCCT
2851 GCCACTCAG CTTAGTTGT CTCTGTTGTC TTATAGAGGT CTACTTGAG
2901 AAGGAAAAAC AGGGGTCATG GTTTGACTGT CCTGTGAGCC CTTCTTCCCT
2951 GCCTCCCCCA CTCACAGTGA CCCGGAATCT GCAGTGCTAG TCTCCCGGAA
3001 CTATCACTCT TTCACAGTCT GCTTTGGAAG GACTGGGCTT AGTATGAAAA
3051 GTTAGGACTG AGAAGAATTT GAAAGGCGGC TTTTTGTAGC TTGATATTCA
3101 CTACTGTCTT ATTACCCTGT CATAGGCCCA CCCCAAATGG AAGTCCCATT
3151 CTTCCTCAGG ATGTTTAAGA TTAGCATTCA GGAAGAGATC AGAGGTCTGC
3201 TGGCTCCCTT ATCATGTCCC TTATGGTGCT TCTGGCTCTG CAGTTATTAG
3251 CATAGTGTTA CCATCAACCA CCTTAACTTC ATTTTTCTTA TTCAATACCT
3301 AGGTAGGTAG ATGCTAGATT CTGGAAATAA AATATGAGTC TCAAGTGGTC
3351 CTTGTCTCT CTCCCAGTCA AATTCTGAAT CTAGTTGGCA AGATTCTGAA
3401 ATCAAGGCAT ATAATCAGTA ATAAGTGATG ATAGAAGGGT ATATAGAAGA
3451 ATTTTATTAT ATGAGAGGGT GAAACCCTCA AAATGAAATG AAATCAGACC
3501 CTTGTCTTAC ACCATAAACA AAAATAAATT TGAATGGGTT AAAGAATTAA
3551 ACTAAGACCT AAAACCATAA AAATTTTTAA AGAAATCAA AGAAGAAAAT
3601 TCTAATATTC ACGTTGCAGC CGTTTTTGAA TTTGATATGA GAAGCAAAGG
3651 CAACAAAAGG AAAAATAAAG AAGTGAGGCT ACATCAAAC TAAAAATTC
3701 CACACAAAA AGAAAACAAT GAACAAATGA AAGGTGAACC ATGAAATGGC

3751 ATATTTGCAA ACCAAATAT TCTTAAATAT TTTGGTTAAT ATCCAAAATA
3801 TATAAGAAAC ACAGATGATT CAATAACAAA CAAAAAATTA AAAATAGGAA
3851 AATAAAAAAA TTAAAAAGAA GAAAATCCTG CCATTTATGC GAGAATTGAT
3901 GAACCTGGAG GATGTAAAAAC TAAGAAAAAT AAGCCTGACA CAAAAGACA
3951 AATACTACAC AACCTTGCTC ATATGTGAAA CATAAAAAAG TCACTCTCAT
4001 GGAAACAGAC AGTAGAGGTA TGGTTTCCAG GGGTTGGGGG TGGGAGAATC
4051 AGGAACTAT TACTCAAAGG GTATAAAAT TCAGTTATGT GGGATGAATA
4101 AATTCTAGAG TCGACCTGCA GGCATGCAAG CTTGGCGTAA TCATGGTCAT
4151 AGCTGTTTCC TGTGTGAAAT TGTATCCGC TCACAAATCC ACACAACATA
4201 CGAGCCGGAA GCATAAAGTG TAAAGCCTGG GGTGCCTAAT GAGTGAGCTA
4251 ACTCACATTA ATTGCGTTGC GCTCACTGCC CGCTTTCAG TCGGAAACC
4301 TGTCGTGCCA GCTGCATTAA TGAATCGGCC AACGCGCGGG GAGAGCGGT
4351 TTGCGTATTG GGCCTCTTC CGCTTCCCTG CTCACTGACT CGCTGCGCTC
4401 GGTGCTTCGG CTGCGGCGAG CGGTATCAGC TCACTCAAAG GCGGTAATAC
4451 GGTATCCAC AGAATCAGGG GATAACGCAG GAAAGACAT GTGAGCAAAA
4501 GGCCAGCAAA AGGCCAGGAA CCGTAAAAAG GCCGCTTGC TGGCGTTTTT
4551 CCATAGGCTC CGCCCCCTG ACGAGCATCA CAAAAATCGA CGCTCAAGTC
4601 AGAGGTGGCG AAACCCGACA GACTATAAA GATACCAGGC GTTCCCCCT
4651 GGAAGCTCCC TCGTGCCTC TCTGTTCCG ACCCTGCCGC TTACCGGATA
4701 CCTGTCCGCC TTTCTCCCTT CGGGAAGCGT GCGCTTTCAT CATAGCTCAC
4751 GCTGTAGGTA TCTCAGTTCG GTGTAGGTCG TTCGCTCCAA GCTGGGCTGT
4801 GTGCACGAAC CCCCCGTTCA GCCCGACCGC TGCCTTTAT CCGGTAACTA
4851 TCGTCTTGAG TCCAACCCGG TAAGACACGA CTTATCGCCA CTGGCAGCAG
4901 CCACTGGTAA CAGGATTAGC AGAGCGAGGT ATGTAGGCGG TGCTACAGAG
4951 TTCTTGAAGT GGTGGCTTAA CTACGGCTAC ACTAGAAGGA CAGTATTTGG
5001 TATCTGCGCT CTGCTGAAGC CAGTTACCTT CGGAAAAAGA TTTGTAGCT
5051 CTTGATCCGG CAAACAAACC ACCGCTGGTA GCGGTGGTTT TTTTGTTTGC
5101 AAGCAGCAGA TTACGCGCAG AAAAAAAGGA TCTCAAGAAG ATCCTTTGAT
5151 CTTTTCTACG GGGTCTGACG CTCAGTGGAA CGAAAACCTCA CGTTAAGGGA
5201 TTTTGGTCAT GAGATTATCA AAAAGGATCT TCACCTAGAT CTTTTTAAAT
5251 TAAAAATGAA GTTTTAAATC AATCTAAAGT ATATATGAGT AAAC TTGGTC
5301 TGACAGTTAC CAATGCTTAA TCAGTGAGGC ACCTATCTCA GCGATCTGTC
5351 TATTTGCTTC ATCCATAGTT GCCTGACTCC CCGTCGTGTA GATAACTACG
5401 ATACGGGAGG GCTTACCATC TGGCCCCAGT GCTGCAATGA TACCGCGAGA
5451 CCCACGCTCA CCGCTCCAG ATTTATCAGC AATAAACAG CCAGCCGGAA
5501 GGGCCGAGCG CAGAAGTGGT CCTGCAACTT TATCCGCCCT CATCCAGTCT
5551 ATTAATTGTT GCCGGGAAGC TAGAGTAAGT AGTTCGCCAG TTAATAGTTT
5601 GCGCAACGTT GTTGCCATTG CTACAGGCAT CGTGGTGTCA CGCTCGTCGT
5651 TTGGTATGGC TTCATTGAGC TCCGGTTCCC AACGATCAAG GCGAGTTACA
5701 TGATCCCCCA TGTTGTGCAA AAAAGCGGTT AGCTCCTTCG GTCTCCGAT
5751 CGTTGTCAGA AGTAAGTTGG CCGCAGTGTT ATCACTCATG GTTATGGCAG
5801 CACTGCATAA TTCTCTTACT GTCATGCCAT CCGTAAGATG CTTTCTGTG
5851 ACTGGTGAGT ACTCAACCAA GTCATTCTGA GAATAGTGTA TGCAGGACC
5901 GAGTTGCTCT TGCCCGCGT CAATACGGGA TAATACCGCG CCACATGCA
5951 GAAC TTTAAA AGTGCTCATC ATTGGA AAC GTTCTTCGGG CCGAAAAC TC
6001 TCAAGGATCT TACCGCTGTT GAGATCCAGT TCGATGTAAC CCAC TCGTGC
6051 ACCCAACTGA TCTTCAGCAT CTTTACTTTT CACCAGCGTT TCTGGGTGAG
6101 CAAAAACAGG AAGGCAAAAT GCCGCAAAA AGGGAATAAG GGCGACACGG
6151 AAATGTTGAA TACTCATACT CTTCTTTTTT CAATATTATT GAAGCATTTA
6201 TCAGGGTTAT TGTCTCATGA GCGGATACAT ATTTGAATGT ATTTAGAAAA
6251 ATAAACAAAT AGGGGTTCG CGCACATTT CCCGAAAAGT GCCACCTGAC
6301 GTCTAAGAAA CCATTATTAT CATGACATTA ACCTATAAAA ATAGGCGTAT
6351 CACGAGGCC TTTGCTCTCG CGGTTTTCGG TGATGACGGT GAAAACCTCT
6401 GACACATGCA GCTCCCGGAG ACGGTCACAG CTTGTCTGTA AGCGGATGCC
6451 GGGAGCAGAC AAGCCCGTCA GGGCGCGTCA GCGGGTGTG GCGGGTGTG
6501 GGGCTGGCTT AACTATGCGG CATCAGAGCA GATTGTACTG AGAGTGCACC
6551 ATATGCGGTG TGAAATACCG CACAGATGCG TAAGGAGAAA ATACCGCATC
6601 AGGCGCCATT CGCCATTCAG GCTGCGCAAC TGTGGGAAG GGCGATCGGT
6651 GCGGGCCTCT TCGCTATTAC GCCAGCTGGC GAAAGGGGGA TGTGCTGCAA
6701 GCGGATTAAG TTGGGTAACG CCAGGGTTTT CCCAGTCACG ACGTTGTAAA
6751 ACGACGGCCA GTGAATTCGA GCTCGGTACG GTACCAGTGG GGCTCTAAG

6801 ACTAAGTCAC TCTGTCTCAC TGTGTCTTAG CCAGTTCCTT ACAGCTTGCC
6851 CTGATGGGAG ATAGAGAATG GGTATCCTCC AACAAAAAAA TAAATTTTCA
6901 TTTCTCAAGG TCCAACCTTAT GTTTTCTTAA TTTTAAAAAA AATCCTTGACC
6951 ATTCTCCACT CTCTAAAAATA ATCCACAGTG AGAGAAACAT TCTTTTCCCC
7001 CATCCCATAA ATACCTCTAT TAAATATGGA AAATCTGGGC ATGGTGTCTC
7051 ACACCTGTAA TCCAGCACT TTGGGAGGCT GAGGTGGGTG GACTGCCTGG
7101 AGCTCAGGAG TTCAAGACCA TCTTGGACAA CATGGTGATA CCCTGCCTCT
7151 ACAAAAAGTA CAAAAATTAG CCTGGCATGG TGGTGTGCAC CTGTAATCCC
7201 AGCTATTAGG GTGGCTGAGG CAGGAGAATT GCTTGAACCC GGGAGGCGGA
7251 GGTTGCAGTG AGCTGAGATC GTGCCACTGC ACTCCAGCCT GGGGGACAGA
7301 GCACATTATA ATTAAGTGT ATTTTTTACT TGGACTCTTG TGGGGAATAA
7351 GATACATGTT TTATTCTTAT TTATGATTCA AGCACTGAAA ATAGTGTTTA
7401 GCATCCAGCA GGTGCTTCAA AACCATTTGC TGAATGATTA CTATACTTTT
7451 TACAAGCTCA GCTCCCTCTA TCCCTTCCAG CATCCTCATC TCTGATTAAA
7501 TAAGCTTCAG TTTTTCCTTA GTTCTGTGTTA CATTTCTGTG TGTCTCCATT
7551 AGTGACCTCC CATAGTCCAA GCATGAGCAG TTCTGGCCAG GCCCTGTGCG
7601 GGGTCAGTGC CCCACCCCG CCTTCTGGTT CTGTGTAACC TTCTAAGCAA
7651 ACCTTCTGGC TCAAGCACAG CAATGCTGAG TCATGATGAG TCATGCTGAG
7701 GCTTAGGGTG TGTGCCCAGA TGTCTCAGC CTAGAGTGAT GACTCCTATC
7751 TGGGTCCCCA GCAGGATGCT TACAGGGCAG ATGGCAAAAA AAAGGAGAAG
7801 CTGACCACCT GACTAAAACT CCACCTCAA CGGCATCATA AAGAAAATGG
7851 ATGCCTGAGA CAGAAATGTGA CATATTCTAG AATATATTAT TTCTGAATA
7901 TATATATATA TATACACATA TACGTATATA TATATATATA TATATATTTG
7951 TTGTTATCAA TTGCCATAGA ATGATTAGTT ATTGTGAATC AAATATTTAT
8001 CTTGCAGGTG GCCTCTATAC CTAGAAGCGG CAGAATCAGG CTTTATTAAT
8051 ACATGTGTAT AGATTTTATG GATCTATACA CATGTATTAA TATGAAACAA
8101 GGATATGGAA GAGGAAGGCA TGAAAACAGG AAAAGAAAAC AAACCTTGTT
8151 TGCCATTTTA AGGCACCCCT GGACAGCTAG GTGGCAAAAAG GCCTGTGCTG
8201 TTAGAGGACA CATGCTCACA TACGGGGTCA GATCTGACTT GGGGTGCTAC
8251 TGGGAAGCTC TCATCTTAAG GATACATCTC AGGCCAGTCT TGGTGCATTA
8301 GGAAGATGTA GGCAACTCTG ATCCTGAGAG GAAAGAAACA TTCTCCAGG
8351 AGAGCTAAAA GGGTTCACCT GTGTGGGTAA CTGTGAAGGA CTACAAGAGG
8401 ATGAAAAACA ATGACAGACA GACATAATGC TTGTGGGAGA AAAACAGGA
8451 GGTCAAGGGG ATAGAGAAGG CTTCCAGAAG AATGGCTTTG AAGCTGGCTT
8501 CTGTAGGAGT TCACAGTGGC AAAGATGTTT CAGAAATGTG ACATGACTTA
8551 AGGAAGTATA CAAAAAGGAA CAAATTTAAG GAGAGGCAGA TAAATTAGTT
8601 CAACAGACAT GCAAGGAATT TTCAGATGAA TGTATGTCT CCACCTGAGCT
8651 TCTTGAGGTT AGCAGCTG

Appendix II – Calibration curves used for total protein quantification via Bradford assay and for analysis of several biomarkers

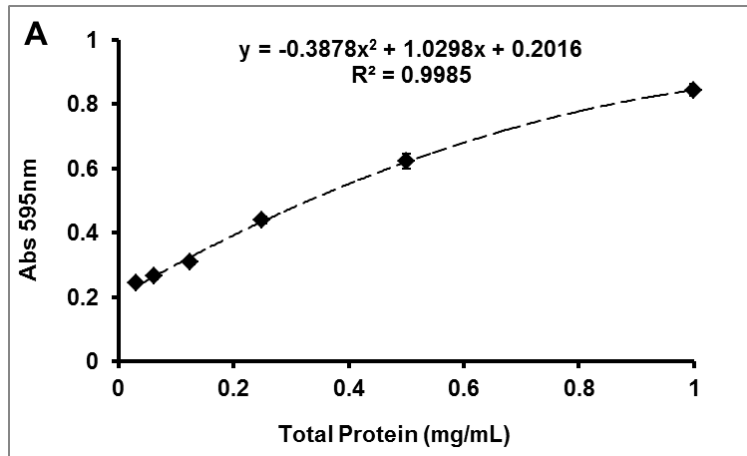


Figure A.1. BSA calibration curve used for quantification of total protein in goldfish samples.

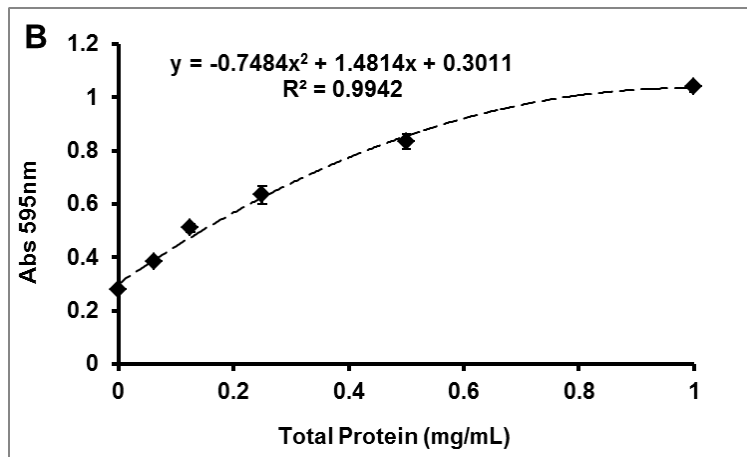


Figure A.2. BSA calibration curve used for quantification of total protein in mussel samples.

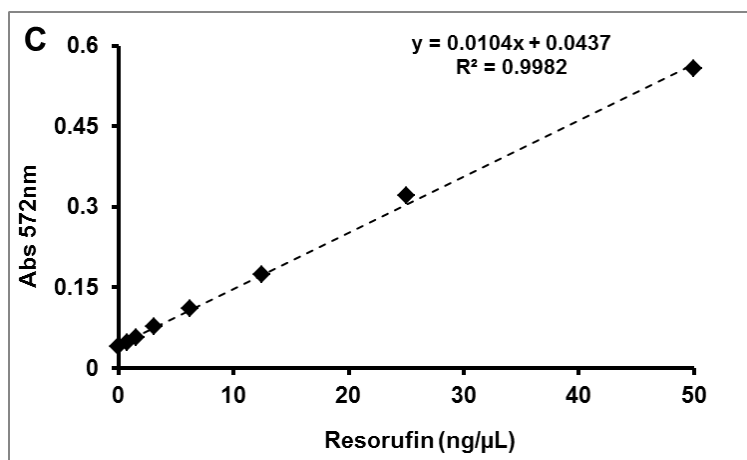


Figure A.3. Resorufin calibration curve used for analysis of EROD in mussel samples.

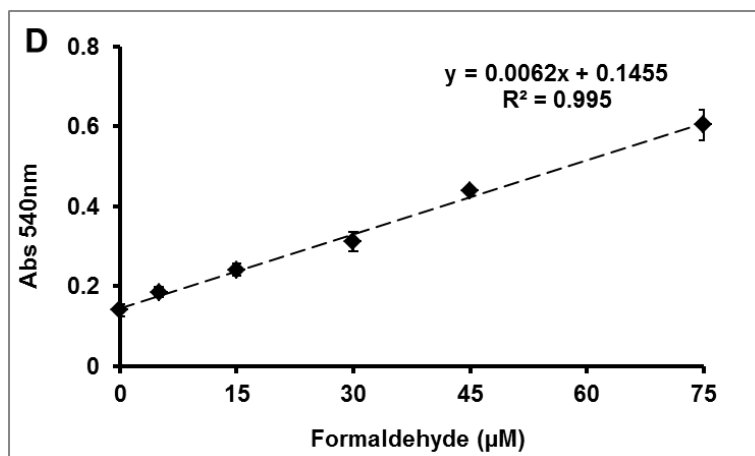


Figure A.4. Formaldehyde calibration curve used for analysis of catalase (CAT) in mussel samples.

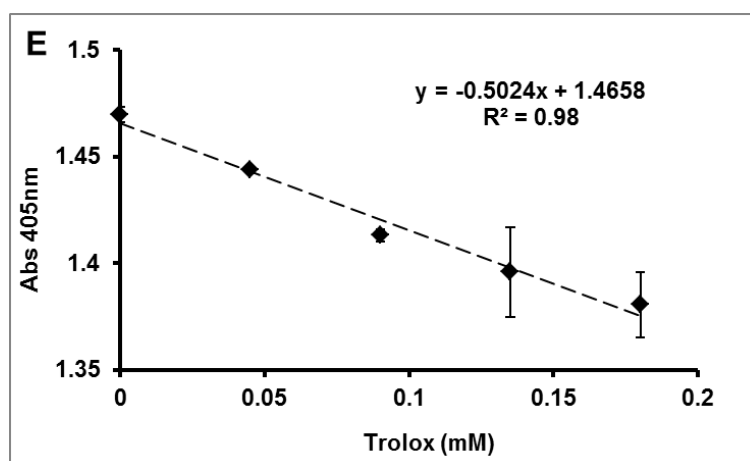


Figure A.5. Trolox calibration curve used for analysis of total antioxidant capacity (TAC) in mussel samples.

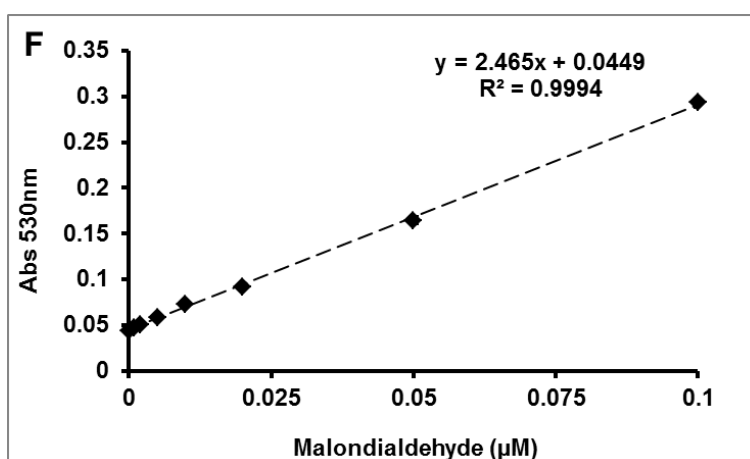


Figure A.6. Malondialdehyde calibration curve used for analysis of lipid peroxidation in mussel samples.

Appendix III – Characterisation of organic matrices: UV-Vis and MALDI-MS

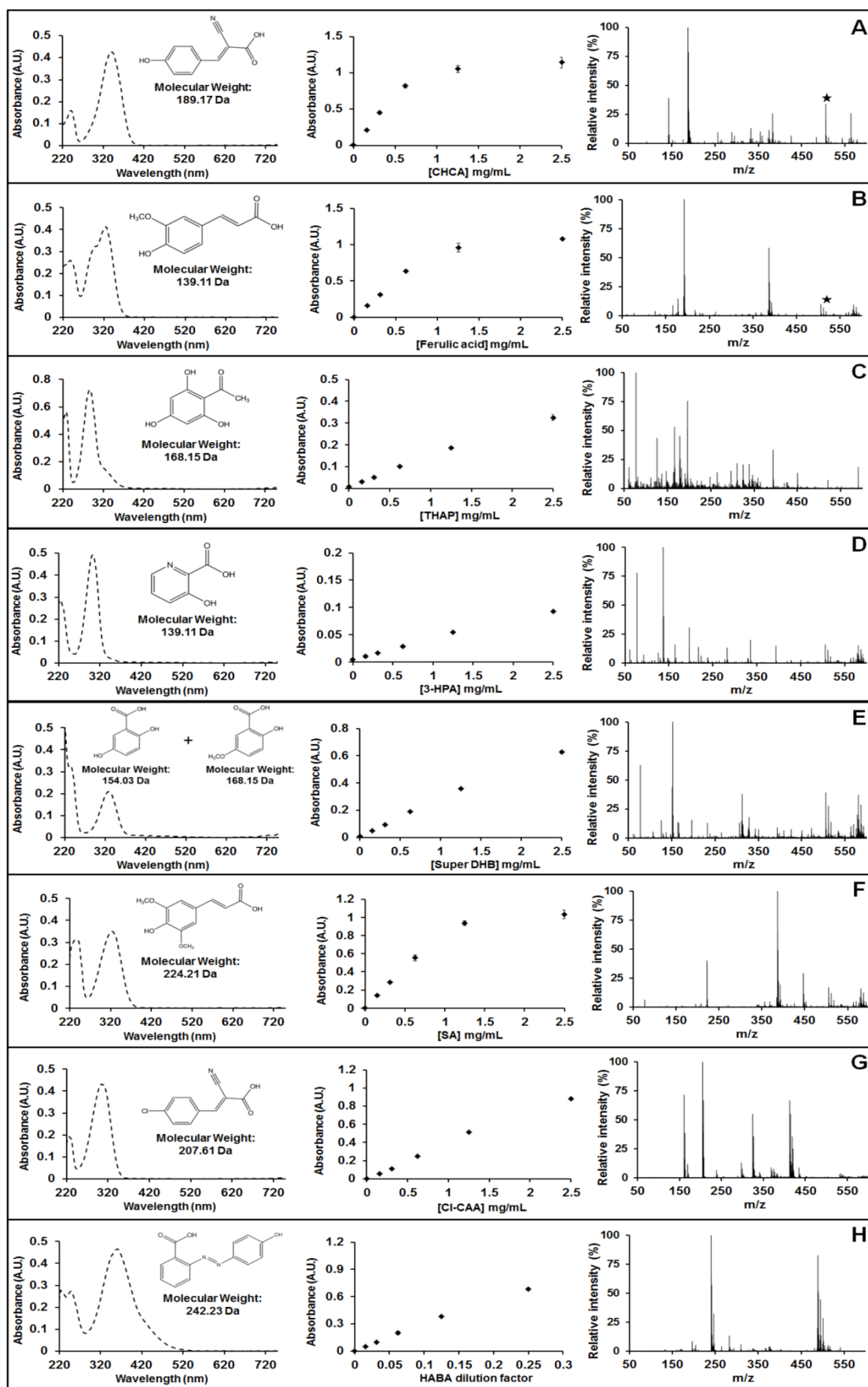


Figure A.7. Characterisation of the utilised organic matrices: UV-Vis spectrum (on the foremost left), Absorbance at 337 nm (on the center) and MALDI spectrum with dGTP (on the right). A) CHCA; B) Ferulic acid; C) THAP; D) 3-HPA; E) Super DHB; F) Sinapinic acid (SA); G) chloro-phenyl-acrylic acid (Cl-Ph-AA); H) HABA. Black stars on the MALDI spectra identify dGTP molecular ion signals when using CHCA and ferulic acid. Other matrices did not allow the identification of the analyte.